"STRUCTURE OF FLOW IN THE FREEBOARD REGION
OF GAS/SOLID FLUIDISED BEDS"

BY

IAIN LANG   B.Sc.

Thesis presented for the Degree of Doctor of Philosophy

University of Edinburgh

March, 1986

The work described in this thesis
is the original work of the author
except where specific reference
is made to other sources. It has
not been submitted, in whole or
in part, for any degree at
any other University.

                                    Iain Lang

Acknowledgments

The author would like to express his gratitude to the following people and organisations who have contributed to the successful completion of the research project and this manuscript:

Abstract

A standard Laser Doppler Anemometry (L.D.A.) system has been developed to operate above fluidised beds where entrained solids travel relatively large distances vertically. The statistical properties of the gas flow i.e. the mean velocity and the rms fluctuating velocity have been measured in the 3 Cartesian co-ordinate directions at different superficial gas flowrates, bed depths and positions in the freeboard space.

Measurements were taken in three fluidised systems, a small bed of 7.5 * 7.5 cm square cross section fluidising glass ballotini beads and round sand and catalyst particles fluidised in a 0.48 * 0.28 m rectangular cross section bed. Comparison of the results obtained from the last two systems showed the effect of minimum fluidising velocity on the structure of the gas flow in the freeboard region.

The effect of an immersed tube bank on the structure of flow was investigated by placing a horizontal arrangement of rods in the dense phase. Results were compared under identical operating conditions in the presence and absence of the rod bundle. The mean velocity profiles were investigated along the axes of symmetry in each system, and in one case measurements were taken off these reference axes. The results obtained indicate the form of the 3 dimensional velocity profile and also that continuity is satisfied. In addition, existing theoretical models for the decay of turbulence above fluidised beds have been tested.

In the course of this investigation a substantial amount of information has been obtained on the structure of gas flow above various fluidised beds. This information has significant implications for the motion of particles in the freeboard space, a number of which are not accounted for in existing theoretically based models for particle motion.

Table of Contents

Chapter 1
Introduction

Fluidisation is defined as the operation whereby solids behave as a liquid. If a gas is forced through a bed of solids at a low rate, the gas will percolate through the interstices of the bed and leave. If the gas flow rate is increased, a flow rate is reached where the drag force on an individual particle becomes equal to the weight of the particle and it becomes suspended in the passing fluid. This is called the Minimum Fluidising Velocity and the bed of particles is said to be incipiently fluidised.

When the gas flow is increased further bubbles develop which rise through the bed of particles, this behaviour is termed aggregative fluidisation. The classical model of this type of fluidised bed is the two phase model, one phase being the particulate phase and the other the bubble phase. At the surface of the bed bubbles erupt and it is generally accepted that there are two consequences of this. Firstly, bed material is ejected into the space above the bed, the freeboard region, and secondly, fluctuations in gas velocity are generated in the freeboard region.

Fluidised Beds have a number of characteristics which make them very attractive for gas solid contacting. There are very good rates of heat transfer from the bed to internals or to the walls, and the bed itself should operate isothermally. Rates of mass transfer are also very good. The mobility of individual particles of bed material is an advantage and mixing is very thorough. As a result Fluidised Beds have been utilized commercially for a number of processes. Some of these processes are physical in nature e.g. drying, coating and granulation. Other operations involve chemical reaction e.g. Catalytic Cracking of long chain hydrocarbons and regeneration of spent catalyst. In recent years fluidised beds have been of special interest because of their potential as an important process in the utilization of coal as a future

source of energy, notably in coal combustion and gasification processes.

In the freeboard region of a fluidised bed bed material is thrown upwards by erupting bubbles and acted on by the fluid flow field. The characteristics of this flow have yet to be fully established. The purpose of this study was to use Laser Doppler Anemometry, L.D.A., to obtain information on local fluid mean velocities and turbulence intensities in three dimensions and relate these to available information on bubbling properties of fluidised beds. The structure of flow may be used to predict the motion of particles and hence the carry over of material from the system. In particular the distance that particles can be expected to travel is important. The Transport Disengaging Height, T.D.H., is defined as the height above which no particles will be disengaged and this will be dependent on the motion of particles in the fluid flow field. In many commercial fluidised systems heat is removed from the bed by passing coolant through tubes passing through the bed. The effect of immersed rods on the properties of the flow field was investigated in this project.

It has become apparent that the phenomena in the freeboard region and the motion of particles will have a significant effect on a number of processes in which fluidised beds are used. For example, in a fluidised system where a chemical reaction is taking place a significant proportion of the reaction will take place in the freeboard as a result of contact between gas and entrained solids. Also, in Fluidised Bed Combustion, the loss of material as a result of carry over will decrease the efficiency of the combustion process and may make the combustion less efficient than in existing furnace configurations. The possibility of combined cycle power generation is currently under consideration, in which the

exhaust gases could be expanded through turbines to recover energy. However, the presence of solid particles in the exhaust gases would cause rapid wear and the accurate prediction of particle carry over for use in the design of gas / solid separation plant is necessary.

Chapter 2
Survey of Literature

2.1 Bubbling Properties of Fluidised Beds

2.1.1 Introduction

In aggregative fluidised systems, the dense bed is characterised by bubbles. The development of models of fluidised beds has been based on the study of bubbling properties. It is important to understand the bubbling phenomenon as a first step in the analysis of gas and solid flow in the freeboard region above the bed. A very large amount of published work is available on the subject, and an attempt has been made to review briefly aspects of dense bed behaviour which are felt to be directly relevant to the present work.

2.1.2 Bubble Rise Velocity and Bubble Size

When a fluidised bed is freely bubbling the bubbles are generated at the distributor and increase in size and velocity as they rise upwards through the bed. The bubble size range in the fluidised bed will be determined by system parameters such as distributor design, superficial gas velocity, bed depth and bed geometry. Leung [38] gives a method for designing the distributor plate and predicting the bubble sizes. The main method of bubble growth is by coalescence.

If one bubble is within one bubble diameter behind another, it will accelerate and eventually catch up with the leading bubble. This phenomenon is described by Clift and Grace [11]. The measurement of bubble size in fluidised beds has been performed by many researchers. Mojtahedi [50] used a compound fibre optic probe, Parks et. al. [59] used a conductivity probe, Rowe and Everett [63] used X-Rays, Geldart [22] used Cine Films and Orcutt and Carpenter [57] used Gamma Ray Absorption. From the evidence provided by these studies, the conclusion is

drawn that the bubble size is related to the excess gas flow, $U_G - U_{MF}$. The prediction of bubble size for fluidised beds has also been the subject of much work. It forms the basis of several fluidised bed models, e.g. that of Kato and Wen [36]. However, it was felt that the correlation that best represented the system used in this work was that of Mori and Wen [51]. A semi-empirical correlation for bubble growth in fluidised beds of various sizes was presented. The correlation has the form:

$$\frac{D_{BM} - d_e}{D_{BM} - D_{B0}} = \exp(-0.3h/D_t) \qquad (2.1)$$

where D_{BM} = bubble diameter that would exist in a fluidised bed if all the fluidising gas above that required for minimum fluidisation went to form a single train of bubbles along the centre line of the bed. D_{BM} can be calculated from:

$$D_{BM} = 0.652 \ (A(U_G - U_{MF}))^{2/5}$$

where A = Cross sectional area of the bed and D_{B0} = Initial bubble diameter at the distributor.
The value of D_{B0} for a porous plate distributor can be calculated from:

$$D_{B0} = 0.00376 \ (U_G - U_{MF})^2$$

where h = Bed depth,
D_t = Diameter or equivalent diameter of the bed.

There is a relationship between bubble size and bubble rise velocity of the form:

$$U_a = (U_G - U_{MF}) + a(gd_e)^b \qquad (2.2)$$

The rise velocity of bubbles may dictate the fluctuations

of gas velocity in the freeboard and its estimation is important in this context. Davidson and Harrison [14] give the following relationship:

$$U_a = (U_G - U_{MF}) + 0.711(gd_e)^{1/2} \qquad (2.3)$$

There have been various values suggested for the constants a and b in equation (2.2) to fit particular experimental data e.g. Mojtahedi [50]. There have also been exponents suggested for the $(U_G - U_{MF})$ term, depending on the fluidised system. A review of this is given by Yates [76].

An equation that predicts reasonably well bubble rise velocites in fluidised beds of particles in the range 40 - 260 µm was proposed by Rowe and Yacono [65]:

$$U_a = (U_G - U_{MF}) + 9.36k_v(h + h_0)^{3/8}(U_G - U_{MF})^{1/4} \qquad (2.4)$$

where k_v = velocity coefficient $U_a/\sqrt{g(d_e/2)}$ and increases from about 1 for a particle size of 260 µm to about 1.3 for those of 40µm.

h_0 = constant characteristic of the distributor and is approximately zero for a porous plate distributor. N.B. the constant 9.36 is dimensional = $0.707g^{3/8}$ and velocities and distances have units of cm s^{-1} and cm respectively.

2.1.3 Spatial Distribution of Bubbling

The distribution of bursting bubbles at the surface of a fluidised bed may affect the local variation of gas velocity in the freeboard region, particularly near the bed surface. Levy and Lockwood [42] suggested this to explain the relatively high local velocities near the wall in the freeboard of their fluidised system. Mojtahedi's findings, too, were that, at low elevations above the distributor

plate, the bubbles were more frequent near the walls [50]. At greater elevations, bubble concentrations moved nearer the bed centre. This being the case, a larger volumetric flow may be expected near the walls in the freeboard when bubbles burst at the surface of a shallow bed.

Werther and Molerus [75] also found that the local bubble volume fraction and local bubble gas flow were greater at the walls than in the centre near the distributor plate, but the converse was true at greater distances from the distributor.

2.1.4 Particle Circulation Patterns

Rowe and Partridge [64] presented experimental evidence on the particle motion induced by single bubbles in 2D and 3D fluidised beds. Photographs were taken in the 2D bed and tracer particles were used in the 3D bed. A reproducible pattern was found in which particles were drawn up by the bubble in a spout with a mushroom shaped wake in its rear.

Particle circulation patterns have been suggested as phenomena that are very closely related to the spatial distribution of bubbling. It is open to question whether particle circulation patterns are caused by bubble maldistribution, particle circulation patterns cause the bubble maldistribution or whether one phenomenon perpetuates the other.

This movement was suggested by Mojtahedi [50] and Werther and Molerus [75]. In regions of the bed where particle movement is upwards bubble rise velocities will be larger than in regions where particle movement is downwards. Ohki and Shirai [56] made measurements of particle velocities in a fluidised bed with a fibre optic

probe, and found particles moving upward near the wall and downwards at the centre. The bed used was shallow. Lin et. al. [45] used a radioactive tracer technique for measurement of solids motion in gas fluidised beds. They found that at low fluidising gas velocity particles tended to move upwards at the wall and downwards at the centre whereas, at increased gas velocity, the converse was true. Yates [76] gives a review of particle movement in fluidised beds.

2.1.5 Pressure Fluctuations

Fan et. al. [18] give measurements of pressure fluctuations at different positions in gas fluidised beds. They concluded that the fluctuations were caused by the passage of bubbles. The amplitude of the pressure fluctuations was related both to the bed density and size of bubbles. The pressure fluctuations at the surface of the bed may be important with respect to the fluctuations in gas velocity in the freeboard. Given the linkage of pressure and velocity in the Bernoulli Equation it may reasonably be expected that fluctuations of pressure at the bed surface are related to fluctuations of gas velocity above it.

Hsieh et. al. [34] made measurements of velocity fluctuations in the freeboard of a fluidised bed with a hot wire anemometer and correlated the results with bubble diameters in the dense phase. They found that there was a correlation between the two phenomena, which in turn indicates that perhaps velocity fluctuations are related to the amplitude of pressure fluctuations at the bed surface.

Nicastro and Glicksman [54] made measurements of differential pressure fluctuations to verify the scaling

laws for fluidised beds proposed by Glicksman [26]. Glicksman proposed parameters that would govern the dynamics of fluidised beds by nondimensionalising the differential equations governing fluid and particle behaviour. By investigating two different fluidised systems with the same parameter values the scaling laws were verified. It was concluded, therefore, that it should be possible to relate information obtained in relatively small scale laboratory equipement to large scale commercial units.

Fan et. al. [19] proposed a dynamic model of a fluidised bed which gave the intensity of pressure fluctuations as proportional to the parameter:

$$M_S/2A \ (U_G - U_{MF}) \hspace{2cm} (2.5)$$

where M_S = Mass of solids in the bed, and
A = Cross sectional area of the bed.

2.2 Entrainment and Elutriation

2.2.1 Introduction

When a fluidised bed is operated at gas velocities in excess of U_{MF} particles are ejected into the space above the bed by bursting bubbles. This phenomenon is known as entrainment and the mass of particles ejected increases with increase in superficial fluidising velocity. The solids are acted on by the gas flow field and, if the gas flow is greater than the terminal velocity of a particle, the particle will be carried over out of the system. In most cases a fluidised bed contains a range of particle sizes and as a result only some of the particles may be carried over. These will be the small particles whose terminal velocities are relatively small. This phenomenon is known as Elutriation. Larger particles will travel for a certain distance before their velocity is reversed and and they fall back towards the bed. There is therefore a decrease in the mass of entrained solids with distance from the bed surface. The distance above the bed at which no further disengagement of solids occurs and the concentration of particles at still greater distances from the bed surface is constant is called the Transport Disengaging Height, (T.D.H.).

In the first section, the development of models to analyse solids movement in the freeboard is described. Because of a lack of mechanistic understanding many of the models are based on empirical correlations and relationships. The second section reviews published literature on bubble eruption and solids ejection which is the first stage in the entrainment process. Finally, available mechanistic models of entrainment and their applications are described.

2.2.2 Historical Development

Leva [39] and Osberg and Charlesworth [58] considered the carry over of fines from a two component bed. The results that were obtained prompted the proposal of a rate equation as for a first order chemical reaction. This work can be summarized by the equation:

$$Log \ C/C_0 = -Mt \qquad (2.6)$$

where C = Concentration of fines after time t

C_0 = Initial concentration of fines

M = Velocity rate constant

Leva also concluded that the velocity rate constant for elutriation was proportional to the fourth root of the superficial fluidising velocity. In addition, he found that at a low fines concentration the simple relationship above broke down. He termed this the "Breakdown Point". He also observed that there was an equilibrium concentration of fines associated with any fluidised system and as a result a fluidised bed has a certain capability to retain fines. Osberg and Charlesworth [58] made a more comphrehensive investigation. Correlation was attempted along the same lines as Leva [39].

Wen and Hashinger [74] correlated data from Osberg and Charlesworth and Leva to give a correlation for a specific elutriation rate constant, K, as opposed to the velocity rate constant used by Leva. K is a proportionality constant in an equation of the form:

$$dC/dt = -K(A/M_S)C \qquad (2.7)$$

where M_S = Mass of solids in bed,

A = Cross sectional area of the bed.

They also assumed that the driving force for elutriation was the difference between the superficial fluidising

velocity and the terminal velocity of the particle. A velocity distribution was assumed for the freeboard which was used to explain the fact that fines near the walls fell back to the bed. The assumed velocity profiles are given in Figure 2.1.

A critical height was proposed which is required for the gas to fully develop the velocity profile. Dimensional analysis was applied based on the following:

$$K = f \left[d_p, U_t, (U_G - U_{MF}), \varrho_g, (\varrho_s - \varrho_g), \mu, g \right] \qquad (2.8)$$

where U_t = Particle terminal velocity
d_p = Particle diameter
ϱ_g = Density of gas
μ = Dynamic viscosity of gas
g = Gravitational constant

The resulting equation was:

$$\frac{K}{\varrho_g (U_G - U_t)} = \beta \left[\frac{(U_G - U_t)^2}{g d_p} \right]^a \left[\frac{d_p U_t \varrho_g}{\mu} \right]^b \left[\frac{\varrho_s - \varrho_g}{\varrho_g} \right]^c \left[\frac{U_G - U_t}{U_t} \right]^d \qquad (2.9)$$

They found by examination of the experimental data that the power of the last group was negligible, and the group was eliminated. The evaluation of the constants was arrived at by plotting the group against the specific elutriation rate constant.

Thomas et. al. [70] proposed that the simple first order rate equation postulated by Leva [39] would be applicable if the fluidised bed was perfectly mixed. They found that this was not the case, and finer particles, which were incapable of elutriation, accumulated at the bed surface. They also found that the initial rate of elutriation was lower than predicted by the equation proposed by Leva

and suggested that the layer of finer particles at the bed surface acted as a resistance to elutriation. They proposed that:

$$-dX/dt \propto X \, e^{aX} \qquad (2.10)$$

where X = Weight of fines in the bed at time t

    a = constant depending on the segregation tendency

This relationship after expansion, rearrangement and integration yields:

$$\frac{X}{(1 + aX)} = \left[\frac{X_0}{1 + aX_0}\right] e^{-kt} \qquad (2.11)$$

where k = Elutriation constant
The authors however, were unable to correlate values of a and k with the characteristics of the bed and the model has not been developed.

Lewis et. al. [44] made an extensive study of entrainment from fluidised beds of glass beads, polystyrene, iron and cracking catalyst particles. Their work was restricted to single particle size solids fluidised by air at atmospheric conditions. They particularly wanted to investigate the effect of column diameter on elutriation rate. To interpret the results of their entrainment experiments dense phase effects were separated from disperse phase effects. As a result of plots of E/U_G vs. $1/U_G^2$, where E = Entrainment rate ($kgm^{-2}s^{-1}$), they proposed the equation:

$$E/U_G = C \exp (-b/U_G^2) \qquad (2.12)$$

where C = the value of E/U_G obtained by extrapolation of $1/U_G^2$ to zero in the plot of E/U_G vs. $1/U_G^2$,

    b = Negative slope of E/U_G vs. $1/U_g^2$ plot.

They went a step further by considering b as a function of U_G to give:

$$E/U_G = C \exp (-b_0 + AZ'U_G)/U_G^2 \qquad (2.13)$$

where $A = aU_G$, and a = Freeboard exponential coefficient in the equation $E \propto \exp (-aZ')$, where Z' = Distance above the bed surface.

Reference was also made to the effect of turbulence on the entrainment rate and motion of particles. The conclusion was reached that the mechanism by which upward moving solids in the freeboard reverse their direction is associated with the eddies generated in the turbulent flow field.

Hanesian and Rankell [28] studied elutriation from a multisize particle fluidised bed. The variables studied were particle size distribution and superficial fluidising velocity. By plotting C/C_0 against time and fitting a curve to the data, they came up with the fit:

$$C/C_0 = b \exp(-k_1 t) + (1-b)\exp(-k_2 t) \qquad (2.14)$$

where b is defined by $C/C_0 = b \exp(-k_1 t)$, i.e. b = value of the intercept in the plot of $Ln(C/C_0)$ vs. t.

This is really an extension of the equation by Leva with an additional term accounting for relatively coarse fractions. The rate constants k_1 and k_2 have dimensions of time^{-1} and were investigated relative to superficial fluidising velocity and particle size distribution. The ideal would be with this and other correlations involving rate constants that values of the constants could be found for any fluidised system. However, their variation with parameters such as gas velocity make this difficult.

Kunii and Levenspiel [35] postulate that there are three distinct phases in the freeboard:

1 Gas stream with completely dispersed solids. These solids are transported pneumatically with velocity V_1

2 Projected agglomerates moving upwards with velocity V_2

3 Descending agglomerates and parcels of thick dispersion moving downwards with velocity V_3

Using this model they were able to explain the exponential decay of entrainment with freeboard height. The empirical equation of Lewis et. al. [44] was modified to:

$$E/U_G = C \exp[-(b/U_G^2) + aZ'] \qquad (2.15)$$

It should be noted that this expression is for elutriation below the T.D.H., where the phenomenon is complex with many interacting variables. The understanding is far from satisfactory, and basic investigation of the structure of flow in the freeboard would help to clarify the situation.

Fournol et. al. [21] obtained experimental data from a 2ft diameter, 26ft high column with a bed of fresh cracking catalyst fluidised by air. They measured entrainment rates at points in the freeboard using isokinetic sampling techniques, and the existence of the transport disengaging height (Section 2.2.1) was confirmed. Both the elutriation rate and the entrained particle mean diameter were plotted against the inverse Froude Number $(Z'g/U_G^2)$ and trends discussed.

Guha et. al. [27] emphasise the idea of an equilibrium concentration of fines in the fluidised bed. Two empirical correlations were proposed, one for C_E the equilibrium fines concentration, and one for K the specific elutriation rate constant. Again, this work was done by setting each parameter as a function of several groups and fitting

them to experimental data. They investigated and discussed the effect of system parameters on elutriation.

Nazemi et. al. [53] measured the pressure drop in the freeboard region of a large scale fluidised bed, and used this to estimate the solids holdup. They found that the hold up increased with increased superficial fluidising velocity and decreased with increased freeboard height before remaining constant above the T.D.H.; Measurements of the pressure drop were taken radially, and at relatively large freeboard heights there was found to be little local variation. This indicated that the gas velocity and solids hold up were nearly constant over the cross section.

Tanaka et. al. [69] carried out experiments on continuous systems i.e. where the fines were returned to the bed. They found that the concentration of fines was kept at a constant value, C_s, throughout the bed except in the space near the overflow pipe. This may be similar to the equilibrium fines concentration correlated by Guha et. al. [27]. Dimensionless groups were introduced based on the physical properties of the bed material and the momemtum balance equations for a particle. They suggest that:

$$\frac{K}{\varrho_g (U_G - U_t)} = f\left[\frac{\varrho_s - \varrho_g}{\varrho_g}, \frac{gd_p}{(U_G - U_t)^{2}}^{-}, \frac{C_{d'} \varrho_g}{\varrho_s}, \right.$$

$$\left. \frac{d_p (U_G - U_t)\varrho_g}{\mu}, \frac{D_t}{d_p}\right] \qquad (2.16)$$

where C_d = Drag coefficient

D_t = Diameter of the vessel

They say that as C_d is a function of Reynolds Number it can be eliminated, and as D_t has no effect on the specific

elutriation constant D_t/d_p can be eliminated. Finally, from the correlation of the data it was found that $d_p U_t \rho_g/\mu$ was better than $d_p(U_G - U_t)\rho_g/\mu$ and this was used in the final form of the correlation. Hence, they got to the same basic form of correlation proposed by Wen and Hashinger [74]. The effect of system parameters on modified elutriation rate coefficients based on C_S was also investigated.

Merrick and Highley [49] did extensive work on a large pilot scale fluidised bed combustion plant. They developed a new form of correlation which gave good agreement with their results. An important point in their work was that they took bed hydrodynamics into consideration by introducing U_{MF} into the correlation. They comment that correlations of the form given by Wen and Hashinger [74] predict rate constants for a very small range of operating conditions, as well as for small diameter slugging beds. They finally concluded that the important factors affecting elutriation were (1) The particle terminal velocity, (2) The superficial fluidising velocity, (3) The minimum fluidising velocity and (4) The gas mass flow rate. Dimensional analysis isolated the following groups as being important:

$$E_i/G, \quad U_t/U_G, \quad (U_G - U_{MF})/U_{MF} \qquad (2.17)$$

where E_i = Specific Elutriation rate constant for particles of size i
G = Mass flow rate of gas.

They fitted coefficients to the groups above using experimental data to give the correlation:

$$E_i = 130 \, G \, \exp[-10.4(U_t/U_G)^{0.5}((U_{MF})(U_G - U_{MF}))^{0.25}] \qquad (2.18)$$

The value of the specific elutriation rate constant is

therefore dependent on the terminal velocity of the particle size fraction according to the above correlation.

Geldart et. al. [23] investigated the effect of fines in the dense phase on the elutriation of coarse particles. This effect exists in many practical systems and previous correlations did not take it into consideration. On the basis of data collected they proposed a simple correlation:

$$K/(\varrho_e U_G) = B \exp(-C(U_t/U_G)) \qquad (2.19)$$

where ϱ_e = Effective density of gas = $\varrho_g + \Sigma \varrho_i$, and ϱ_i = solids loading of ith size fraction in exit gas,
B and C = constants obtained from the plot of $K/(\varrho_e U_G)$ vs. U_t/U_G.

A procedure was outlined for predicting carry over based on the above equation and the summation of estimates for each size fraction.

Bachovchin et. al. [5] made measurements of elutriation from a fluidised bed of a mixture of two size fractions of non-elutriable sand and fines. The size distribution of the elutriated material was also measured. In addition, the effects of freeboard height and superficial fluidising velocity were investigated. They found that the choking velocity correlations based on pneumatic transport gave the best predictions of elutriation rates. They used a choking velocity correlation which was modified for surface concentration of fines, which compared reasonably well with their experimental data.

Colakyan et. al. [13] measured the elutriation of sand particles in a 0.9 * 0.9 m cross section bed with and without bed internals. They concluded that the specific elutriation rate constant could be correlated very well by a simple expression implying that elutriation above the

T.D.H. is a function of particle terminal velocity and superficial fluidising velocity. The expression was of the form:

$$K = C (1 - (U_t/U_G))^2 \qquad (2.20)$$

where C = Constant obtained from the plot of K vs. 1 - (U_t/U_G).

Lin et. al. [46] found that existing correlations could not predict the specific elutriation rate constant in their fluidised system. The bed was a sand and char mixture. The correlation that best fitted their data was of the form:

$$K/\varrho_g U_G = C ((U_G)^2/(gd_\rho))^{1.65} \qquad (2.21)$$

George and Grace [24] obtained measurements of entrainment in relatively large beds of silica sand. They found that the correlation which best fitted their data was the saturation carrying capacity correlation of Zenz and Weil [79]. A mechanistic manner of looking at entrainment was outlined based on the fraction of ejected particles that were carried over. Reference was made to the work of Horio et. al. [33], and it was stated that mechanistic models of particle motion and entrainment in gas/solid fluidised beds would have to account for the generation and decay of turbulence in the freeboard.

Wen and Chen [73] proposed a model of entrainment and elutriation. The entrainment model was based on the experimental evidence that below the T.D.H. entrainment decreased exponentially with freeboard height, and the total entrainment rate at the bed surface. It was assumed that, in the freeboard region, solid particles rise or fall depending on the size of the particle and the local gas velocity. Hence:

$$E = E_\infty + (E_0 - E_\infty) \exp(-aZ') \qquad (2.22)$$

where E_∞ = total elutriation rate of particles,
a = constant dependent on the fluidised system. It was recommended that a value of 4.0 be taken for a system in which no entrainment data was available,·
E_0 = Total entrainment rate of particles at the bed surface.

The entrainment rate at the bed surface was correlated with the excess gas velocity using available experimental data:

$$\frac{E_0}{Ad_e} = 3.07*10^{-9} \; \frac{\rho_g^{3.5} g^{0.5}}{\mu^{2.5}} (U_G - U_{MF})^{2.5} \qquad (2.23)$$

The fines specific elutriation rate constant was given by:

$$K = \rho_s (1 - \epsilon_i) U_{ri} \qquad (2.24)$$

where ϵ_i = Voidage in the freeboard for elutriation of single sized particles,
U_{ri} = Relative particle velocity $\approx (U_G - U_t)$.

ϵ_i may be obtained from a force balance on the wall of the vessel:

$$\epsilon_i = 1 + \left[\frac{\lambda'(U_G - U_t)^2}{2gD_t} \right]^{-0.213} \qquad (2.25)$$

where λ' = The friction coefficient due to the bouncing of the particles against the walls and each other. This is given by the following correlations:

$$\frac{\lambda' \rho_s \mu^{2.5}}{d_p^2 \rho_g} = \begin{array}{ll} 5.17 Re_p^{-1.5} D_t^2 & \text{for } Re_p \leqslant Re_{pc} \\ 12.3 Re_p^{-2.5} D_t^2 & \text{for } Re_p \geqslant Re_{pc} \end{array} \qquad (2.26)$$

22

where $Re_{pc} = 2.38/D_t$,

$$Re_p = \varrho_g(U_G - U_t)d_p/\mu.$$

It was found that the specific elutriation rate constant calculated by the above method predicted 80% of the published data to ±50%. It was suggested that this deviation was within experimental accuracy. It is interesting to note that the elutriation rate was found to be independent of bed hydrodynamics. The elutriation rate will therefore be independent of the presence of an immersed tube bank in the dense phase. The effect of an immersed tube bank on the structure of gas flow is presented in Chapters 5 and 6.

Matsumo et. al. [47] proposed a model assuming that the fine particles were transported by convection of gas only. The model included two parameters; one was a critical height above which the transport of fine particles was controlled by convection of the gas, and the other was the elutriation rate constant. The accumulated weight of fines elutriated from a small scale bed of two particle sizes of glass beads was obtained, and this information used to establish the elutriation rate constant.

2.2.3 Bubble Eruption and Solids Ejection

The first stage in the entrainment process is when solid particles are projected from the bed surface by erupting bubbles and become entrained in the gas flow. Mechanistic models of entrainment and elutriation are based on the initial conditions at the bed surface.

Andrews [4] developed equations which provided the basis for estimating catalyst entrainment in the freeboard region of a fluidised bed. He suggested that when the energy of an interparticle collision in the fluidised bed was equal to or greater than a threshold value, entrainment of one particle from the vessel occurred.

The origin of ejected particles has been investigated by a number of workers. Lewis et. al. [44] made an extensive study of entrainment from fluidised beds (Section 2.2.2). The origin of ejected particles was assumed to be from the bulge formed at the surface of the bed as a bubble approached. Their reason for this assumption was that it led to a prediction of entrainment rate strongly dependent on the bubbling properties of the bed such as bubble size and rise velocity. This was in fact found to be the case.

Leva and Wen [40] followed a procedure for estimating initial levels of entrainment from the bed surface by assuming that the origin of ejected particles was in the wake of the bubble. The rate of entrainment was found by multiplying the amount of solids per bubble by the number of bubbles per unit time. This procedure has been criticized because it overestimates entrainment in most practical systems.

Do et. al. [16] used photography in a 2-Dimensional fluidised bed to investigate the ejection velocity of particles, and used this as the boundary condition in the

equation of motion to predict the trajectories of particles in the freeboard. They assumed that the origin of ejected particles was the bulge formed at the surface of the bed when a bubble approached.

George and Grace [25] studied the entrainment of particles in the freeboard as a result of single bubbles erupting at the surface of a gently fluidised bed. A mechanistic model of entrainment was proposed based on the equation of motion of particles. This model will be described in Section 2.2.4. The initial experiments were designed to test whether ejected particles originated at the nose or from the wake of bursting bubbles. A layer of coke particles was placed on the surface of the fluidised bed, and the ejected particles collected by suction sampling. They found that, in all cases, irrespective of the weight of the coke layer, the weight fraction of coke particles collected per bubble was less than 3%. They concluded that the main source of ejected particles was the wake, with a small fraction from the bed surface. However, they did not take into account the drainage of particles from the bulge just before bubble eruption which may have transferred the surface layer away from the eruption site.

Chen and Saxena [9] developed a theory for solids projection rate from the surface of a gas fluidised bed as a first step in the analysis of the entrainment process. One of the assumptions made was that the origin of ejected particles was the bulge developed at the surface of the bed when a bubble approached. This was tested by extrapolating elutriation data to zero freeboard height.

Pemberton [60] presents a three phase model of entrainment based on the equation of motion of a particle. This model will be described in Section 2.2.4. He suggests a model for ejection of solids by bubbles as follows:

<u>1</u> Eruption of a single bubble and formation of a dome of particles.

<u>2</u> The drainage of these particles from the bubble's nose.

<u>3</u> The projection of material into the freeboard as the bubble finally bursts.

Furthermore, he suggests that at low bubble flow rates the ejection of particles from the dome predominates, whereas at high bubble flow rates, where coalescing bubble eruption predominates, the origin of ejected particles is the bubble wake.

To summarize the preceding section, there are basically two assumed origins of ejected particles:

<u>1</u> From the bulge formed at the surface of the bed when a bubble approachs. The workers who have supported this, with associated equations if any are:

Lewis et. al. [44]   ——

Do et. al. [16]   ——

Chen and Saxena [9]:

$$E'_0 = \left[\frac{(U_G - U_{MF})A}{4/3\pi R_{b1}{}^3}\right] \left[2\pi\left(\frac{R_{b1} + r_1}{2}\right)^2 (r_1 - R_{b1})\right.$$

$$\left. (1 - \epsilon_{MF})\varrho_s\right] \qquad (2.27)$$

where E'_0 = Entrainment rate at the bed suface (kgs^{-1})

R_{b1} = Bubble radius at the bed surface

r_1 = Distance between apex of bulge and bubble centre at the bed surface

ϵ_{MF} = Bed voidage at minimum fluidisation.

Pemberton [60], for low bubble flow rates:

$$E_0 = 3d_\rho(U_G - U_{MF})\varrho_s(1 - \epsilon_{MF})/d_e \qquad (2.28)$$

26

<u>2</u> From the wake of bursting bubbles. The workers who have supported this mechanism with the associated equations if any are:

Leva and Wen [40]:

$$E_0 = f_w \varrho_s (1 - \varepsilon_{MF})(U_G - U_{MF}) \qquad (2.29)$$

Where f_w = Fraction of bubble volume occupied by the wake.

George and Grace [25]:

$$M_0 = (1/2)\varrho_s (1 - \varepsilon_{MF})\zeta(U_G - U_{MF}) \qquad (2.30)$$

Where M_0 = Mass of solids ejected from the bed surface
ζ = Volume of particles ejected per unit bubble volume

Pemberton [60], for high bubble flow rates:

$$E_0 = 0.1 \varrho_s (1 - \varepsilon_{MF})(U_G - U_{MF}) \qquad (2.31)$$

The bubble eruption process has been investigated by various workers. Levy et. al. [43] studied the bubble eruption process in 2-Dimensional and 3-Dimensional fluidised beds containing glass beads, polystyrene particles and catalyst using a high speed video system. They gave the extent to which each mechanism occurred expressed as a percentage over a large number of observations. They concluded that there were four mechanisms:
<u>1</u> Bulge Burst, where the bulge layer stretches and moves upwards as the bubble approaches.
<u>2</u>/<u>3</u> Mid-Layer Burst and Wake Spike. When a pair of 3-Dimensional bubbles coalesce just below the free bed surface, the bulge material of the leading bubble is

thrown above the bed. As a result of the coalescence of the two bubbles, the layer of solids between the two bubbles combines with the leading bulge layer. The resulting particle cloud expands upwards and outwards. As the eruption process continues, the wake from the trailing bubble forms a spike which is projected above the bed surface, reaching a height in excess of that attained by the bulge and middle layers.

4 Jet Spray. When two or more bubbles coalesce at the bed surface a flow passage may develop between the two bubbles, allowing a jet of gas to form which entrains particles and carries them to relatively large distances above the bed.

They concluded that each mechanism contributes to the entrainment process, but only the first three occur often enough to be important. In addition, they recommend that, because of observed differences in behaviour between the 2-D and 3-D fluidised beds, research on bubble eruption behaviour and particle motion should be carried out in 3-D beds.

Hatano and Ishida [29] investigated entrainment from beds of glass beads using pictures taken in the freeboard and measurements by optical probes which detected bubbles and the velocity of particles ejected from the bed surface. They observed four mechanisms of particle ejection:

1 Isolated Bubble. The bed surface formed a bulge which was the origin of the ejected particles. The ejection velocity of particles was found to be relatively low and particles did not travel a significant distance. This mechanism is comparable to the bulge burst mechanism of Levy et. al. [43].

2 Successively Rising Bubbles. Particles in this case were projected relatively large distances into the freeboard. The entrainment mechanism was characterised by the fact that particles moved as swarms in the freeboard and were

not dispersed. Again, this mechanism is comparable to the bulge burst mechanism of Levy et. al. [43].

3 Coalescent Bubbles. Particles were projected still larger distances into the freeboard and were found to be dispersed more loosely than the particles associated with mechanisms 1 and 2 above. This mechanism is comparable to the mid-layer/wake spike mechanism of Levy et. al.

4 Successively Coalescent Bubbles. In this case the maximum initial velocity of particles was measured, and the particles were again loosely dispersed. This mechanism is comparable to the jet spray mechanism of Levy et. al. [43].

They concluded that, although the frequency of the third and fourth mechanisms was low they nevertheless gave the major contribution to entrained solids.

Hatano and Ishida [30] made similar measurements for a fluidised bed of FCC catalyst with small particle diameter. The bubble properties, particle ejection velocities and solids hold up were measured by optical probes. They found that behaviour was similar to that of the glass beads described above, and that the coalescence mechanisms were the major contributors to entrained solids. A bubble eruption model was proposed based on a normal distribution of distance between successive bubbles. A frequency of ejected particle swarms at any height above the bed surface was derived. Hatano et. al. [31] in a companion paper extended the bubble eruption model to predict the maximum rise height of particle swarms generated by bubble eruption and the entrainment rate below the T.D.H. Experimental values of the entrainment below the T.D.H. were measured by a simple collecting device and FCC catalyst, glass beads and sand particles were used. Probably because a value of the ratio of the voidage of the particle swarm to the bed voidage was set so that the theoretical values fitted the experimental values, the model did predict the effect of superficial

fluidising velocity and bed depth satisfactorally.

Baskakov [7] investigated the eruption of fine grain
material from a non-uniform fluidised bed by simulating
the semiellipsoids formed when bubbles coalesce at the
surface of a fluidised bed. Under this condition particles
will travel their maximum vertical distance because of
very high ejection velocities. The influence of system
parameters on the maximum vertical distance travelled
was investigated, and an empirical correlation presented
for the maximum particle ejection height.

Do et. al. [16] predicted particle trajectories based on
experimental ejection velocities and the equation of
motion for a single particle given below:

$$\frac{dV_z}{dt} = \frac{-3}{4} \frac{C_D \rho_g V_r |V_r|}{\rho_p d_p} - \frac{(\rho_s - \rho_g)g}{\rho_p} \qquad (2.32)$$

where C_D = Drag coefficient,
V_r = Particle velocity relative to the gas stream $\approx V_z - U_G$.

Two simplifying assumptions were made:
1 Because the particle Reynolds Number was low any
influence of turbulence could be neglected.
2 The gas velocity in the freeboard was uniform and equal
to the superficial fluidising velocity.
The validity of these assumptions is questionable in light
of experimental evidence presented in this work (Chapters
5 and 6).

George and Grace [25] used the equation of motion given
above as part of a mechanistic model of entrainment. This
model will be described in Section 2.2.4. A distribution of
ejection velocities was taken based on levels of
entrainment measured in the freeboard.

Peters et. al. [62] investigated the origin of ejected particles and the distribution of initial particle velocities experimentally using an image carrying fibre optic probe. The discussion was limited to cases in which surface coalescence of bubbles did not occur. It was shown that when a bubble bursts at the surface of the bed, particles are thrown along a spherical radius from the centre of the bubble. Making the simple assumption that the radial solids velocity was equal to the bubble rise velocity at the surface of the fluidised bed, solids velocities along the axial direction could be given by the following:

$$V_z = V_h \, Cos\theta' = U_a \, Cos\theta' \qquad (2.33)$$

where V_z = Particle ejection velocity vertically

V_h = Particle ejection velocity radially

θ' = Angle of ejection.

To partially verify the above equation the equation of motion, Equation (2.32) was used to predict the trajectory of a solid particle. Reasonable agreement was found between the trajectory predicted and that found experimentally.

Pemberton [60] within a mechanistic model of entrainment solved the equation of motion of a particle to predict the particle velocity at any freeboard height. He took into account the fact that not all the particles were ejected vertically therefore giving a distribution of initial vertical components of particle ejection velocity. The entrainment model will be described in Section 2.2.4.

2.2.4

Mechanistic Models for Entrainment and Elutriation in the Freeboard Space

The preceding section refers to published work on the ejection of particles by bursting bubbles. The entrainment of solids and its variation with height above the bed surface is very important. The work presented in subsequent chapters is related primarily to the structure of flow in the freeboard region of fluidised beds and the implications for particle motion. The information given will be related to some of the assumptions made in the mechanistic models referred to in this section.

Zenz and Weil [79] proposed a theoretical approach to particle entrainment through forces acting on the particles. It was assumed that particles were ejected into the freeboard at a velocity equal to the bubble rise velocity in the bed and were then acted on by constant gas velocity equal to the superficial fluidising velocity. The equation was solved for a particle and a stepwise procedure outlined to enable the calculation of an entrainment curve given by the summation of the entrainment of different size fractions. The current research gives valuable information on the gas flow field in which particles travel.

George and Grace [25] outline a mechanistic model for entrainment. The expression for initial mass flux of particles was given in Section 2.2.3. Expressions for gas velocity dissipation with distance were given based on jet dissipation theory. This was assumed to describe the gas velocity. Particle velocities were then calculated using the equation of motion for a particle, equation (2.32). The local concentration of particles of size d_{pi} having an initial ejection velocity V_{0j} was given by:

$$C_{ij} = E_0 x_i y_i / V_{ij} \qquad (2.34)$$

where x_i = Weight fraction of particles of size d_{pi},

y_i = Weight fraction of particles with ejection velocity V_{0j}

V_{ij} = Absolute upward velocity of particle of size d_{pi} with ejection velocity V_{0j}.

The overall concentration of particles at any level was given by:

$$C = \sum_i \sum_j C_{ij} \qquad (2.35)$$

Morooka et. al. [52] measured entrainment rate, hold up of solid particles and local velocities of particles in the freeboard of a small scale fluidised bed of FCC particles. The effect of superficial fluidising velocity was confirmed and the existence of particle downflow at the walls substantiated. Three regions were proposed:

1 Solid particles ascending with a velocity V_a and hold up ε_a in the central region of the freeboard, where the gas flow is unaffected by the solid boundary.

2 Solid particles descending in the central region described above.

3 Solid particles descending at the walls. This wall region usually takes up a relatively small part of the freeboard space but is important in terms of a mass balance of solids.

They suggested that a mechanism exists for transport of solid particles from the central region to the peripheral region near the wall where they descend.

Horio et. al. [33] presented a model for freeboard particle transport assuming that:

1 Particles are transported by gas turbulence which is not much affected by the presence of fine particles.

2 The freeboard is divided into a particle ascending zone

33

and a particle descending zone.

3 The fraction of area occupied by the particle descending
zone is much smaller than unity.

4 The motion of particles in the descending zone is more
stable than in the ascending zone. Transport of particles
from the decending zone to the ascending zone may be
neglected.

The equation of motion described in Section 2.2.3 was used
to predict particle velocity in the freeboard and mass
balances were made taking into account lateral transport
of particles in the turbulent gas flow field. The
mechanism was assumed to be turbulent diffusion, and the
diffusivity of particles, α_p, was given by:

$$\alpha_p \equiv (u')^2/f \qquad (2.36)$$

where f = Characteristic frequency of the gas velocity
fluctuations,
and u' = rms value of the fluctuations in velocity.

A mass transfer coefficient was defined as:

$$k_g = \alpha_p/l \qquad (2.37)$$

where l = the effective diffusion length.

An equation was obtained relating the volume fraction of
particles in the ascending zone, ε_{pa}, at freeboard height Z'
to the volume fraction of particles at an arbitrary
freeboard height $Z'=Z'_0$. After integration of the mass
balance equation the following equation was obtained (this
includes an expression for the decay of turbulence which
will be described in Section 2.3.3):

$$\varepsilon_{pa}/\varepsilon_{pa(Z'=Z_0')} = \exp \left[\; ((a'/l) \, V_a f_b) \; (u_{v0}'^2 d_e \, (1/Z' - 1/Z') \right.$$

$$\left. - 2u_{v0}' u_{v\infty}' d_e \, \ln(Z'/Z_0') - u_{v\infty}'^2 (Z'-Z_0')) \right] \qquad (2.38)$$

where a' = Specific interface area between the ascending and descending zones averaged over the cross section,

V_a = Particle velocity in ascending zone,

f_b = Bubble eruption frequency, which was assumed equivalent to the characteristic frequency of the gas velocity fluctuations,

u_{v0}' = Slope of the plot of u_z' vs. d_e/Z',

$u_{v\infty}'$ = Intercept of the plot of u_z' vs. d_e/Z' = intensity of fully developed turbulence.

It seems that the arbitrary freeboard height was set so that the predicted values matched up with those obtained by experiment. The expression is therefore of limited general use.

An estimate of the T.D.H. was made assuming that the turbulence intensity had decayed to a small percentage value. This is not consistent with the definition of the T.D.H. which is in terms of disengagement of the solid particles. However, the intensity of turbulence may dictate the rate of lateral transport of particles which may be one of the mechanisms of disengagement.

Pemberton [60] assumed that there were three phases in the freeboard region of a gas fluidised bed:

1 Ascending particles in the central zone where gas flow is unaffected by the walls.

2 Descending particles in the central zone.

3 Descending particles in the wall region where low gas velocity exists due to the influence of the wall.

The lateral movement of particles to the wall region in

the freeboard was was assumed to be an additional method of disengagement of particles, as well as the reversal of the vertical velocity. This phenomenon was modelled on turbulent diffusion, and an estimate of a particle mass transfer coefficient, k_g, was made as follows. An estimate of α_g the turbulent diffusion coefficient for the gas was obtained from an analytical expression given by Weinstock [72]:

$$\alpha_g = (((m - 1)/m)(\sqrt{\pi}/2)(u'/k_0) \tag{2.39}$$

where m = wave number power index for the turbulent energy spectrum,
k_0 = Characteristic wave number of energy containing eddies.
The particle turbulent diffusion coefficient was obtained from a relationship by Yuu et. al. [78]:

$$\alpha_g/\alpha_p = 1 + St/12 \tag{2.40}$$

where St = Particle Stokes Number = $\varrho_s d_p^2 U_z/18\mu D_t$.
The Stokes Number expresses the effect of particle inertia. The assumption was then made that the particle turbulent diffusion coefficient was related to a turbulent mass transfer coefficient by a turbulent Sherwood Number:

$$Sh = k_g D_t/\alpha_p \tag{2.41}$$

Assumptions were then made concerning m, k_0 and Sh. m was taken as 5/3 assuming a Kolmogoroff energy spectrum, k_0 was based on the estimate for pipe flow suggested by Brodkey [6]:

$$k_0 = 2/L \tag{2.42}$$

where L = Characteristic length of turbulence = radius in pipe flow.

In this case, as the turbulence is bubble induced the characteristic length of turbulence was taken as the bubble diameter. Therefore,

$$k_0 = 4/d_e \qquad (2.43)$$

The Sherwood Number was assumed to be 4 which is consistent with the diffusion path length model. An expression for k_g was therefore obtained:

$$k_g = \frac{\sqrt{\pi} \ u'_0 \ \exp(-\beta Z') \ d_e}{10 \ D_t \ (1 + St/12)} \qquad (2.44)$$

where β = Turbulent decay constant (Section 2.3.3).

One of the assumptions made was that turbulence was isotropic. This may not be the case in the light of evidence given in subsequent chapters. Mass balances were derived for each phase, and integrals obtained which expressed the concentration of particles expected at any height Z'. The equation of motion (2.32) was solved as particle velocity was contained in the integral mass balances. One of the assumptions made was that the gas velocity in the central region of the freeboard was constant and equal to the superficial fluidising velocity. Entrainment at the bed surface was estimated by expressions described in Section 2.2.3 and decay of turbulence was modelled by methods referred to in Section 2.3.3. The predictions of the model compared well with entrainment data obtained by isokinetic sampling. This method of sampling collected only particles in the ascending phase in the central region of the freeboard and it was assumed that particles were travelling upwards at their terminal velocity.

The T.D.H. was predicted assuming that:

$$\frac{E_{aOi} - E_{ai}}{E_{aOi} - E_{a\infty i}} = 0.99 \qquad (2.45)$$

where E_{aOi} = Initial particle flux in the ascending zone with particle diameter d_{pi},

E_{ai} = Freeboard particle flux in the ascending zone, particles of size d_{pi},

$E_{a\infty i}$ = Particle flux carried over, particle size d_{pi}.

The T.D.H. was calculated from the mass balance equations for freeboard hold up in the ascending zone.

2.2.5 Applications

The influence of the freeboard region in processes using fluidised beds must be taken into account, as a significant proportion of gas/solid contact occurs in this region.

Yates and Rowe [77] presented a model for reaction in the freeboard. The model was based on an entrainment fraction, which was assumed to be the fraction of wake solids ejected into the freeboard (Section 2.2.3). The freeboard was treated alternatively as a plug flow reactor in which the reactant gas had a fully developed turbulent profile and a well mixed reactor. Using data for a typical catalytic reactor the results of the model were presented for different values of the entrainment fraction and reaction rate constant. The fluidisation conditions that were considered were such that the fluidising velocity was many times the minimum fluidising velocity. The assumption of constant voidage in the freeboard region was therefore considered reasonable at large freeboard heights.

Ford et. al. [20] found that the freeboard region of an industrial scale catalytic regenerator played an important

role in the overall reaction. De Lasa and Grace [15] used the mechanistic model of entrainment developed by George and Grace (Section 2.2.4) to predict particle concentrations in the freeboard and integrate these into a model for reaction in a fluidised bed catalytic cracking regenerator. The model was based on different size fractions and it was possible to investigate the influence of each particle size on the overall coke conversion. The effect of solids feed rate and superficial gas velocity were also investigated.

2.3 Structure of Flow in the Freeboard

2.3.1 Introduction

Many assumptions have been made concerning the gas flow in the freeboard e.g. those of Wen and Hashinger [74] and Do et. al. [16]. Detailed measurements of the gas flow have only recently been made with the advent of techniques such as Hot Wire Anemometry and Laser Doppler Anemometry. The local properties of the gas flow in the freeboard have been investigated by a few workers. This information is referred to in the subsequent sections.

2.3.2 Velocity and Turbulence Profiles

Fournol et. al. [21] developed a hot wire probe to investigate the gas velocity profile above their fluidised bed. The superficial flow was 0.149 m s^{-1} which was $9.8*U_{MF}$ and the distance from the bed surface was 12 ft. A flat velocity profile was found characteristic of turbulent flow.

Levy and Lockwood [42] used a modified L.D.A. system to make measurements of gas velocity and turbulence intensity in the freeboard of fluidised beds of sand. Two grades of sand were used each of which was monosize. The fluidising velocities ranged from 0.65 to 1.17 m s^{-1}. It was found that the vertical component of velocity had a maximum at the walls and a minimum at the centre. Measurements of the fluctuating velocity expressed as the rms value of the fluctuations in the vertical component of velocity were also taken; this can be considered as the vertical component of the turbulent energy. It was found that the turbulence profile showed a maximum at the walls and a minimum at the centre of the cross section.

These findings were discussed with reference to the spatial distribution of bubbling (Section 2.1.3) and vortex ring motion caused by bursting bubbles. Information was presented on the gas and particle velocities near the bed surface after a bubble had burst for single bubble releases into an incipiently fluidised bed. Near the bed surface the gas velocity was found to reach a maximimum, later become negative because of falling particles and then reach the fluidising velocity after the sand had settled. By consideration of the gas and sand measurements away from the bubble axis a toroidal circulation created by a bursting bubble was deduced. Sand velocities were taken above freely bubbling fluidised beds and it was found that the distribution of velocities at relatively large freeboard height had two peaks, one for ascending particles and one for descending particles.

Levy [41] presented additional measurements of gas and sand velocities. These measurements gave similar profiles to those described above. The distances from the bed surface at which these measurements were taken were quite low. The development of the gas flow was therefore not fully investigated.

Pemberton and Davidson [61] used hot wire anemometry to make axial measurements of the turbulence intensities generated by single bubble releases from a stagnant liquid, an incipiently fluidised bed and freely bubbling fluidised beds. They used different theories to predict the decay of turbulence with increase in freeboard height. This will be described in Section 2.3.3. Measurements were not taken in the radial direction.

Pemberton [60] used isokinetic sampling to measure the entrainment rate above fluidised beds. To ensure that the velocity used for sampling was correct the axial vertical component of velocity was measured by a hot wire

anemometer. It was found that the measured velocity decreased with increase in freeboard height. The local vertical component of gas velocity was greater than the superficial fluidising velocity near the bed surface and of the same order of magnitude at large freeboard heights. These measurements were assumed to give the gas velocity in the central region of the freeboard, which was used in the three phase model of entrainment proposed (Section 2.2.4). Even though the local gas velocities radially were not taken these results suggest that no dip profile was evident in this system.

Horio et. al. [33] used hot wire anemometry to make measurements of velocity fluctuations in the vertical direction and velocity fluctuations in the horizontal direction above fluidised beds of glass ballotini beads. It was concluded that the fluctuations were bubble induced and increased with increasing superficial flow, increasing bed depth and decrease in particle size. The effect of freeboard height on turbulence was investigated and its decay empirically analysed. This will be reported in Section 2.3.3. There were no fines associated with the system and it was assumed that this did not affect the structure of flow. Particle velocities were measured by an optical probe and it was shown that particles fell in the region near the walls.

2.3.3 Decay of Turbulence

Horio et. al. [33] observed exponentially decaying turbulence from the measurements taken with a hot wire anemometer (Section 2.3.2). The average velocity fluctuation over the cross section was correlated with d_e/Z' and an empirical correlation proposed. This was based on the assumption that the decay of a pulsed jet, on which the gas leaving the bed was modelled, was

similar to the decay of a steady free jet.

Levy [41] fitted an exponential function to turbulence intensity/freeboard height data obtained by laser doppler anemometry (Section 2.3.2). It seems that no attempt was made to relate this to available theories.

Pemberton and Davidson [61] compared two theories to predict motion in the freeboard. Firstly, ghost bubbles are assumed to be generated at the surface of the bed and travel up through the bulk fluid decelerating due to entrainment of bulk fluid. Alternatively, assuming that turbulence is isotropic, a power law decay can be used to predict decay in the freeboard. When analysing the ghost bubble theory, it was assumed that the rise velocity of the ghost bubble was twice the rms fluctuating component of velocity obtained experimentally. Expressions were derived assuming that the circulation in the ghost bubble was laminar i.e. a vortex ring, or that the circulation was turbulent i.e. a puff. For a vortex ring the velocity should decay according to the the expression:

$$u = u_0 \exp(-\beta_1 Z') \qquad (2.46)$$

where u = Ghost bubble velocity,
u_0 = Initial ghost bubble velocity,
β_1 = Constant defining rate of decay.

For puff motion the velocity should decay according to the expression:

$$u/u_0 = (1 + (Z'/na_0))^{-3} \qquad (2.47)$$

where a_0 = Initial value of the ghost bubble radius,
n = Constant, assumed to be 4 which is applicable to buoyant puffs.

The expression for turbulent energy dissipation per unit mass given by Brodkey [6] for pipe flow was used to express the decay of isotropic turbulence. The assumption was made that the characteristic length of the turbulent flow field was the bubble diameter at the bed surface (Section 2.2.4). The resulting expression for the decay of turbulence with freeboard height was:

$$1/u' = 1/u'_0 + 2.45(Z'/U_G d_e) \qquad (2.48)$$

The initial velocity of the ghost bubble was estimated from the absolute rise velocity of bubbles (Section 2.1.2). Exponential decay was found best to represent the experimental data and β was determined by regression analysis.

2.3.4 Horizontal or Transverse Components

The only information available in the literature concerning horizontal or transverse components of velocity or turbulence is by Horio et. al. [33] who measured turbulence intensity in the horizontal direction. There does not appear to be any available data on horizontal components of velocity to the best of the authors knowledge, though Levy [41] discussed the possible importance of such phenomena in relation to the gas motion generated by bursting bubbles.

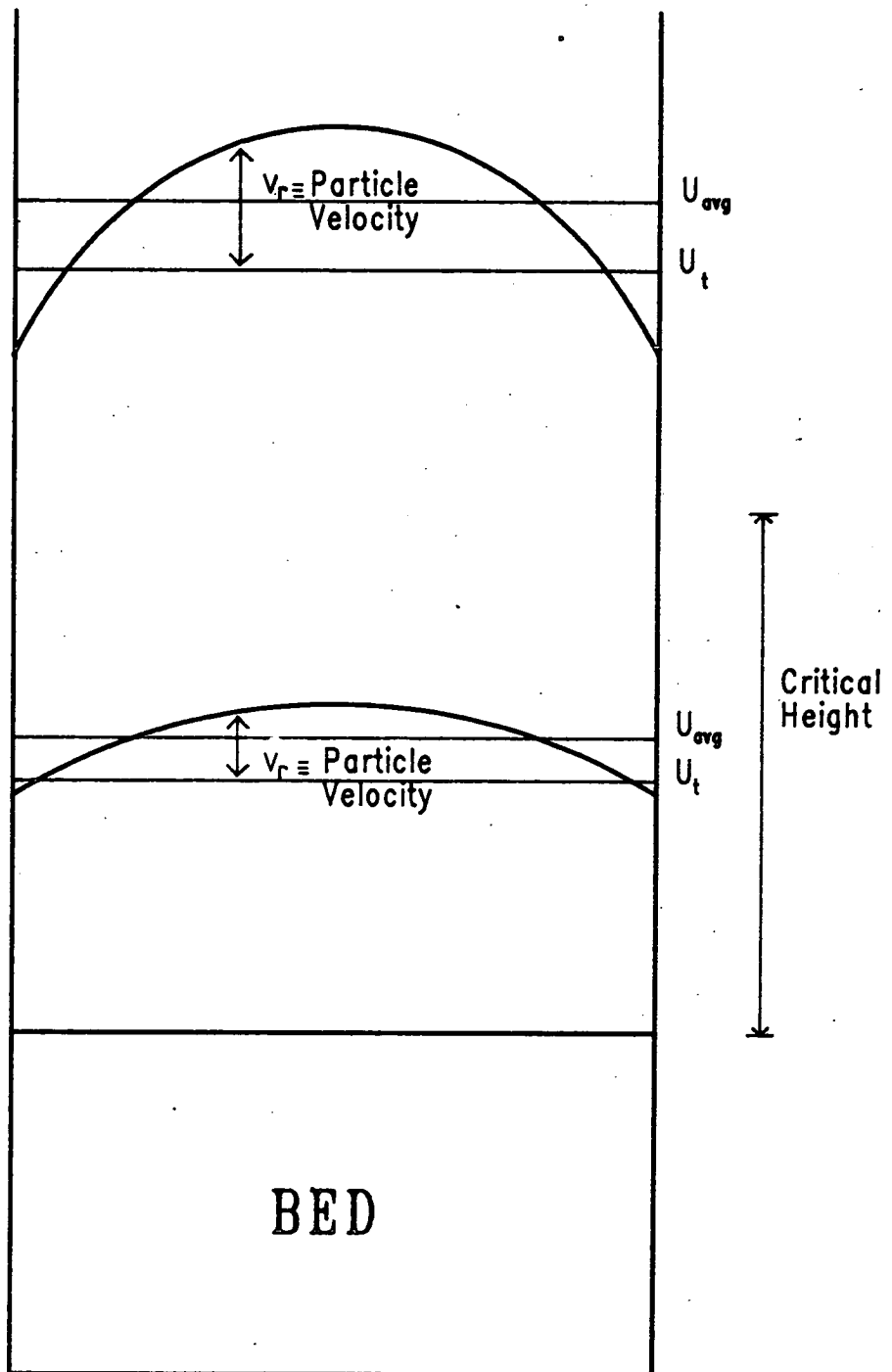Wen and Hashinger's Assumed Velocity Profile in Freeboard
of a Fluidised Bed.

$V_r \equiv$ Particle Velocity

U_{avg}

U_t

$V_r \equiv$ Particle Velocity

U_{avg}

U_t

Critical Height

BED

Figure 2.1

(From Wen and Hashinger (74))

Chapter 3
Laser Doppler Anemometry and Development

3.1 Introduction

Measurements of flow in the freeboard region of gas fluidised beds have been described in Section 2.3.2. The methods used included hot wire anemometry, high speed photography and optic probes. The use of Laser Doppler Anemometry ,(L.D.A.) has a number of advantages:

1 No disturbance to the flow
2 High degree of accuracy
3 Detection of direction of flow
4 Velocities can be measured in 3 dimensions.

Some experimental work has been done by Levy [41] and the results presented here will complement that work. The principles of L.D.A. are outlined in the first section. The signal processing technique used is described in the next section, based on the principles outlined previously. The development of signal processing to enable measurements of the gas flow to be made in the freeboard of fluidised beds where significant entrainment of bed material exists is then described. The selection of a suitable technique is discussed and the principle of its operation outlined. The use of Phase Modulation and its effect on the Doppler Signal are discussed in the final section. Detailed review of the L.D.A. technique is given by Durst et. al. [17] and Abbiss et. al. [1].

3.2 Laser Doppler Anemometry

3.2.1 The Doppler Effect

The principles of L.D.A. are given by Abbiss et. al. [1]. The frequency of the radiation scattered by an object moving relative to a radiating source is changed by an amount which depends on the velocity of the object and the scattering geometry (Figure 3.1).

If V is the particle velocity, the doppler shift is given by:

$$\Delta \upsilon = (k_s - k_0) V \qquad (3.1)$$

where k_0 = Incident wave vector = $2\pi/\lambda$, and λ = Wavelength of incident light.
k_s = Scattered wave vector.

The accuracy of this frequency measurement is not very good, and the optical geometry is difficult. The disadvantages have encouraged the development of units crossing two incident beams of the same colour. The source of the radiation is a laser beam which is split and then focused to a point. The difference of the two doppler shifted frequencies can be measured. The schematic arrangement is shown in Figure 3.2:

$$\Delta \upsilon_1 = (k_s - k_{01}) V$$

and

$$\Delta \upsilon_2 = (k_s - k_{02}) V$$

where k_{01} and k_{02} = Incident wave vectors.

Therefore $\quad \Delta \upsilon_1 - \Delta \upsilon_2 = (k_{02} - k_{01}) V = K_0 . V$

But $\qquad |k_{01}| = |k_{02}| = 2\pi/\lambda$, so

$$|K_0| = |(k_{02} - k_{01})| = (2 \, \text{Sin} \, \theta/2) \, 2\pi/\lambda$$

and $\qquad \Delta\upsilon_1 - \Delta\upsilon_2 = (4\pi U_z/\lambda) \, \text{Sin} \, \theta/2$

where U_z = the component of V in the direction of K_0.

Or $\qquad \Delta f = 2U_z \, \text{Sin}(\theta/2)/\lambda \qquad\qquad (3.2)$

The change in frequency measured using two incident beams is independent of the angle at which the scattered radiation is collected. The system is therefore more flexible than a velocimeter using single beam optics and the scattering direction can be chosen to met particular requirements. The equipment used in this study was a Spectra Physics He/Ne 15 mW Laser and Malvern Instruments Optics Unit RF 340M. The latter consists of an offset prism, phase modulator (the operation of this equipment will be described in Section 3.5) and a focussing lens. The scattered radiation was detected by a photomultiplier, Malvern Instruments type RF 313. The optical arrangement used is termed the Doppler Difference System.

3.2.2 Fringe Model for Laser Doppler Signals

This is an alternative way of analysing the scatttered radiation, first proposed by Rudd [66]. Two coherent coherent light beams having plane wave fronts, as would be present in the waist region of two Gaussian light beams, intersect having been focused by a lens. The properties of laser light and the crossover point will be discussed in more detail in Section 3.2.3. A pattern of plane interference fringes is formed. This can be confirmed by projecting the image at the crossover point

on to a screen using a short focal length lens. The fringe spacing is given by:

$$s = \lambda/(2 \, Sin(\theta/2)) \qquad (3.3)$$

A particle crossing this fringe pattern will scatter light whose intensity will vary according to the variations in light intensity at the cross over point. The frequency of this scattered radiation will be:

$$\Delta f' = U_z/s$$

$$= 2U_z \, Sin(\theta/2)/\lambda$$

$$= \text{Equation (3.2)}$$

The fringe model is very useful as a visual representation and can be used to explain several features of Laser Doppler Signals.

3.2.3

Characteristics of Laser Beams and the Measurement Control Volume (M.C.V)

In the preceding section reference was made to the properties of laser beams when describing the fringe pattern set up when two laser beams are focused to a point. In this section the properties of laser beams and the cross over point or Measurement Control Volume are described. In addition, the information given explains the importance of the optical arrangement e.g. the focal length of the lens, in relation to the characteristics of the M.C.V.

The laser operates in the lowest order transverse mode (TEM$_{ooq}$). The beam has a Gaussian intensity profile and hyperbolic beam contour. A schematic diagram of the beam

profile is given in Figure 3.3. At the beam waist, where the diameter is a minimum, the wave front is planar. At a distance z from the waist, the beam radius, defined as the radial distance to the e^{-2} (0.135) intensity point, is given by:

$$(r_{(z)})^2 = r_0^2 \, 1 + ((\lambda z)/(\pi r_0^2))^2 \qquad (3.4)$$

where r_0 = Radius at beam waist.

The divergence of the waist ϕ is defined as the angle between the axis and the hyperbolic asymptotes (Figure 3.3). It can be shown that:

$$\phi = \lambda/\pi r_0 \qquad (3.5)$$

The Radius of Curvature of the wavefront at distance z is given by:

$$R(z) = z[1 + (\pi r_0^2/\lambda z)^2]^2 \qquad (3.6)$$

For the Spectra Physics model 124B Helium Neon Laser, r_0, the radius at the $1/e^2$ intensity points is 0.55 mm and the beam divergance is 0.75 mrad.

When two beams of the above characteristics are focused to a point by a lens a fringe pattern is formed. A typical pattern is shown in Figure 3.4. The fringe spacing assuming that the beams cross at or near their waists is given by Equation 3.3. Therefore for the Helium - Neon laser used in this work, with the following characteristics:

    Wavelength, λ, = 632.8 nm
    Beam separation at focusing lens = 20 mm
    Focal length of lens = 50 cm

the Fringe Spacing, s, is 15.82 μm.

Using the $1/e^2$ peak intensity points to define its boundaries the measurement control volume is ellipsoidal in shape and can be visualised as a set of parallel fringes in space in a plane perpendicular to the plane of the focused laser beams.

3.3 Photon Correlation Signal Processing

The photomultiplier used was a Malvern Instruments type RF313; the tube operates at a voltage of -1650 Volts. Durst et. al. [17] describe the characteristics of an electrical signal obtained from scattered radiation. The signal from a particle contains a low frequency element corresponding to the passage of particles through the laser beams and a high frequency element corresponding to the velocity of particles passing through the M.C.V. observed by the photomultiplier. The laser doppler signal is made up of contributions from the individual photoelectrons emitted when a photon is absorbed on the photomultiplier tube followed by secondary emission amplification in the dynode chain of the photomultiplier. The output from the photomultiplier is amplified and fed to a comparator where the signal is compared to a preset threshold level. The output from the comparator is a clean pulse for each photo-detection event. When a scattering particle crosses a bright fringe in the M.C.V., there will be a greater probability of photon detection and the density of the pulses in the pulse train is greater. The period of the intensity variations is related to the particle velocity and can be found by performing an autocorrelation procedure on the pulse train. The autocorrelation function is defined mathematically as follows:

$$G(\tau) = \langle\ n(t,T)\ n(t+\tau,T)\ \rangle \qquad (3.7)$$

Where τ = Correlation delay,

T = Sample time set in the correlator.

n(t,T) = Number of pulses counted during sample time at time t.

The pulse train is processed in a Multibit Correlator, Malvern Instuments type K7025. The correlator gives an approximation to the autocorrelation function as follows.

53

A schematic diagram of the hardware is given in Figure 3.5. During every sample time period the number of pulses applied to the input of the correlator is counted by a 4 bit counter. This value is entered into the first stage of the shift register, and values previously in the shift register are shifted up one stage. In addition, during every sample time period the number of pulses applied to the input is multiplied by the values in each stage of the shift register. Associated with each multiplier is a 4 bit adder with a carry bit. Each carry is counted into a 24 bit memory corresponding to a correlator channel. After a time the contents of the jth correlator channel will be:

$$G(j\Delta\tau) = \sum_{i=1}^{N} n_i n_{i-j} \qquad (3.8)$$

Where n_i represents the number of times the contents n_{i-j} of the jth stage of the shift register was added into the jth channel memory.

As the number of samples N grows large the approximation becomes exact.

The a.c.f. is made up of contributions from a series of signals obtained from many particles to provide information on the average particle velocity and the statistical properties of the velocity fluctuations. When experiments are run in this way the a.c.f. is characterised by a sinusoidal fluctuation with decaying amplitude. The a.c.f. sits on a base line which represents the detection of photons from stray light sources whose arrival times are uncorrelated with those from the scattering particles. A typical a.c.f is given in Figure 3.6.

The data in the a.c.f. is input to a microcomputer, the Malvern Data Processor type MDP 7025, which is based on the Commodore P.E.T. 2001-32N computer. The software package contains an algorithm which tests the a.c.f. for turning points and as a result the period is calculated.

The turbulence is calculated from the decay in amplitude of the turning points.

The velocity is obtained from the expression derived from the fringe model of the scattered radiation (Section 3.2.2):

$$U_1 = s/t_{av}$$

Where t_{av} = Average of the time of each turning point.

Two independent estimates of turbulence can be made using the information of the turning points (Figure 3.6):

$$u''_{12} = \frac{1}{\pi} \frac{2}{3} \ln\left[\frac{a_1 - (g_1 - a'_0)}{(g_2 - a'_0) - a_1}\right] \qquad (3.9)$$

$$u''_{23} = \frac{1}{\pi} \frac{2}{5} \ln\left[\frac{(g_2 - a'_0) - a_1}{(a_1 - (g_3 - a'_0)}\right] \qquad (3.10)$$

where a'_0 = Amplitude of coefficient which represents uncorrelated data,

a_1 = Beam profile coefficient.

a'_0 is obtained from the monitor channels of the correlator as follows:

$$a'_0 = AI/(16 * TS)$$

where AI = Total number of input pulses to input A (Figure 3.5),

TS = Total number of samples.

The value of a_1, the beam profile coefficient, is unknown and is determined by an iterative procedure such that the estimates of turbulence described above differ by less than 0.0001.

The true velocity estimate is then given by the following equation using the turbulence estimate above:

$$U_2 = U_1[1 - (u'')^2 - 1/(m_1^2 N_\sigma^2 \pi^2 (1 + m_1^2/2)] \qquad (3.11)$$

where m_1 = Fringe visibility, and is given from the a.c.f. by:

$$m_1 = 2(g_2 - g_1)/(g_2 - g_1 - 2a_0)$$

and, N_σ = Number of fringes in beam diameter.

The above formulae are based on the assumption that the distribution of velocities in the turbulent flow field is Gaussian. There is some disagreement on this assumption, which is discussed in Durst et. al. [17], but it is felt that in this case the model gives realistic results for the mean velocity and turbulence estimates.

The advantage of the Photon Correlation Technique is that it is extremely sensitive as individual photons are counted. This is important in gas flows where seeding is usually necessary. The technique does not need a continuous signal which proved to be an advantage when developing signal processing in two phase flows (Section 3.4.3).

3.4 Development of Signal Processing for Two Phase Flows

3.4.1 Outline of Flow Sytems

Work was initially done in a single phase flow above beds of glass ballotini beads fluidised by air. The gas flow in many cases has to be seeded with very fine particles to give a transmitted doppler signal. However, it was found that the scattering centres associated with the gas flow were sufficient to give a processable signal by photon correlation. In the large bed, the material used was a round sand, the physical properties of which are given in Chapter 4. At the superficial fluidising velocities used in this work significant entrainment of particles of sand to large freeboard heights was evident. Scattered radiation was therefore received from scattering centres associated with the gas phase as described above and also from entrained bed material. It was felt that the velocity distribution of the sand particles was unlikely to be the same as the velocity distribution of the gas phase. This prompted the development of the existing L.D.A. system to discriminate between the signals received from the gas phase and the solid phase.

There were two methods considered to overcome the problem of discriminating between the two phases.
1 Obtaining a Power Spectrum of the autocorrelation function obtained from the signals given by both phases over a period of time.
2 Discrimination between the signals obtained from each phase based on a threshold photon count rate.
These methods will be discussed in the subsequent sections.

3.4.2 Fourier Transforms of Autocorrelation Functions

It is known that the autocorrelation function and the power spectrum are a Fourier Transform pair [1]. This is expressed mathematically below:

$$P(\omega) = 2/\pi \int G(\tau) \, Cos\omega\tau \, d\tau \qquad (3.12)$$

The Power Spectrum, $P(\omega)$, is a function of frequency and provides means of frequency analysis. It expresses the fraction of energy of radiation in the doppler signal which lies between frequencies ω and $\omega + d\omega$.

The Discrete Fourier Transform of a sequence of N real data values, (in this case the contents of the correlator channels making up the a.c.f.) F(O), F(1),............F(N-1) is given by Steiglitz [67]:

$$F^*(k) = \sum_{n=0}^{N-1} F(n) \, exp(-jnk2\pi/N) \qquad k=0,1,......,N-1 \qquad (3.13)$$

Expanding,

$$F^*(k) = \sum_{n=0}^{N-1} F(n)[\, Cos(2\pi nk/N) - j\, Sin(2\pi nk/N)] \qquad (3.14)$$

Consider the value of $F^*(N - k)$,

$$F^*(N - k) = \sum_{n=0}^{N-1} F(n)[\, Cos(2\pi n(N-k)/N) - j\, Sin(2\pi n(N-k)/N)]$$

But $Cos(2\pi n(N-k)/N) = Cos(2\pi n - 2\pi nk/N)$

$$= Cos(2\pi nk/N)$$

and $\qquad -j\, Sin(2\pi n(N-k)/N = -j\, Sin(2\pi n - 2\pi nk/N)$

$$= -j\, (-Sin\, (2\pi nk/N)$$

$$= j\, Sin(2\pi nk/N)$$

Therefore,

$$F^{*}(N-k) = \sum_{n=0}^{N-1} F(n)[\ \text{Cos}(2\pi nk/N) + j\ \text{Sin}(2\pi nk/N)] \qquad (3.15)$$

From the derivation above of the component of the Power Spectrum, $F^{*}(N-k)$, it is shown that the component is a complex conjugate with the component $F^{*}(k)$ (Equation 3.14). This is true for any value of k, and the Discrete Fourier Transform will therefore give a series of complex conjugates about the data point k=N/2. Furthermore, from Equation 3.14 it is shown that the Fourier Cosine Transform is given by the real part of the Discrete Fourier Transform.

This technique was used for some measurements in the small bed fluidising round sand. The bed was freely bubbling, and the superficial fluidising velocity was 0.09 m s^{-1}. Under these conditions significant entrainment of bed material occurred. Radiation was scattered from the gas phase and also from the particles of bed material. The autocorrelation function of this signal was not periodic in nature (Figure 3.6) and could not therefore be analysed by the data processor available.

The data from the a.c.f. was used as input to a Discrete Fourier Transform package from the Nag Fortran Library. The real part of the transform gave the Power Spectrum as shown above. From the initial experiments carried out it seemed that the high intensity scattered light from the particles of bed material was dominating the autocorrelation function and consequently the power spectrum. An attempt was therefore made to artificially "seed" the gas flow. This was done by adding Lycopodium Powder to the bed fill which presumably followed the gas flow after the bed was fluidised. Autocorrelations were taken of the signals from this flow system and used as input to the Discrete Fourier Transform routine described above. It was found that the real part of the transform

i.e. the power spectrum had two peaks, indicating that there were two dominant frequencies. A power spectrum obtained under the conditions described above is given in Figure 3.6. The general shape of the transform is symmetrical about the k=N/2 data point as expected from the expansion of the Discrete Fourier Transform given previously. In addition, the two peaks are clearly defined. From this figure it is possible to estimate the dominant frequencies of the signal from the photomultiplier.

The frequency is given by:

$$f = k/N\Delta t \qquad (3.16)$$

Where Δt = The time difference between data points in the a.c.f.,

        = Sample time set

        = T (under these conditions the sample time was 1.5µs).

N = Number of the data point.

The peaks in the power spectrum occur at (1) k≈2 and (2) k≈6.5. Using equation 3.16 the corresponding frequencies are (1) 2.083 kHz and (2) 6.875 kHz. These are the dominant frequencies of the signal given by the photomultiplier and correspond to the characteristic Doppler Frequencies given by particles passing through the measurement control volume at the intersection of the two laser beams. Using the Fringe Model (Section (3.2.2) equation (3.2)) the characteristic velocities may be estimated. (The Fringe spacing was 15.82 µm), therefore:

(1) For a doppler frequency of 2.083 kHz, velocity = 0.033 ms^{-1}

(2) For a doppler frequency of 6.785 kHz, velocity = 0.108 ms^{-1}

Presumably the reason for the Power Spectrum having two peaks is that the gas and sand phase have different mean velocities. The results indicate that the sand phase has a mean velocity of 0.033 ms^{-1} and the gas phase has a mean velocity of 0.108 ms^{-1}. In addition, Figure 3.6 shows that the spread of the "gas" peak is greater than the spread of the "sand" peak. The reason for this may be that velocity fluctuations were not induced in the solid particles because of their size and the characteristics of the turbulent gas flow (Section 7.2).

It is possible therefore to use this technique to obtain estimates of velocities in flows that have a gas phase and a solid phase. However, two major problems arose:

1 The gas phase had to be seeded to give the signal obtained from it reasonable strength. It was found that this was a major problem in a fluidised bed. The method described above of seeding by adding seeding material to the bed fill was itself not entirely satisfactory as the length of the experiment duration was limited, and the properties of the fluidised bed may have been affected by the presence of the seeding material.

2 The resulting power spectrum did not suit the data processing facility available. Accurate results for mean velocity would have been difficult to measure, and results for turbulence would have required substantial development.

An alternative technique was therefore developed.

3.4.3 Threshold Photon Count Rate

This technique of discriminating between the gas phase and the solid phase is based on the much higher photon count rate associated with the scattered radiation from a solid particle compared to the photon count rate associated with scattered radiation from the gas phase.

This in turn means that there will be higher pulse rates in the pulse train from the photomultiplier. This was investigated using an oscilloscope, and bursts of high pulse rate were detected when a sand particle passed through the measurement control volume.

A similar flow system was investigated in some detail by Levy [41] and it was found that the pedestal amplitude of the solid phase was many times more than the pedestal amplitude of the gas phase. Agarwal and Johnson [3] say that as a general rule, a particle's ability to scatter light increases with its diameter and its refractive index. The increase in intensity of scattered light with particle diameter has been used as the basis for particle size measurement which may be carried out simultaneously with particle velocity measurement. Ogden and Stock [55] optimized the angle at which scattered radiation was received so that there was a nearly linear relationship between scattered light intensity and particle size. The possibility of particle size measurement · was not investigated in this work, though it may be possible to develop the system to investigate particle size distribution. However, extensive studies of the scattered radiation from the particles used would be necessary.

A device was developed in co-operation with the Wolfson Microelectronics Institute at Edinburgh University which would sum the pulse rate over a period of time, and if this rate was greater than a preset threshold the device would switch off the pulse train to the correlator. A block diagram, Figure 3.8, is given to show the main parts of the unit. Calibration was initially carried out to determine the threshold count rate. The unit was tested in single phase gas flow and the rate found at which the gas phase signal did not quite trigger the unit. In two phase flow therefore triggering of the device would imply that a sand particle had passed through the M.C.V.

<u>1</u> Rate Detector: The input from the photomultiplier is branched, one branch going to the rate detector. In this section pulses charge up an integrating capacitor at a rate determined by the calibration threshold rate. The value of the capacitance is important as it determines the integration time. The threshold will be an average rate over this integration time. For example, the threshold rate was 3 pulses per μs over an integration time of 100 μs for two phase flow in the freeboard above fluidised beds of round sand. If a higher average pulse rate is detected over the integration time the capacitor will discharge and a semiconductor gate triggers an integrated circuit.

<u>2</u> Delay Timer: In this section of the unit a delay timer is included to cut off the signal for a predetermined time. This was found to be necessary to avoid the device switching on because of the relatively low pulse rates that exist even in a pulse train associated with a solid particle. The output is actually switched off by a logic gate and the "switch off" logic was maintained for a delay time which was set at 440 μs. Also included is a retrigger oscillator which will maintain the "switch off" logic if rate above threshold is detected within the delay time.

<u>3</u> Delay Line: The other input branch passes the pulse train through a delay line. This is a digital memory around which information is clocked. The delay time has to be longer than the time taken for the capacitor to discharge having detected rate over threshold and the trigger to be activated. The output line from the delay line is then shut. This part of the device is designed to ensure that pulses from high rate signals are not input to the correlator in the time it takes for the rate detector to operate. The delay time was 200 μs.

The unit was also fitted with an event counter which gives an output pulse every time the device is triggered. This gives a facility for counting the number of solid particles passing through the M.C.V. over a period of time. A counter was built based on a universal counter integrated circuit with four L.E.D. displays which could batch count the number of times the device switched off.

The Pulse Rate Discriminator could be operated in high cut mode, in which rates over threshold switched the unit off or high pass mode where rates over threshold were passed through. The signals passed in this mode of operation could be assumed to be from solid particles, and a limited number of runs were done with the unit in this mode. However, most runs were taken with the device in high cut mode giving information on the structure of the gas flow which was the primary objective.

3.5 Phase Modulation

A Malvern Instruments type K9023 Phase Modulator was contained in the optics unit. The phase modulator contains an Electro-optic crystal through which the two laser beams pass after being split in the beam splitting prism. By application of a sawtooth voltage to the Electro-optic crystal the phase of one outgoing beam is advanced whilst the phase of the other beam is retarded. The fringes at the cross over point will as a result move linearly in space at the frequency of the sawtooth voltage applied to the crystal.

The phase modulator can be operated in two modes from the drive unit, these modes are called Drive and Invert. Changing the mode changes the direction in which the fringe pattern is driven. The movement of the fringes may be in the same direction as the flow or against the flow. The result is to decrease or increase the apparent frequency of the a.c.f., and hence enable the directional sense of the flow to be resolved. Phase modulation is also used when the turbulence intensity is high and the a.c.f. obtained with a stationary fringe pattern is heavily damped. The apparent turbulence is decreased when phase modulation is used and the true turbulence is given by:

$$Turb_t = Turb_{app} * U/(U - U_c) \qquad (3.17)$$

where $Turb_t$ = True turbulence estimate,
$Turb_{app}$ = Turbulence estimate from the a.c.f.,
U = Velocity estimate obtained from the a.c.f.,
U_c = Velocity equivalent of the modulator frequency.

Phase Modulation was used in this work for both vertical and horizontal components of velocity, and valuable information was obtained on the directional sense. When used for horizontal components of velocity the phase modulation frequency was large relative to the

65

mean doppler frequency of the velocity component, and the interpretation of the results was in terms of a dominant direction. This however, will be discussed in more detail in Chapter 6.

In addition, phase modulation was used in the initial stages to artificially produce doppler signals that could be used to test the operation of the L.D.A. system. The beams were crossed over in open space and the phase modulator used to move the fringes in space. Particles suspended in the space gave a doppler signal as a result of the moving fringes. This was found to be useful when primary alignment of the L.D.A. was necessary.

Single and Dual Beam Laser Doppler Anemometer Vector
Diagrams.
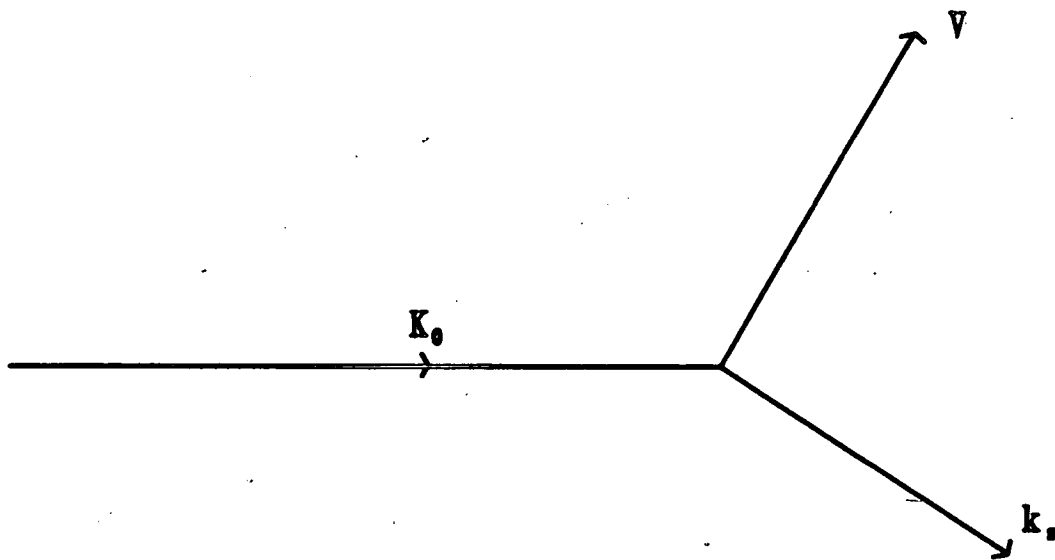
Figure 3.1
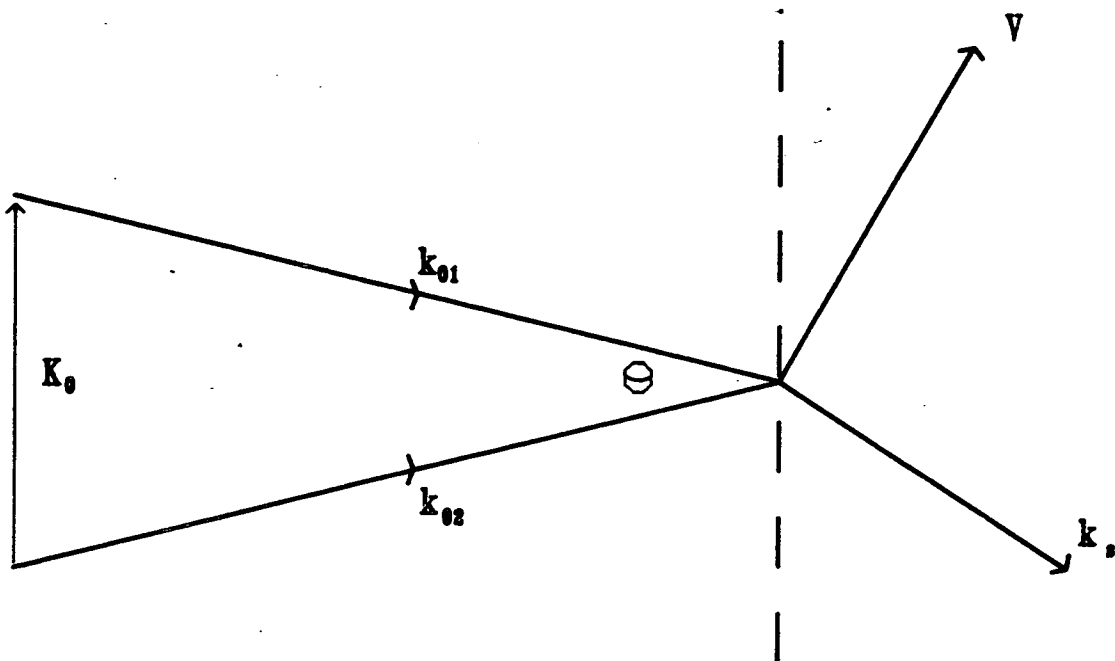
Figure 3.2

Waist and Divergence of Laser Beam.
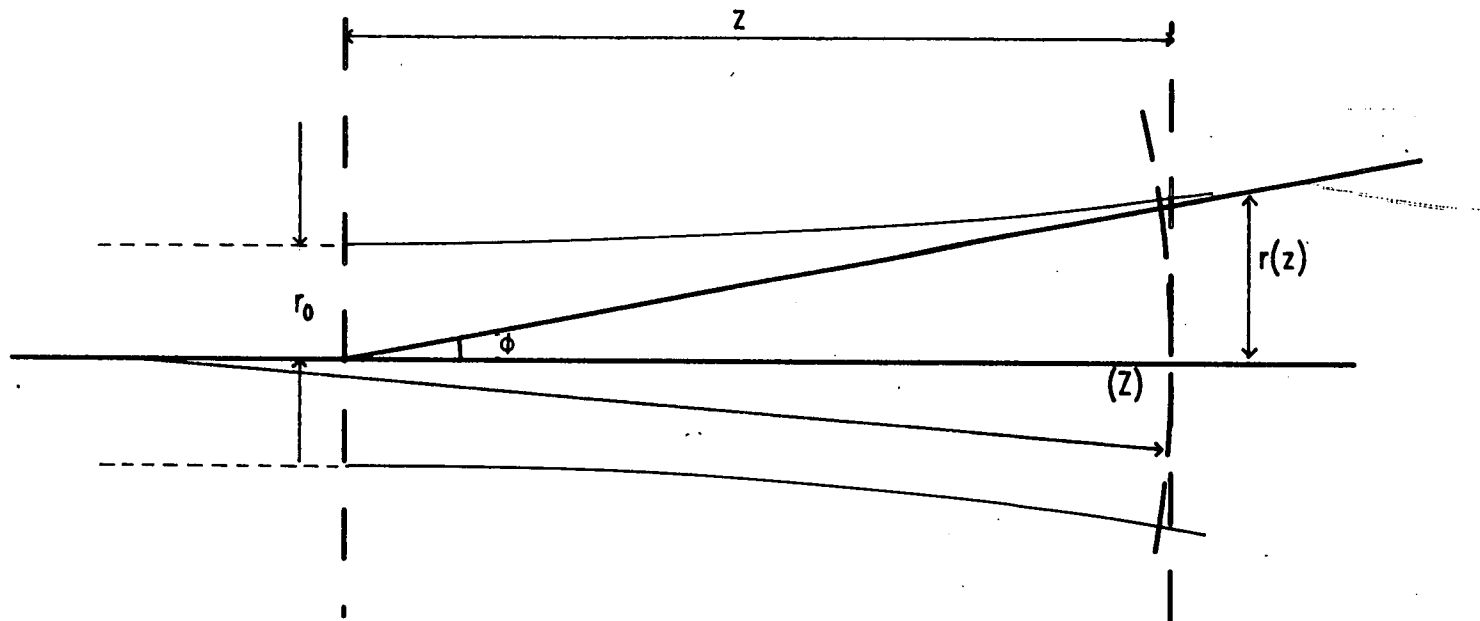
Figure 3.3

Fringe System Formed at Intersection of Two Laser Beams.
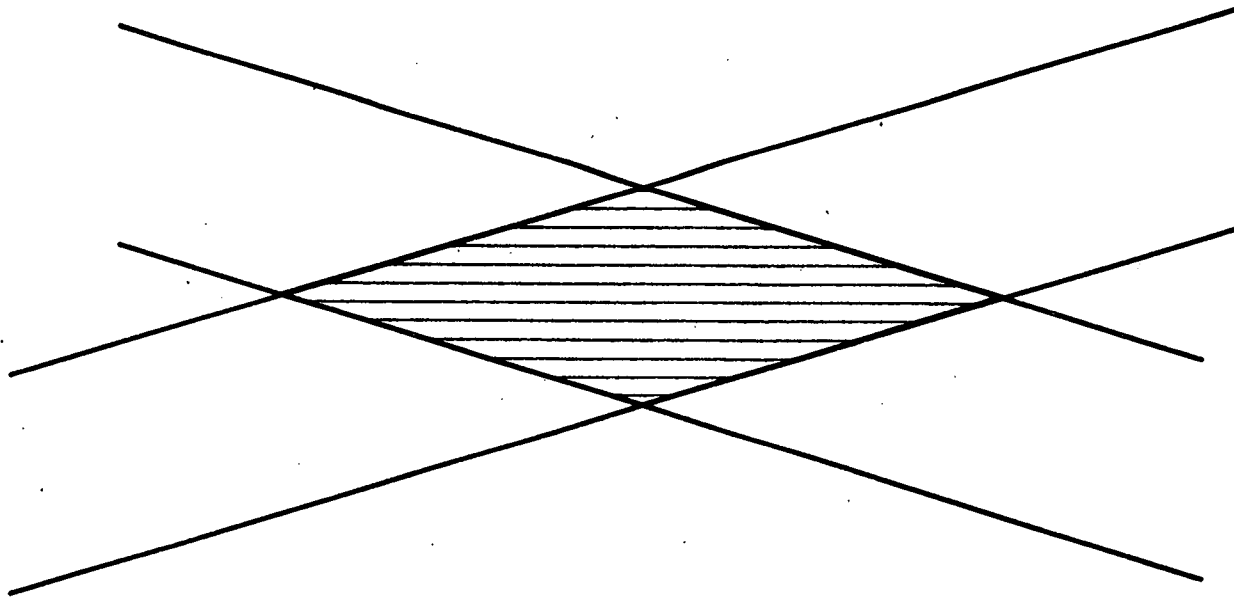
Figure 3.4

Signal Correlator - Schematic Diagram.
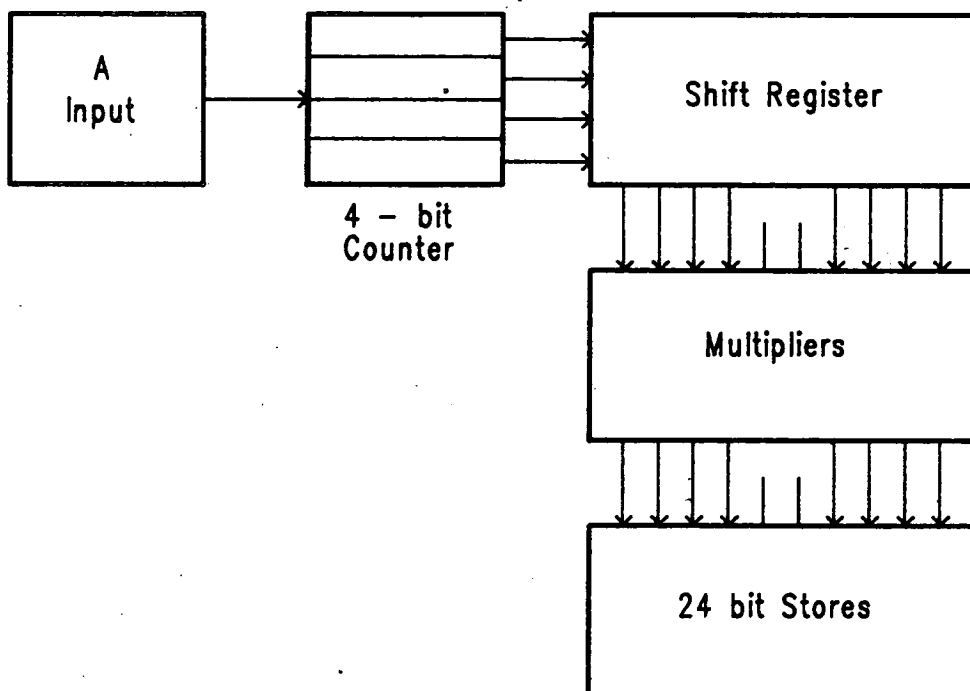
Figure 3.5

Typical Autocorrelation Function.
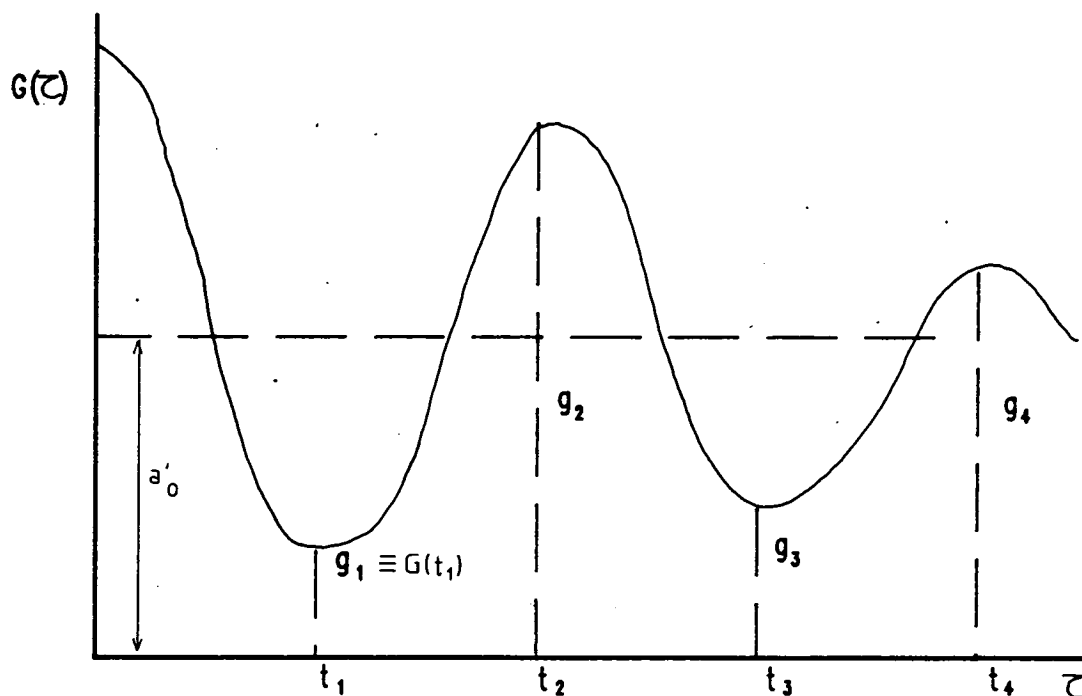
Figure 3.6

Figure 3.7

Power Spectrum of Autocorrelation Function of L.D.A. Signal from a Seeded Gas Flow containing Large Particles.
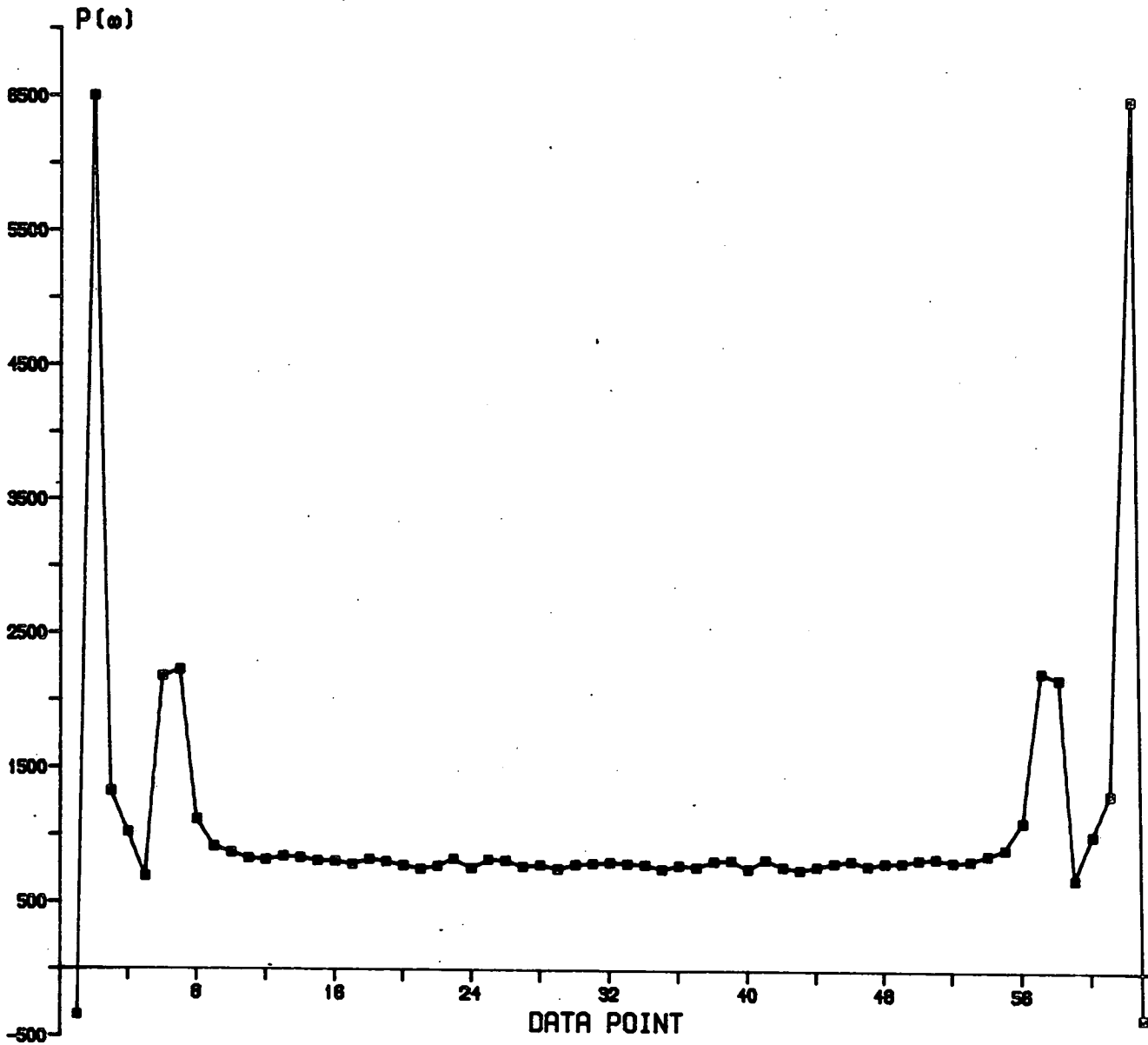
Block Diagram of Pulse Rate Discriminator.
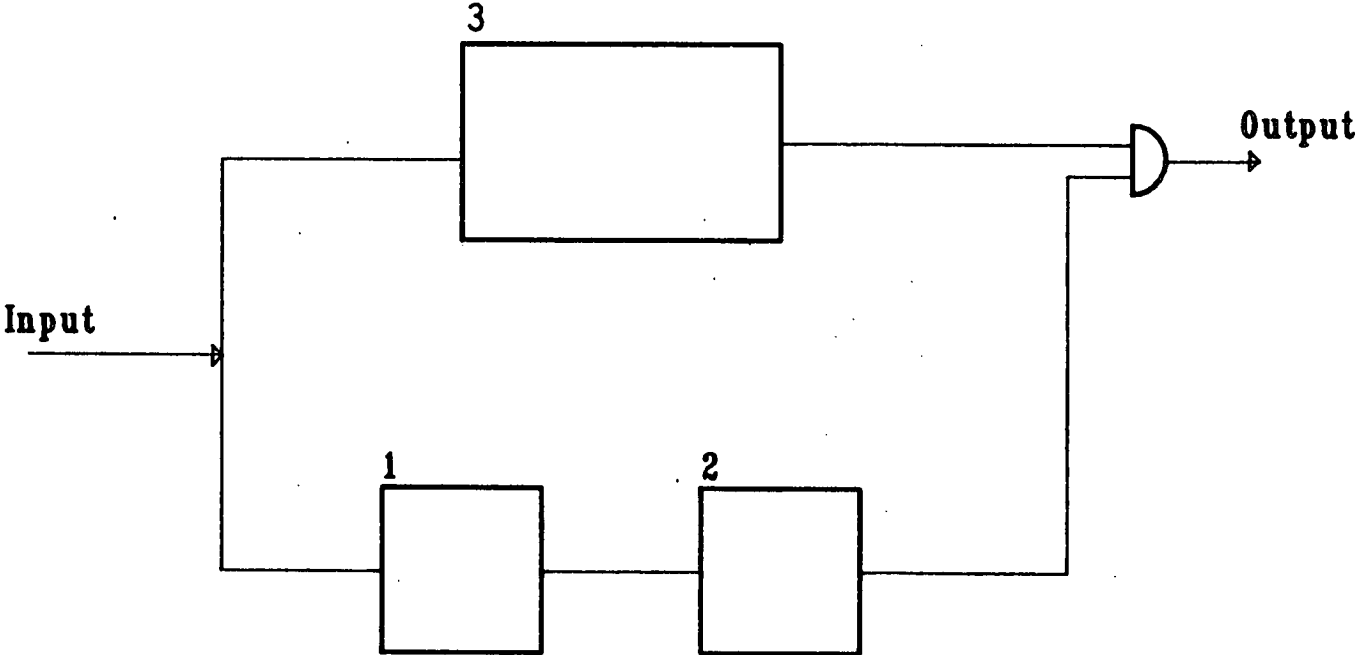
Figure 3.8

Chapter 4
Experimental Apparatus and Procedure

4.1 Fluidised Systems

4.1.1 The Fluidised Beds

Two geometries were used:

1 A small scale fluidised bed of 7.5 * 7.5 cm cross section. The gas distributor was porosint sheet 5 mm thick and pore size 30-40 µm. Compressed air was passed through a coarse filter and a rotameter to measure the flow rate before entering the plenum chamber below the distributor plate. The total height from the distributor to the top of the vessel was 50 cm. A glass wool filter was used on the exit flow to retain any solid particles. Reference axes were defined in the cross section along which the local properties of the flow were investigated. This is shown in Figure 4.1.

2 A fluidised bed of rectangular 48.6 * 28.6 cm cross section. The gas distributor was porosint sheet as described above. The material of construction was 1 cm perpex. Compressed air was passed through a coarse filter and a rotameter before entering the plenum chamber below the distributor plate. The bed depth used was up to 60 cm, and the total height of the apparatus was 1.95 m. This enabled the development of the flow field to be investigated. A schematic diagram is given in Figure 4.2. Reference axes were defined along which the local properties of the flow field were investigated. These definitions are given in Figure 4.3.

4.1.2. Materials Used

Three materials were used as bed fill,

1 Glass Ballotini beads

2 Round Sand

3 Catalyst Particles

1 Glass Ballotini Beads: This material was used in the 7.5 * 7.5 cm square bed. The beads had a size range of 440-530 μm and bulk density of 1830 kg m^{-3}. The specific gravity of the particles was 2.48. When the material was fluidised entrained particles travelled only a short distance before returning to the bed. Flow in the freeboard was essentially single phase.

The bed pressure drop - superficial flow characteristics were measured in the 7.5 * 7.5cm square bed with the top open to atmosphere. The results are given in Figure 4.4. The minimum fluidising velocity was found to be 21 cm s^{-1}.

2 Round Sand: This material was used in the 48.6 * 28.6 cm rectangular bed. The sand had a size distribution that was measured by sieve analysis. This is given in Table 4.1. The particle density was 2500 kg m^{-3} and the bulk density was 1500 kg m^{-3}. When the material was fluidised entrained solids travelled large distances into the bed. The solids that travelled the greatest distances would be from the small size fractions.

The bed pressure drop - superficial flow characteristics were measured in a 15 cm diameter bed, with bed depth 25 cm and a porous paper distributor. The results are shown in Figure 4.5. The minimum fluidising velocity was found to be 0.95 cm s^{-1}.

3 Catalyst Particles: kindly supplied by I.C.I. (plc) Mond Division. This material was used in the 48.6 * 28.6 cm rectangular bed. The particles had a range of particle sizes which were measured by sieve analysis. This

analysis is given in Table 4.2. The arithmetic mean diameter was calculated as 450 µm, and the bulk density was found to be 954 kgm^{-3}. When this material was fluidised much of the small size fraction solids was carried over in the gas flow in the freeboard. In the present system this material was not returned to the bed. However, after an initial period the remaining particles were entrained but not elutriated.

The bed pressure drop - superficial flow characteristics were measured in the large rectangular bed. The results are shown in Figure 4.6. The minimum fluidising velocity was found to be 11 cms^{-1}.

4.1.3 Tube Bank

Heat removal from gas fluidised beds may be carried out by the use of tubes, containing a circulating coolant. Since the mobile particles surrounding the tubes are solid and have a high heat capacity, a heat transfer coefficient of about five times greater than for gas flow alone in the empty apparatus can be obtained.

A tube bank shown in Figure 4.7 was assembled and immersed in the bed to study the effect on the mean velocities and velocity fluctuations in the freeboard.

A staggered array of wooden rods 1.9cm in diameter in 7cm * 7cm pitch was constructed which could be lowered down to rest ≈ 11cm above the distributor plate. The rods were fixed into chipboard which is 1.8 cm thick, thus narrowing the bed slightly. A horizontal rod arrangement was chosen since this is used in coal combustion fluidised bed furnaces.

Skinner [48] reported that a pitch/diameter ratio of 2 to 8 is used over a wide range of industrial applications.

For a tube diameter of 35mm, a decrease in pitch/diameter ratio (over the range investigated), decreased the heat transfer coefficient by 15-20%. A pitch/diameter ratio of 3.5 was therefore used in these experiments, as representing common industrial practice with heat transfer tubes in fluidised beds. Three rows of rods were used.

4.1.4 Traversing Mechanism

Measurements were taken throughout most of the freeboard space. This meant building a rig that would travel the three dimensions given in Section 4.1.1. whilst carrying the optical system including the laser and optics unit. A vertical lift trolley was adapted so that this was possible.

4.1.5 Smoke Generator

Visualisation of the flow in the freeboard was studied by use of a smoke generator. This unit used the smoke generated by the incomplete combustion of paraffin which was output via a fan. It was found that the internal pressure in the freeboard was large enough to made direct input of smoke to the freeboard impossible. The smoke plus carrier gas was passed through a peristallic pump which gave the stream some pressure head. Smoke was admitted to the freeboard through a nozzle.

The procedure used was that smoke was admitted when the fluidised bed was in operation. This was done over a time period of 5 minutes. After five minutes had elapsed the generator was switched off and the smoke allowed to leave in the gas flow. A sequence of photographs was taken at 5 second intervals.

4.2 Experimental Procedure

For every measurement point the location of the Measurement Control Volume was checked by carefully targeting the cross over point using a piece of photographic film. The image was focused on to the pinhole at the front of the photomultiplier tube. The size of this pinhole was 200 μm. The position of the M.C.V. was moved along the reference axes specified in Section 4.1.1. as well as some positions off these reference axes. Five different planes were used in the 7.5 * 7.5 cm square bed, 10, 20, 29.5, 40 and 47.5 cm above the distributor plate. The planes used in the large rectangular bed were 30, 60, 120 and 150 cm above the fluidised bed surfaces.

For each experimental run, the bed was fluidised and the sample time and experiment duration specified to the correlator. The value of the modulator frequency if used was checked and specified to the data processor. The experiment time used throughout this work was five minutes, during which time the autocorrelation function is made up of contributions from many signals and provides information on the average velocity and statistical properties of velocity fluctuations.

4.3 Measurement Errors

The position of the MCV was determined relative to the walls of the fluid bed container (and hence to the centre of this, taken as the origin of the coordinates) by direct measurement on a millimetre scale. The consequent error in each spatial coordinate of the MCV is estimated to be ±2 mm.

The standard deviations on the measurements of mean and rms velocity, as found from replicate determinations ata fixed location, were different for the two fluid bed containers, and to some extent for the different bed materials used:

For the 7.5 * 7.5 cm bed, the standard deviation on each mean velocity component measurement was ≯±5% for U_z, ≯±20% for U_x and U_y and on the components of rms velocity was ≯±10%.

For the 48.6 * 28.6 cm bed, the standard deviation on each mean velocity component measurement was ≯±20%, and on the rms velocity component was ≯±20% when sand was used. For a bed of catalyst particles the corresponding standard deviation values were ≯±5% for U_z, ≯±20% for U_x and U_y and ≯±10% for the rms velocity components.

Coordinate System for Small Fluidised Bed.
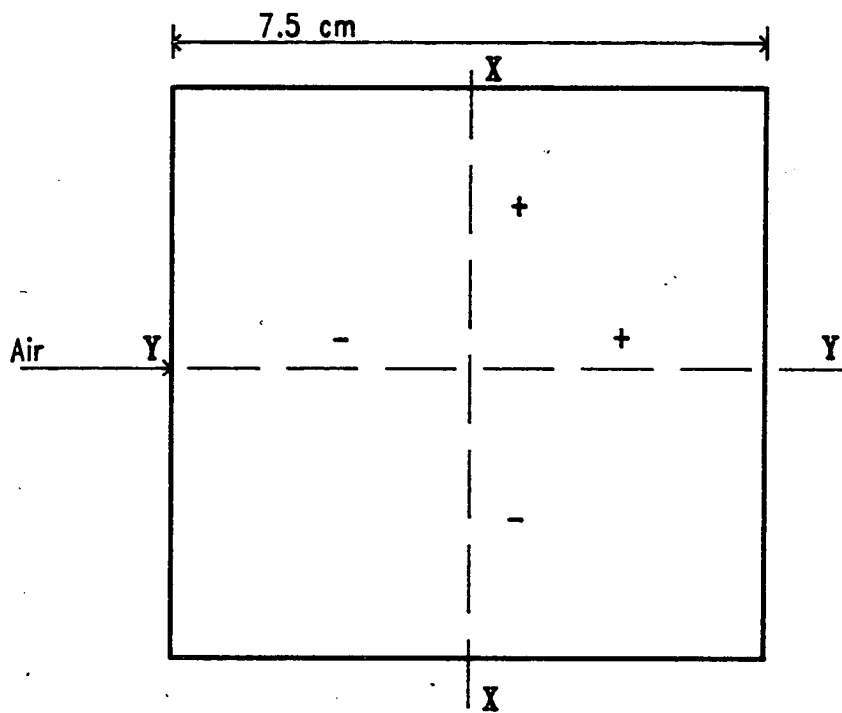
Figure 4.1

Schematic Diagram of Large Fluidised Bed Apparatus.
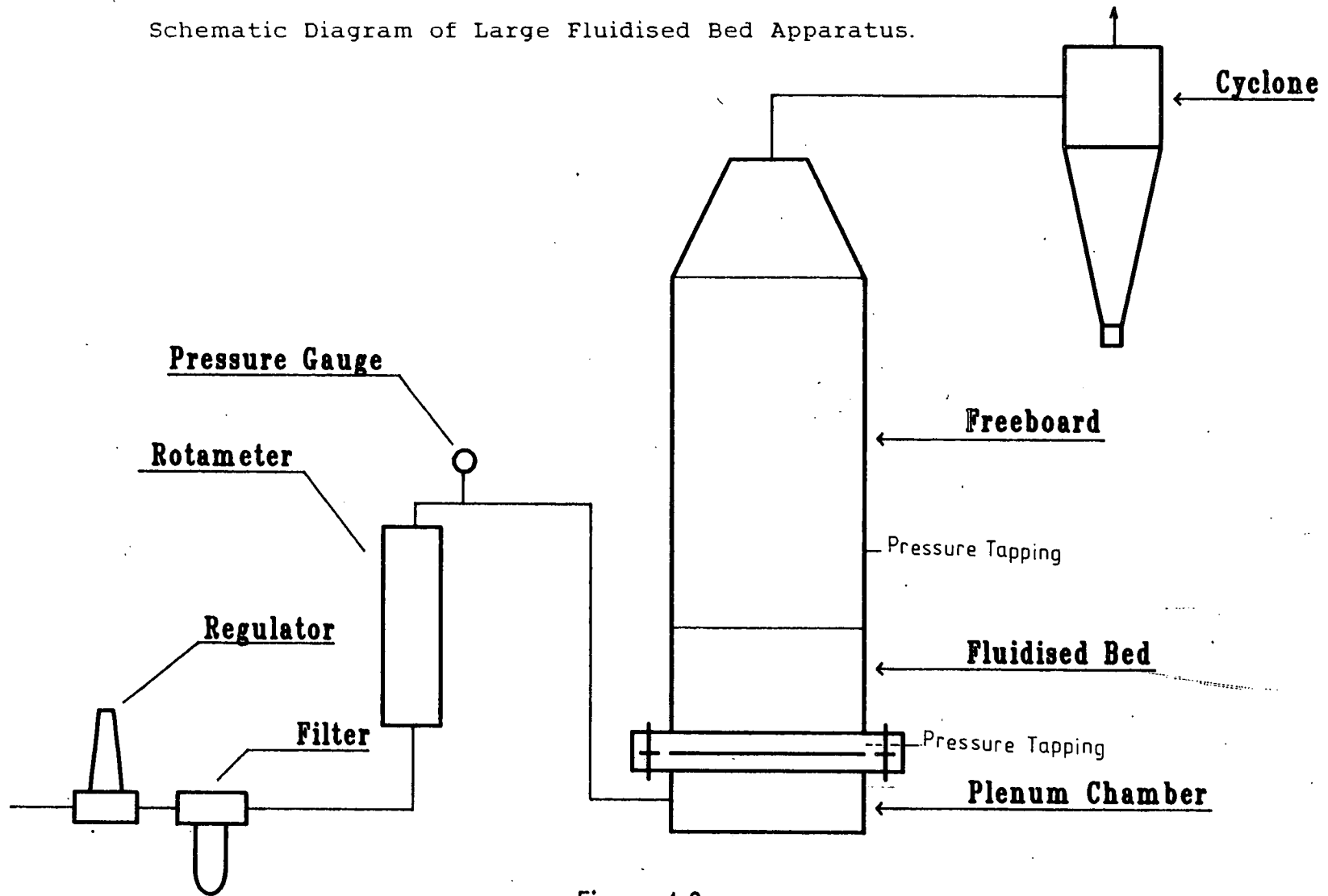
Figure 4.2

Coordinate System for Large Fluidised Bed.
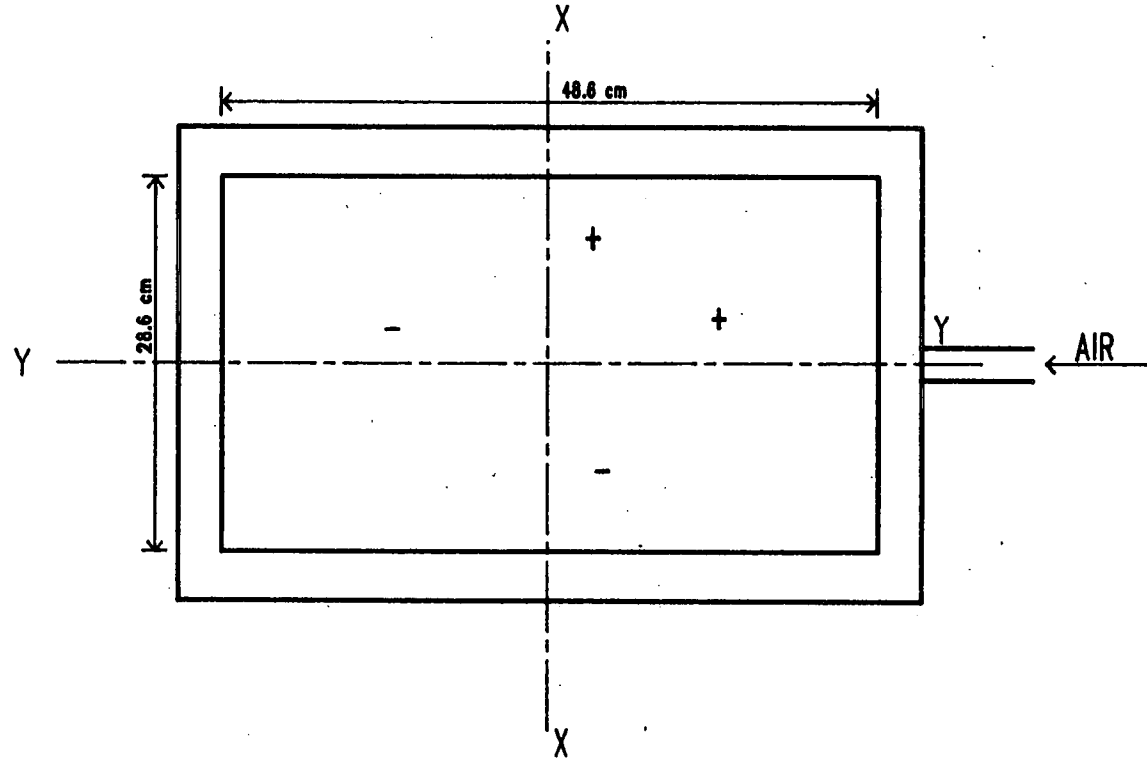
Figure 4.3

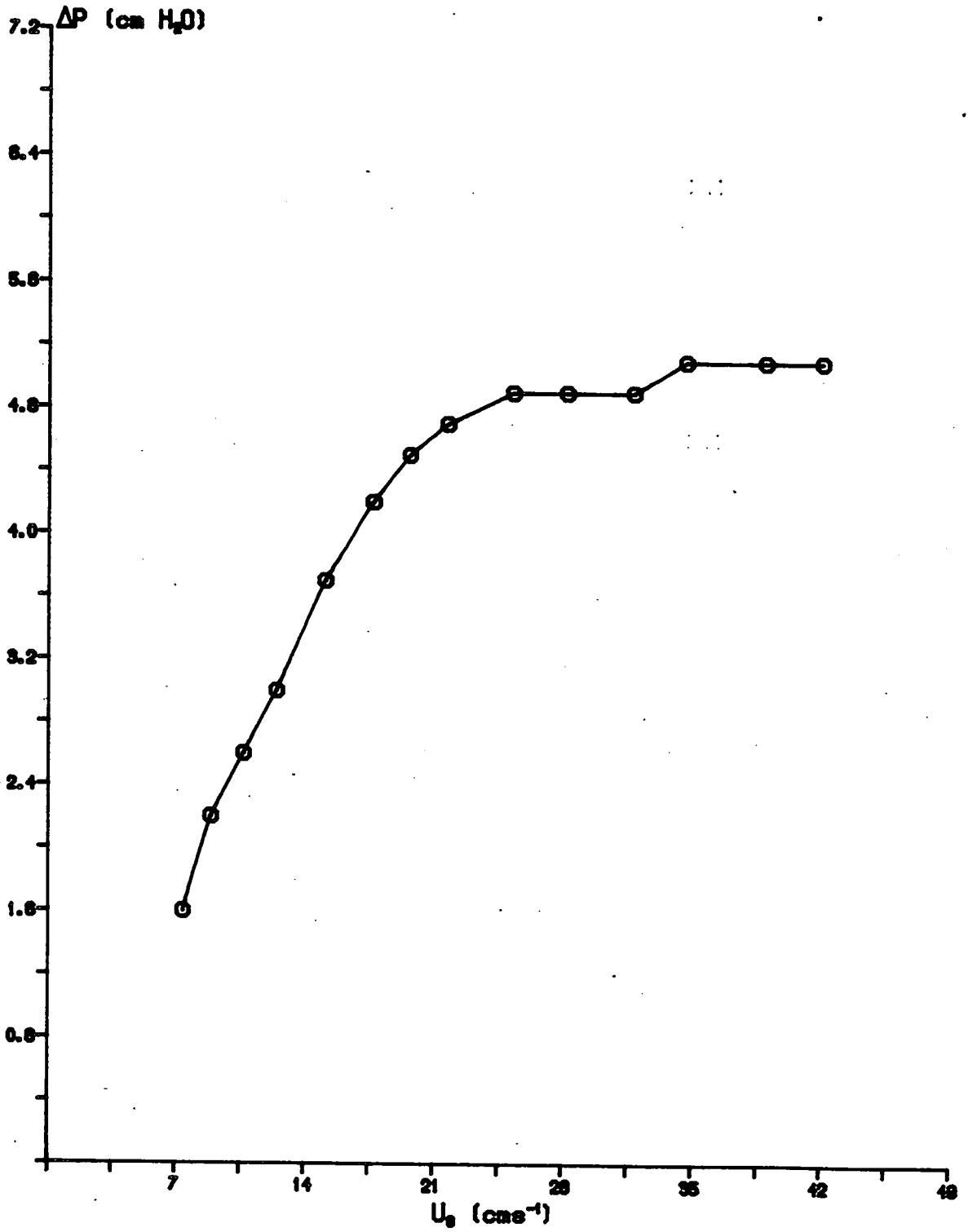Figure 4.4

$\Delta P - U_s$ Relationship For Ballotini

Figure 4.5
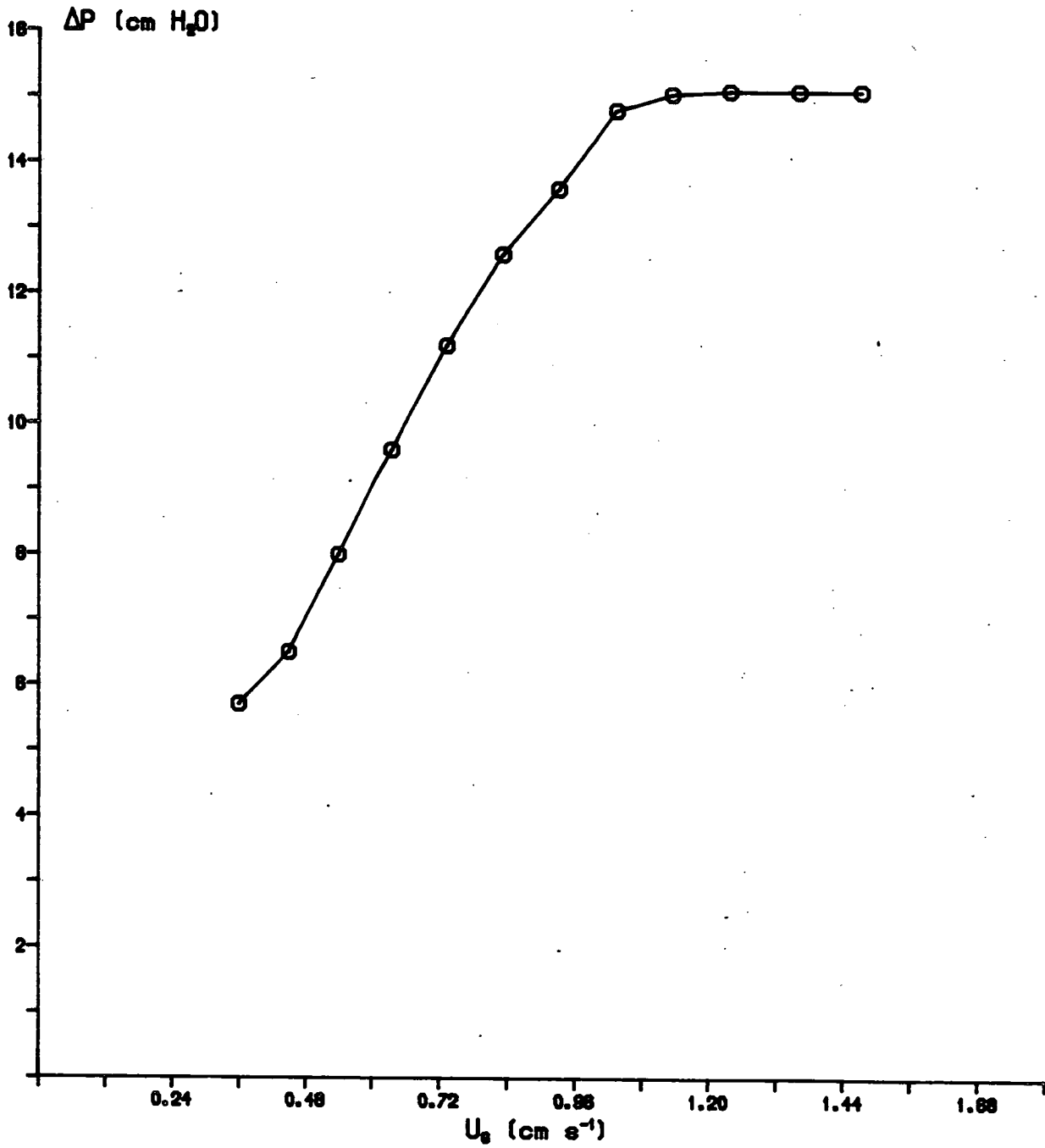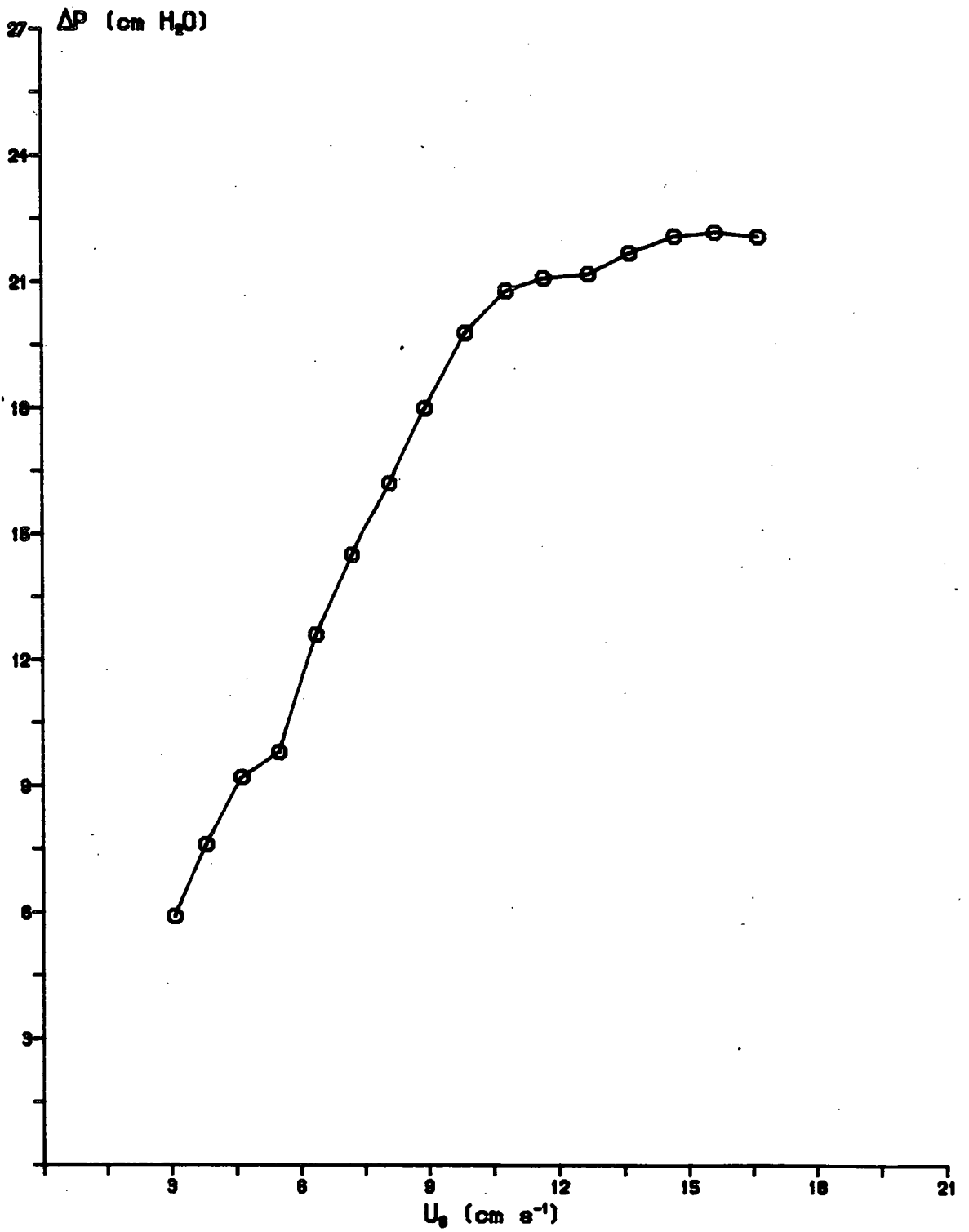
$\Delta P - U_8$ Relationship for Round Sand

Figure 4.6

ΔP – U_s Relationship for Catalyst
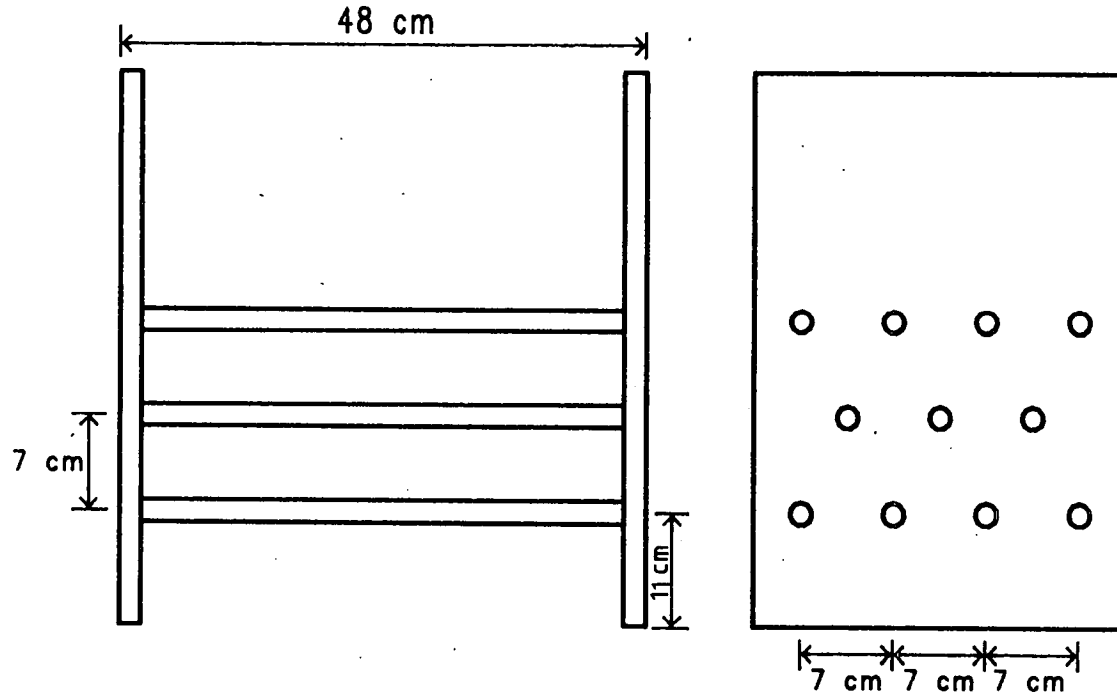
Dimensions of Model Tube Bank.

Figure 4.7

Sieve Aperture (µm)	Weight Retained (%)
250	1.8
210	1.7
180	1.8
150	35.4
125	36.2
105	10.3
90	7.3
75	2.9
45	1.6
-45	1.1

Table 4.1

Sieve Analysis of Sand.

Sieve Aperture (µm)	Weight Retained (%)
850	0.3
710	0.7
500	32.4
420	26.5
355	17.1
300	13.2
250	4.8
210	1.5
180	0.8
150	0.6

Table 4.2

Sieve Analysis of Catalyst Particles.

Chapter 5
Vertical Component of Velocity and Turbulence

5.1 Introduction

The various theoretically based attempts to predict entrainment and elutriation rates have had to make assumptions about the gas flow to predict the motion of particles. There is very little information on the structure of gas flow in the freeboard, particularly the distribution over the cross section. The motion of a particle is determined by two parameters; the initial ejection velocity and the gas flow field in the freeboard. The results presented in this work give useful information on the gas flow field which may enable the motion of particles to be predicted. The estimation of T.D.H. and particle carry over is therefore rendered possible.

The vertical velocity profiles in a number of systems have been investigated. The materials and bed geometries are given in Chapter 4. These results show a rather bewildering variation, but an attempt is made to explain the variations in subsequent sections. The fluidised beds in all cases were freely bubbling.

The characteristics of flow below the T.D.H. and the development of the flow with distance from the erupting bed surface have been investigated. The influence of system parameters and the effect of an immersed tube bank have also been studied.

5.2 Measurements in the 7.5 * 7.5 cm Square Bed

The particulate material used was glass ballotini beads with minimum fluidising velocity 22 cm s^{-1}. The number of particles ejected from the dense phase is small and these travel only a small distance into the freeboard region before falling back into the bed. The flow in the freeboard was therefore single phase gas flow. This fluidised system is similar to that used by Horio et. al. [33] and it was hoped to repeat and expand on that work. The effect of superficial flow, bed depth and freeboard height were investigated.

Standard deviations on the mean and rms velocity measurements are given in Section 4.3.

5.2.1 Effect of Superficial Flow

An increase in superficial flow when a fluidised bed is freely bubbling will increase the volumetric flow in the bubble phase of the dense bed. The bubble size distribution will shift to larger sizes, and there will therefore be a larger proportion of faster rising bubbles because of the relationship between bubble rise velocity and bubble size.

The superficial flow will also affect the bubble frequency. Information on bubble frequencies and bubble size distributions is given by Mojtahedi [50], who also made measurements of the spatial dsitribution of bubbling over the cross section. It was found that bubble frequency increased with increase in superficial flow, but the spatial distribution of bubbling was not affected.

Work has been done on particle circulation patterns in a fluidised system similar to the one used in this work by Lin et. al. [45]. It was found that an increase in superficial flow changed the particle circulation pattern from particles ascending at the walls to particles ascending at the centre of the cross section. This effect in the dense bed is important to bear in mind when describing the results obtained for gas flow in the

freeboard.

Figure 5.2.1 shows the local vertical component of velocity across the YY axis for superficial flows of 0.3 and 0.4 m s^{-1}. The profile for a superficial flow of 0.4 m s^{-1} shows a maximum at the centre with minina near the walls. The profile for a superficial flow of 0.3 m s^{-1} is nearly flat. These profiles are as expected for conventional duct flow. All the measured velocities in the Z direction are greater than the superficial fluidising velocity. Continuity can only be satisfied if a region of low velocity or downward flow exists near the walls as suggested by Horio et. al. [33]. Unfortunately, the reflectance of the walls made measurement difficult in this region and demonstration of the existence of this zone was made in the larger rectangular bed (Section 5.3.3). The effect of increasing the superficial flow is to increase the local vertical component in the centre of the freeboard cross section.

Figure 5.2.2 shows the rms value of the fluctuations in the vertical component of velocity across the YY axis for superficial flows of 0.3 and 0.4 m s^{-1}. These measurements express the magnitude of the fluctuating velocities about the mean velocity values given in Figure 5.2.1. The increase in superficial flow gives an increase in the magnitude of the velocity fluctuations measured in the freeboard, in other words the turbulence intensity is increased.

A simple model of the behaviour described can be based on the rise velocity of bubbles in the bed. Mori and Wen [51] give a correlation for the characteristic bubble size in a fluidised bed (Section 2.1.2). This correlation predicts that an increase in superficial flow will increase the characteristic bubble size in the fluidised bed. The rise velocity of bubbles can be estimated from the expression given by Davidson and Harrison [14] (Section 2.1.2). This

predicts that the rise velocity of bubbles is greater for larger bubbles. Assuming that fluctuations in gas velocity are generated by bursting bubbles, the increase in the magnitude of the fluctuating velocity in the freeboard with increasing superficial flow can be explained by the bubble rise velocity in this system. Details of this method of analysis will be given in Chapter 7.

Measurements were also taken across the XX axis to confirm the local properties of the flow field over the cross section. Figures 5.2.3 and 5.2.4 show the mean velocities and rms values of the fluctuations in the vertical component of velocity on the XX axis under the same conditions as Figures 5.2.1 and 5.2.2, and the effect of increase in superficial flow. The profiles obtained on the XX axis are basically the same as those obtained on the YY axis. The velocity profile for a superficial flow of 0.4 m s^{-1} is distinctly skew indicating that the distribution of bubbling activity across the XX axis at the bed surface is not uniform and affects the velocity profile at this relatively low freeboard height. There is the expected increase in local mean velocities and rms values of the fluctuations in velocity with increase in superficial flow.

The effect of superficial flow was investigated at several freeboard heights and along both reference axes for this fluidised system. The presentation of all this experimental data is impractical, but the effects described in Figures 5.2.1 to 5.2.4 were found in other parts of the freeboard. This information enables the following conclusions to be made:

1 The increase in superficial flow does not affect the shape of the mean velocity profiles. The assumption of constant gas velocity in the central region of the freeboard is resonable in this system. For continuity to

be satisfied there must be a region of low vertical component of velocity near the wall. It is assumed that particles of bed material would fall back towards the fluidised bed in this region, as was found by Horio et. al. [33].

2 Increase in superficial flow gives an increase in the amplitude of velocity fluctuations at all positions in the freeboard. It is assumed that the fluctuations in gas velocity are generated by gas bubbles bursting at the surface of the fluidised bed. At higher superficial flow the rise velocity of bubbles is expected to be greater and therefore the amplitude of the velocity fluctuations in the freeboard will be greater.

5.2.2 Effect of Bed Depth

The bed depth has the effect of modifying particle circulation patterns in the bed. These circulation patterns will give discrepancies in bubble rise velocity so that rise velocity will be enhanced by upward movement of particles and retarded by downward movement of particles. These effects on the dense bed have been investigated by Mojtahedi [50] and Werther and Molerus [75].

The characteristics of bubbles erupting at the surface of the fluidised bed should be dependent on the bed depth. However, there are conflicting trends e.g. according to Mojtahedi [50] in the fluidised bed there will be a larger proportion of smaller bubbles generated at the distributor at greater bed depths which will develop into larger bubbles as they travel upwards before erupting at the bed surface. Consequently the rise velocity of bubbles may not be significantly affected by change in bed depth.

The bubbling activity or bubble frequency may be reduced at larger bed depths because of bubble coalescence and as

93

a result the distribution of bubbling activity at the surface of the bed may be relatively poor.

The characteristic bubble size correlation of Mori and Wen [51] predicts that the bubble size will increase with increase in bed depth. The bubble rise velocity and therefore the magnitude of the velocity fluctuations in the freeboard expressed as the rms velocity fluctuation are expected to be greater.

The most striking effect of bed depth is shown in Figure 5.2.5 which shows the vertical component of velocity on the YY axis for superficial flows of 0.3 and 0.4 m s^{-1}. The bed depth was 3 cm and the freeboard height was 10 cm. The mean velocity profile for a superficial flow of 0.3 m s^{-1} shows an inversion of the behaviour described in Section 5.2.1 with maxima in vertical velocity near the walls and a minimum at the centre of the cross section. This profile is interesting in being similar to those described by Levy and Lockwood [42]. The minimum velocity is in fact almost exactly the minimum fluidising velocity. Mojtahedi [50] in studying bubble statistics in a freely bubbling fluidised bed, found that at low freeboard heights above the distributor plate bubbling activity tended to be concentrated at the bed walls, but at greater bed depths was more prevalent near the bed centre. This fact, assuming that the gas flow in the bubble phase is transferred to the region of the freeboard above the point where it surfaces, could explain the peaks of vertical velocity measured near the walls. The mean velocity profile for a superficial flow of 0.4 m s^{-1} shows the same behaviour as that described in Section 5.2.1 with low velocity near the wall and higher local velocity at the centre of the cross section. The distribution of bubbling activity has presumably changed at the larger superficial flow to give more uniform distribution over the bed surface.

The existence of this inverted profile under low bed depth, low superficial flow conditions is confirmed on the XX axis in Figure 5.2.6. The velocity profile at the lower superficial flow shows the inversion of behaviour described above. The velocity profile at the higher superficial flow has relatively low local velocities near the walls.

The effect of bed depth on the rms values of the fluctuations in the vertical component of velocity is shown in Figure 5.2.7. The rms fluctuation was measured on the YY axis at a freeboard height of 20 cm for a superficial flow of 0.4 m s^{-1}. The magnitude of the rms fluctuation is greater at each position for the larger bed depth. The model of the fluctuations in gas velocity based on the rise velocity of bubbles can explain this. For an increase in bed depth it is predicted that the bubble diameter in the bed will increase, therefore the rise velocity of bubbles will increase. Hence, it is expected that the fluctuations in gas velocity will be greater at the greater bed depth.

From the measurements taken, it is possible to confirm this observation at a different superficial fluidising velocity, on the alternative reference axis and at several freeboard heights.

5.2.3 Effect of Freeboard Height

As the distance from the erupting bed surface increases the bubble induced turbulence should decrease. The mechanism of this decay will depend on the flow stucture developed in the freeboard by bursting bubbles.
The effect of freeboard height on mean velocity profiles will also depend on the structure of flow, in particular any tendency for flow in the transverse direction. The

mean velocity profile that develops at large distances from the erupting bed surface will be important, as the assumption has always been made in models to predict particle motion in the freeboard that gas velocity is constant.

The vertical component of velocity and turbulence were measured at several freeboard heights and along reference axes YY and XX. Superficial flows of 0.3 and 0.4 m s^{-1} were used and bed depths of 3 and 5 cm. Some of these results are presented below. Additional information if required can be obtained from the Department of Chemical Engieering, University of Edinburgh.

Figure 5.2.8 shows the vertical component of velocity at a bed depth of 5 cm and a superficial flow of 0.4 m s^{-1} on the YY axis and the variation with freeboard height. The mean velocity profile at a height of 20 cm above the distributor plate is distinctly skew, but profiles at successively increased heights are less skew. In each case the velocity near the centre of the cross section was greater than that at the walls, as might be expected for conventional duct flow. The profiles do not seem to be significantly affected by increase in freeboard height.

Figure 5.2.9 shows the rms value of the fluctuations in the vertical component of velocity on the YY axis at several freeboard heights. The experimental conditions are as described above. The rms fluctuation or in other words the turbulence intensity decreases steadily as height above the bed surface increases. This decay of turbulence will be analysed and discussed in Chapter 7. At the lower elevation turbulence is more or less uniform in accordance with the supposition that it is generated by bubbles bursting at the bed surface. At a freeboard height of 47.5 cm however, turbulence is at a minimum at the centre of the bed and is highest at the greatest distance from

the centre. This might well suggest, again, a region of
high velocity gradient near the walls with consequent high
generation of turbulence.

Similar measurements were taken on the XX axis and at
a superficial flow of 0.3 m s^{-1}. The same conclusions as
made above can be drawn from this information which is
available at the Department of Chemical Engineering,
University of Edinburgh.

In Section 5.2.2 it was shown that the velocity profile
under low superficial flow and shallow bed depth
conditions was inverted with maxima in local velocity near
the walls at low freeboard height. Figure 5.2.10 shows
how the profile develops with increasing freeboard height.
As height above the bed increases the profile flattens out
and finally, 47.5 cm above the bed, a familiar duct type
profile is obtained. Figure 5.2.11 shows the rms values of
the fluctuations in the vertical component of velocity
associated with the mean velocities given in Figure 5.2.10.
At the lowest freeboard height, Z=10 cm, there is high
turbulence near the walls. The reason for this may be
that in the dense bed under these conditions bubbling
activity is greater near the walls, as a result particle
circulation patterns exist with particles moving upwards
near the walls and downwards at the centre. The rise
velocity of bubbles will be enhanced by the upward
movement of the particles and therefore the turbulence
intensity near the walls in the freeboard will tend to be
greater than the turbulence intensity at the centre of
the cross section. At successively larger freeboard
heights the turbulence intensity profile becomes nearly
flat and finally at a freeboard height of 47.5 cm a
turbulence profile is attained with relatively high
turbulence near the walls. This may well be a result of a
region of high velocity gradient near the walls with
consequent high generation of turbulence as suggested in

the description of Figure 5.2.9.

5.3 Measurements in 0.48*0.28m Rectangular Bed

Having first of all taken measurements in a small bed with single phase flow in the freeboard, measurements were taken in a larger bed fluidising round sand with a range of particle diameters, the size distribution is given in Chapter 4. When this material is fluidised at 3-4 * U_{MF} bed material is projected large distances into the freeboard of the system by bursting bubbles. The development of the Laser Doppler Anemometry system to enable measurements of gas flow to be made under such conditions is covered in Chapter 3. The generation of large scale turbulence was anticipated in this case and the characteristics of the turbulent gas flow were measured to investigate this. Mojtahedi [50] made extensive measurements on the statistics of bubble flow in this particular system, and it was hoped to relate the mean velocity profiles near the bed surface to this information. Levy [41], in a similar system took measurements at a maximum freeboard height of 70 cm. In this work measurements of the local structure of flow were taken at large freeboard heights up to 150 cm. Conclusions could therefore be drawn on the development of the flow field.

Standard deviations on the mean and rms velocity measurements are given in Section 4.3.

5.3.1 Effect of Superficial Flow

From section 5.2.1 it was found that for the small bed fluidising glass ballotini an increase in superficial flow caused an increase in the fluctuations of velocity over the whole cross section. This was explained by a bubble rise velocity model. It was expected that increases in superficial flow would have the same effect in the large bed fluidising sand.

Figure 5.3.1 shows the vertical component of velocity measured on the YY axis for superficial flows of 3 and 4

cm s^{-1}. The bed depth was 60cm and freeboard height 120 cm. The vertical components of velocity at both 3 and 4 cm s^{-1} have distinct "dip" profiles with maxima near the walls and a minimum at the centre. The effect of superficial flow is to increase the local vertical component of velocity at all positions on the reference axis.These are similar to the profiles found by Levy [41]. The results of Mojtahedi [50] indicated that in shallow beds such as were used by Levy surface bubbling activity was concentrated in the wall region. Assuming that this part of the flow is directly transferred to the region of the freeboard immediately above the surface, this would lead to maxima in the vertical velocity profile near the bed wall. The bed depth in Figure 5.3.1 is 60 cm, at which it would be expected that bubbling activity would be concentrated at the bed centre. Using a similar argument to that used in Section 5.2.2 a velocity profile with a maximum at the centre of the cross section would be expected in the freeboard. This behaviour is significantly different from that observed in the smaller bed with glass ballotini.

Figure 5.3.2 shows the rms value of the fluctuations in the vertical component of velocity. This expresses the magnitude of the fluctuations associated with the mean velocities given in Figure 5.3.1. The magnitude of the rms fluctuating velocity is consistently greater for the larger superficial flow. This is the expected effect of superficial flow, found in Section 5.2.1, and is predicted by the the bubble rise velocity model. The turbulence intensity gets progressively greater with increasing distance from the centre of the cross section, rising to a maximum near the walls. This may be because of the high velocity gradients which may be inferred, from the mean velocity profiles Figure 5.3.1, to exist near the wall. Such regions would be expected to generate substantial turbulence.

Measurements were taken on the XX axis to extend the coverage of the bed cross section. Figure 5.3.3 shows the vertical component of velocity on the XX axis for superficial fluidising velocities of 3 and 4 cm s^{-1}. The bed depth is 60 cm and freeboard height is 120cm. At both superficial flows the mean velocities have a dip profile across the reference axis. The shape of the profiles on the XX and YY axes are therefore the same and variations in the magnitude of local velocities are probably due to uneven distribution of the bubble phase in the freeboard after bubbles erupt at the bed surface, but not predicted by the bubble rise model.

Figure 5.3.4 shows the rms value of the fluctuations in the vertical component of velocity on the XX axis under the experimental conditions already described. The values for superficial flows of 3 and 4 cm s^{-1} are not distinctly separated as was the case for values taken on the YY axis. Further, the actual magnitude of the fluctuations is less than in the previous case. Values near the wall seem to be greater than those in the bed centre which could be due to the region of wall induced turbulence mentioned above.

As freeboard height increases the turbulence intensity decays. Axial measurements of turbulence have been taken by Pemberton [60], but variation over the cross section was not investigated. Levy [41] found that at low freeboard heights increases in superficial flow resulted in increases in turbulence intensity at all positions on the reference axes. In this work measurements were taken for superficial flows of 3 and 4 cm s^{-1} at larger freeboard heights than were used by Levy. The results for the rms value of the fluctuations in the vertical component of velocity at a freeboard height of 180 cm are shown in Figure 5.3.5. The bed depth was 60 cm. The level of turbulence at the bed axis is greater for the higher

superficial flow. At other positions on the YY axis, however, there seems to be no clear trend in the results. The absolute levels of turbulence are low but higher values are evident near the wall, particularly for negative values of Y.

5.3.2 Effect of Bed Depth

Measurements were taken at a bed depth of 30 cm so that comparison could be made with the information obtained at a bed depth of 60 cm. The reasoning introduced in section 5.2.2 would suggest that, since the distribution of bubbling at the bed surface has been reported to vary significantly with bed depth, mean velocity profiles and turbulence levels might also depend strongly on this parameter, particularly at low freeboard heights.

Figure 5.3.6 shows the vertical component of velocity on the YY axis at superficial flows of 3 and 4 cm s^{-1}. The bed depth is 30 cm and the height above the static bed surface, Z', is 60 cm. For both superficial flows there is no distinct dip profile, as there was for a bed depth of 60 cm. In fact, the assumption of constant velocity in the central zone of the freeboard is not unreasonable for the superficial flow of 4 cm s^{-1}. For a superficial flow of 3 cm s^{-1} the local vertical component of velocity is greater at -ve positions on the YY axis suggesting, according to the bubble flow model, that bubbling activity is not symmetrical about the centre of the bed surface. The bed depth used in this set of experiments was similar to those used by Levy [41]. He found that the vertical velocities at low freeboard height had a distinct dip profile. The behaviour described above is significantly different from that observed by Levy and also from that

observed in the smaller bed with glass ballotini (Section 5.1.2).

The effect of bed depth in the small bed fluidising glass beads was shown in Section 5.2.2. There it was found that the bed depth affected the mean velocity profiles and that the intensity of turbulence expressed as the rms value of the fluctuations of the vertical component was less at smaller bed depths. This effect could be explained by a bubble rise velocity model. It has been found by Mojtahedi [50] that bubble rise velocity can vary significantly at different elevations in a fluidised bed. Most theories assume that the only parameter affecting the bubble rise velocity is the bubble size regardless of how the bubble reached its volume. Enhanced velocity of bubbles can be found at low bed depths. Mojtahedi ascribed this mainly to particle circulation patterns, but a little to possibly high coalescence rates near the distributor.

Figure 5.3.7 shows the rms value of the fluctuations in the vertical component of velocity on the YY axis at bed depths of 30 and 60 cm. The superficial flow was 3 cm s^{-1} and the height above the static bed surface was 60 cm. The turbulence intensities are consistently larger at the lower bed depth; this is the opposite effect to that described for the small bed and is presumably related to the properties of bubble velocities in the dense phase described above. In both cases turbulence intensity tends to be larger near the walls. For the bed depth of 60 cm this is probably due to the relatively large velocity gradients that exist in the gas flow with consequent high turbulence. For the bed depth of 30 cm the high turbulence intensity measured near the wall may be because of enhanced bubble velocities in this region in the dense phase. At positions close to the wall i.e. <2 cm the turbulence intensity decreases which is characteristic of

103

wall turbulence.

Figure 5.3.8 shows the rms value of the fluctuations in the vertical component of velocity on the YY axis for bed depths of 30 and 60 cm. The superficial flow was 4 cm s^{-1} and the distance above the static bed surface was 60 cm. At this higher superficial flow there is no significant difference between the turbulence intensities measured at each bed depth. This may be related to the properties of bubble velocity in the dense bed, but in addition there may be different rates of decay from initial levels at the bed surface for each superficial fluidising velocity such that the magnitude of gas velocity fluctuations at a distance of 60 cm from the static bed surface are not significantly different (section 7.1).

Figure 5.3.9 shows the rms value of the fluctuations in the vertical component of velocity on the YY axis for three superficial flows. The bed depth is 30 cm and the height above the static bed surface is 60cm. The turbulence intensity is low at a superficial flow of 2 cm s^{-1} and increases markedly for a superficial flow of 3 cm s^{-1}. However, there is no significant difference between the turbulence intensities measured at superficial flows of 3 and 4 cm s^{-1}. Assuming the magnitude of velocity fluctuations is dependent on the rise velocities of bubbles, it would seem that rise velocities of bubbles are similar in a bed of depth 30 cm for superficial flows of 3 and 4 cm s^{-1}. However, different rates of decay of turbulence may exist under different experimental conditions as mentioned above.

5.3.3 Effect of Freeboard Height

Measurements of the vertical component of velocity were taken at heights above the distributor of up to 180 cm. The effect of height on the mean velocity profiles should show whether horizontal or transverse components of velocity are present which would be important for particle disengagement from the gas flow.

Figure 5.3.10 shows the vertical mean velocities on the YY axis for various freeboard heights. The bed depth was 60 cm and superficial flow was 4 cm s^{-1}. At Z=120 cm the mean velocity profile has a distinct dip as was shown in Figure 5.3.1. For increasing freeboard height there are changes in the local magnitudes of mean velocity, but the dip profile persists at a freeboard height of 180 cm. There is no evidence that the velocity profile is affected by secondary flows that would tend to flatten the profile shape.

Figure 5.3.11 shows the vertical mean velocity measurements on the YY axis for various freeboard heights. The bed depth was 30 cm and superficial flow was 3 cm s^{-1}. At Z=90 cm the mean velocities do not exhibit a distinct dip profile as was shown in Section 5.3.2. However, at freeboard height of 150 cm the flow has developed to give a distinct dip profile. Horizontal components of velocity are presumably present which transfer gas from the bed centre, particularly in the negative Y direction. At Z=180 cm the mean velocity profile has still smaller local velocities at the centre of the cross section with very large velocities near the wall. Local velocities of up to 8 cm s^{-1} were measured in the freeboard (at position -23.3cm on the YY axis at Z=180 cm). This has important implications for particle motion and carry over which will be discussed in Chapter 7.

Measurements of U_z were made at a distance of 1cm
from the walls. In the apparatus as originally constructed
it was not possible to make measurements closer to the
wall because of the high intensity scattered radiation
resulting from the laser beams passing through the
perspex walls of the fluidised bed. This scattered
radiation was picked up as noise by the photomultiplier
and the signal to noise ratio became very poor. It was
therefore impossible to get a processable autocorrelation
function of the output from the photomultiplier. To
enable measurements to be made at distances <1 cm from
the wall an observation port was used. A diagram is
given in Figure 5.3.12. The laser beams leave through the
end of the observation port and the cross over point can
therefore be located very near the wall without excessive
scattering of light. The piece was located at a·freeboard
height, Z, of 180 cm at the +ve end of the YY axis.
Measurements were taken at a bed depth of 30 cm for
superficial flows of 3 and 4 cm s^{-1}. The results obtained
are given in Figure 5.3.13. From these results it is
confirmed that there is a region of low gas velocity at
distances of less than 1 cm from the wall. However, if
particles of bed material associated with the gas flow
are transferred towards the wall they will first of all be
acted on by very high gas velocities measured near the
wall.

Figure 5.3.14 shows the rms value of the vertical
component of velocity on the YY axis at various freeboard
heights. The bed depth was 60 cm and the superficial
flow was 4 cm s^{-1}. The rms value of the fluctuations is
expected to decrease with increase in freeboard height as
was found in Section 5.2.3. The rms value or turbulence is
lower at a freeboard height of 150 cm compared to the
turbulence intensities measured at Z=120 cm. However, at
Z=180 cm there are several positions where the measured
turbulence intensity is greater than that measured at

Z=150 cm. This may be because of the relatively low values of turbulence intensity at these freeboard heights and the relatively high mean velocity gradients that exist at Z=180 cm, particularly at the -ve end of the YY axis (Figure 5.3.10).

Figure 5.3.15 shows the rms values of the fluctuations in the vertical component of velocity on the YY axis at various freeboard heights. The fluidised bed had a depth of 30 cm and a superficial flow of 3 cm s^{-1}. This figure gives the turbulence intensity associated with the mean velocities given in Figure 5.3.11. The turbulence intensity decreases steadily from Z=90 cm to Z=150 cm, however, at Z=180 cm relatively high levels of turbulence are measured particularly near the walls. This may be a result of the high mean velocity gradients that exist near the walls at this freeboard height (Figure 5.3.11).

5.3.4 Effect of Tube Bank

In many industrial fluidised systems tubes, through which coolant is passed, are immersed in the bed to remove heat from the system. The effect of an immersed tube on the properties of the gas flow in the large rectangular bed was therefore investigated.

In addition the measurements will provide a test for the assumption that the magnitude of gas velocity fluctuations in the freeboard is dependent on the rise velocity of gas bubbles in the fluidised bed, as Mojtahedi [50] found that the effects of an immersed tube bank on the bubbling properties of this system are as follows:

1 Bubble rise velocities are significantly lower than those found in an unobstructed bed.

2 The bubble size distribution is not significantly affected.

3 The spatial distribution of bubbling is improved i.e. it is more even.

Hence, if the rms velocities of the fluctuations in the vertical component of gas velocity in the freeboard are significantly lower in the prescence of an immersed tube bank in the fluidised bed, the dependence of turbulence intensity on the rise velocity of bubbles will have been verified. The design of the tube bank is given in Section 4.1.3.

Figure 5.3.16 shows the vertical mean velocity component on the YY axis in the presence and absence of the tube bank. The bed depth was 60 cm and the superficial flow 3 cm s^{-1}. The profile of mean velocity shows a minimum at the bed centre and maxima near the walls both in the presence and absence of the tube bank. In fact, there is little significant difference between the two cases. Figure 5.3.17 shows the comparison of the vertical components of velocity on the YY axis in the presence and absence of an immersed tube bank for a superficial flow of 4 cm s^{-1}. The bed depth and freeboard height are as described above. The mean velocities measured in the presence of the tube bank agan have a dip profile and are not significantly different from those measured in the unobstructed bed. If the gas flow in the freeboard is closely related to bubbling activity in the corresponding area of the the bed surface, one would expect an even velocity above the the tube bundle which has the effect of making the bubbling activity more uniform. The pronounced nonuniformity of the experimental profiles suggests that the gas flow in the freeboard is less dependent on the bubbling activity in the same region at the bed surface than was hitherto believed.

Figure 5.3.18 shows the rms values of the fluctuations in the vertical component of velocity on the YY axis at a freeboard height of 120 cm. The bed depth was 60 cm and

superficial flow was 3 cm s^{-1}. This expresses the magnitude of velocity fluctuations associated with the mean velocities given in Figure 5.3.16. At all positions on the YY axis the rms fluctuating velocity is lower in the presence of the immersed tube bank. This therefore gives positive evidence that the turbulence intensity in the freeboard is dependent on the rise velocity of bubbles in the bed, as Mojtahedi [50] found that the rise velocity of bubbles is lower in a fluidised bed with internals as mentioned above.

Figure 5.3.19 confirms the above observation at a superficial flow of 4 cm s^{-1}. The rms values of the fluctuations in velocity with the tube bank immersed in the bed are significantly lower at all positions.

Figure 5.3.20 shows a sequence of photographs taken after smoke had been admitted to the freeboard gas flow above a fluidised bed of round sand containing the immersed tube bank. The experimental procedure is given in Section 4.1.5. The superficial flow was 3 cm s^{-1} and the bed depth was 60 cm. These are the experimental conditions under which the results shown in Figure 5.3.16 were obtained. It is shown in Figure 5.2.20 that smoke tends to clear near the walls leaving smoke in the centre of the cross section. This is consistent with the measurements obtained with L.D.A. which indicated that relatively large local gas velocities existed near the walls. There is also evidence that swirling flow exists as a result of the bubble eruptions at the bed surface. This is consistent with the model of gas motion after bubble eruption given in Figure 5.3.23.

5.3.5 Measurements with uneven Distribution of Gas

It was at first assumed that, at low freeboard heights, the mean vertical gas velocity would be closely related to the intensity of bubbling activity at the corresponding point on the bed surface. This however was not observed in the the experimental investigations.

It was decided to investigate this phenomenon further by using a distributor plate in which the gas flow was confined to the central regions of the bed. If there was close correspondence between dense phase bubbling activity and gas velocity in the freeboard this should lead to velocity profiles with maxima at the bed centre and minima at the walls rather than the observed profiles which had a minimum at the bed centre and very high velocities towards the walls. Although the distributor used in the previous experiments was fabricated of porous bronze, for this purpose a multiorifice distributor was used. The orifices near the wall were blanked off with threaded plugs and the remainder of the orifices were backed with gauze to prevent dumping of sand (Figure 5.3.21). Visual inspection of the bed surface during operation confirmed that bubbling activity was confined to the central region.

Figure 5.3.22 shows the vertical velocity profile on the YY axis at a freeboard height of 120 cm. The profile shows a minimum at the bed centre and maxima near the walls, exactly as did the profiles taken using the unobstructed porous metal distributor. It must therefore be concluded that the assumed correspondence between areas of high bubbling activity and high vertical velocities in the freeboard is not valid.

It has been shown in Figure 5.3.22 that the nett effect of bubbles bursting at the centre of the bed surface under the experimental conditions given is to transfer the

bubble phase gas to the wall region in the freeboard giving large local gas velocities. This is consistent with the evidence given by Levy and Lockwood [42] for single bubble releases at the surface of an incipiently fluidised bed. They took measurements of sand and gas velocities at low freeboard height over a one second period and found that gas velocities in excess of the superficial gas velocity were measured away from the bubble axis. A sketch was given for the suggested flow near the bursting bubble (Figure 5.3.23). At time t_1 the flow issuing from the bursting bubble entrains air, after eruption the drag of descending particles on the gas is sufficient to reverse the gas flow ($t=t_2$) and generates a ring vortex which is carried vertically by the mean flow ($t=t_3$). The mean flow for the conditions used in Figure 5.3.21 would be the minimum fluidising velocity. The generation of ring vortices will result in the transfer of gas towards the walls as was found in Figure 5.3.22. The magnitude of the minimum fluidising velocity may be important, as the extent to which the vortex will expand in the time after generation will depend on it. From Figure 5.3.22 it seems that the bubble phase is transfered to the wall region in the freeboard. However, at larger minimum fluidising velocities the distance that bubble phase gas is transferred horizontally may be less (Section 5.3.7).

Using the explanation above of the behaviour of the gas from bursting bubbles the profiles above freely bubbling beds of round sand may be analysed.

1 Profiles above a deep (60 cm) bed: The profiles above a bed of depth 60 cm were found to have a distinct dip profile with maxima in local gas velocity at the walls (Figure 5.3.1). Mojtahedi [50] found that bubbling activity was greater at the centre of the bed surface for this bed depth. This being the case, the bubble phase gas from this region of the bed surface must be transferred to the

wall region in the freeboard (Figure 5.3.22). The relatively low number of gas bubbles bursting near the walls at the bed surface will transfer some gas to the centre of the freeboard cross section, but gas will also be retained in the wall region of the freeboard. The nett effect is that larger gas velocities exist in the wall region in the freeboard.

<u>2</u> Profiles above a shallow (30 cm) bed: It was found that the profiles of gas velocity at low freeboard height above a shallow bed did not have a distinct dip profile (Figure 5.3.6). Mojtahedi [50] found that bubbling activity at the bed surface was greater near the walls at this bed depth. This being the case a larger proportion of the bubble phase gas will be transferred to the centre of the freeboard cross section and larger mean gas velocities were measured in this region than were measured above fluidised beds of depth 60 cm.

A schematic diagram of the gas flow above deep and shallow beds is given in Figure 5.2.24.

5.3.6 Effect of Position on Cross Section

Measurements were taken off the reference axes defined in Chapter 4 to verify the velocities and turbulence intensities expected. The results for the mean velocities are particularly interesting as this indicates the form of the profile over a cross section defined by a freeboard height Z. The profile expected can be visualised as a crater with high local velocities near the walls and low velocities at the centre of the cross section.

Measurements were taken at a freeboard height, Z, of 150 cm above a fluidised bed of depth 60 cm with an immersed tube bank. Figure 5.3.22 shows the mean velocities measured at a superficial flow of 3 cm s^{-1}. The magnitude of the local velocities on the X=-8 cm axis are

greater than those measured on the YY axis at all positions. The velocities on both axes have distinct dip profiles. It would appear that continuity would be satisfied if the velocity profile over the whole cross section was integrated. A rough check can be made by estimating the areas under each of the profiles shown in Figure 5.3.22. The volumetric flow is given by the integral of these values over the XX axis i.e.

$$Q = \int \left[\int U_z \, dY \right] dX$$

Admittedly, the form of the integral $\int U_z \, dY$ must be assumed over most of the values of X (two points are given by Figure 5.3.22), but a reasonable assumption for this shows that continuity is satisfied to within 5%.

Figure 5.3.26 shows the results obtained at a superficial flow of 4 cm s^{-1}. Again, the magnitudes of the velocities measured on the X=-8 cm axis are consistently greater than those measured on the YY axis. Furthermore, the velocities on both reference axes have distinct dip profiles. The three dimensional velocity profile has a crater shape, and it would appear that continuity is satisfied. A rough check can be made by estimating the areas under each of the profiles given in Figure 5.3.26, using the same procedure outlined above.

Previous measurements taken by Levy and Lockwood [42] were questioned by Pemberton and Davidson [61] because the results did not appear to satisfy continuity. The measurements shown above give further experimental evidence that the crater profile suggested by Levy [41] is reasonable for systems that exhibit a dip profile for the vertical component of velocity. It is encouraging that the velocity profile satisfies continuity, as this implies that the measurement technique is accurate.

Figure 5.3.27 shows the rms values of the fluctuations in the vertical component of velocity associated with the mean velocities given in Figure 5.3.25. There is no consistent difference in the results obtained, though at the +ve end of the X=-8 cm axis does have a relatively high value. This may be because of the high local velocities measured (Figure 5.3.25). Figure 5.3.28 shows the rms values of the fluctuations in the vertical component of velocity associated with the mean velocities shown in Figure 5.3.26. There is no consistent difference between the results obtained, but again relatively large turbulence intensities exist at the +ve end of the X=-8 cm axis, where large mean velocities were measured (Figure 5.3.26).

Figure 5.3.29 gives a sketch of the 3-D velocity profile, based on the measurements of local gas velocity presented in this section.

5.3.7 Effect of Minimum Fluidising Velocity

Measurements were taken in the freeboard above fluidised beds of catalyst particles, the physical properties of which are given in Chapter 4. The minimum fluidising velocity, U_{MF}, is 11 cm s^{-1} whereas the minimum fluidising velocity for round sand was 0.95 cm s^{-1}.

A superficial flow was used such that U_G-U_{MF} was similar to that used for round sand. The important difference is the flow which is necessary to maintain the material in the fluidised state. Comparison of the results obtained above a bed of catalyst particles with those obtained above a bed of round sand will show the effect of U_{MF} and may give a basis for predicting the vertical velocity profiles above fluidised beds. The motion of particles in the freeboard will depend on the gas velocity profile, therefore the ability to predict it is important. Existing

theoretically based models for particle carry over assume that gas velocity profiles are constant in the central region of the freeboard where the influence of the containing walls is negligible.

Initially measurements were taken in the absence of bubbling. This was done to show that the dip profile found above fluidised beds of round sand was not the result of systematic error in gas distribution through the distributor plate. Figure 5.3.30 shows the vertical component of velocity on the YY axis. The superficial flow was 10 cm s^{-1}, bed depth was 30 cm, and the freeboard height, Z, was 60 cm. The Reynolds Number for the gas flow in the freeboard was therefore 2200. The local mean velocities have a laminar type profile. There is no evidence therefore of systematic error in the gas distribution through the distributor.

Figure 5.3.27 shows the results obtained for the vertical component of velocity on the YY axis at a freeboard height of 150 cm. The bed of catalyst was 60 cm deep and superficial fluidising velocity was 16.4 cm s^{-1}. The difference between the superficial fluidising velocity and the minimum fluidising velocity was therefore 5.4 cm s^{-1}. This represents the gas flow in the bubble phase. The mean velocities are nearly constant at positions up to 6 cm from the wall, though a slight increase towards the wall is evident. The velocity than starts to fall under the influence of the solid boundary. The mean velocity profile for round sand at this bed depth had a distinct dip profile with low velocities at the centre of the cross section (Figure 5.3.1). There is no evidence that this is the case in this system. In Section 5.3.5 a model of the motion of bubble phase gas following bubble eruption at the surface of a fluidised bed was proposed. This model can be extended to explain the effect of minimum fluidising velocity described above. When bubbles burst at

the surface of the fluidised bed vortex rings are generated. The extent to which the ring develops horizontally will depend on the magnitude of the gas velocity after bubble eruption. This velocity will be the minimum fluidising velocity. In this case the value of U_{MF} is 11 cm s^{-1}, whereas the value of U_{MF} for round sand was 0.95 cm s^{-1}. Therefore the extent to which the vortex ring develops horizontally may be limited in this fluidised system. As mentioned above there is evidence of larger local gas velocities near the wall, but the very low values of gas velocity found in the freeboard of fluidised beds of round sand are not evident in the freeboard of this fluidised bed of catalyst.

Figure 5.3.32 shows the results obtained above a bed of depth 30 cm at freeboard heights of 90 and 150 cm on the YY axis. The superficial flow was 16.4 cm s^{-1}. The velocities measured at both freeboard heights are nearly constant across the YY axis, but some increase in velocity is evident near the wall. At the position nearest the wall the velocity is lower under the influence of the solid boundary. The behaviour above is similar to that described in the small bed fluidising ballotini, where the profile was flat at intermediate freeboard height.

Table 5.3.1 shows the variation of the axial vertical component of velocity with freeboard height. The bed depth was 30 cm and the superficial flow was 16.4 cm s^{-1}. The measurement at $Z'=30$ cm is lower than the superficial fluidising velocity of 16.4 cm s^{-1}. This implies that a dip profile exists for the vertical component of velocity. At this bed depth bubble frequency is expected to be greater near the walls at the surface of the bed. It has been suggested that in this system bubble phase gas will travel nearly vertically after bubble eruption. Therefore, at low freeboard heights high local velocities will exist near the walls. This is presumably the velocity profile present at

Z'=30 cm. As freeboard height increases the profile develops into a turbulent profile expected for duct flow, with nearly constant velocity at the centre of the cross section. The local mean velocities measured on the YY axis at Z'=60 and 120 cm are shown in Figure 5.3.32. The variation of vertical mean velocity profiles with freeboard height is very similar to that described in Section 5.2.3 for the small bed fluidising ballotini. The general properties of the gas flow must be similar in particular the behaviour of bubble phase gas.

Figure 5.3.33 shows the rms values of the fluctuations in the vertical component of velocity on the YY axis at a freeboard height, Z, of 150 cm. The bed depth was 60 cm and superficial flow was 16.4 cm s^{-1}. The turbulence intensities are nearly constant over the reference axis, though a slight increase near the wall is evident. This profile is similar in shape to those measured in the small bed fluidising ballotini. The magnitude of the turbulence intensity is dependent on the rise velocity of bubbles in the bed.

Figure 5.3.34 shows the rms fluctuating velocity on the YY axis at freeboard heights of 90 and 150 cm. The bed depth was 30 cm and the superficial flow was 16.4 cm s^{-1}. It is interesting to compare the shape of the turbulence intensity profile shown to the turbulence intensity profile given in Figure 5.3.33 for a bed depth of 60 cm. At the shallow bed depth higher levels of turbulence are measured near the walls than at the centre of the cross section. At the deep bed depth the turbulence intensity profile is nearly constant. An explanation of this is that at the shallow bed depth bubble frequency will be relatively large near the walls, and the rise velocity of bubbles will also be relatively large because of the particle circulation patterns induced which have upward movement at the walls. Therefore, assuming that the

117

amplitude of gas velocity fluctuations in the freeboard is dependent on the rise velocity of bubbles in the bed, the turbulence intensities near the walls in the freeboard will be greater. For the deep bed, bubble frequency will·be greater at the centre of the cross section and the rise velocities of bubbles will be larger. Hence, the turbulence intensities at the centre of the freeboard will be larger in a deep bed than in a shallow bed. This is the case, as shown by Figures 5.3.33 and 5.3.34. Figure 5.3.34 also shows the decrease in turbulence intensity evident with increase in freeboard height.

5.4 Conclusions

1 In the small bed fluidising glass beads mean velocity profiles in the freeboard are directly affected by the distribution of bubbling activity at the surface of the fluidised bed. This is illustrated by Figure 5.2.5, where under low superficial flow and low bed depth conditions the mean gas velocity profile has maxima at the walls at low freeboard height. Under these operating conditions bubbling activity is greater near the walls in the fluidised bed, and bubble phase gas is transferred to the corresponding region in the freeboard giving high local velocities.

Trends in the rms value of the fluctuations in velocity, or in other words the turbulence intensity, can be explained by a bubble rise velocity model. The assumptions made in the model are that fluctuations in gas velocity are a consequence of gas bubbles erupting at the surface of the fluidised bed and that the magnitude of the fluctuations is dependent on the rise velocity of bubbles in the bed.

At large freeboard heights the mean velocity profiles develop into those expected for conventional duct flow. This is true in all cases including that where the mean velocity profile is inverted at low freeboard height. Turbulence intensity decreases with increase in freeboard height. The form of this decay will be investigated in Chapter 7.

It is concluded that the turbulence generated in this system may be isotropic as it is not possible for large scale turbulence effects to exist. This conclusion will be tested by results obtained for horizontal components of velocity presented in Chapter 6.

2 In the large rectangular bed fluidising round sand with a minimum fluidising velocity of 0.95 cm s^{-1} the mean velocity profiles were dependent on the fluidisation operating conditions. However, the simplistic explanation of freeboard velocity and turbulence distributions which sufficed for results from the small bed were found to be inadequate to explain results from the big bed fluidising round sand. When bubbles burst at the surface of this fluidised system significant horizontal components of velocity are imparted to the bubble phase gas. In this case, because the dense phase gas velocities are low, bubble phase gas is transferred to the wall in the freeboard. Hence, at large bed depths where more bubbles erupt at the centre of the cross section large local vertical components of velocity were measured near the walls in the freeboard.

The rms value of the fluctuations in velocity or the turbulence intensity is dependent on the rise velocity of bubbles in the fluidised bed. However, there is discrepancy between the trends predicted by simple bubble rise velocity models and trends found by experiment. It

seems that this is due to inadequate methods of predicting bubble rise velocities in geometries where they can be affected by movement of the particulate phase. Further work on bubble rise velocity models is necessary but is outside the scope of this work.

It was found that profiles for the vertical component of velocity were different when using catalyst with a minimum fluidising velocity of 11 cm s^{-1}. When the gas velocity in the dense phase is greater the extent to which bubble phase gas is transferred horizontally is reduced. The local vertical gas velocity components measured in the freeboard are dependent on the bubbling activity in the same region at the bed surface. There is, however, some evidence of horizontal movement of the bubble phase gas in the case of the catalyst bed, but the vertical velocity profiles are not significantly affected.

For gas flow in the freeboard above fluidised beds of round sand there is evidence that mean velocity profiles are modified at increasing freeboard height by, presumably, horizontal components of velocity. The existence of horizontal components of velocity will be investigated in Chapter 6 for this system. Turbulence decreases with increase in freeboard height, the form of this decay is discussed in Chapter 7.

It is suggested that turbulence generated in this system is the result of vortex rings generated by eruptions of gas bubbles at the surface of the bed. The turbulence in this case particularly at low freeboard height may be anisotropic. This conclusion will be tested in Chapter 6.

Figure 5.2.1 YY Profile of Average Vertical Velocity - Small Bed.

SYSTEM PARAMETERS
BED DEPTH 5cm
Z=20cm
BED FILL BALLOTINI
○ U_g 0.3 ms⁻¹
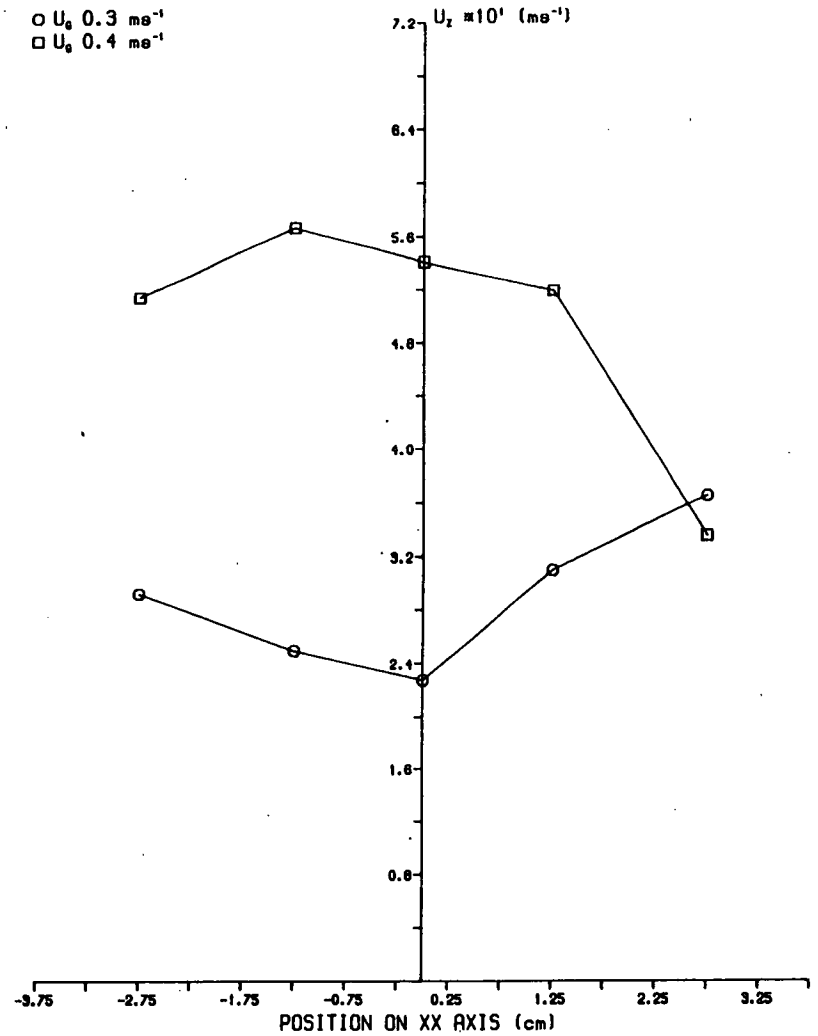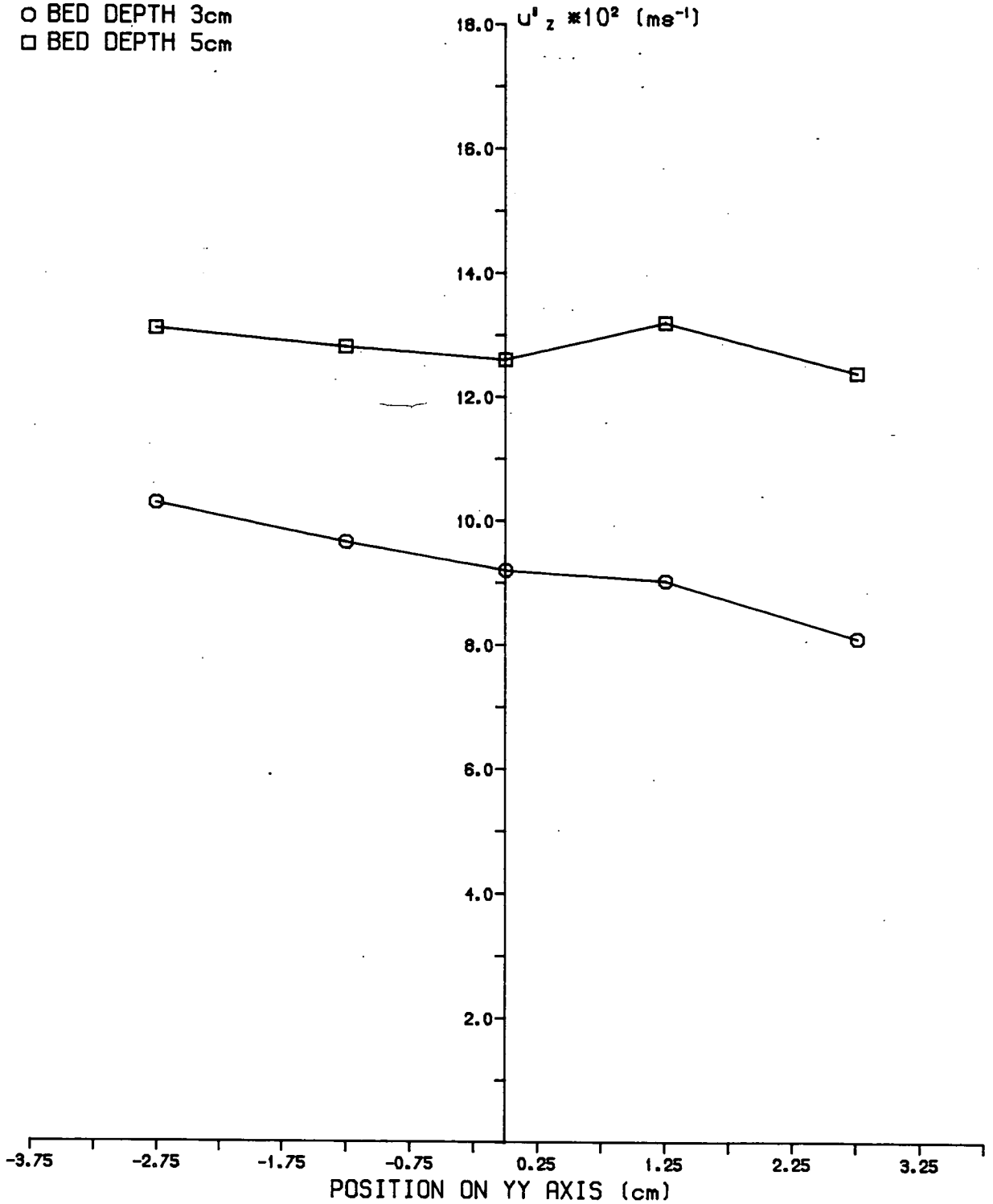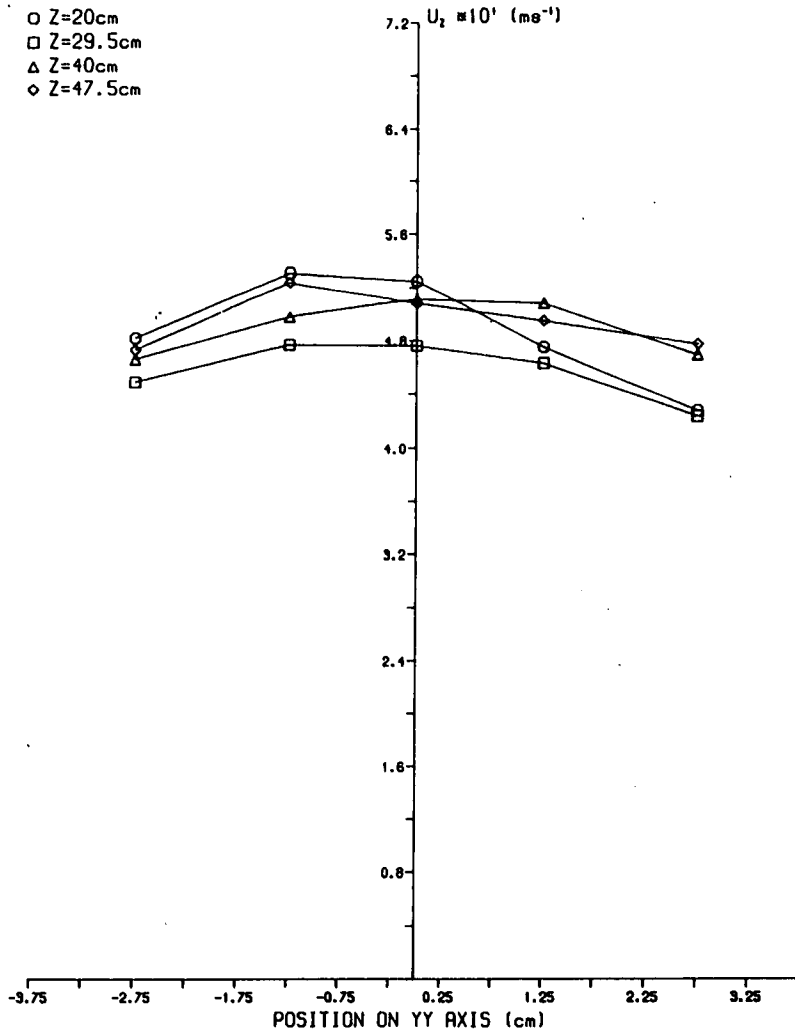□ U_g 0.4 ms⁻¹

U_z ×10¹ (ms⁻¹)

POSITION ON YY AXIS (cm)
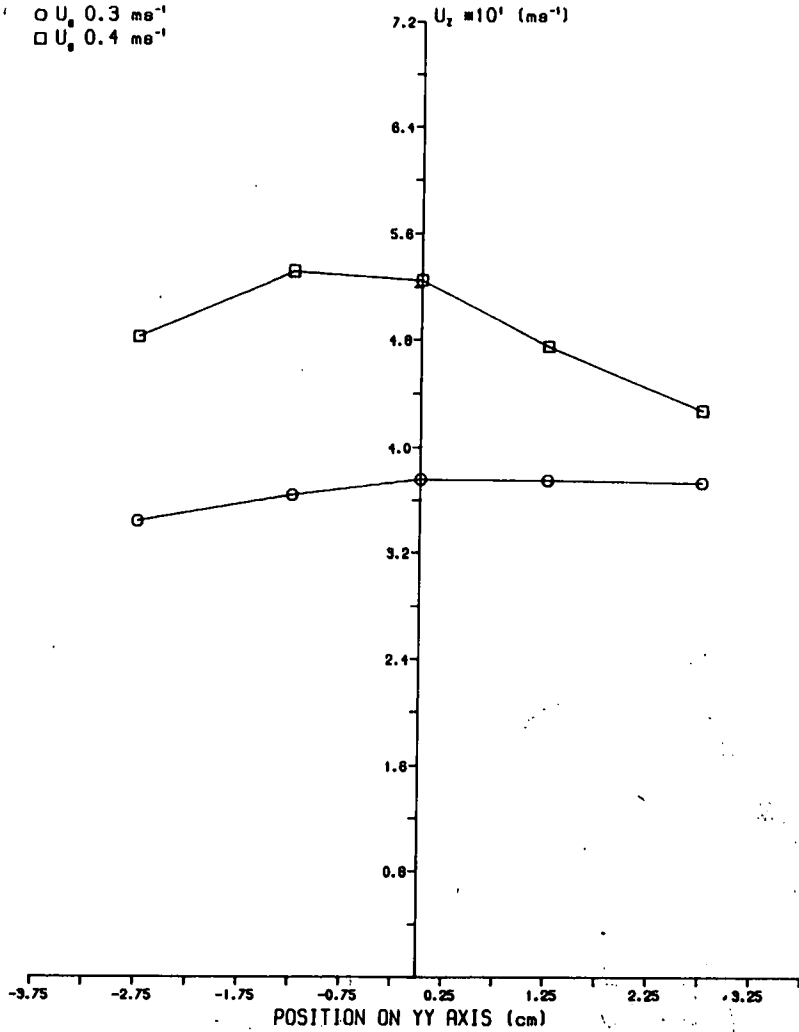
Figure 5.2.2 YY Profile of rms Vertical Velocity Fluctuations - Small Bed.

SYSTEM PARAMETERS
BED DEPTH 5cm
Z=20cm
BED FILL BALLOTINI
○ U_g 0.3 ms⁻¹
□ U_g 0.4 ms⁻¹

U'_z ×10² (ms⁻¹)

POSITION ON YY AXIS (cm)

121
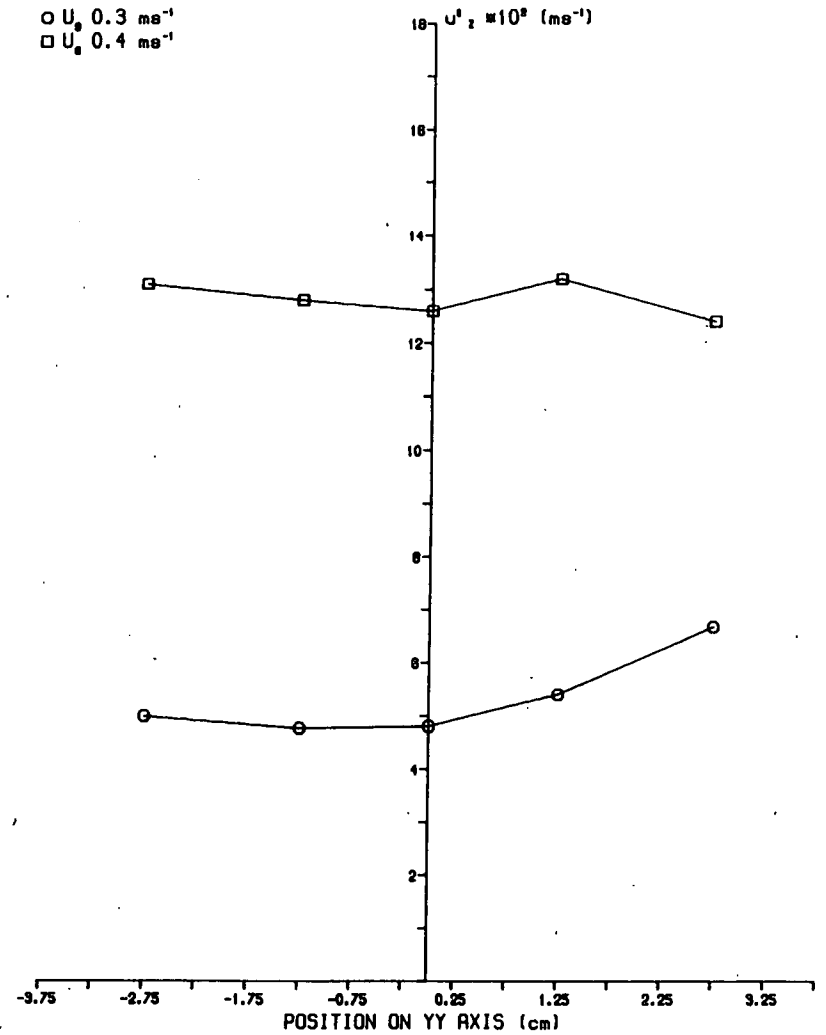
Figure 5.2.3 XX Profile of Average Vertical Velocity - Small Bed.
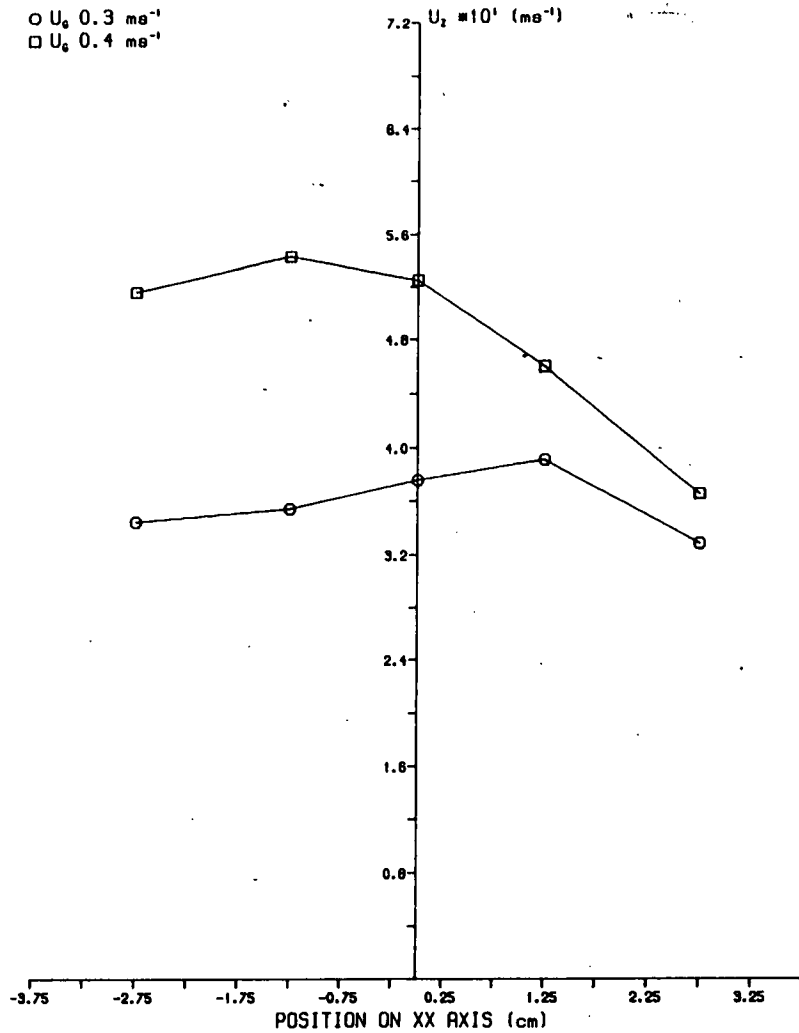
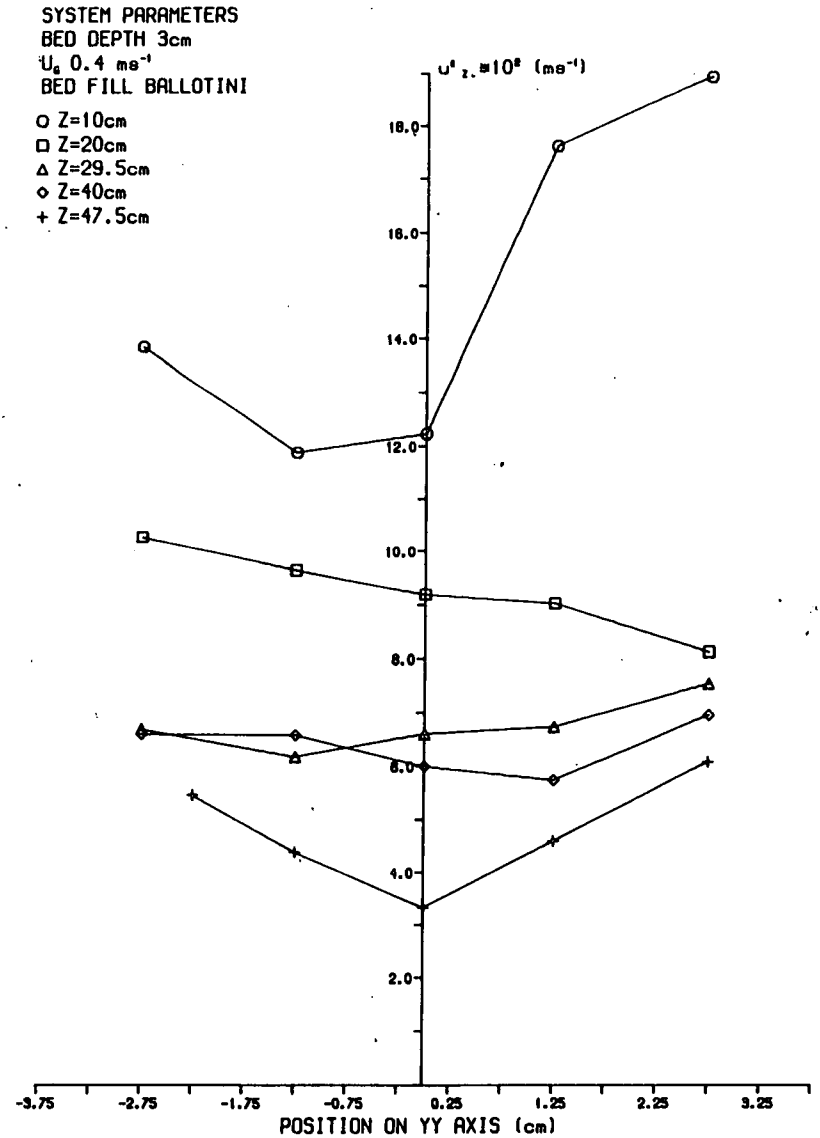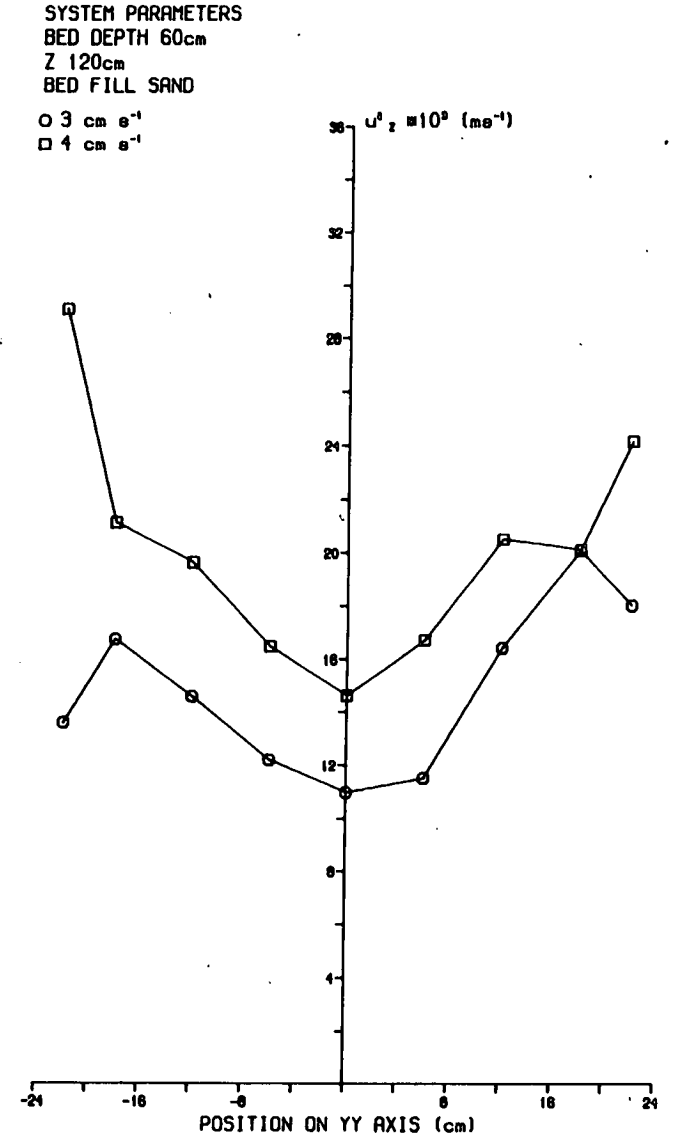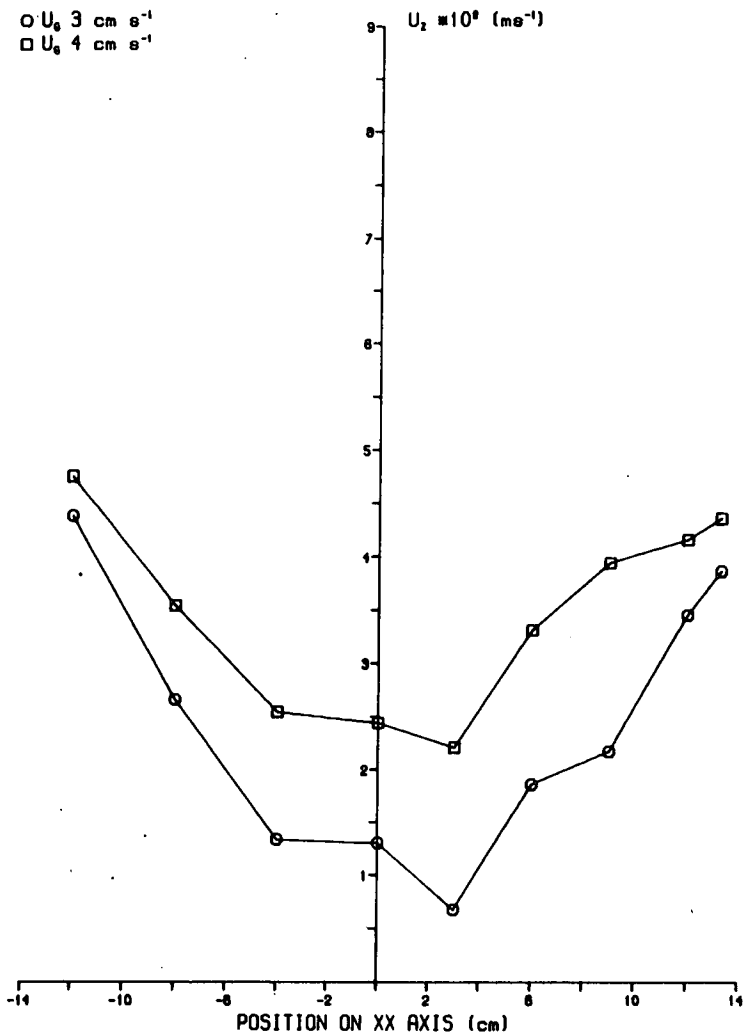Figure 5.2.4 XX Profile of rms Vertical Velocity Fluctuations - Small Bed.

SYSTEM PARAMETERS
BED DEPTH 5cm
Z=20cm
BED FILL BALLOTINI

o U_6 0.3 ms^{-1}
□ U_6 0.4 ms^{-1}

U_z ×10^1 (ms^{-1})

POSITION ON XX AXIS (cm)

SYSTEM PARAMETERS
BED DEPTH 5cm
Z=20cm
BED FILL BALLOTINI

o U_6 0.3 ms^{-1}
□ U_6 0.4 ms^{-1}

u'_z ×10^2 (ms^{-1})

POSITION ON XX AXIS (cm)

122
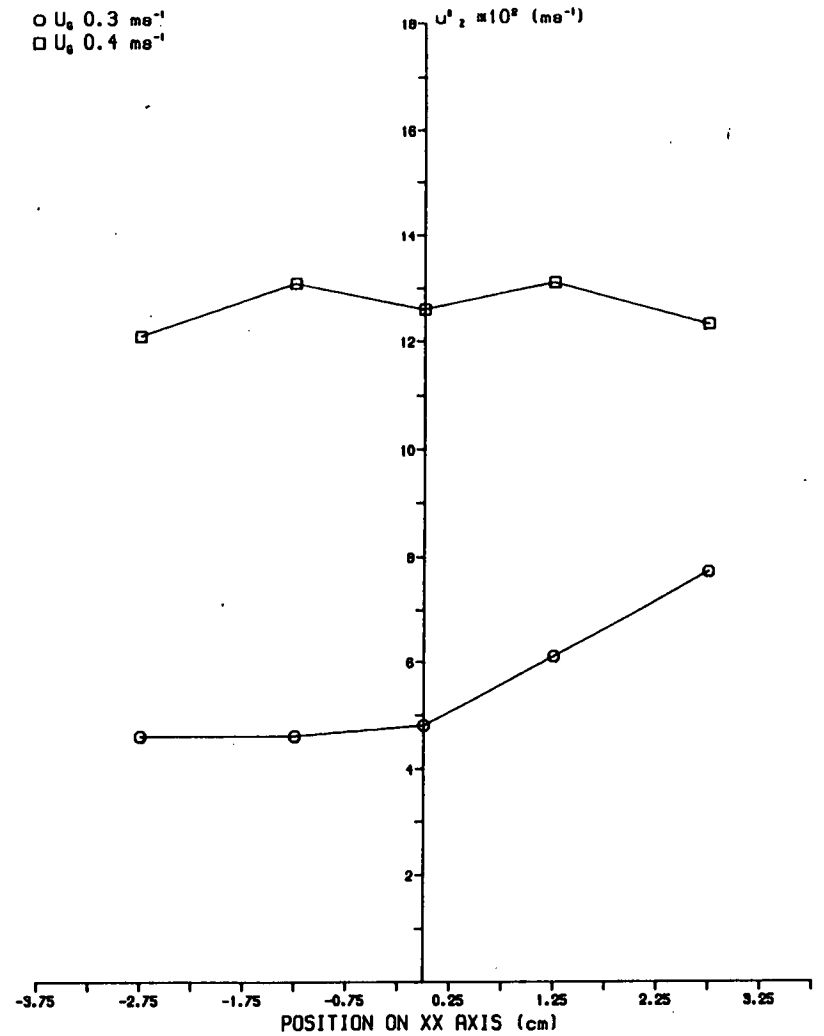
Figure 5.2.5 YY Profile of Average Vertical Velocity - Small Bed.

SYSTEM PARAMETERS
BED DEPTH 3cm
Z=10cm
BED FILL BALLOTINI

o U_G 0.3 ms^{-1}
□ U_G 0.4 ms^{-1}

U_z ×10^1 (ms^{-1})

POSITION ON YY AXIS (cm)
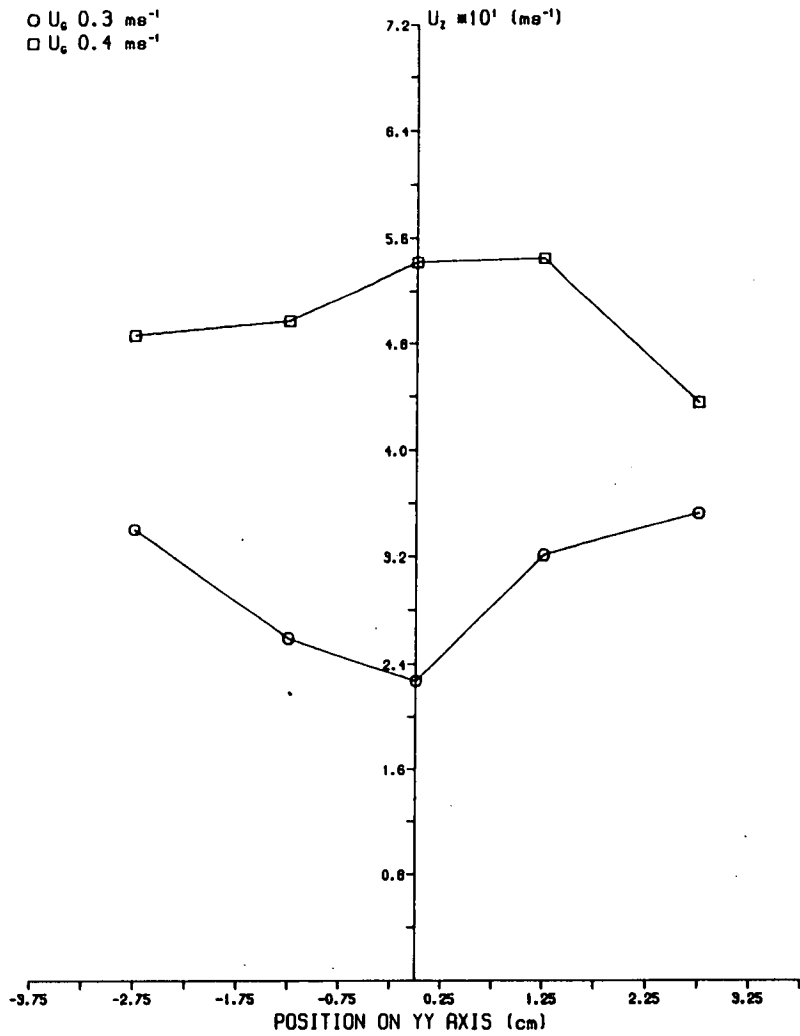
Figure 5.2.6 XX Profile of Average Vertical Velocity - Small Bed.

SYSTEM PARAMETERS
BED DEPTH 3cm
Z=10cm
BED FILL BALLOTINI

o U_G 0.3 ms^{-1}
□ U_G 0.4 ms^{-1}

U_z ×10^1 (ms^{-1})

POSITION ON XX AXIS (cm)

123

Figure 5.2.7 YY Profile of rms Vertical Velocity
Fluctuations - Small Bed.

SYSTEM PARAMETERS
U_G 0.4 ms^{-1}
Z=20cm
BED FILL BALLOTINI

o BED DEPTH 3cm
□ BED DEPTH 5cm

Figure 5.2.8 YY Profile of Average Vertical Velocity - Small Bed.

SYSTEM PARAMETERS
BED DEPTH 5cm
U_g 0.4 ms^{-1}
BED FILL BALLOTINI

o Z=20cm
□ Z=29.5cm
△ Z=40cm
◇ Z=47.5cm

U_z ×10^1 (ms^{-1})

POSITION ON YY AXIS (cm)

Figure 5.2.9 YY Profile of rms Vertical Velocity Fluctuations - Small Bed.

SYSTEM PARAMETERS
BED DEPTH 5cm
U_g 0.4 ms^{-1}
BED FILL BALLOTINI

o Z=20cm
□ Z=29.5cm
△ Z=40cm
◇ Z=47.5cm

U'_z ×10^2 (ms^{-1})

POSITION ON YY AXIS (cm)
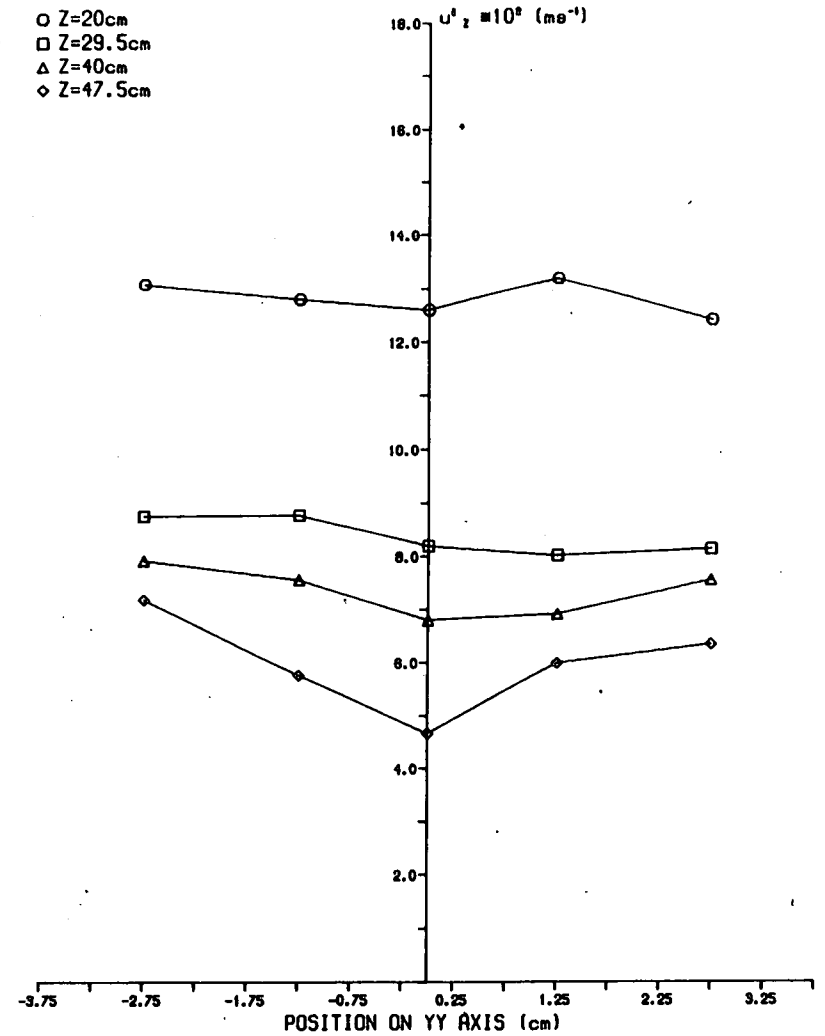
Figure 5.2.10 YY Profile of Average Vertical Velocity – Small Bed.

SYSTEM PARAMETERS
BED DEPTH 3cm
U_a 0.3 ms^{-1}
BED FILL BALLOTINI

O Z=10cm
□ Z=20cm
△ Z=29.5cm
◇ Z=40cm
+ Z=47.5cm

U_z ≈10^1 (ms^{-1})

POSITION ON YY AXIS (cm)
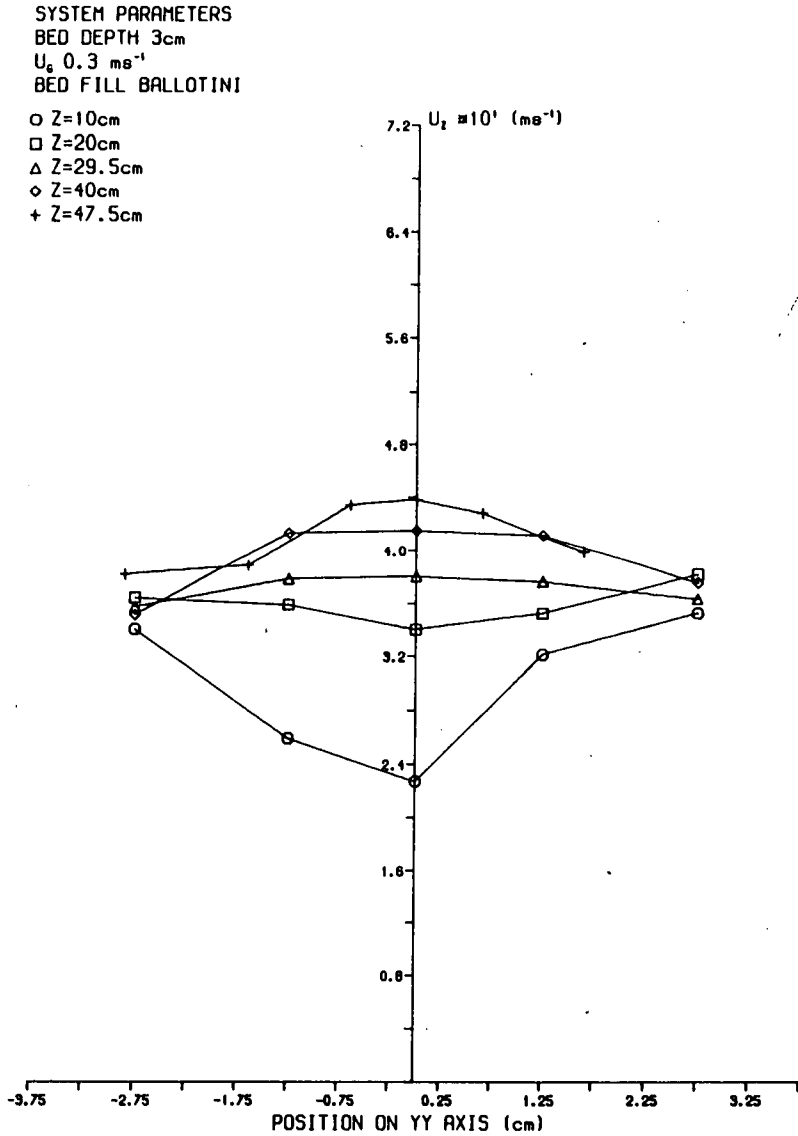
Figure 5.2.11 YY Profile of rms Vertical Velocity Fluctuations – Small Bed.

SYSTEM PARAMETERS
BED DEPTH 3cm
U_a 0.4 ms^{-1}
BED FILL BALLOTINI

O Z=10cm
□ Z=20cm
△ Z=29.5cm
◇ Z=40cm
+ Z=47.5cm

u'_z ≈10^2 (ms^{-1})

POSITION ON YY AXIS (cm)

126

Figure 5.3.1 YY Profile of Average Vertical Velocity - Large
Bed.

SYSTEM PARAMETERS
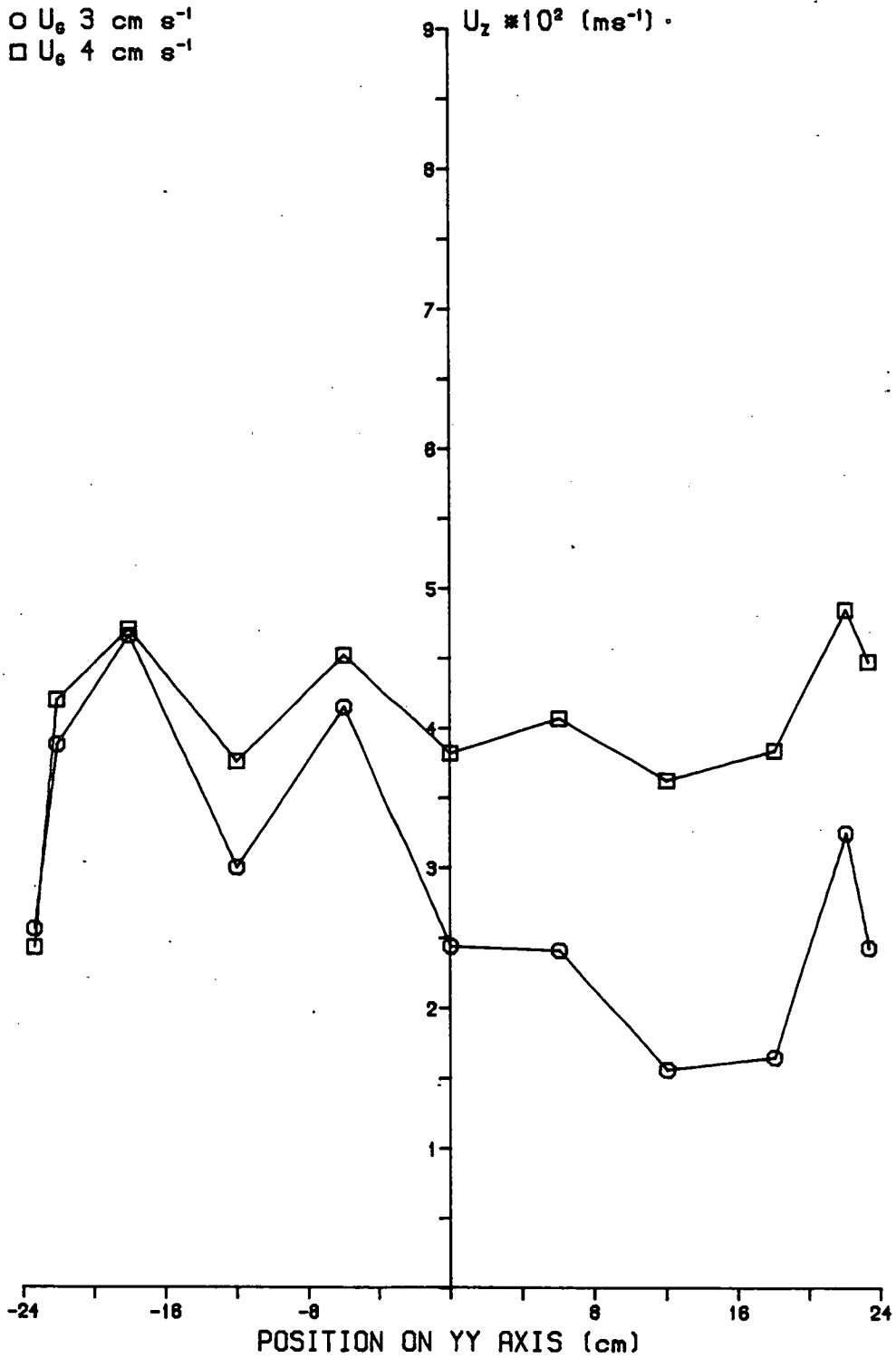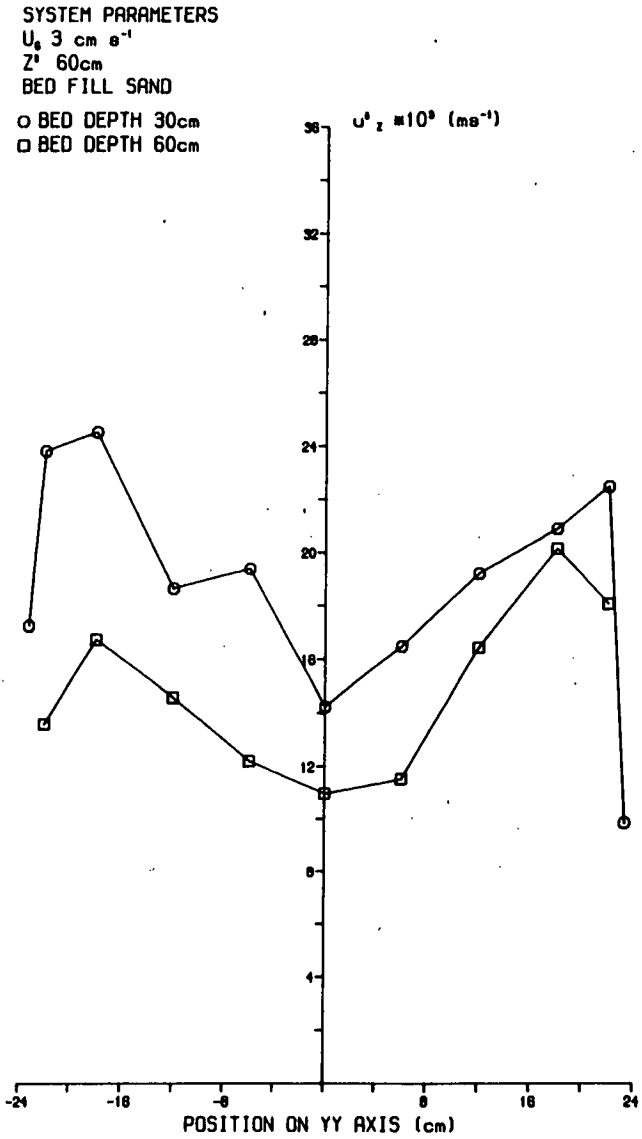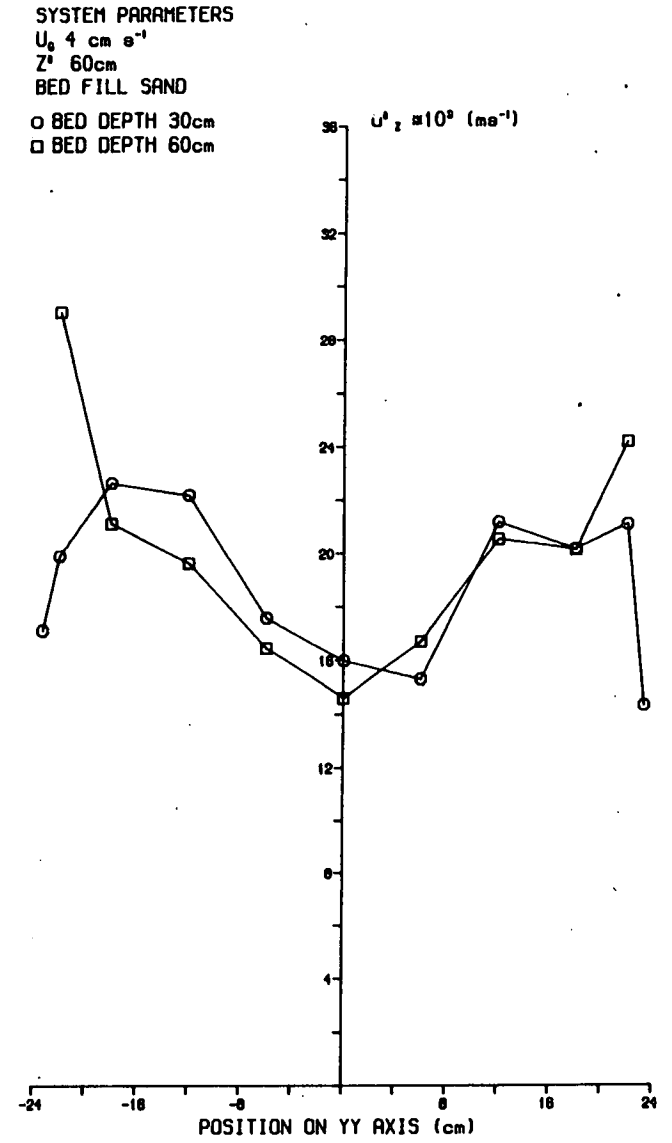BED DEPTH 60cm
Z 120cm
BED FILL SAND
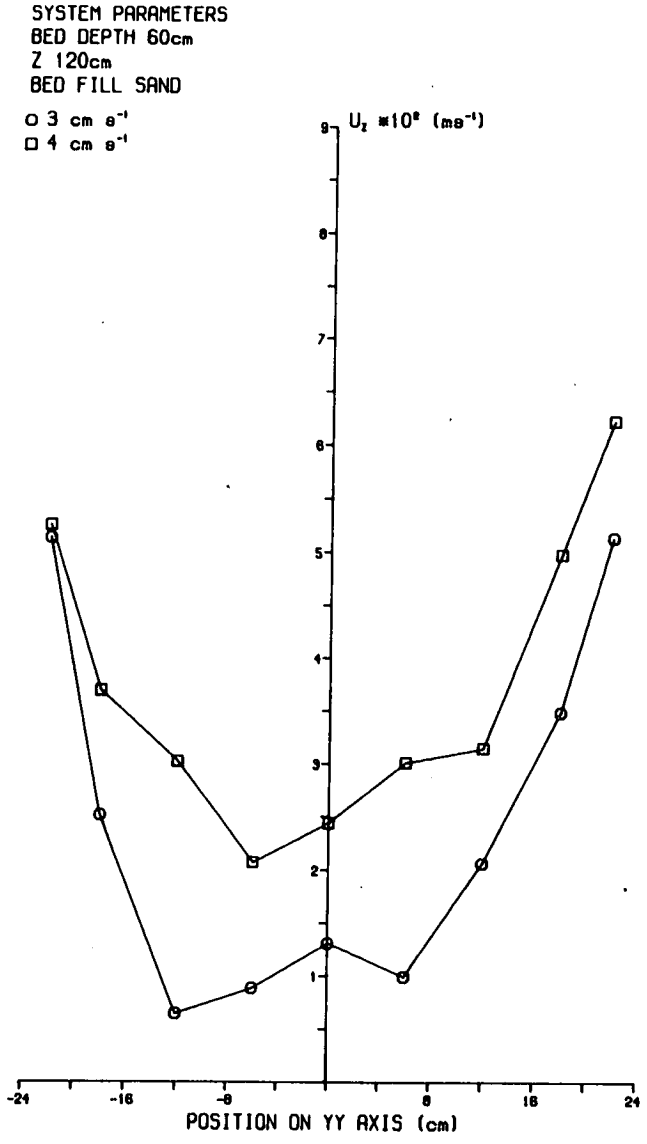
O 3 cm s^{-1}
□ 4 cm s^{-1}

Figure 5.3.2 YY Profile of rms Vertical Velocity
Fluctuations - Large Bed.

SYSTEM PARAMETERS
BED DEPTH 60cm
Z 120cm
BED FILL SAND

O 3 cm s^{-1}
□ 4 cm s^{-1}

Figure 5.3.3 XX Profile of Average Vertical Velocity - Large Bed.

SYSTEM PARAMETERS
BED DEPTH 60cm
Z 120cm
BED FILL SAND

○ U_s 3 cm s^{-1}
□ U_s 4 cm s^{-1}

U_z ×10^8 (ms^{-1})

POSITION ON XX AXIS (cm)

Figure 5.3.4 XX Profile of rms Vertical Velocity Fluctuations - Large Bed.

SYSTEM PARAMETERS
BED DEPTH 60cm
Z 120cm
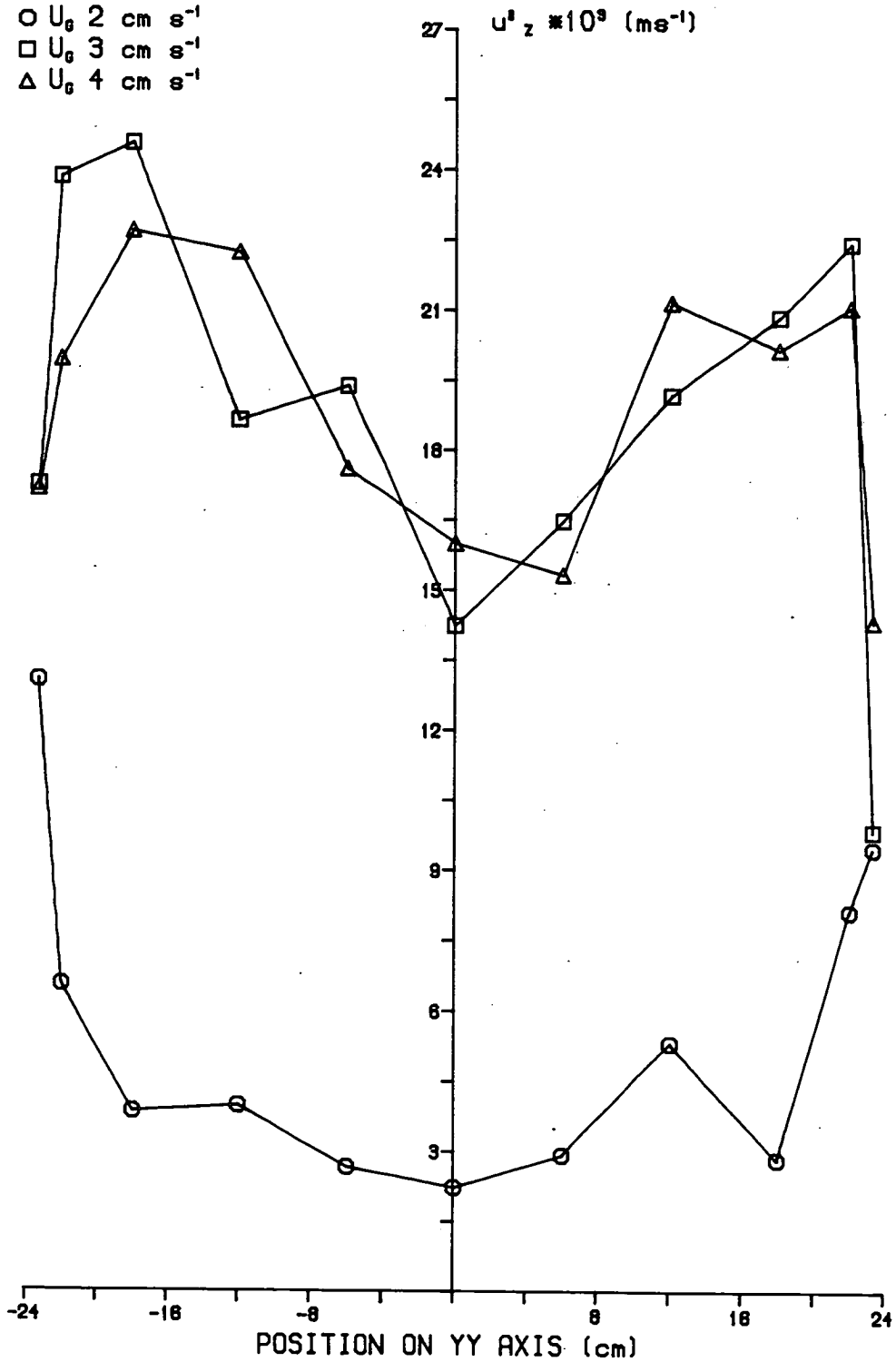BED FILL SAND

○ U_s 3 cm s^{-1}
□ U_s 4 cm s^{-1}

u'_z ×10^9 (ms^{-1})

POSITION ON XX AXIS (cm)

128
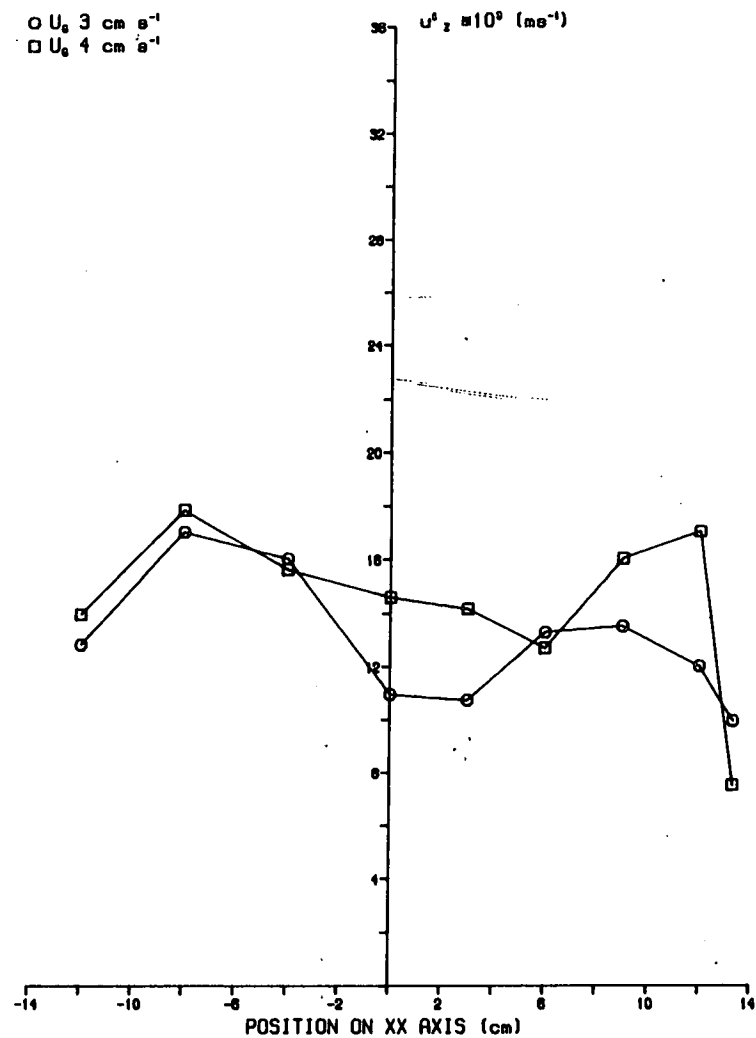
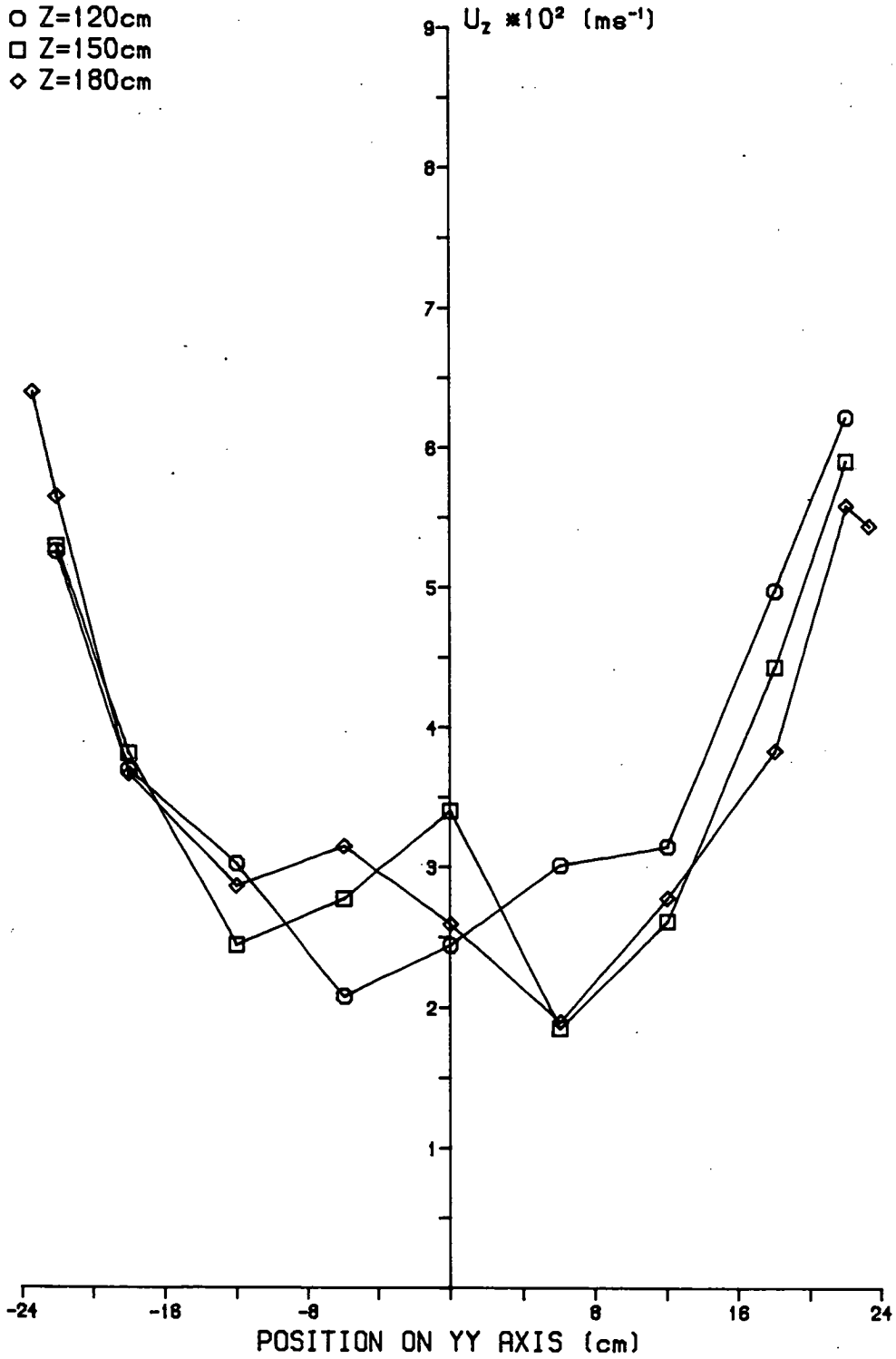Figure 5.3.5 YY Profile of rms Vertical Velocity Fluctuations – Large Bed.
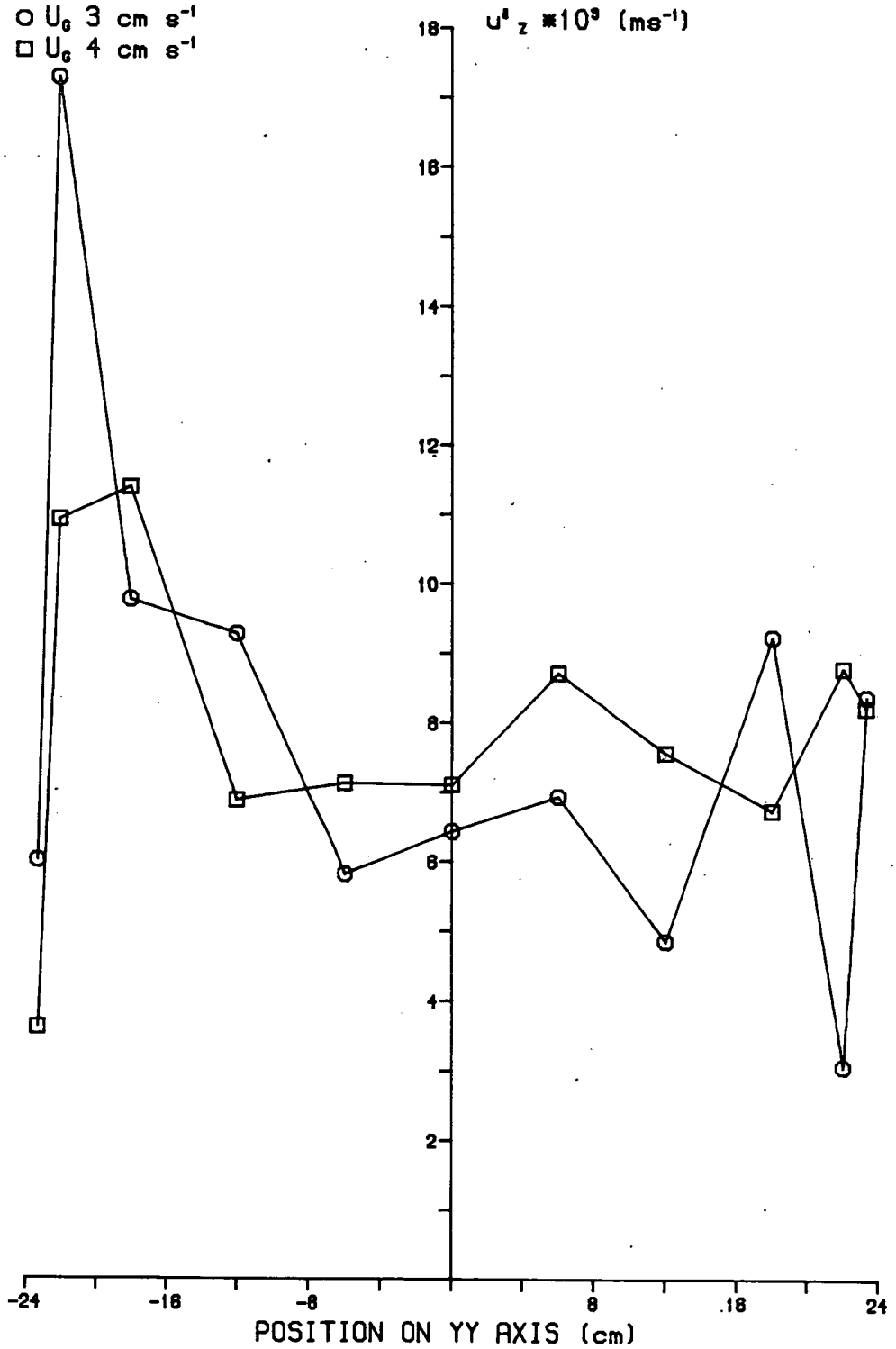
Figure 5.3.6 YY Profile of Average Vertical Velocity - Large Bed.

SYSTEM PARAMETERS
BED DEPTH 30cm
Z' 60cm
BED FILL SAND

o U_G 3 cm s^{-1}
□ U_G 4 cm s^{-1}

U_z *10² (ms⁻¹)

POSITION ON YY AXIS (cm)

Figure 5.3.7 YY Profile of rms Vertical Velocity
Fluctuations - Large Bed.

SYSTEM PARAMETERS
U_6 3 cm s⁻¹
Z' 60cm
BED FILL SAND

O BED DEPTH 30cm
□ BED DEPTH 60cm

POSITION ON YY AXIS (cm)

Figure 5.3.8 YY Profile of rms Vertical Velocity
Fluctuations - Large Bed.

SYSTEM PARAMETERS
U_6 4 cm s⁻¹
Z' 60cm
BED FILL SAND

O BED DEPTH 30cm
□ BED DEPTH 60cm

POSITION ON YY AXIS (cm)

Figure 5.3.9 YY Profile of rms Vertical Velocity
Fluctuations - Large Bed.

SYSTEM PARAMETERS
BED DEPTH 30cm
Z' 60cm
BED FILL SAND

O U_G 2 cm s^{-1}
□ U_G 3 cm s^{-1}
△ U_G 4 cm s^{-1}

u'_z $*10^3$ (ms^{-1})

POSITION ON YY AXIS (cm)

132

Figure 5.3.10 YY Profile of Average Vertical Velocity –
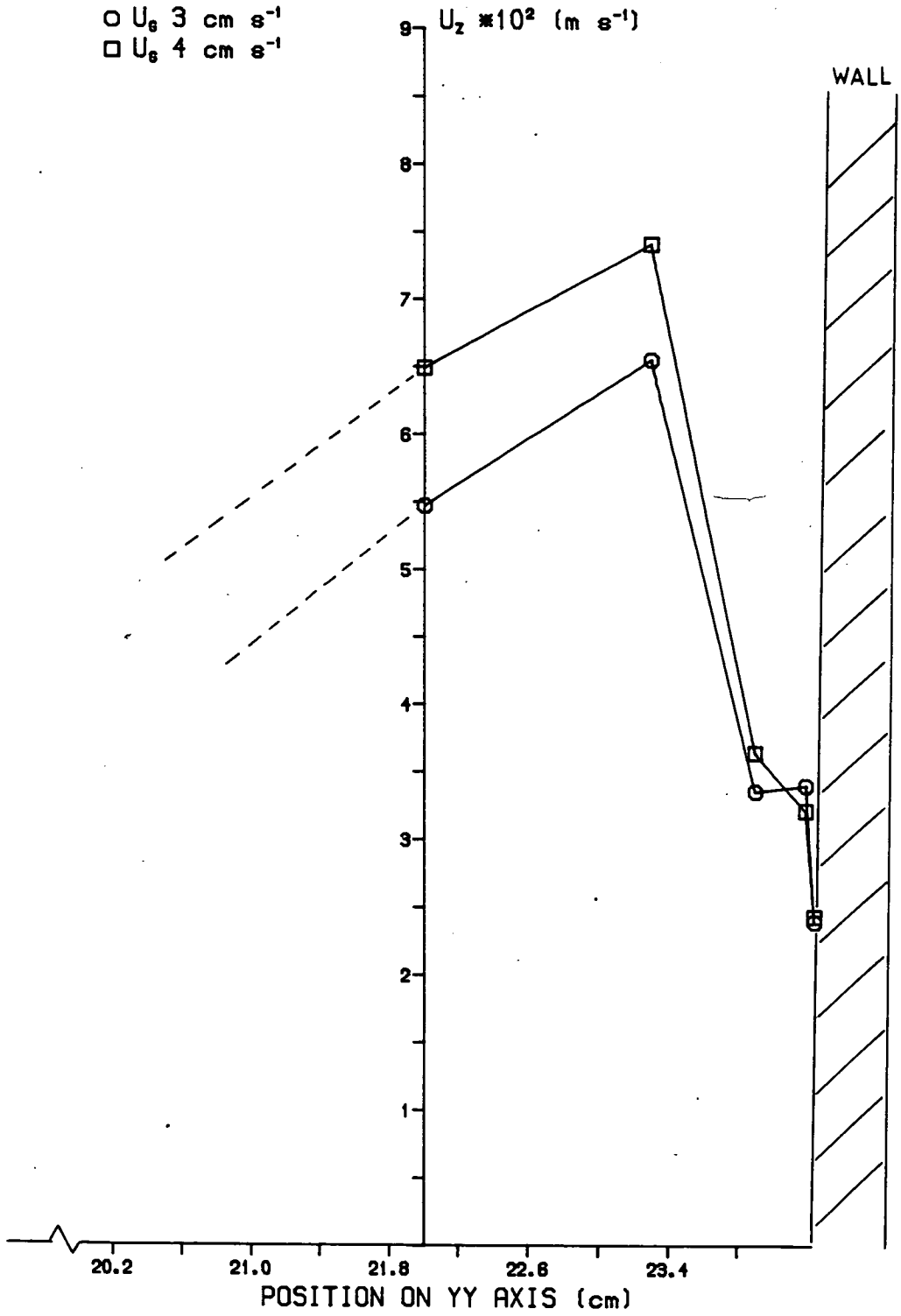Large Bed.

SYSTEM PARAMETERS
BED DEPTH 60cm
U_G 4 cm s^{-1}
BED FILL SAND

o Z=120cm
□ Z=150cm
◇ Z=180cm

Figure 5.3.11 YY Profile of Average Vertical Velocity – Large Bed.

SYSTEM PARAMETERS
BED DEPTH 30cm
U_g 3 cm s^{-1}
BED FILL SAND

O Z=180cm
□ Z=150cm
◇ Z=120cm
△ Z=90cm

U_z $*10^2$ (ms^{-1})

POSITION ON YY AXIS (cm)
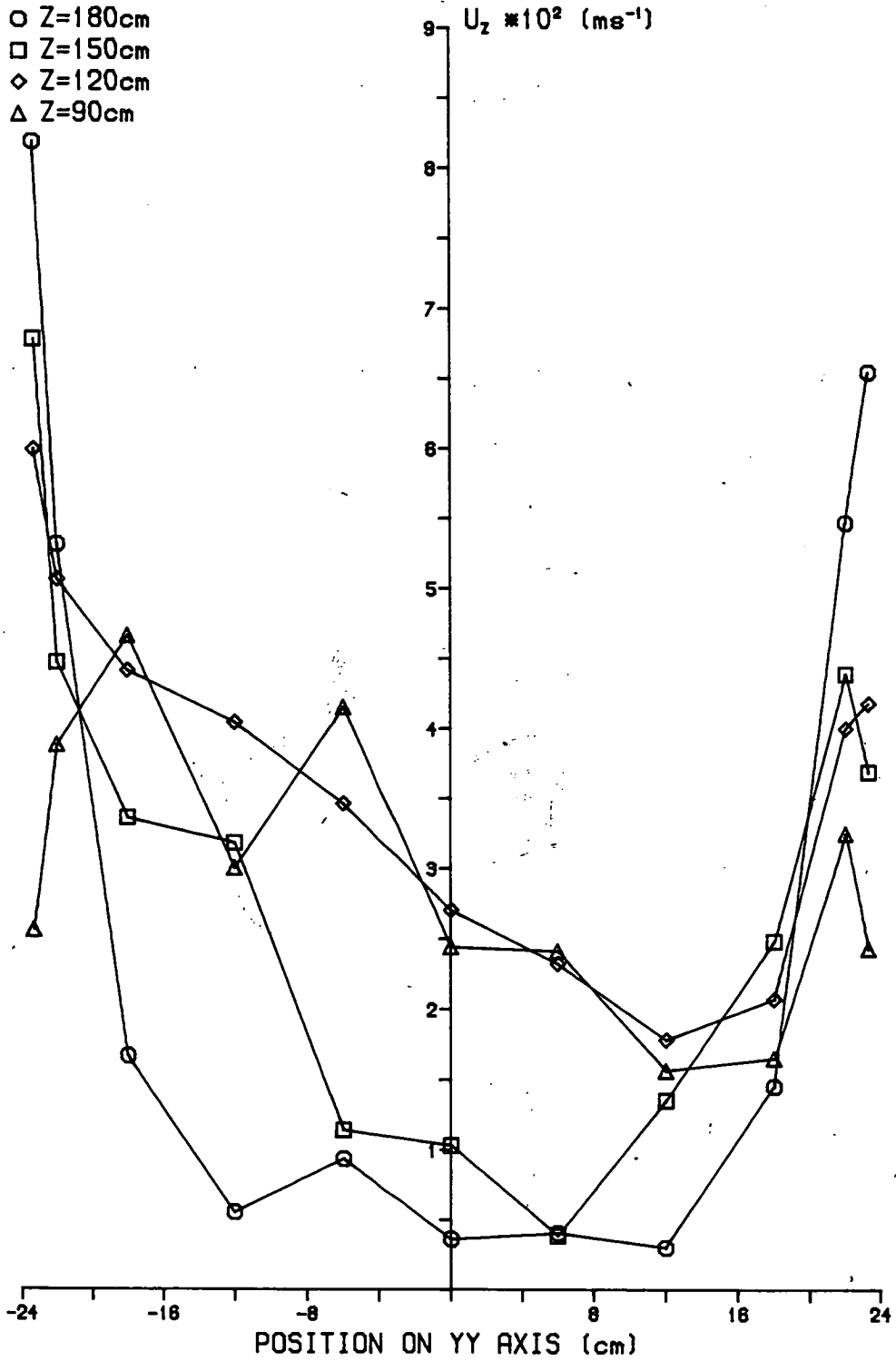
4 cm

Observation Port for Large Bed.
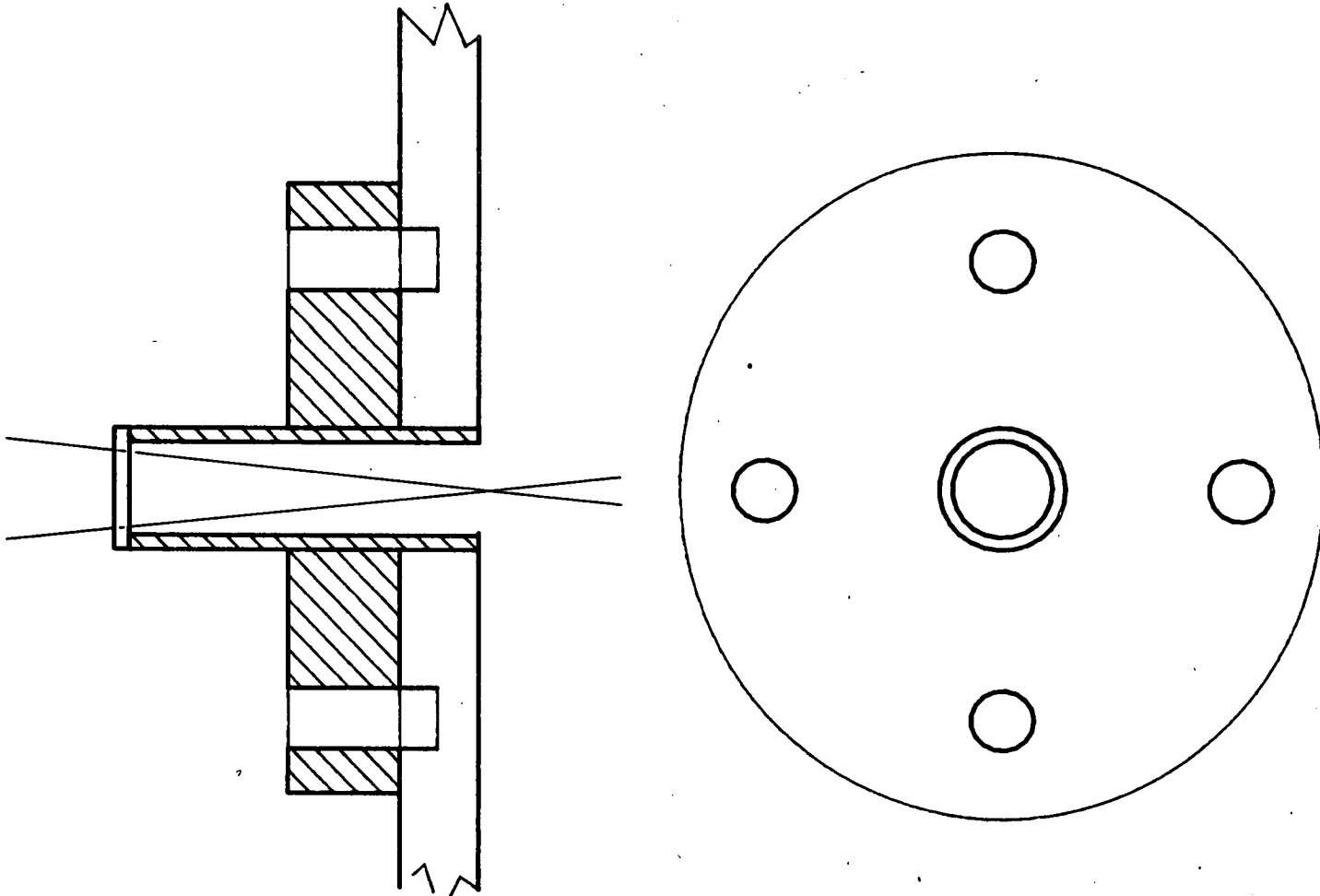
Figure 5.3.12

Figure 5.3.13 YY Average Vertical Velocity Profile for Large
Bed with Observation Port.

SYSTEM PARAMETERS
BED DEPTH 30cm
Z 180cm
BED FILL SAND

o U_6 3 cm s^{-1}
□ U_6 4 cm s^{-1}

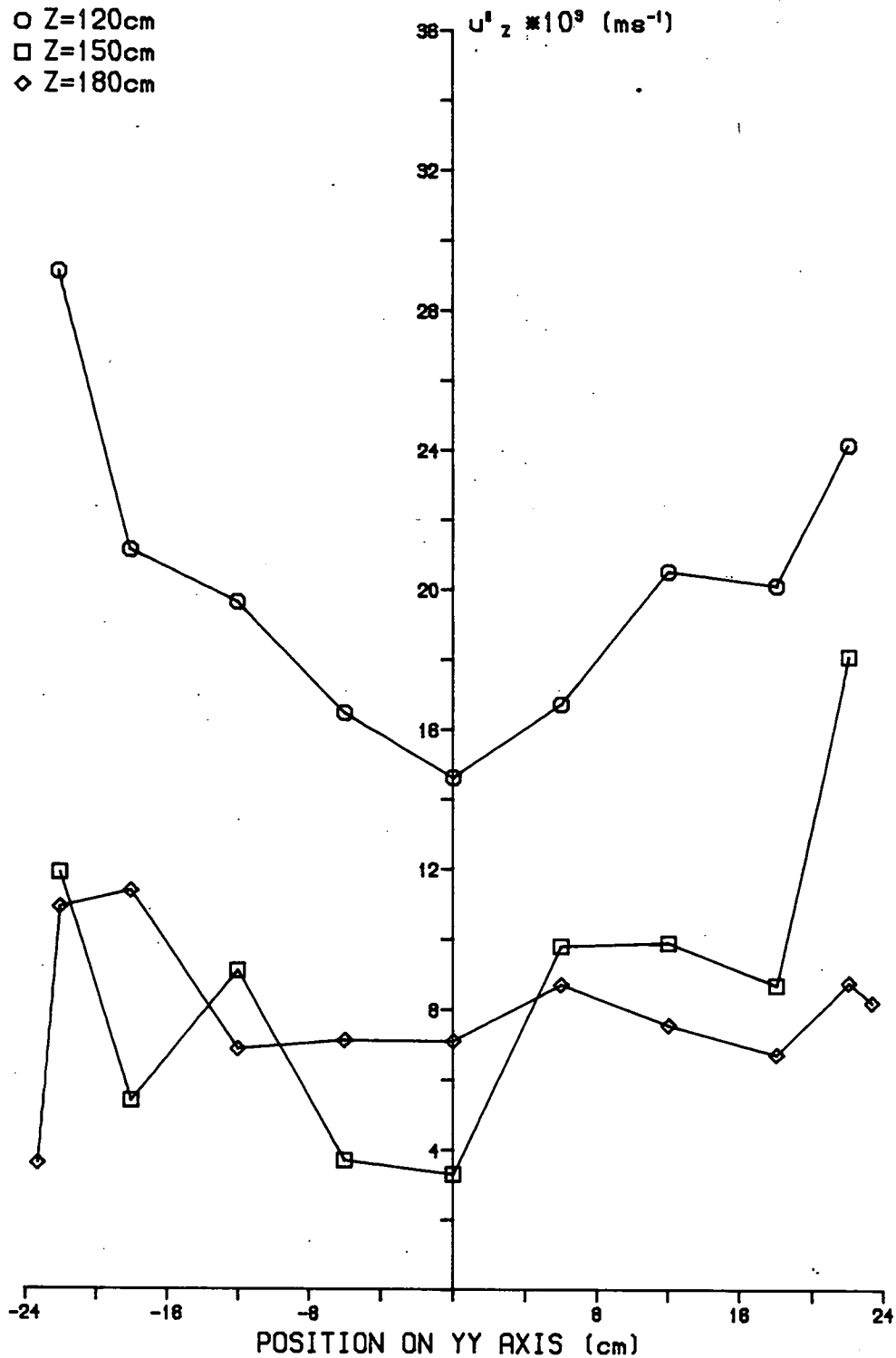U_z *10^2 (m s^{-1})

WALL

POSITION ON YY AXIS (cm)

Figure 5.3.14 YY Profile of rms Vertical Velocity Fluctuations - Large Bed.

SYSTEM PARAMETERS
BED DEPTH 60cm
U_G 4 cm s^{-1}
BED FILL SAND

O Z=120cm
□ Z=150cm
◇ Z=180cm

$u^s{}_z$ *10^3 (ms^{-1})

POSITION ON YY AXIS (cm)

137

Figure 5.3.15 YY Profile of rms Vertical Velocity Fluctuations - Large Bed.

SYSTEM PARAMETERS
BED DEPTH 30cm
U_G 3 cm s^{-1}
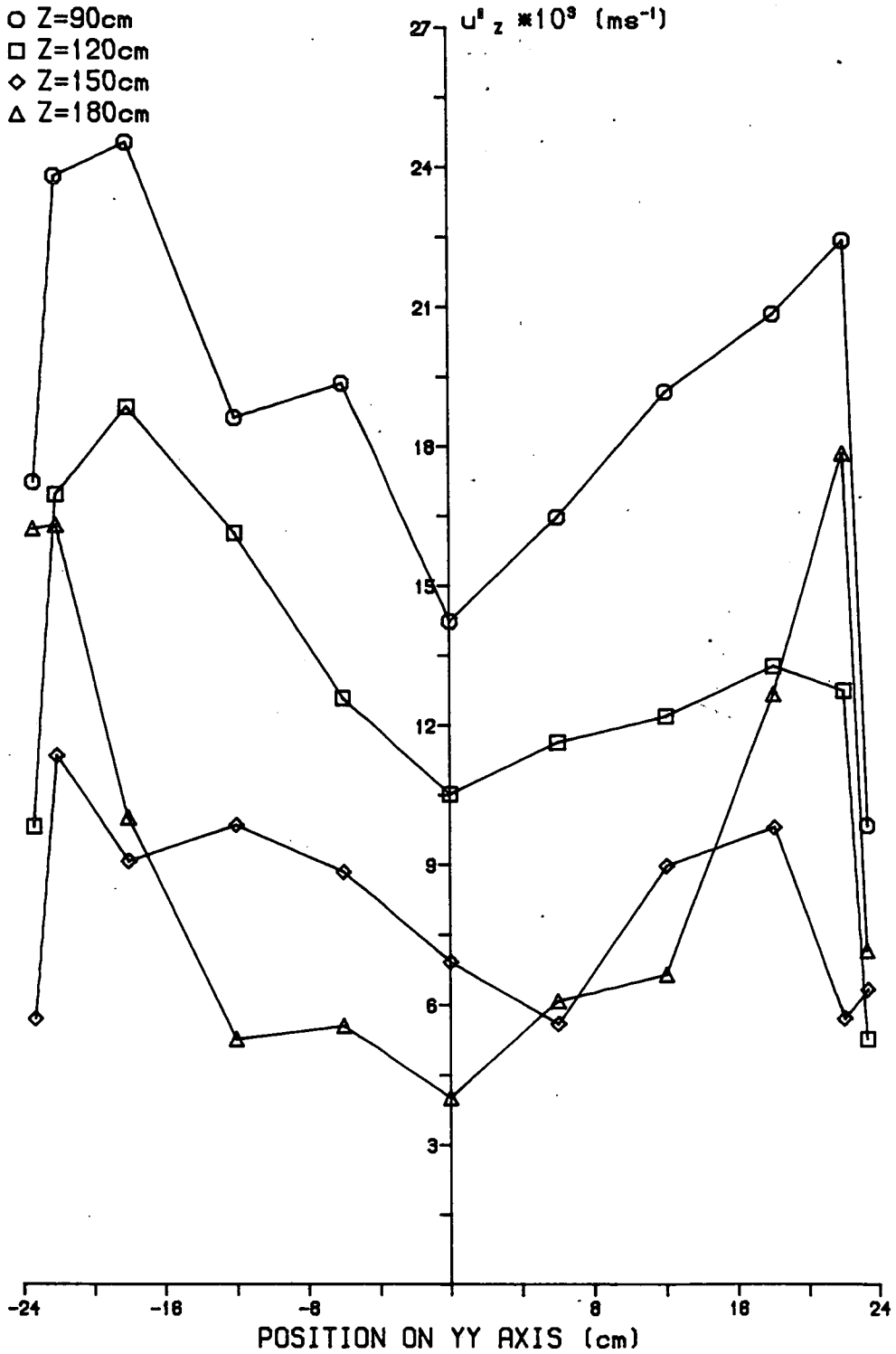BED FILL SAND

O Z=90cm
□ Z=120cm
◇ Z=150cm
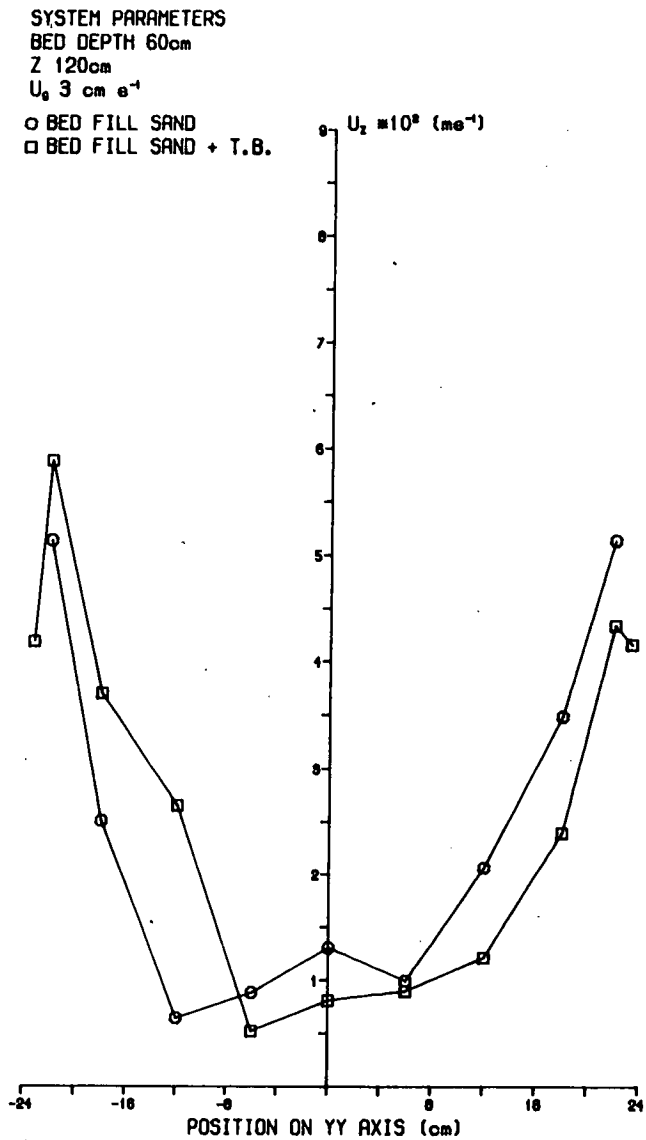△ Z=180cm

$u''_z *10^3$ (ms^{-1})

POSITION ON YY AXIS (cm)

Figure 5.3.16 YY Profile of Average Vertical Velocity – Large Bed.

Figure 5.3.17 YY Profile of Average Vertical Velocity – Large Bed.

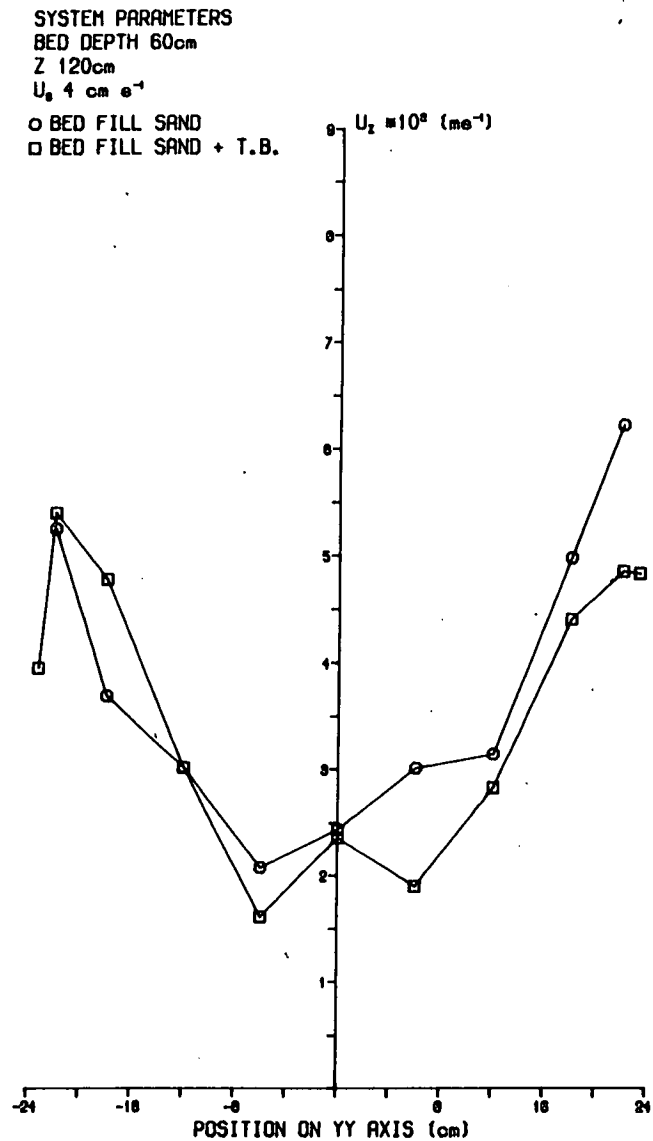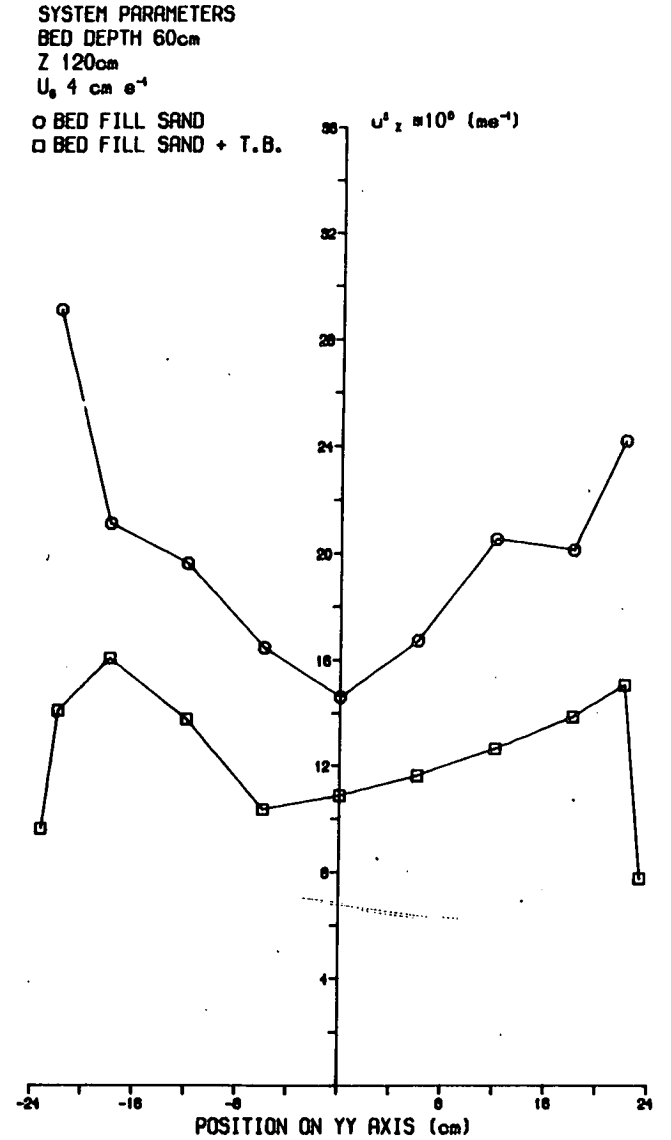SYSTEM PARAMETERS
BED DEPTH 60cm
Z 120cm
U_e 3 cm e⁻¹

o BED FILL SAND
□ BED FILL SAND + T.B.

U_z *10² (me⁻¹)

POSITION ON YY AXIS (cm)

SYSTEM PARAMETERS
BED DEPTH 60cm
Z 120cm
U_e 4 cm e⁻¹

o BED FILL SAND
□ BED FILL SAND + T.B.

U_z *10² (me⁻¹)

POSITION ON YY AXIS (cm)

Figure 5.3.18 YY Profile of rms Vertical Velocity
Fluctuations - Large Bed.

SYSTEM PARAMETERS
BED DEPTH 60cm
Z 120cm
U_s 3 cm e^{-1}

o BED FILL SAND
□ BED FILL SAND + T.B.
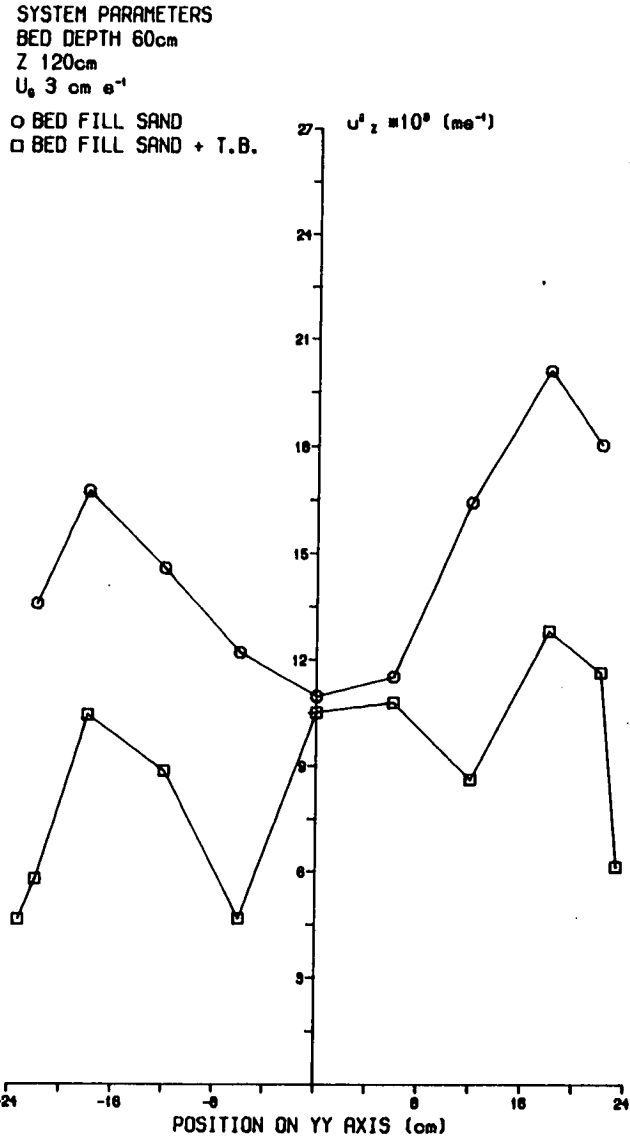
Figure 5.3.19 YY Profile of rms Vertical Velocity
Fluctuations - Large Bed.

SYSTEM PARAMETERS
BED DEPTH 60cm
Z 120cm
U_s 4 cm e^{-1}

o BED FILL SAND
□ BED FILL SAND + T.B.

Smoke Clearance from Freeboard of Large Sand Bed. Views at 5 sec. intervals, $U_G = 3$ cm s^{-1}.

A

Z 180cm

Z 150cm

Z 120cm

B

C

D

E

F

Figure 5.3.20

Figure 5.3.22 YY Average Vertical Velocity Profile with Partially Occluded Distributor.

SYSTEM PARAMETERS
BED DEPTH 60cm
Z 120cm
BED FILL SAND
$O\ U_a\ 3\ cm\ s^{-1}$

$U_z \times 10^2\ (ms^{-1})$

POSITION ON YY AXIS (cm)
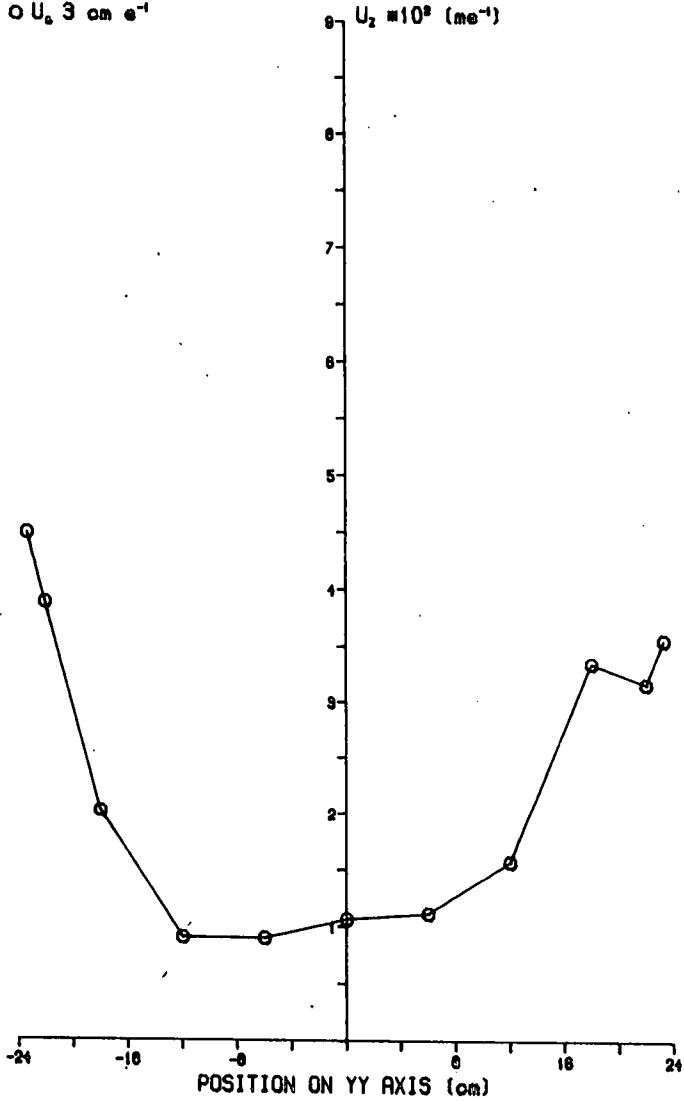
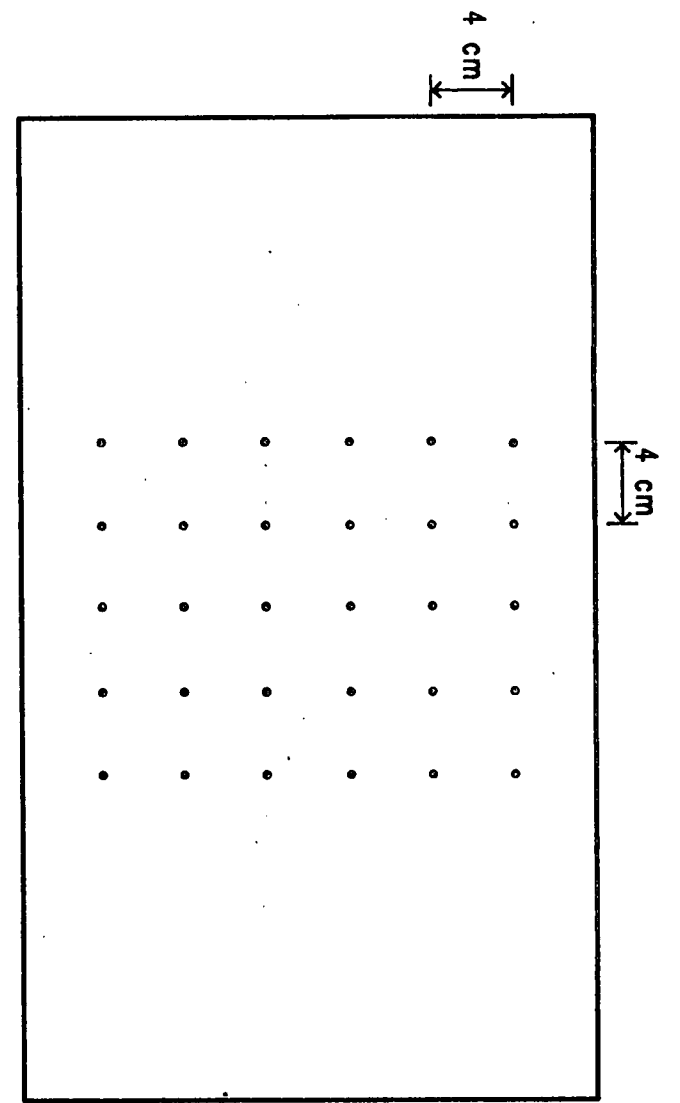Figure 5.3.21

Dimensions of Partially Occluded Distributor.

4 cm

4 cm

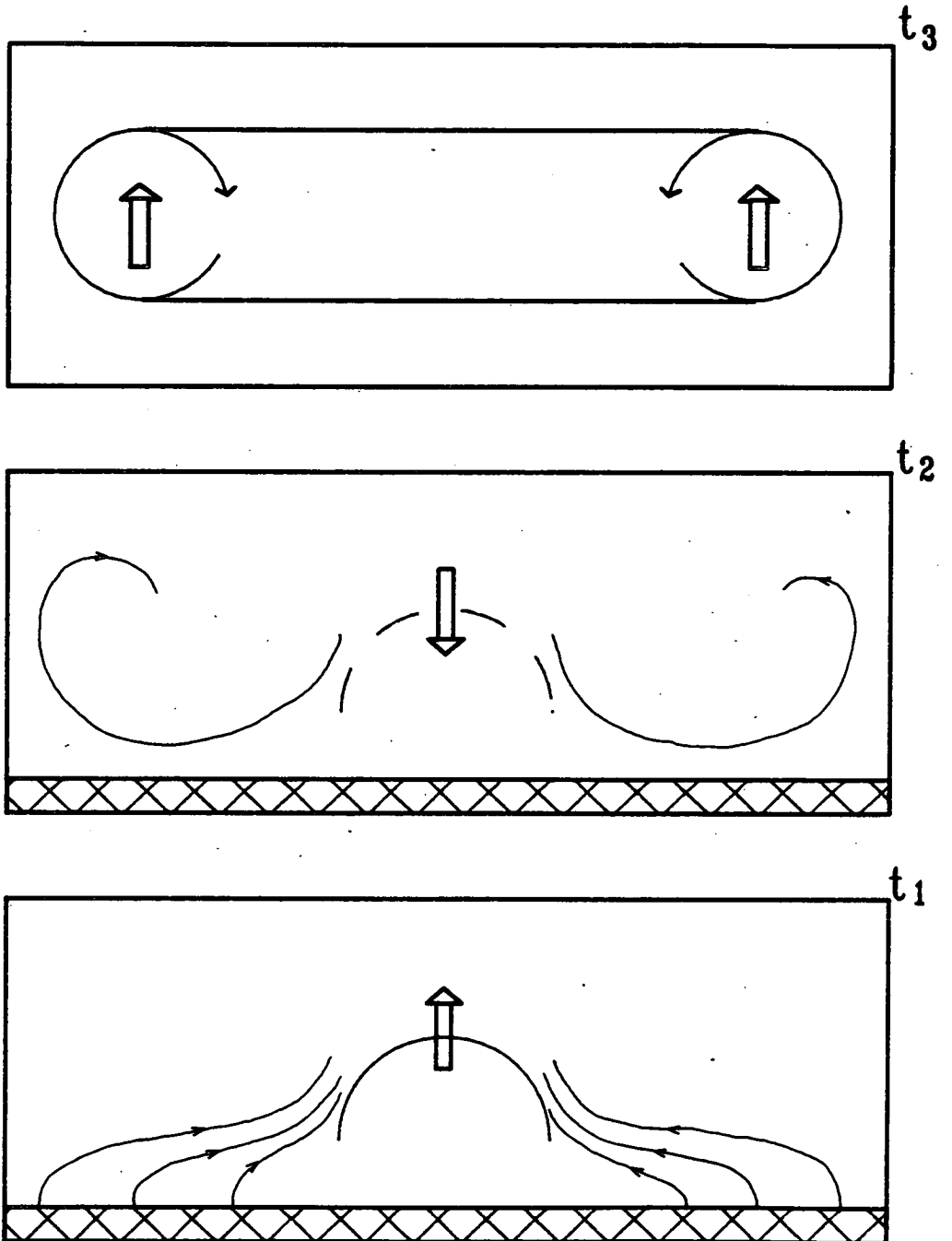Proposed Freeboard Gas Flow Pattern at Three Stages of Bubble Eruption.

Figure 5.3.23

(From Levy and Lockwood (42))

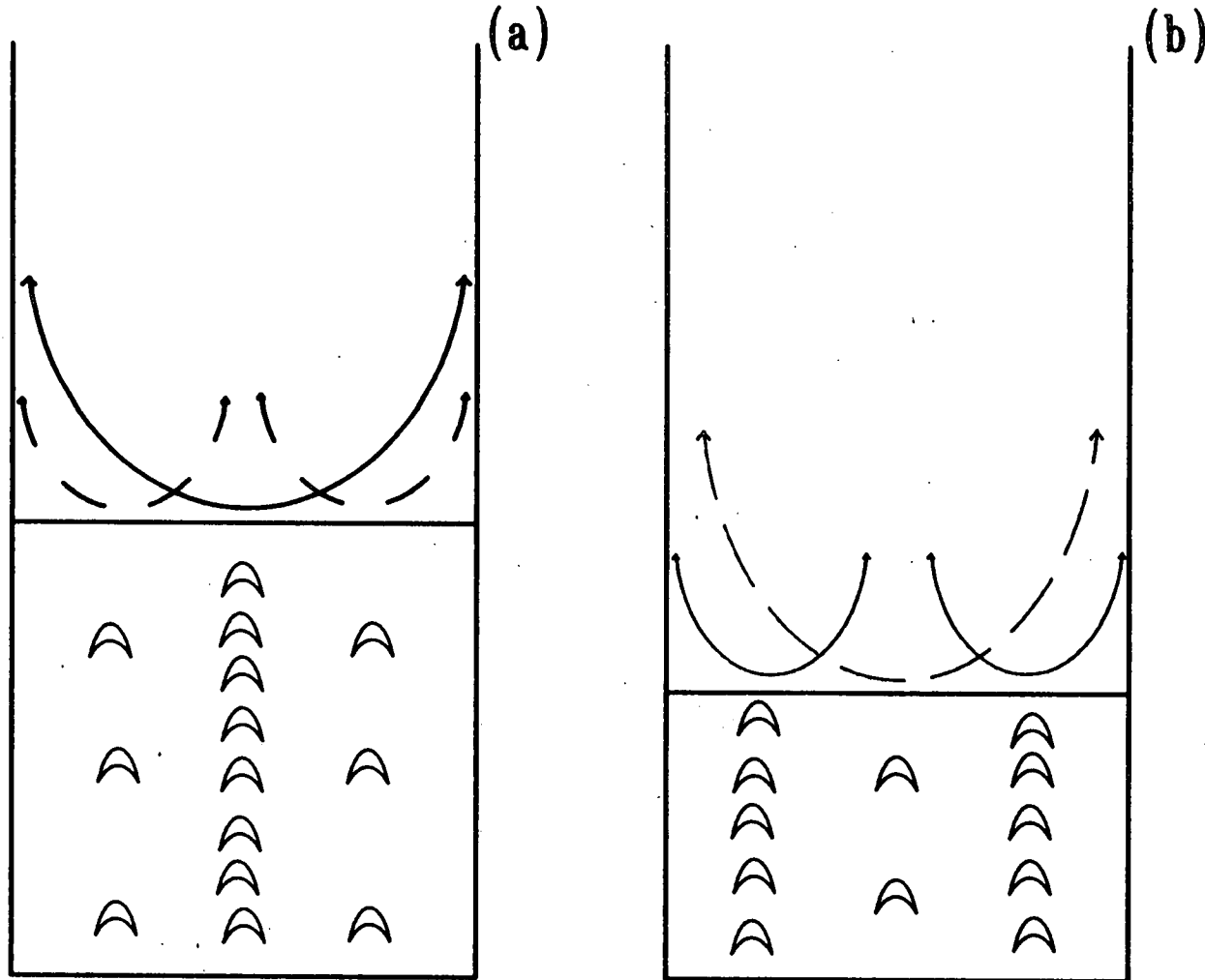Possible Gas Flow Patterns in Bed and Freeboard for (a) Deep, (b) Shallow Fluidised Beds.

Figure 5.3.24

Figure 5.3.25 Average Vertical Velocity Profiles Along and Parallel to YY Axis for Fluid Bed with Tube Bank Model.
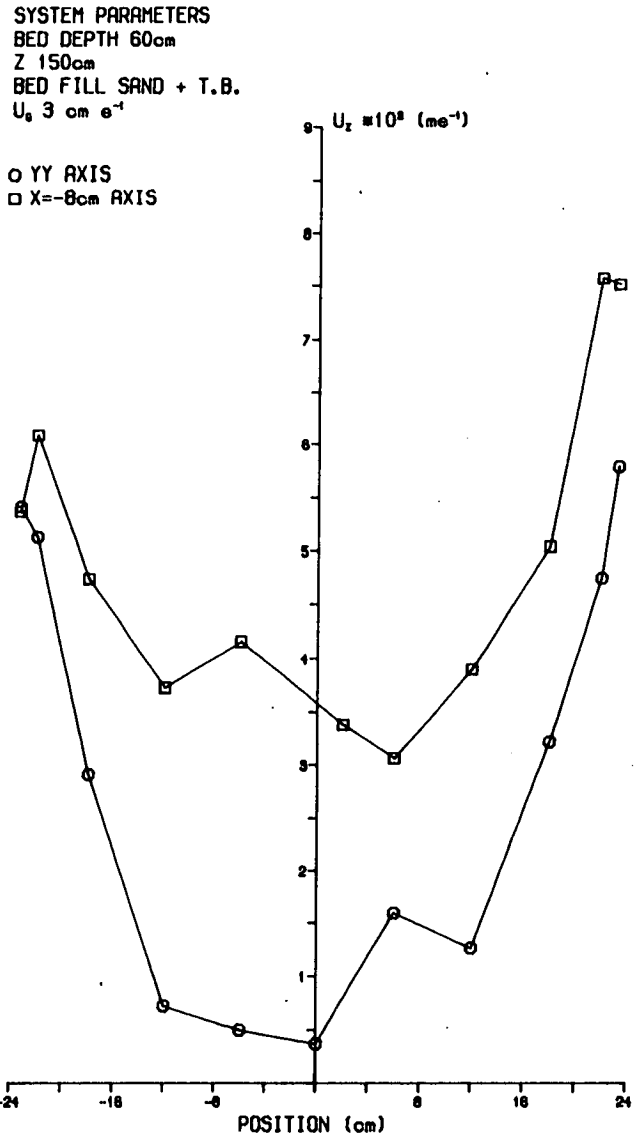

Figure 5.3.26 Average Vertical Velocity Profiles Along and Parallel to YY Axis for Fluid Bed with Tube Bank Model.
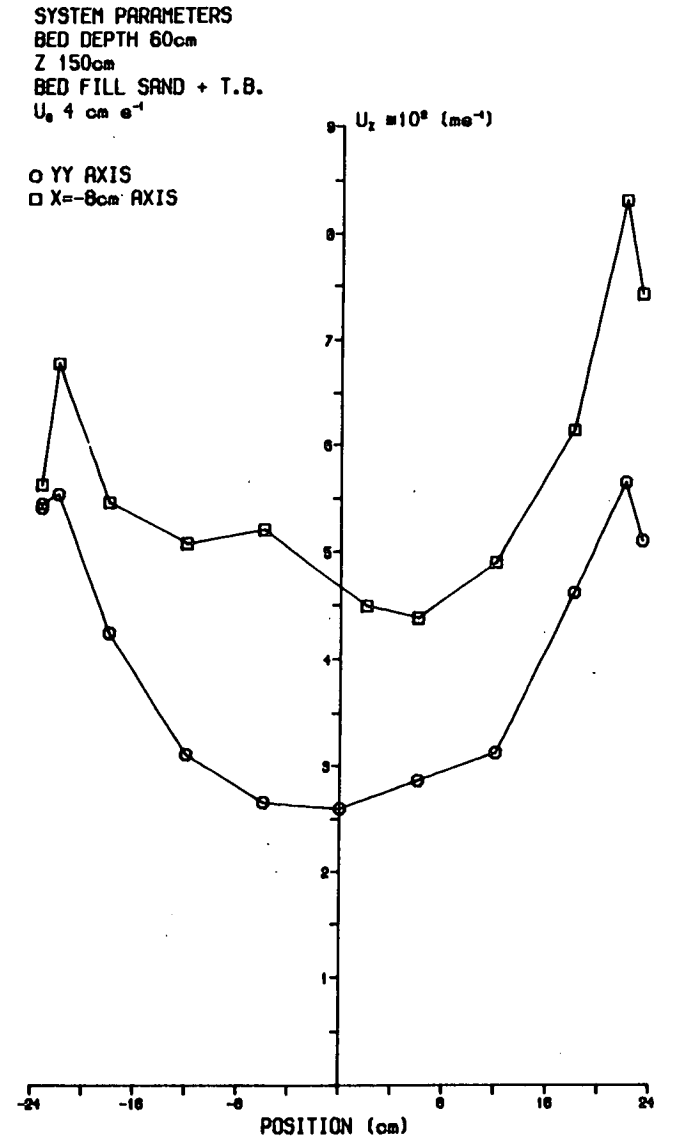
Figure 5.3.27 Profile of rms Vertical Velocity Fluctuations
Along and Parallel to YY Axis for Fluid Bed with Tube Bank
Model.

SYSTEM PARAMETERS
BED DEPTH 60cm
Z 150cm
BED FILL SAND + T.B.
U_0 3 cm e^{-1}

o YY AXIS
□ X=-8cm AXIS

u'_z #10^9 (me^{-1})

POSITION (cm)
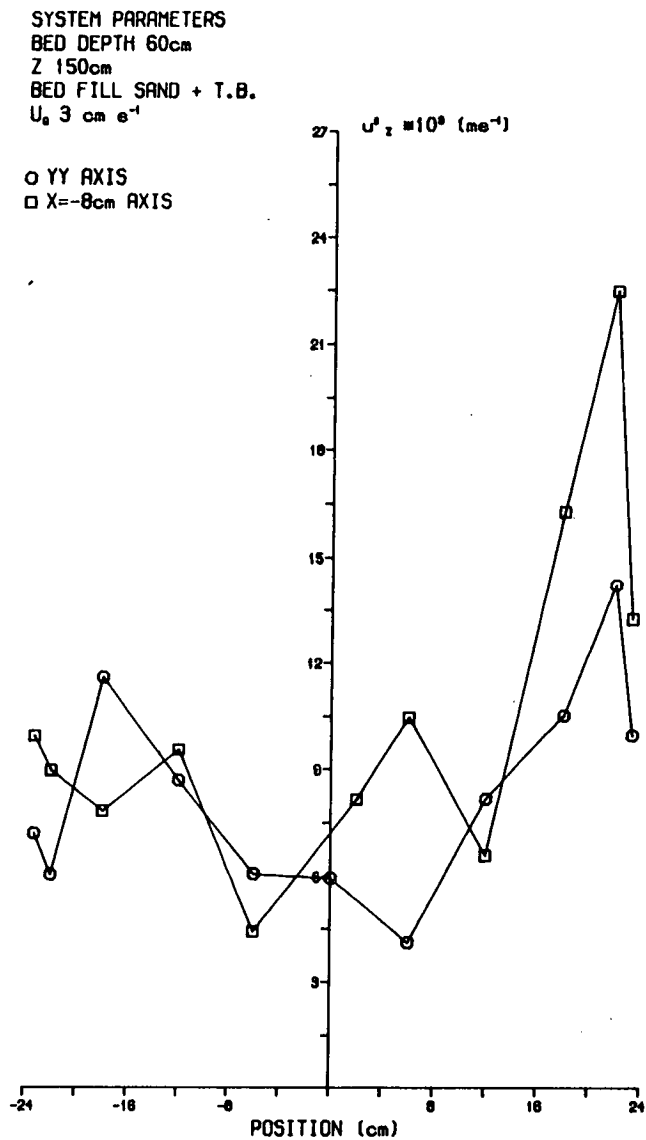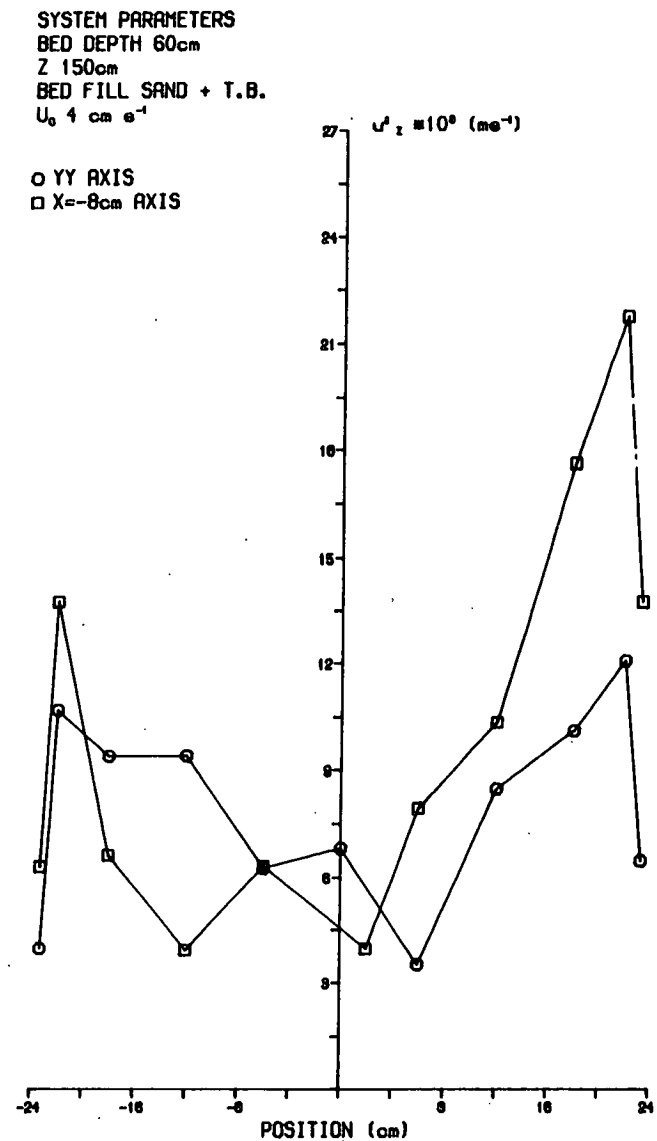
Figure 5.3.28 Profile of rms Vertical Velocity Fluctuations
Along and Parallel to YY Axis for Fluid Bed with Tube Bank
Model.

SYSTEM PARAMETERS
BED DEPTH 60cm
Z 150cm
BED FILL SAND + T.B.
U_0 4 cm e^{-1}

o YY AXIS
□ X=-8cm AXIS

u'_z #10^9 (me^{-1})

POSITION (cm)

146
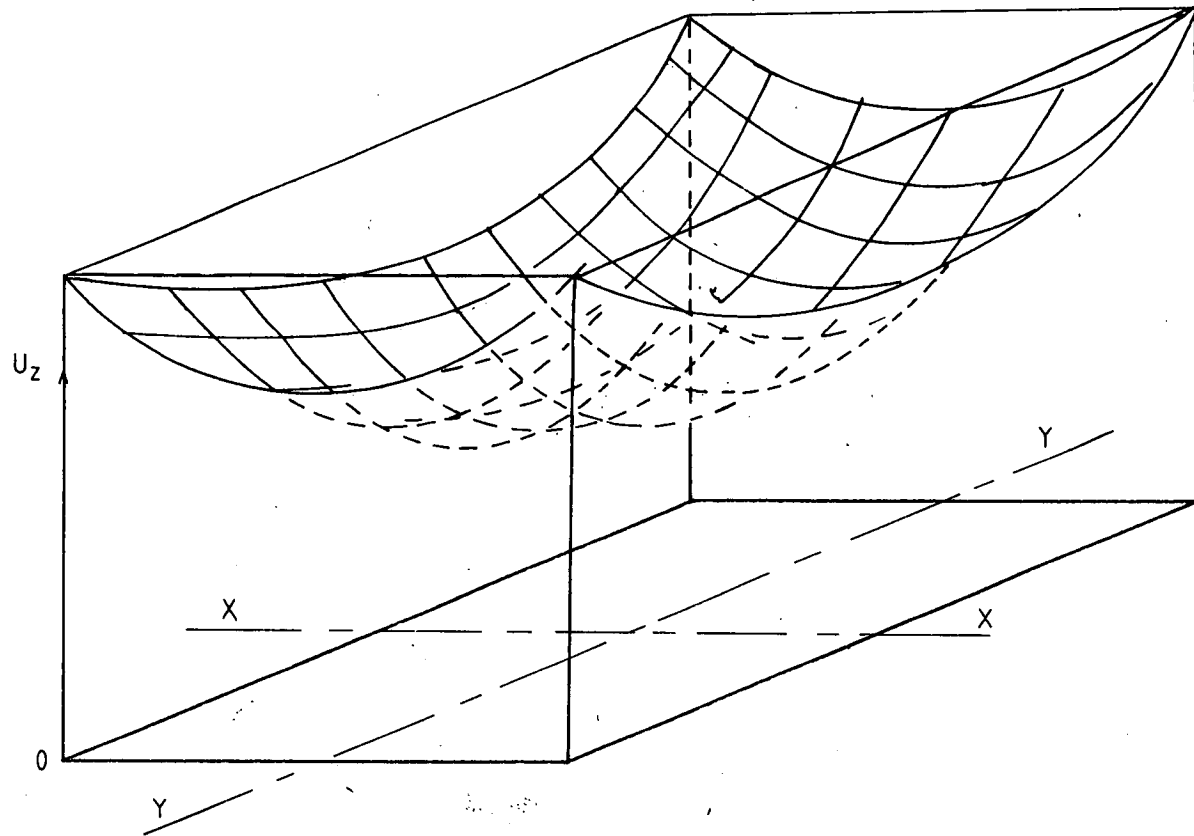
Figure 5.3.29

General Form of U_z Variation with X and Y - Large Sand
Bed.

Figure 5.3.30 YY Profile of Average Vertical Velocity - Large Bed.

SYSTEM PARAMETERS
BED DEPTH 30cm
U_e 10 cm e^{-1}
BED FILL CATALYST

O Z=60cm

U_z ⅹ 10^2 (me^{-1})

POSITION ON THE YY AXIS (cm)
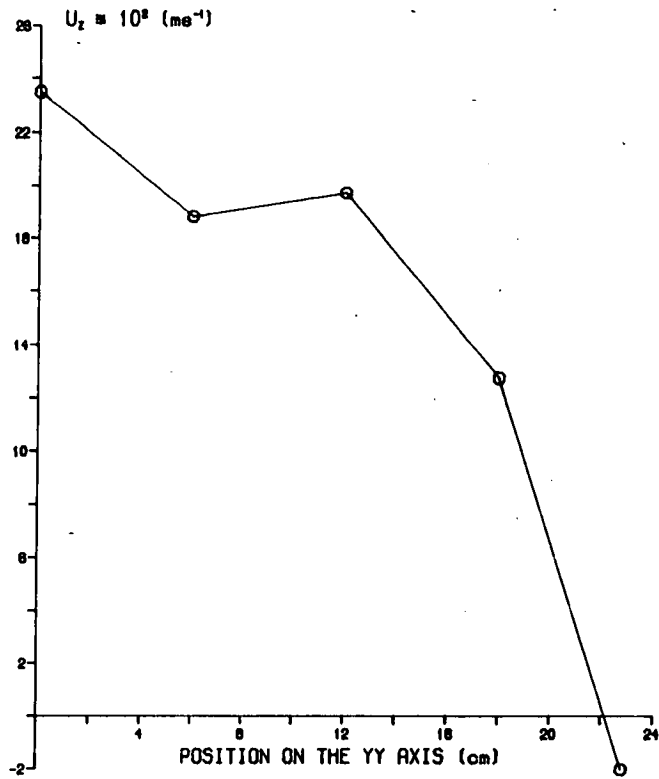
Figure 5.3.31 YY Profile of Average Vertical Velocity - Large Bed.

SYSTEM PARAMETERS
BED DEPTH 60cm
U_e 16.4 cm e^{-1}
BED FILL CATALYST

O Z=150cm

U_z ⅹ 10^2 (me^{-1})

POSITION ON THE YY AXIS (cm)

148

Figure 5.3.32 YY Profile of Average Vertical Velocity - Large Bed.

SYSTEM PARAMETERS
BED DEPTH 30cm
U_s 16.4 cm e^{-1}
BED FILL CATALYST

o Z=90cm
□ Z=150cm

Figure 5.3.33 YY Profile of rms Vertical Velocity Fluctuations - Large Bed.

SYSTEM PARAMETERS
BED DEPTH 60cm
U_e 16.4 cm e^{-1}
BED FILL CATALYST

o Z=150cm

Figure 5.3.34 YY Profile of rms Vertical Velocity Fluctuations - Large Bed.

SYSTEM PARAMETERS
BED DEPTH 30cm
U_e 16.4 cm e^{-1}
BED FILL CATALYST

o Z=90cm
□ Z=150cm

Variation of Average Vertical Velocity on Z Axis with Height above Bed Surface (Freeboard Height) - Large Bed.

Freeboard Height Z'(cm)	Vertical Component of Velocity U_z(cms^{-1})
30	13.8
60	20.4
90	18.5
120	20.3
150	21.3

Table 5.3.1 Bed Depth 30cm, Superficial Flow 16.4 cms^{-1}, Bed Fill Catalyst.

Chapter 6
Horizontal Components of Velocity and Turbulence

6.1 Introduction

The significance of horizontal components of velocity in the freeboard region of fluidised beds has been described in Chapter 5. There is at present no experimental data on this subject in the literature to the best of the authors knowledge, so the information presented will provide confirmation or otherwise of ideas previously proposed. These ideas are :

1 Horizontal components of velocity exist in the freeboard which tend to transfer gas towards the wall, so affecting the vertical velocity profile.

2 Large horizontal components of velocity exist near the bed surface as a result of gas bubbles bursting.

The transfer of ejected bed material towards the wall has been suggesed by Horio et. al. [33] and Pemberton [60] as an additional method of particle disengagement in the freeboard region, because particles can be transported to the low velocity gas flow region assumed to exist near the wall and fall back to the bed.

The technique of phase modulation was used in this work primarily because the mean velocity estimates were an order of magnitude less than the vertical component of velocity, and the relative turbulence in many cases was well over 100%. The physical situation therefore seems to be one of eddy type diffusion accompanied by directional drift of the gas phase. Because of this mean velocities were measured as an average over five minute experiment durations. The directional sense of the horizontal components was investigated by using the Phase Modulator in its two modes of operation, Drive or Invert. Because of the nature of the horizontal components it was found that there was flow in both directions over the experiment duration. For example consider the horizontal component U_Y on the YY axis. At any point on the reference axis there were found to be horizontal

components in the +ve and -ve Y directions over the experiment duration. Two five minute experiments were taken in each mode of operation and the result was classified in terms of a dominant direction. Three classifications were possible;

I = Dominant Direction opposite to the direction of movement of fringes in invert mode.

D = Dominant Dominant direction opposite to direction of movement of fringes in drive mode.

N = No Dominant Direction.

A larger value of the mean velocity estimate implies that the degree of dominance in the dominant direction is relatively large. Each result obtained at a particular position in the freeboard for the mean horizontal component of velocity will be classified in this way.

6.2 Measurements in the 7.5*7.5 cm Square Bed

Measurements were taken in both horizontal directions on both reference axes, (Figure 4.1), and several freeboard heights. In its entirety the experimental program gives comphrehensive information on this system. However, it is not practical to present all the data and an effort has been made to present selected data that will illustrate the structure of flow. Additional information if required is available from the Department of Chemical Engineering, University of Edinburgh.

In Section 6.1 the classification of drift velocities was outlined. In this section the labels for each drift velocity have the following meaning.

For U_X:

D = Dominant direction in the +ve X direction.

I = Dominant direction in the -ve X direction.

For U_Y:

D = Dominant direction in the +ve Y direction.

I = Dominant direction in the -ve Y direction.

Standard deviations on the mean and rms velocity measurements are given in Section 4.3.

6.2.1 Effect of Superficial Flow

Consider first the YY axis at a bed depth of 5 cm and a height above the distributor, Z, of 20cm. Figure 6.2.1 shows the mean velocities, U_Y, for superficial flows of 0.3 and 0.4 m s^{-1}. The measurements labelled D have a dominant direction in the +ve Y direction, measurements labelled I have a dominant direction in the -ve Y direction. The increase in superficial flow does not affect the dominant direction, except at position +2.75 cm where the dominant direction is in the -ve direction at the higher superficial flow. For a superficial flow of 0.3 m s^{-1} there is a steady decrease in the magnitude of the mean velocity estimate with increasing Y, while for a superficial flow of 0.4 m s^{-1} the same trend is evident, though in this case reversal of the dominant direction is detected at position +2.75 cm. Horizontal components of velocity will therefore tend to transfer momentum to the +ve end of the YY axis for a superficial flow of 0.3 m s^{-1} and to the centre of the cross section for a superficial flow of 0.4 m s^{-1}.

At this point it is informative to present the rms fluctuating velocities associated with the mean velocity estimates. These are shown in Figure 6.2.2. It is clearly shown that the effect of increasing superficial flow is to increase the magnitude of the rms fluctuating velocity. In other words the distribution of velocities has increased

and the turbulence intensity is increased. This is the same effect found for the vertical component of rms fluctuating velocity (Section 5.2.1). For a superficial flow of 0.4 m s^{-1} the turbulence intensity tends to decrease approaching the wall. The presence of the wall has the effect of limiting the turbulent motion, in this case the direction of measurement is perpendicular to the walls so the turbulence will tend to be smaller.

As mentioned in the introduction the rms fluctuating velocity in many cases is greater than 100% of the mean velocity. Consider the measurement of the turbulent flow taken at the centre of the cross section for a superficial flow of 0.4 m s^{-1}. From Figure 6.2.1, $U_Y = 2.00 *10^{-2}$ m s^{-1} and from Figure 6.2.2 the rms fluctuating velocity $u'_Y = 10.94 *10^{-2}$ m s^{-1}. The relative turbulence intensity expressed as the mean velocity divided by the rms fluctuating velocity is 547%. The distribution of velocity components is therefore very large and the physical situation seems to be eddy type diffusion accompanied by directional drift as mentioned above. The velocity distribution implied by the above result is shown in Figure 6.2.3. The turbulence is such that there are velocities in both directions over a five minute experiment duration, but a drift velocity is detected which for this position is in the +ve Y direction. It is useful to think of changes in the mean velocity as shifts in the velocity distribution.

Figure 6.2.4 shows the drift velocities, U_X, measured on the YY axis. This completes the measurements in three dimensions on this reference axis. It can be seen that in comparison with Figure 6.2.1 the magnitudes of the drift velocities are greater than those detected in the Y direction, particularly at the centre of the cross section. At all positions on the YY axis the dominant direction is in the +ve X direction for both superficial fluidising

velocities. However, the magnitude of the drift velocity is increased for increase in superficial flow.

Figure 6.2.5 shows the rms fluctuating velocities, u'_x, associated with the drift velocities shown in Figure 6.2.4. The effect of an increase in superficial flow is to increase the turbulence intensity measured in the X direction. According to Launder and Spalding [27] the measurements u'_x, u'_y and u'_z may be considered as the components of the turbulent energy. The rms fluctuating velocity near the wall in this direction tends to be greater than at positions at the centre of the cross section. The direction of measurement in this case is parallel to the wall so continuity does not affect the magnitude of the fluctuations as it would those towards the wall. This behaviour is characteristic of wall turbulence.

The results obtained on the XX axis will now be presented which will confirm observations made on the YY axis. The results as a whole will give measurements of the flow field in three dimensions at this freeboard height and the effect of superficial flow on the measured values.

Figure 6.2.6 shows the horizontal component of velocity U_x on the XX axis. It is expected that these results will show similar trends to those found for U_y on the YY axis. The dominant direction at all positions for a superficial flow of 0.3 m s^{-1} is in the +ve X direction with larger magnitudes of the mean velocity or drift velocity at -ve positions on the XX axis. For a superficial flow of 0.4 m s^{-1} there is flow reversal at +ve positions on the XX axis, at positions +1.25 and +2.75 cm the dominant direction is in the -ve X direction. The drift velocity is in fact very near zero at +1.25 cm which suggests that the point of flow reversal is close to this position. This means that,

157

particularly at the larger superficial flow, momentum will tend to be transfered to the centre of the cross section by horizontal components of velocity. The results shown in Figure 6.2.6 show similar behaviour to those shown in Figure 6.2.1 for U_Y on the YY axis.

Figure 6.2.7 shows the rms fluctuating velocities associated with the drift velocities shown in Figure 6.2.6. The expected increase in magnitude with increase in superficial flow is clearly shown. The relative turbulence intensities are very large and the velocity distribution is of the same form as shown in Figure 6.2.3. High local turbulence levels were found at +ve positions on the XX axis at a superficial flow of 0.3 m s^{-1} which may be the result of relatively large bubble rise velocities in this area at the bed surface. The decrease in rms fluctuating velocity towards the wall is seen most clearly at -ve positions on the XX axis, the decrease is probably due to the fact that the direction of measurement is perpendicular to the walls.

Figure 6.2.8 shows the horizontal component of velocity, U_Y, on the XX axis. There tend to be larger drift velocities at positions in the centre of the cross section with low values at the walls. The dominant direction at postions near the centre is in the +ve Y direction and this is unaffected by increase in superficial flow. At positions near the walls the dominant direction is affected by increase in superficial flow. The measurements show similar trends to those for U_X on the YY axis, but the magnitudes of the drift velocities U_Y are lower, and in this case there does not appear to be a significant increase in the magnitude of the drift velocity with increase in superficial flow. Figure 6.2.9 shows the rms fluctuating velocity u'_Y for positions on the XX axis. The turbulence intensity is consistently increased for increase in superficial flow as has been found in all cases.

To summarize the results obtained in this section the drift velocities in both directions are presented for each position in a vector diagram. This is shown in Figure 6.2.10 for superficial flows of 0.3 and 0.4 m s^{-1}. The dimensions of the cross section are approximately to scale and the arrows representing each drift velocity are scaled according to:

$$1 \text{ cm} \equiv 4 \text{ cm s}^{-1}$$

Over a five minute experiment duration the gas flow will tend to be transferred horizontally in the directions indicated. It is of interest to consider the components of velocity measured at a particular position in three dimensions e.g. consider position +1.25 cm on the YY axis at a superficial flow of 0.3 m s^{-1}. The values of the vertical component of velocity and the drift velocities are given below:

$$U_z \quad 37.5 *10^{-2} \text{ m s}^{-1}$$
$$U_Y \quad 2.42 *10^{-2} \text{ m s}^{-1}$$
$$U_X \quad 3.28 *10^{-2} \text{ m s}^{-1}$$

The drift velocities are therefore an order of magnitude less than the vertical component of velocity and transfer of momentum in this case would only be significant over a large freeboard height.

6.2.2 Effect of Bed Depth

It was found in Section 5.2.2 that the bed depth affected the vertical velocity distribution under conditions of low freeboard and low superficial flow. This can be explained by the effect of bed depth on the spatial distribution of bubbling at the surface of the bed. It is therefore of interest to investigate the effect of

bed depth on the horizontal mean velocities or drift velocities and the turbulence intensities measured in the horizontal directions.

Figure 6.2.11 shows the effect of bed depth on the drift velocities U_Y on the YY axis for a superficial flow of 0.4 m s^{-1}. The magnitudes of the drift velocities are greater at all positions on the YY axis for the fluidised bed with the lower static bed depth. This would indicate that different bubbling properties at the bed surface generate different structures of flow in the freeboard. The trend is the same at both bed depths, the drift velocity tends to get smaller at +ve positions on the YY axis. In addition the dominant direction is the same at -ve positions on the YY axis for both bed depths, but reversal of the dominant direction is detected near the wall at the +ve end of the YY axis.

Figure 6.2.12 shows the effect of bed depth on the rms value of the fluctuations in the horizontal component of velocity, u'_Y. This expresses the amplitude of velocity fluctuations associated with the mean velocities given in Figure 6.2.11. The amplitude of the velocity fluctuations, or the turbulence intensity, is lower at the lower bed depth. This is the same effect found for the turbulence intensity measured in the vertical, Z, direction. It is interesting to note that at the lower bed depth the turbulence intensity is lower than at the higher bed depth, but the drift velocities measured at the lower bed depth are greater. It would appear therefore that the magnitudes of the drift velocities are not solely dependent on the turbulence intensity, but are also related to the system parameters.

Figure 6.2.13 shows the mean velocities U_X on the YY axis for a superficial flow of 0.4 m s^{-1}. The drift velocities tend to be greater for the greater bed depth,

except at position +2.75 cm where the converse is true. The dominant direction is in the +ve X direction for both bed depths. Figure 6.2.14 shows the rms fluctuating velocity u'_X associated with the drift velocities given in Figure 6.2.13. The effect of bed depth on the turbulence intensity measured in this direction is that a decrease in bed depth gives a decrease in turbulence intensity. This is consistent with the effect of bed depth on the turbulence intensities u'_Z (Figure 5.2.5) and u'_Y (Figure 6.2.12).

Results are now presented for the drift velocities on the XX axis. This will conclude the effect of bed depth on the drift velocities over the cross section at this freeboard height. Figure 6.2.15 shows U_X on the XX axis. There are two effects evident, firstly, the magnitude of the drift velocity is greater at the greater bed depth, and secondly, at the lower bed depth there is no change in the dominant direction at +ve positions on the XX axis. Similar effects were found for U_X on the YY axis, (Figure 6.2.13). Figure 6.2.16 shows that the rms fluctuating velocities associated with the drift velocities decrease with decrease in bed depth.

Figure 6.2.17 shows U_Y on the XX axis. The drift velocity tends to be greater at the lower bed depth and there is no change in dominant direction evident at the lower bed depth. At the greater bed depth there is reversal of the dominant direction at the +ve end of the XX axis. Figure 6.2.18 shows that the rms velocities or turbulence intensities measured in this direction decrease with decrease in bed depth.

All this appears to be consistent with the view that bed depth affects the drift velocities and associated turbulence intensities in the following way: for decrease in bed depth

<u>1</u> Turbulence intensity is decreased at all positions and in both directions.

<u>2</u> The magnitudes of the drift velocities U_Y are increased and the magnitude of the drift velocities U_X are decreased. The reason for this may be that the spatial distribution of bubbling is different as larger drift velocities have been shown to exist at lower levels of turbulence (Figure 6.2.11 and Figure 6.2.12), indicating that the magnitudes of the drift velocities are not solely dependent on the intensity of turbulence.

<u>3</u> There is no change in the dominant direction across the reference axes. Reversal of the dominant direction was found at the larger bed depth under which conditions the turbulence intensity was consistently greater. The reversal of the dominant direction of the drift velocity across the reference axes therefore tends to occur under relatively large turbulence intensity conditions.

The results for the horizontal components of velocity from the figures above are presented as a vector diagram in Figure 6.2.19a. Comparison with Figure 6.2.10b shows the effect of bed depth on the magnitude and direction of the drift velocities and illustrates the points made above.

Additional information is available at a bed depth of 3cm and a superficial flow of 0.3 m s^{-1}. The figures are not presented due to lack of space, but a vector diagram is given in Figure 6.2.19b. This figure shows similar behaviour to that described above for a superficial flow of 0.4 m s^{-1}.

6.2.3 Effect of Freeboard Height

Measurements of the drift velocities and associated rms fluctuating velocities were taken on the XX and YY axes at various freeboard heights under the four experimental conditions. The results will show if freeboard height has a consistent effect on the magnitude and dominant direction of the drift velocities, and also whether the same effect found for the rms fluctuating velocities measured in the vertical, Z, direction (Section 5.2.3) is evident for measurements of turbulence intensity in the X and Y directions.

Figure 6.2.20 shows the effect of freeboard height on the drift velocity U_Y on the YY axis. The bed depth was 3 cm and the superficial flow was 0.4 m s^{-1}. The drift velocities are generally greater at a freeboard height of 20 cm and decrease with increasing Y. At freeboard height of 40 cm they are smaller and increase with increasing Y. Furthermore, the drift velocities at Z=20 cm are in the +ve Y direction while those at Z=40 cm are towards decreasing values of Y. This reversal of dominant flow direction with height suggests a circulation like secondary flow pattern in the freeboard space. Figure 6.2.21 shows the effect of freeboard height on the rms fluctuating velocities associated with the drift velocities in Figure 6.2.20. There is a general decrease with increase in freeboard height which was the effect found for the rms fluctuating velocity measured in the vertical, Z, direction. The turbulence maintains a nearly constant value at large freeboard heights.

Figure 6.2.22 shows the effect of freeboard height on the drift velocity U_X on the YY axis. The bed depth was 5 cm and the superficial flow was 0.4 m s^{-1}. The magnitude of the drift velocities are once again generally greater at Z=20 cm and decrease with increasing Y. At Z=29.5cm the magnitude is lower and the drift velocity tends to

increase with increasing Y. At -ve positions on the YY axis the dominant direction is reversed to be towards decreasing values of X whereas at +ve positions on the YY axis the dominant direction remains in the +ve X direction. At Z=40 cm the magnitude of the drift velocity is nearly constant and the dominant direction is now in the -ve X direction at all positions. Once again this information suggests that secondary flow patterns exist in the freeboard. Figure 6.2.23 shows that the rms fluctuating velocities or turbulence intensities measured in this direction on the YY axis decrease with increasing freeboard height as found for u'_z and u'_Y.

Figure 6.2.24 shows the effect of freeboard height on the drift velocity U_X measured on the XX axis. Similar behaviour is evident to that found in the preceding figures. However, in this case measurements were taken at a freeboard height of 47.5 cm, the results show that the drift velocity tends to increase in magnitude after flow reversal particularly near the wall. This is consistent with point 2 (p.162), made in section 6.2.2 that the magnitude of the drift velocity is not dependent on the level of turbulence intensity and seems to be related to the structure of flow generated by bubbles bursting at the bed surface. Figure 6.2.25 shows that the same general relationship between freeboard height and turbulence intensity holds for measurements in the X direction on the XX axis.

Figure 6.2.26 shows the effect of freeboard height on the drift velocity U_Y measured on the XX axis. The bed depth was 3 cm and the superficial flow was 0.3 m s^{-1}. Reversal in the dominant direction of the drift velocity is again found with increase in freeboard height. Figure 6.2.27 shows the variation of rms fluctuating velocity with freeboard height. There is the expected general decrease in turbulence intensity with increase in

freeboard height. It is interesting to note the variation of turbulence intensity across the XX axis at a freeboard height of 10 cm. Under these experimental conditions it was found that there were maxima of the local vertical components of velocity and turbulence near the walls (section 5.2.2). The turbulence measured in the Y direction near the wall at Z=10 cm shows a maximum as was found for the turbulence measured vertically. The profiles for turbulence at increasing freeboard height become nearly flat.

In conclusion, it has been shown by figures 6.2.20 to 6.2.27 that:

1 Reversal of the dominant flow direction of the drift velocities U_X and U_Y occurs under each experimental condition.

2 The magnitude of the drift velocities tends to be larger at low freeboard height and gets smaller as freeboard height increases. With further increase in freeboard height the drift velocity increases once again after reversal of the dominant direction.

3 Under each experimental condition a general decrease in turbulence intensity is found with increase in freeboard height as was the case for the turbulence intensity measured in the vertical direction.

A velocity component diagram is given in Figure 6.2.28, the bed depth was 3 cm, superficial flow was 0.4 m s^{-1} and freeboard height was 40 cm. This gives all the drift velocities measured under one set of experimental conditions. Comparison with Figure 6.2.19a gives the effect of freeboard height i.e. the reversal of dominant direction of the drift velocities.

Further information is available for each horizontal component of velocity under different experimental conditions and at different positions in the cross section.

This information confirms the observations made above, and if required, is available from the Department of Chemical Engineering, University of Edinburgh.

6.2.4 Isotropic/Anisotropic Turbulence

Having made measurements of turbulence intensity in three dimensions it is possible to find if the turbulence generated by erupting bubbles at the surface of this fluidised bed is isotropic or anisotropic. In other words, are the turbulence intensities measured in the X, Y, and Z directions at a point in the turbulent flow field the same or different ?.

The results are important as they give an indication of the type of structure formed by gas from the bubble phase when it erupts into the gas flow above the bed. Also of interest are the characteristics at low and high freeboard heights. Initially turbulence may exhibit a large degree of anisotropy whereas, at greater freeboard heights, after turbulence has decayed it may exhibit less anisotropy and be nearly isotropic.

Table 6.2.1 shows the measurements of turbulence in the X,Y and Z directions on the XX axis. The bed depth was 5 cm, superficial flow was 0.4 m s^{-1} and freeboard height was 20 cm. The measurements in the Z direction tend to be larger than the measurements in the X and Y directions. At the centre of the cross section the differences are less than the differences at the walls. However, wall turbulence, where the structure is directly influenced by the presence of the solid boundary, will have a relatively large degree of anisotropy.

Table 6.2.2 shows the measurements at a freeboard height of 40 cm under the same experimental conditions

described above. Again the measurements at the centre of the cross section show a very low degree of anisotropy, whereas measurements at the wall show a relatively large degree of anisotropy particularly for the measurement taken perpendicular to the wall.

Table 6.2.3 shows the measurements at a bed depth of 3 cm. The trends found are similar to those described in Table 6.2.1 with increased degree of anisotropy near the walls. Table 6.2.4 shows the measurements at a larger freeboard height of 40 cm. The same trends are shown under these experimental conditions.

In conclusion, the following have been found for this fluidised system.

1 The degree of anisotropy is greater at the walls than at the centre of the cross section.

2 The intensity of turbulence measured vertically has the highest value, that of the transverse component measured perpendicular to the wall has the smallest value.

3 Because of the close values of the rms fluctuating velocities in the X, Y and Z directions, the assumption of isotropic turbulence is reasonable at all freeboard heights in this system.

6.3 Measurements in the 0.48*0.28 m Rectangular Bed

The measurements of the vertical component of gas velocity in this system gave results which suggested that horizontal components of gas velocity transferred momentum towards the walls. The comparison of the magnitude of the horizontal mean velocities or drift velocities to the vertical mean velocities given in Chapter 5 should indicate the significance of the horizontal components. The presence of fine particles in the freeboard flow may also affect the gas flow structure. Comparison of the results with those obtained in the small bed will test the generality of the conclusions drawn for that system.

It was found that at many positions in the freeboard above the large bed fluidising sand the horizontal component of velocity did not have a dominant direction. The procedure used was to run two experiments in each mode of operation of phase modulation. If the results in one mode of operation gave larger mean velocity estimates it was concluded that the this mode of operation gave the dominant direction. However, if results from each mode of operation gave comparable values it was concluded that there was no dominant direction.

The mean velocity estimates or drift velocities at each position are labelled I, D or N, this indicates the dominant direction, if any. For U_X (Figure 4.3)

I = Dominant direction in the -ve X direction.
D = Dominant direction in the +ve X direction.
N = No dominant direction.

For U_Y

I = Dominant direction in the +ve Y direction.
D = Dominant direction in the -ve Y direction.

N = No dominant direction.

Standard deviations on the mean and rms velocity measurements are given in Section 4.3.

6.3.1 Effect of Superficial Flow

Increase in superficial flow increases the gas flow in the bubble phase. The effect on horizontal components of velocity in the small bed was described in section 6.2.1. Results are now presented for the horizontal components of velocity U_X and U_Y on the XX and YY axes for a bed depth of 60cm and superficial flows of 3 and 4 cm s^{-1}. The minimum fluidising velocity is 0.95 cm s^{-1}.

Figure 6.3.1 shows the results obtained for U_Y on the YY axis. The magnitude of the drift velocities measured over a five minute experiment duration tend to be larger for the larger superficial fluidising velocity. At some +ve positions on the YY axis a dominant direction in the +ve Y direction was found. However, at -ve positions on the YY axis there was no dominant direction found for data taken over a period of 20 minutes. The magnitudes tend to be smaller near the walls, particularly for the larger superficial flow. This may be because the direction of measurement is perpendicular to the rigid surface.

Figure 6.3.2 shows the rms fluctuating velocities associated with the drift velocities given in Figure 6.3.1. The values of the relative turbulence intensities are again well over 100%, as was found for the horizontal components of velocity above the small bed. The physical situation is similar, and the velocity distributions would have the same form as Figure 6.2.3. The magnitude of the rms fluctuating velocity or turbulence intensity is consistently greater at the larger superficial fluidising velocity. This is the same effect as found for the turbulence intensities measured in the vertical, Z, direction. The turbulence intensity measured near the

wall tends to be smaller than that measured at the centre of the cross section. This may also be because the direction of measurement is perpendicular to the rigid surface, therefore limiting the turbulent motion.

Figure 6.3.3 shows the horizontal components of velocity, U_x, measured on the YY axis. There does not appear to be any consistent effect on the magnitude of the drift velocities for an increase in superficial flow. The dominant direction shows similar trends for both superficial flows, the dominant direction is in the -ve X direction near the walls and at some positions near the centre of the cross section the dominant direction is towards increasing values of X. Large drift velocites are measured near the walls, particularly at the -ve end of the YY axis.

Figure 6.3.4 shows the rms fluctuating velocity associated with the drift velocities given in Figure 6.3.3. The increase in superficial flow gives an increase in the turbulence intensity at all positions as was found for u'_z and u'_Y. The magnitude of the turbulence intensity tends to be greater near the walls, getting progressively lower nearer the centre. The profile at a superficial flow of 3 cm s^{-1} is distinctly skew which may be the result of uneven distribution of bubbling activity at the bed surface.

These figures along with the figures for U_z given in Chapter 5 describe the local structure of flow across the YY axis under the specified experimental conditions. To illustrate the significance of each component consider position +6 cm on the YY axis at a superficial flow of 3 cm s^{-1}. The mean velocity components are as follows:

$$U_z \qquad 9.90 * 10^{-3} \text{ m s}^{-1}$$
$$U_x \qquad 6.30 * 10^{-3} \text{ m s}^{-1}$$

$$U_Y \quad - \quad 7.67 * 10^{-3} \ m \ s^{-1}$$

The horizontal components of velocity are therefore significant relative to the vertical component of velocity. However, at this freeboard height many of the horizontal components of velocity have no dominant direction and tend to disperse the gas phase in no preferred direction. The vertical velocity profiles may not therefore be significantly affected by the horizontal components of velocity as was described in Chapter 5 (section 5.3.1).

Measurements are presented in the following figures for U_X and U_Y on the XX axis under the same experimental conditions described above. This extends the coverage of the cross section and should confirm observations made on the YY axis.

Figure 6.3.5 shows U_X on the XX axis. The magnitudes of the drift velocities are greater for the greater superficial flow, and at most positions there is a dominant direction for both superficial flows. For -ve positions the dominant direction tends to be in the +ve X direction i.e. towards the centre of the cross section. For +ve positions on the XX axis the dominant direction is towards decreasing values of X which again is towards the centre of the cross section. The magnitudes of the drift velocities do not show significant change across the reference axis at each superficial flow.

Figure 6.3.6 shows the rms fluctuating velocities associated with the drift velocities given in Figure 6.3.5. The magnitudes tend to be greater at the larger superficial flow, as was found on the YY axis. In addition, the turbulence intensity tends to smaller near the walls as found for u'_Y on the YY axis. This is expected as the measurement direction in both cases is perpendicular to the wall consequently limiting the turbulent motion. The

absolute values of the turbulence are lower then those measured on the YY axis which may be the result of uneven distribution of bubbling at the surface of the bed.

Figure 6.3.7 shows U_Y on the XX axis. There is no consistent effect of superficial flow on the magnitudes of the mean velocity estimates or drift velocities, though at -ve positions on the XX axis the drift velocities are larger at the greater superficial flow. A very high drift velocity, 1.7 cm s^{-1}, with dominant direction in the +ve Y direction was measured at position -12 cm on the XX axis. For a superficial flow of 3 cm s^{-1} the dominant direction at most positions was in the +ve Y direction. For a superficial flow of 4 cm s^{-1} dominant directions towards decreasing values of Y were found at +ve positions on the XX axis.

Figure 6.3.8 shows the rms fluctuating velocities associated with the drift velocities given in Figure 6.3.7. The effect of increase in superficial flow is to increase the rms fluctuating velocity or, in other words, the turbulence intensity is increased. The magnitude of the turbulence intensity is greater near the walls than in the centre of the cross section, probably because the direction of measurement is parallel to the walls. This figure shows similar characteristics to Figure 6.3.4 for u'_x on the YY axis, but in this case the profile is not skewed which may be because the distribution of bubbling across the XX axis at the surface of the bed is reasonably good.

Figure 6.3.9 shows the results obtained for the drift velocities at a superficial flow of 3 cm s^{-1}, presented as a velocity component diagram. The velocities are scaled according to:

$$1 \text{ cm} = 1 \text{ cm s}^{-1}$$

Generally, it can be seen that at many positions the drift velocities have no dominant direction. Nevertheless, momentum will tend to be transferred in the directions indicated.

6.3.2 Effect of Bed Depth

Bed depth affects the spatial distribution of bubbling in the dense bed, and it was found that in the small bed fluidising ballotini the magnitude of the drift velocities was affected by bed depth. It was also found that turbulence intensity was lower at lower bed depth. Measurements are presented in this section for the drift velocity U_Y on the YY axis at bed depths of 30 and 60 cm.

Figure 6.3.10 shows U_Y on the YY axis for bed depths of 30 and 60 cm. The superficial flow was 3 cm s^{-1} and the distance from the static bed surface, Z', was 60 cm. There does not appear to be any consistent effect on the magnitude of the drift velocity for an increase in the bed depth. At this freeboard height the drift velocities do not have a dominant direction at most positions though, for a bed depth of 60 cm, a dominant direction in the +ve Y direction at +ve positions on the YY axis is detected. For both bed depths the magnitudes of the drift velocities tend to be lower near the walls.

Figure 6.3.11 shows the rms value of the fluctuations in the horizontal component of velocity on the YY axis for bed depths of 30 and 60 cm. These values express the amplitude of the velocity fluctuations about the mean velocities given in Figure 6.3.10. The turbulence is greater at the centre of the cross section in both cases. This is due to the fact that the measurement direction is perpendicular to the solid boundary.

Figure 6.3.12 shows the horizontal components of velocity measured on the YY axis at bed depths of 30 and 60 cm. The superficial flow was 4 cm s^{-1} and the height above the static bed surface was 60 cm. Once again, no consistent effect on the magnitude of the drift velocities is evident for an increase in the superficial flow. At many positions the drift velocities have no dominant direction, but at both bed depths there is a dominant direction in the +ve Y direction at +ve positions on the YY axis and a dominant direction towards decreasing values of Y at -ve positions on the YY axis. This implies that gas may be transferred towards the walls as a result of these horizontal components of velocity. This may show up in the vertical velocity profiles at greater freeboard height (Figure 5.3.10).

Figure 6.3.13 shows the rms values of the fluctuations in the horizontal component of velocity associated with the mean velocities given in Figure 6.3.12. At the larger superficial fluidising velocity the turbulence intensities measured are greater at the larger bed depth. This behaviour is expected assuming that turbulence intensity is dependent on the rise velocity of bubbles in the fluidised bed which will be greater at greater bed depths according to existing correlations (Section 5.2.1). Both profiles of turbulence show a fall in turbulence intensity near the walls because of the measurement direction.

6.3.3 Effect of Freeboard Height

The significance of horizontal components of gas velocity in the freeboard space above fluidised beds of round sand was suggested in Chapter 5. Results presented in this section will give evidence that such components of velocity do exist and in many cases have a dominant direction. The decay of turbulence intensity measured in

this direction is also shown which indicates slightly different behaviour to the decay of turbulence measured in the vertical direction.

Results are presented for the effect of freeboard height under three sets of experimental conditions:

<u>1</u> U_Y on the YY axis for bed depth of 60 cm and superficial flow 4 cm s^{-1}.

<u>2</u> U_X on the YY axis for bed depth of 60 cm and superficial flow 4 cm s^{-1}.

<u>3</u> U_Y on the YY axis for bed depth of 30 cm and superficial flow 3 cm s^{-1}.

Additional measurements were taken, but are not presented here. If required the information is available from the Department of Chemical Engineering, University of Edinburgh.

Figure 6.3.14 shows U_Y on the YY axis at various freeboard heights. The bed depth was 60 cm and the superficial flow was 4 cm s^{-1}. The magnitudes of the drift velocites measured at the lowest freeboard height are significantly greater than those measured at greater heights. In fact, the magnitude steadily decreases with increase in freeboard height. At low freeboard height horizontal components of gas velocity generated by gas bubbles bursting at the surface of the bed exist (Section 5.3.5), whereas at larger freeboard heights the effect of the horizontal components has diminished. There is evidence that at +ve positions on the YY axis the drift velocities have a dominant direction towards increasing values of Y, at -ve positions on the YY axis the drift velocities have a dominant direction towards decreasing values of Y. Gas will therefore tend to be transferred towards the walls from the centre of the cross section, maintaining the dip profiles measured for the vertical component of velocity (Section 5.3.1). It is shown in Figure 6.3.14 that the drift velocity has a dominant

direction in the +ve Y direction near the wall at the -ve end of the YY axis. This means that gas would tend to be transfered away from the wall. However, large vertical components of velocity exist in this region (Section 5.3.3) which means that the resultant mean gas velocity will be nearly vertical i.e. the effect of the drift velocity is limited.

Figure 6.3.15 shows the rms values of the fluctuations in the horizontal component of velocity; this expresses the magnitude of the velocity fluctuations about the mean velocity estimates given in Figure 6.3.14. The rms values of the fluctuations in velocity or the turbulence intensities measured in this direction show a steady decrease at all positions with increase in freeboard height. The measurements do not show the discrepancies detected for the turbulence intensity measured in the vertical, Z, direction (Section 5.3.3). The profiles at each freeboard height have the same shape, with relatively low values of turbulence near the walls.

Figure 6.3.16 shows the horizontal components of velocity measured in the X direction on the YY axis under the experimental conditions described above. This completes the measurements of the turbulent flow in the X, Y and Z directions on this reference axis. The magnitude of the drift velocities are generally lower than those measured in the Y direction (Figure 6.3.14) at low freeboard height. This may be the result of the structure of flow after bubble eruption at the surface of the bed. As found for U_Y there tend to be larger drift velocities at low freeboard height, but relatively large drift velocities exist near the walls for this measurement direction, wheras the converse was true for U_Y (Figure 6.3.14). Near the walls the dominant direction tends to be towards -ve X, and at the centre of the cross section the dominant direction tends to be towards increasing values of X.

Generally, however, the drift velocities at many positions have no dominant direction.

Figure 6.3.17 shows the decay of turbulence intensity, u'_x, associated with the drift velocities given in Figure 6.3.15. In other words the figure shows the turbulence intensities measured in the X direction at the same positions shown in Figure 6.3.15 for the Y direction. The turbulence intensities at Z=120 cm are much greater than those measured at Z=150 cm. However, those measured at Z=180 cm are not significantly different from the values at Z=150 cm, in fact, at some positions the turbulence intensity is greater at Z=180 cm. This behaviour is similar to that described for the turbulence intensity measured in the Z direction (Figure 5.3.14).

Figure 6.3.18 shows the horizontal component of velocity, or drift velocity, U_Y on the YY axis at various freeboard heights. The bed depth was 30 cm and the superficial fluidising velocity was 3 cm s^{-1}. In comparison with Figure 6.3.14 the same general effects are apparent:

<u>1</u> The drift velocities tend to be greater at low freeboard height.

<u>2</u> At +ve positions on the YY axis the drift velocities tend to have a dominant direction in the +ve Y direction, and at -ve positions on the YY axis the dominant direction tends to be towards decreasing values of Y. Gas will therefore tend to be transferred from the centre of the cross section to the wall regions in the freeboard.

<u>3</u> Near the wall at the -ve end of the YY axis drift velocities were measured with a dominant direction in the +ve Y direction i.e. away from the wall. However, because the vertical component of velocity is high at these positions the effect of the drift velocities is limited.

Figure 6.3.19 shows the rms values of the fluctuations in velocity associated with the drift velocities given in

Figure 6.3.18. The decay of turbulence intensity with freeboard height is not as steady as the decay shown in Figure 6.3.15 under different experimental conditions. However, the general decay is as expected. It is worth noting that the measurements indicate that the turbulence intensity near the walls tends to the same value regardless of the turbulence intensity outside the influence of the solid boundary.

6.3.4 Isotropic/Anisotropic Turbulence

From the measurements taken it is possible to investigate the degree of anisotropy present in the turbulent flow above fluidised beds of round sand. The results may give an indication of the nature of the flow generated when bubbles burst at the surface of the bed. It is also of interest to compare the results with the results obtained in the small bed (Section 6.2.4), as the comparison may indicate if the structure of the turbulent flows in each case is similar.

Table 6.3.1 shows the rms values of the fluctuations in velocity measured in the three Cartesian coordinate directions X, Y, and Z on the YY axis. The bed depth was 60 cm, superficial fluidising velocity was 3 cm s^{-1} and the freeboard height, Z, was 120 cm i.e. 60 cm above the static bed surface. At the centre of the cross section the turbulence intensities measured in the X and Y directions are nearly identical, but the value measured in the Z direction is lower. Near the walls the degree of anisotropy increases with the lowest value being that measured in the horizontal direction perpendicular to the walls. This is similar to the behaviour described for the small bed fluidising ballotini (Section 6.2.4).

Comparison of the turbulence intensities measured in the three Cartesian directions at large freeboard height with those measured at low freeboard height will show if the degree of anisotropy is affected. Table 6.3.2 shows the turbulence intensities in the X, Y, and Z directions on the YY axis. The experimental conditions are as described above, except that Z was 180 cm. The degree of anisotropy is low at the centre of the cross section and tends to increase at positions near the walls. There does not appear to be a significant difference between the degree of anisotropy present at this relatively large freeboard height and the degree of anisotropy present at low freeboard height (Table 6.3.1).

Table 6.3.3 shows the results obtained on the YY axis for a bed depth of 60 cm and a superficial flow of 4 cm s^{-1}. The freeboard height was 120 cm. The results show similar behaviour to those obtained with a superficial fluidising velocity of 3 cm s^{-1} (Table 6.3.1). The degree of anisotropy is low at the centre of the cross section, with the lowest value of turbulence intensity being that measured in the vertical, Z, direction. As expected the degree of anisotropy is greater near the walls with the lowest value being that measured in the horizontal direction perpendicular to the walls. Table 6.3.4 shows the results obtained at a freeboard height of 180 cm. The degree of anisotropy does not seem to be affected by the increase in freeboard height as was found for the results obtained using a superficial fluidising velocity of 3 cm s^{-1} (Tables 6.3.1 and 6.3.2).

Generally, the degree of anisotropy of the turbulent flow above fluidised beds of round sand is low. In addition, there does not appear to be any significant difference between the degree of anisotropy present in this system and the degree of anisotropy present above fluidised beds of ballotini in a small bed geometry (Section

179

6.2.4).

6.3.5 Effect of Tube Bank

It was shown in Section 5.3.4 that an immersed tube bank did not significantly affect the mean vertical component of velocity, but the rms value of the fluctuations in velocity were significantly lower. In this section the effect on the horizontal component of velocity, U_Y, and the associated turbulence intensities, u'_Y, is investigated.

Figure 6.3.20 shows the horizontal component of velocity on the YY axis at a freeboard height of 120 cm in the presence and absence of the immersed tube bank. The bed depth was 60 cm and the superficial fluidising velocity was 3 cm s^{-1}. The magnitude of the drift velocity is greater at the centre of the cross section when the tube bank is immersed in the dense bed. At positions nearer the walls there is no significant difference. In both cases the drift velocity tends to be smaller in magnitude near the walls. Generally, more drift velocities measured in the freeboard above a fluidised bed containing an immersed tube bank have a dominant direction. This may be because of a decrease in turbulence intensity caused by the presence of the tube bank (p.162). The suggestion above will be confirmed in the following figure.

Figure 6.3.21 shows the rms values of the fluctuations in velocity associated with the drift velocities given in Figure 6.3.20. The magnitude of the turbulence intensity is consistently lower for gas flow above the fluidised bed containing the immersed tube bank. This is the same behaviour found for turbulence intensity measured in the vertical, Z, direction, and confirms the suggestion made above. This demonstrates the near isotropic nature of the

gas flow above fluidised beds of round sand. In both cases the turbulence intensity is much lower at positions near the walls because the measurement direction is perpendicular to the solid boundary which limits the turbulent motions.

Figure 6.3.22 shows the results obtained for the drift velocity using a superficial fluidising velocity of 4 cm s^{-1}. Under this fluidisation condition the drift velocities differ at the centre of the cross section. At some positions e.g. +6 cm and -6 cm the drift velocity is much smaller in the presence of the immersed tube bank. However, at position +12 cm the converse is true. Nearer the walls there is no significant difference. There is some evidence that more drift velocities have a dominant direction in the freeboard above the bed containing the immersed tube bank, which may be the result of reduced turbulence (p.162). And, furthermore there is evidence that gas will tend to be transferred towards the walls by horizontal components of velocity.

Figure 6.3.23 shows the rms fluctuating velocities associated with the drift velocities given above. There is the consistent decrease in the magnitude of the turbulence intensity with the tube bank immersed in the bed shown in Figure 6.3.21 for a superficial fluidising velocity of 3 cm s^{-1}. This behaviour is also exhibited by the turbulence intensity in the vertical direction (Figure 5.3.20). In both cases the turbulence is lower near the walls because of the direction of measurement.

It seems therefore that the presence of the immersed tube bank affects the magnitude of the drift velocity in the freeboard, particularly near the centre of the cross section, but there are conflicting trends at different fluidising conditions. The turbulence intensity measured in this direction is consistently lower with the tube bank

immersed in the bed, as was found for the turbulence intensity measured in the vertical, Z, direction.

6.3.6 Effect of Position on Cross Section

The local properties of the turbulent flow were investigated off the reference axes defined in Figure 4.3. The results will show if there is any effect on the magnitude of the drift velocities, the dominant direction of the drift velocities and the magnitude of the turbulence intensity measured horizontally. The axes used were those defined by the coordinates X=-8 cm and Y=-18 cm (Figure 4.3).

Figure 6.3.24 shows the drift velocity, U_Y, on the XX axis and the axis defined by Y=-18 cm. The bed depth was 60 cm, superficial flow was 3 cm s^{-1} and freeboard height, Z, was 180 cm. There does not seem to be any consistent effect on the magnitudes of the drift velocities. However, there is evidence that on the Y=-18 cm axis the dominant direction tends to be in the -ve direction at the centre of the cross section i.e. towards the wall closest to the reference axis. There is no evidence of this on the XX axis which is equidistant from the walls in the Y direction. It appears therefore that at positions nearer the wall, the drift velocity in this direction tends to have a dominant direction towards the wall. Near the walls at the ends of the reference axes the dominant direction is in the +ve Y direction. Figure 6.3.25 shows the rms fluctuating velocities associated with the drift velocities described above. The turbulence intensities measured on the Y=-18 cm axis are slightly greater than those measured on the the XX axis.

Figure 6.3.26 shows the drift velocity U_Y on the YY axis and the axis defined by X=-8 cm. The bed depth was 60

cm, superficial fluidising velocity was 3 cm s^{-1} and freeboard height was 150 cm. The drift velocities measured on each reference axis are not significantly different, and the dominant direction tends to be the same at equivalent positions. The reference axis defined by X=-8 cm is closer to the wall at the -ve end of the XX axis (Figure 4.3), but the measurement direction is parallel to the wall whose influence on the measurements may be expected to be insignificant. Figure 6.3.27 shows the turbulence intensities associated with the drift velocities shown in Figure 6.3.26. The turbulence intensities measured on the X=-8 cm axis are larger than those measured on the YY axis at positions away from the walls. It has been shown that the magnitude of the turbulence intensity u$'_Y$ increases near the walls on the XX axis, this explains the greater turbulence intensities measured on the X=-8 cm axis shown above.

Figure 6.3.28 shows the mean velocity estimates or drift velocities measured in the X direction on the YY axis and the X=-8 cm axis. Bed depth was 60 cm, superficial fluidising velocity was 3 cm s^{-1} and freeboard height was 180 cm. The magnitudes of the drift velocities are consistently greater on the X=-8 cm axis. In addition, the drift velocities on the X=-8 cm axis are more likely to have a dominant direction which, particularly at -ve positions on the reference axis is towards decreasing values of X i.e. towards the wall at the -ve end of the XX axis (Figure 4.3). This does not tend to be the case on the YY axis. At +ve positions on the X=-8 cm axis the behaviour described is not clearly evident, and at some positions the dominant direction is in the +ve X direction i.e. away from the wall. Horizontal transfer of momentum will not therefore be symmetrical which will tend to give skewed vertical mean velocity profiles. Figure 6.3.29 shows the rms values of the velocity fluctuations associated with the drift velocities described above. The

magnitude of the rms value or turbulence intensity tends to be greater on the X=-8 cm axis. This indicates that the turbulence is not homogeneous. In other words the turbulence intensity does not have the same value in all parts of the flow field. Figures 6.3.25 and 6.3.27 also illustrate this point.

6.3.7 Effect of Minimum Fluidising Velocity

The effect of increased minimum fluidising velocity is to limit the horizontal transfer of bubble phase gas after bubble eruption (Section 5.3.6). In this section the mean velocity estimates or drift velocities and associated rms values of velocity fluctuations in the Y direction for the gas flow above a fluidised bed of catalyst are presented. The physical properties of the catalyst are given in Section 4.1.2.

Figure 6.3.30 shows the drift velocity U_Y on the YY axis for a superficial fluidising velocity of 16.4 cm s^{-1}. The bed depth was 60cm and freeboard height was 150 cm. The magnitude of the drift velocity is greater at the centre of the cross section as was generally found for the gas flow above fluidised beds of round sand (Section 6.3.1). All the drift velocities have a dominant direction in the +ve Y direction. This indicates that the reproducibility of the velocity distribution measured in this system over the five minute experiment time is good and is similar to the behaviour found in the small bed fluidising ballotini. To give an idea of the significance of the drift velocity for the gas flow, Table 6.3.5 gives the magnitude of the drift velocity and the vertical mean velocity, U_z, (Figure 5.3.32). A resultant velocity based on the time averaged components given in the table would be nearly vertical.

Figure 6.3.31 shows the rms fluctuating velocity associated with the drift velocities given in Figure 6.3.30. The turbulence intensity is relatively high near the centre of the cross section at -ve positions on the YY axis, and tends to decrease with decreasing distance from the wall. The turbulence intensities at +ve positions on the YY axis do not show a steady decrease with decreasing distance from the wall as might be expected.

Table 6.3.6 shows the magnitude of the turbulence intensities measured in the Y direction and the turbulence intensities measured in the Z direction. The experimental conditions are as described above. The comparison shows that the degree of anisotropy in this fluidised system is significantly greater than that detected in the small bed fluidising ballotini or in the large bed fluidising round sand. This is an important effect of increased minimum fluidising velocity. The table also shows that the turbulence intensity measured vertically is much greater than the turbulence intensity measured horizontally, particularly near the wall. Furthermore, increase in the degree of anisotropy is evident near the wall as has been found in the two previous systems (Section 6.2.4 and 6.3.4).

6.4. Conclusions

The mean velocity estimates in the horizontal directions or the drift velocities and the rms fluctuating velocities have been studied. The effect of fluidising conditions and system parameters have been investigated in two bed geometries using various materials. The following conclusions can be drawn:

1 Drift velocities exist in the gas flow above fluidised beds of glass beads. The magnitude of the drift velocities is an order of magnitude less than that of the vertical

mean component of velocity. All the drift velocities had a dominant direction.

Both the magnitude of the drift velocities and the dominant direction can be affected by changes in the fluidisation conditions (Sections 6.2.1 and 6.2.2), but the effect does not appear to be systematic. For example, Figure 6.2.11 and Figure 6.2.12 show that the drift velocities are greater in magnitude at lower levels of turbulence. This indicates that the drift velocities are dependent on the structure of flow generated by erupting bubbles at the surface of the bed.

The dominant direction changes with increase in freeboard height. This suggests that secondary flow patterns exist in the freeboard space which can transfer momentum horizontally in the dominant direction.

The relative turbulence intensities measured in the horizontal directions are usually much greater than 100% and horizontal components of velocity exist in both directions over a period of time. The turbulence intensities measured in the horizontal directions show the same behaviour found for those measured in the vertical direction.

By comparison of the turbulence intensities measured in the three Cartesian coordinate directions (Figure 4.3) it was found that the degree of anisotropy was low in the single phase flow above fluidised beds of glass beads.

2 In the larger rectangular bed fluidising round sand it was found that drift velocities existed for the gas phase in the two phase flow. The magnitudes of the drift velocities were of the same order as the vertical component of velocity at the centre of the cross section

(Section 6.3.1). In many cases the drift velocities were found to have no dominant direction which was different from the behaviour found in the small bed fluidising glass ballotini beads.

The magnitude of the drift velocity and the dominant direction can be affected by the fluidisation conditions. There is some evidence that increase in turbulence intensity is associated with an increase in the magnitude of the drift velocity (Figures 6.3.10-6.3.14), but the converse is true at other positions on the reference axes.

The magnitudes of the drift velocities are greater at low freeboard height. This may be because of the horizontal components of velocity present when gas bubbles erupt at the surface of the fluidised bed (Section 5.4).

The relative turbulence intensities for the horizontal components of velocity were found to be greater than 100% at most positions in the freeboard. The distribution of velocities was such that components of velocity existed in both directions over a five minute experiment time. The turbulence intensity measured horizontally had a more consistent behaviour than that measured in the vertical direction (Section 6.3.1). However, similar deviations from expected behaviour were found for change in bed depth as found for the turbulence intensity measured vertically (Section 6.3.2).

By comparison of the turbulence intensities measured in the X, Y and Z directions it was found that the degree of anisotropy was low in this flow field. This is not consistent with the structure suggested in Section 5.4, and indicates that large scale anisotropic turbulence is not fully developed. This may be because of the low superficial flows used in the fluidised system.

Measurements of the gas flow field above a fluidised bed of catalyst were taken. The minimum fluisidising velocity was approximately ten times that of round sand (Section 4.1.2). It was found that the drift velocities were an order of magnitude less than the vertical components of velocity. Comparison of the turbulence intensities measured horizontally and vertically showed that the degree of anisotropy was high. It is concluded that only in this fluidised system is the structure of the gas flow resulting from gas bubbles bursting into the gas leaving the dense phase anisotropic.
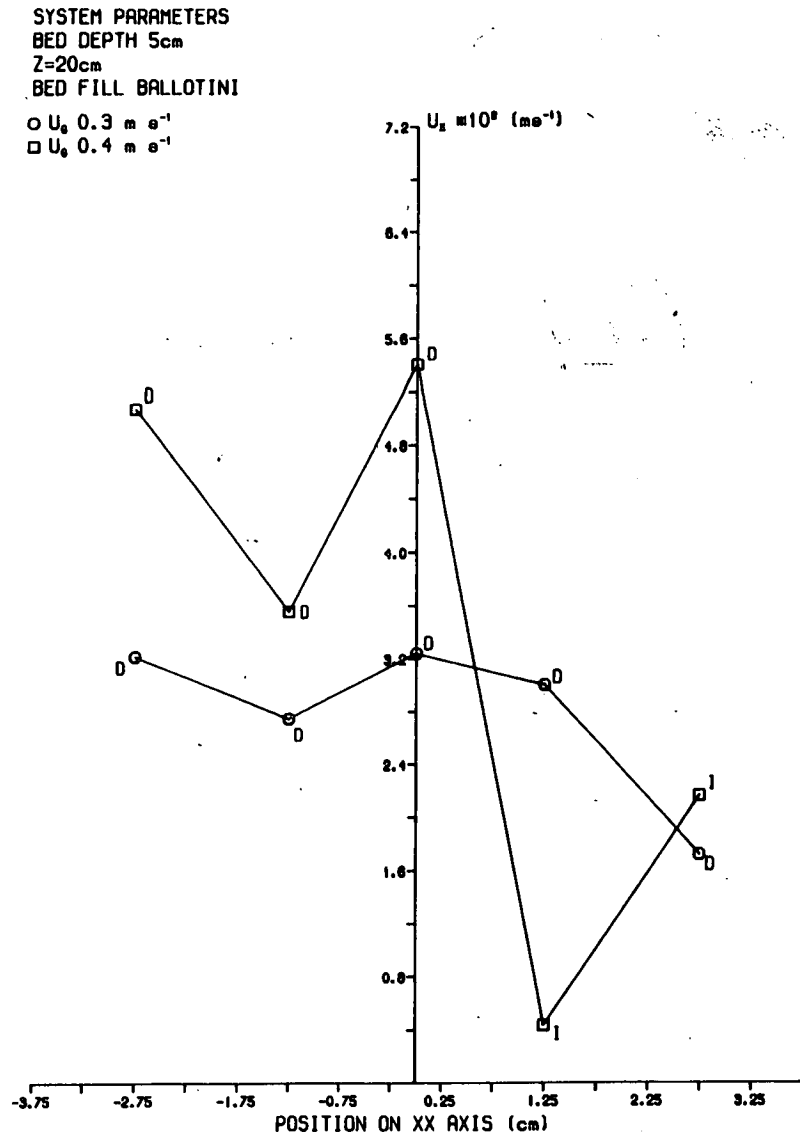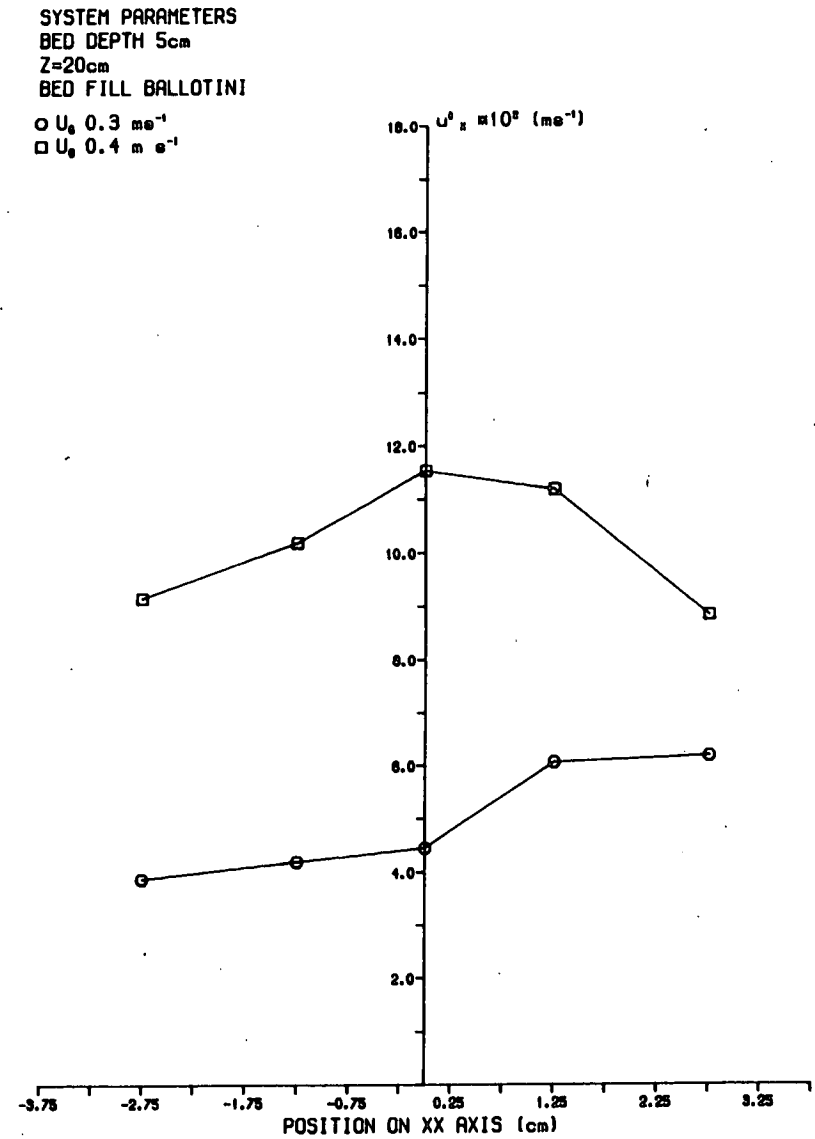
Figure 6.2.1 YY Profile of U_Y - Small Bed.
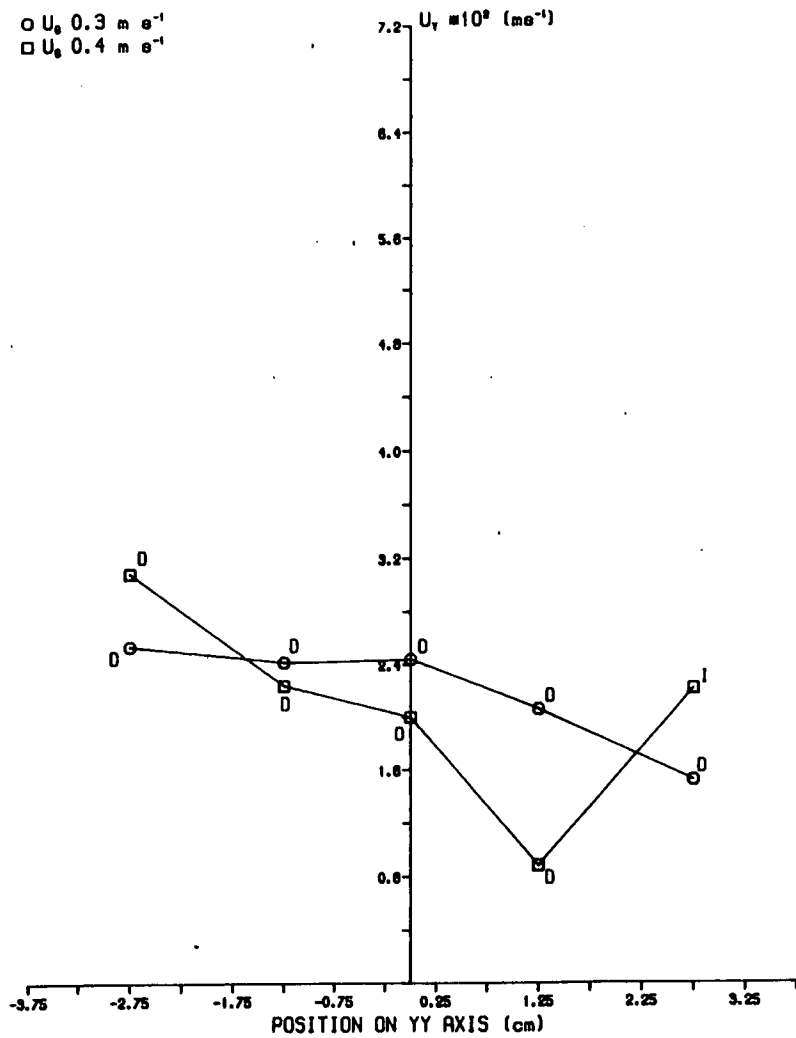
Figure 6.2.2 YY Profile of u'_Y - Small Bed.

SYSTEM PARAMETERS
BED DEPTH 5cm
Z=20cm
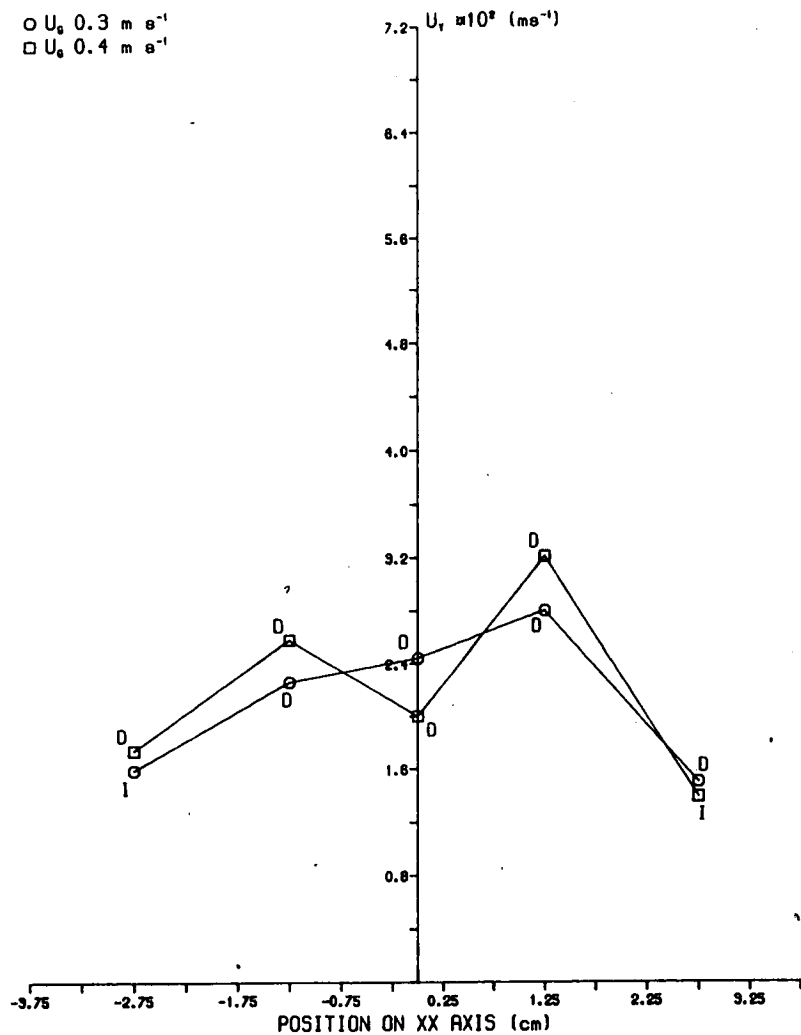BED FILL BALLOTINI

o U_s 0.3 m s^{-1}
□ U_s 0.4 m s^{-1}

SYSTEM PARAMETERS
BED DEPTH 5cm
Z=20cm
BED FILL BALLOTINI

o U_s 0.3 m s^{-1}
□ U_s 0.4 m s^{-1}

189

POSITION ON YY AXIS (cm)

POSITION ON YY AXIS (cm)
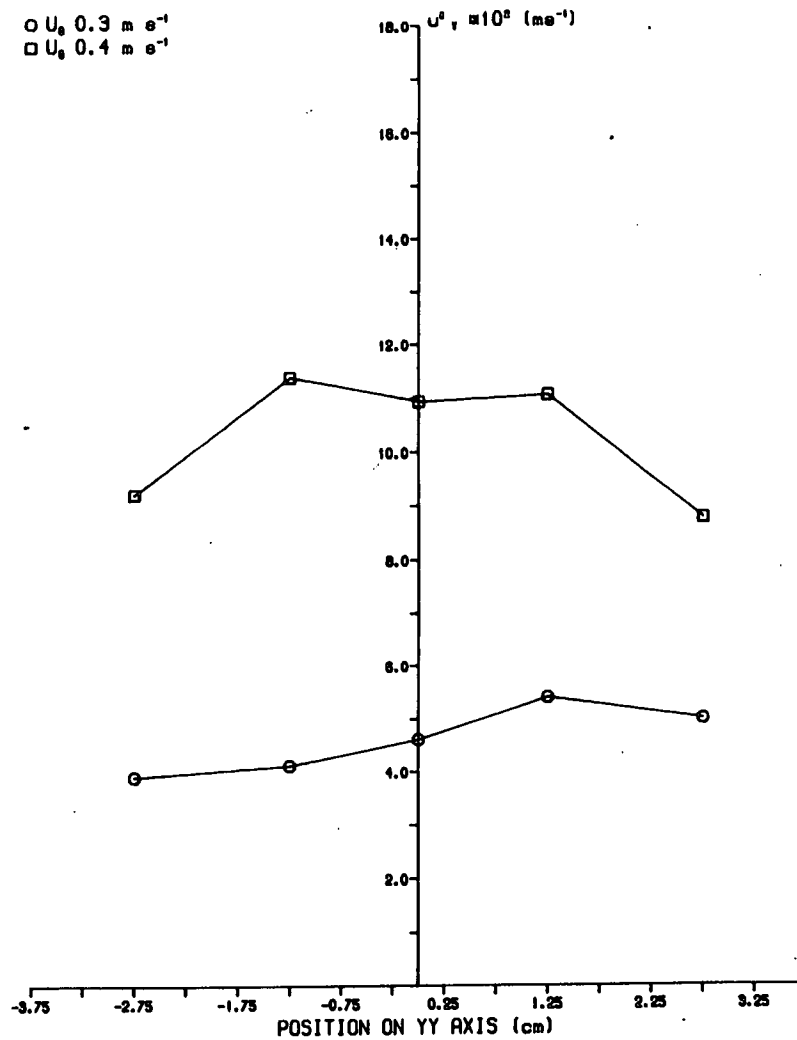
Form of Velocity Spectrum or Distribution of U_y, $P(U_y)$.
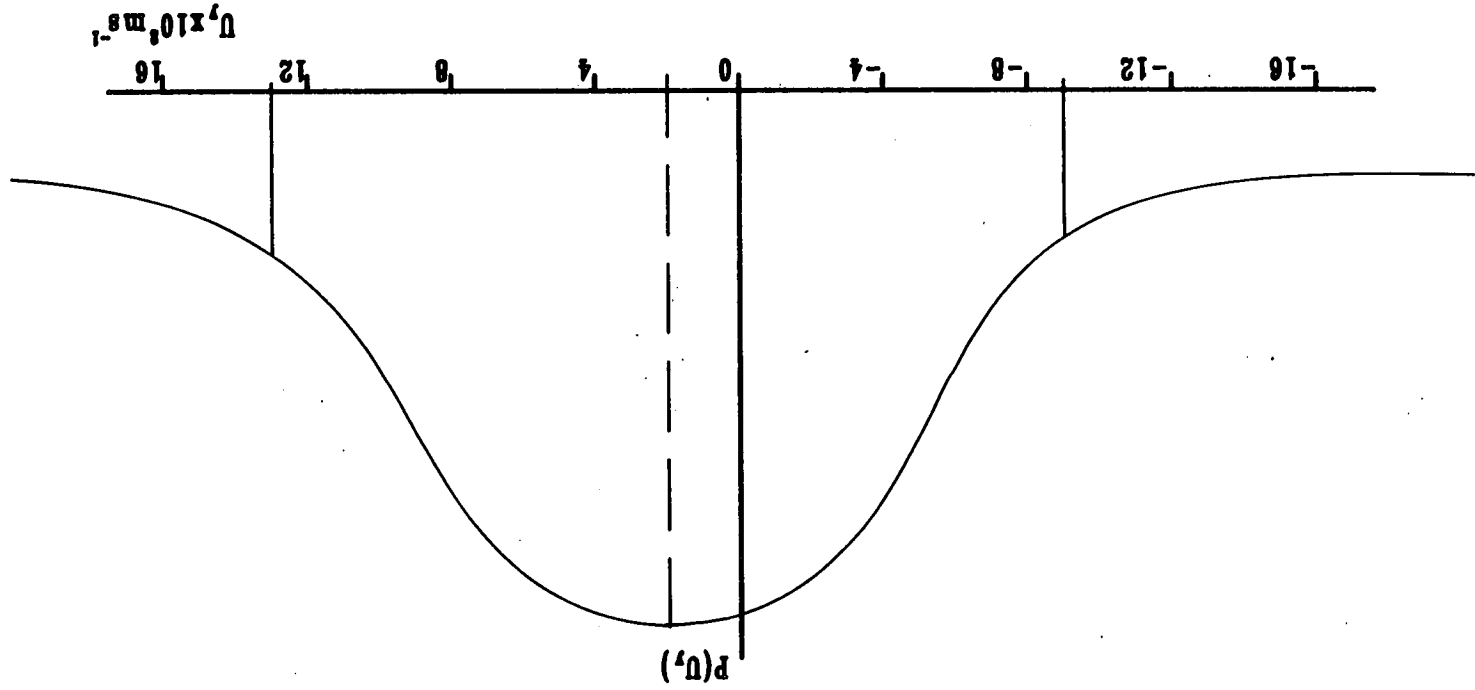
Figure 6.2.3

Figure 6.2.4 YY Profile of U_x - Small Bed.
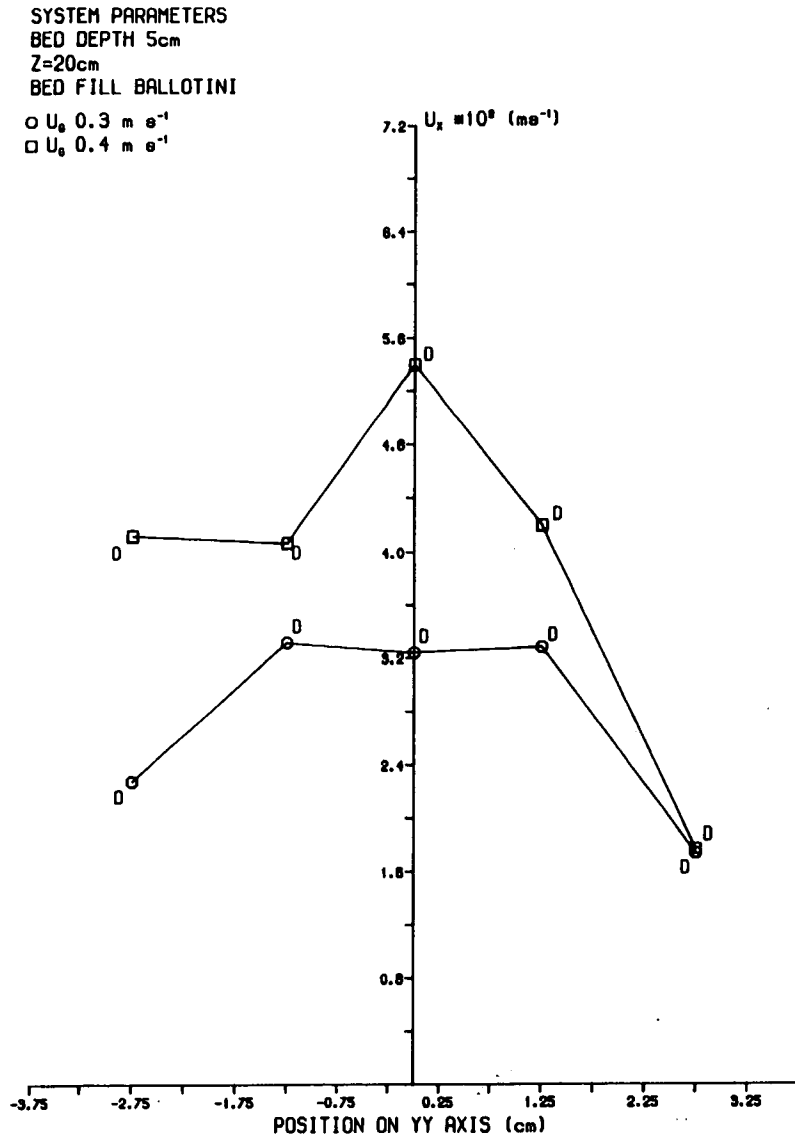
Figure 6.2.5 YY Profile of u'_x - Small Bed.

SYSTEM PARAMETERS
BED DEPTH 5cm
Z=20cm
BED FILL BALLOTINI
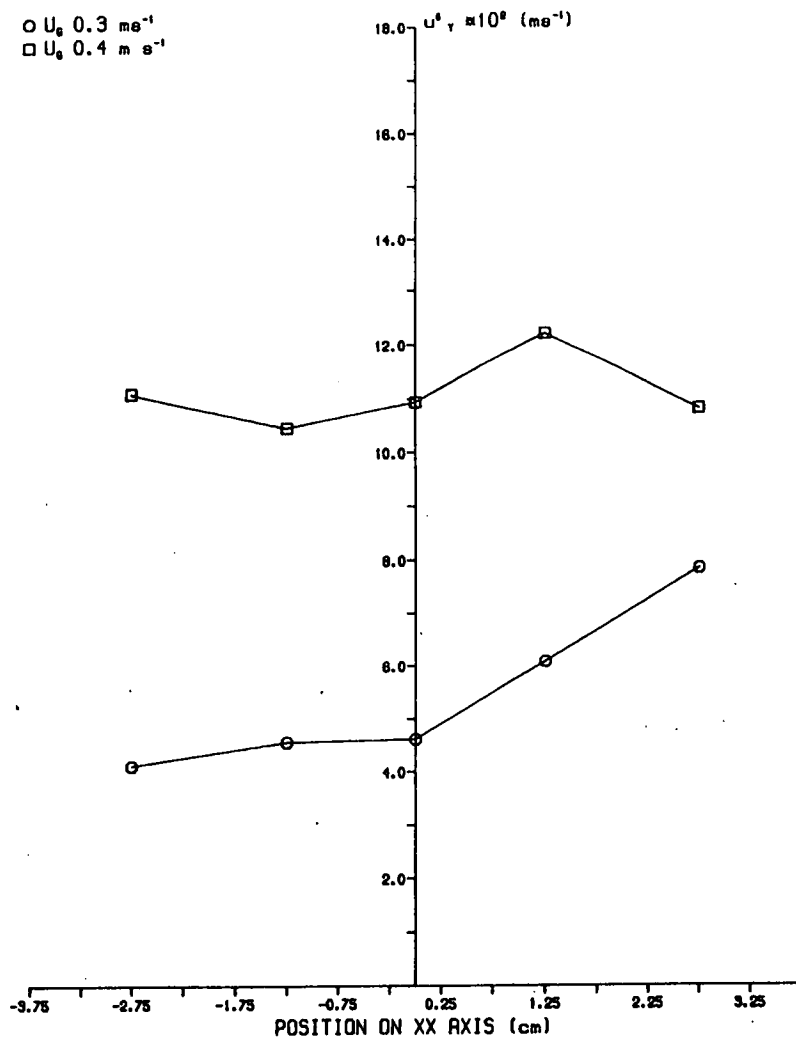
o U_e 0.3 m s^{-1}
□ U_e 0.4 m s^{-1}

U_x ☆10^8 (ms^{-1})

POSITION ON YY AXIS (cm)

SYSTEM PARAMETERS
BED DEPTH 5cm
Z=20cm
BED FILL BALLOTINI

o U_e 0.3 m s^{-1}
□ U_e 0.4 m s^{-1}

u'_x ☆10^8 (ms^{-1})

POSITION ON YY AXIS (cm)

191
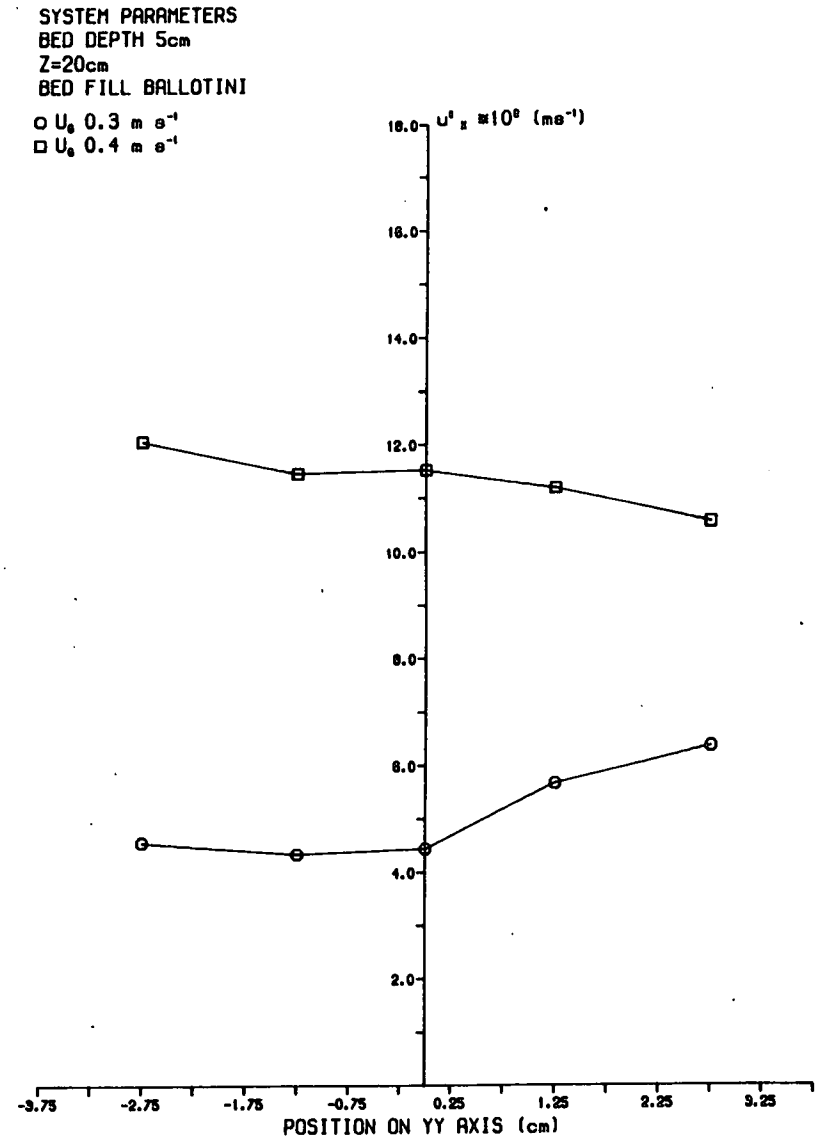
Figure 6.2.6 XX Profile of U_x - Small Bed.

SYSTEM PARAMETERS
BED DEPTH 5cm
Z=20cm
BED FILL BALLOTINI

o U_0 0.3 m e^{-1}
□ U_0 0.4 m e^{-1}

Figure 6.2.7 XX Profile of u'_x - Small Bed.

SYSTEM PARAMETERS
BED DEPTH 5cm
Z=20cm
BED FILL BALLOTINI

o U_0 0.3 m e^{-1}
□ U_0 0.4 m e^{-1}

192

Figure 6.2.8 XX Profile of U_Y - Small Bed.

Figure 6.2.9 XX Profile of u'_Y - Small Bed.

SYSTEM PARAMETERS
BED DEPTH 5cm
Z=20cm
BED FILL BALLOTINI

O U_6 0.3 m s^{-1}
□ U_6 0.4 m s^{-1}

U_Y ×10^2 (ms^{-1})

POSITION ON XX AXIS (cm)

SYSTEM PARAMETERS
BED DEPTH 5cm
Z=20cm
BED FILL BALLOTINI

O U_6 0.3 ms^{-1}
□ U_6 0.4 m s^{-1}

u'_Y ×10^3 (ms^{-1})

POSITION ON XX AXIS (cm)

Pattern of Average Transverse Velocity Variation across
Freeboard of Small Bed, Depth 5 cm, at Freeboard Height =
20 cm.

(a)

U_c **30 cms**$^{-1}$

Figure 6.2.10

(b)

U_c **40 cms**$^{-1}$
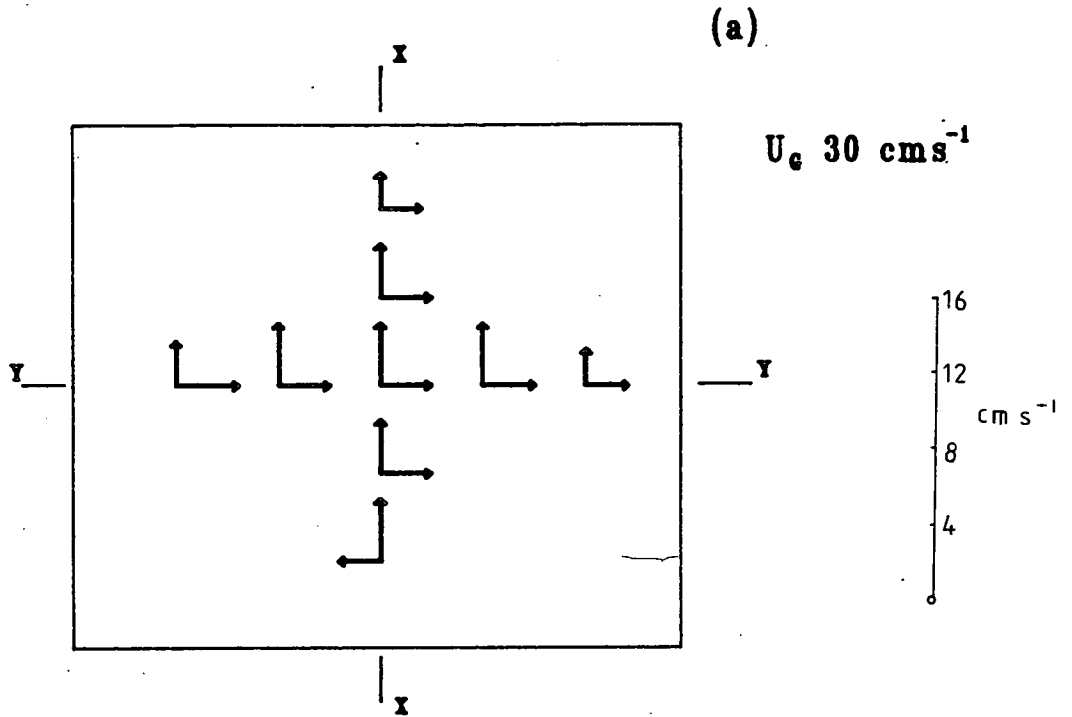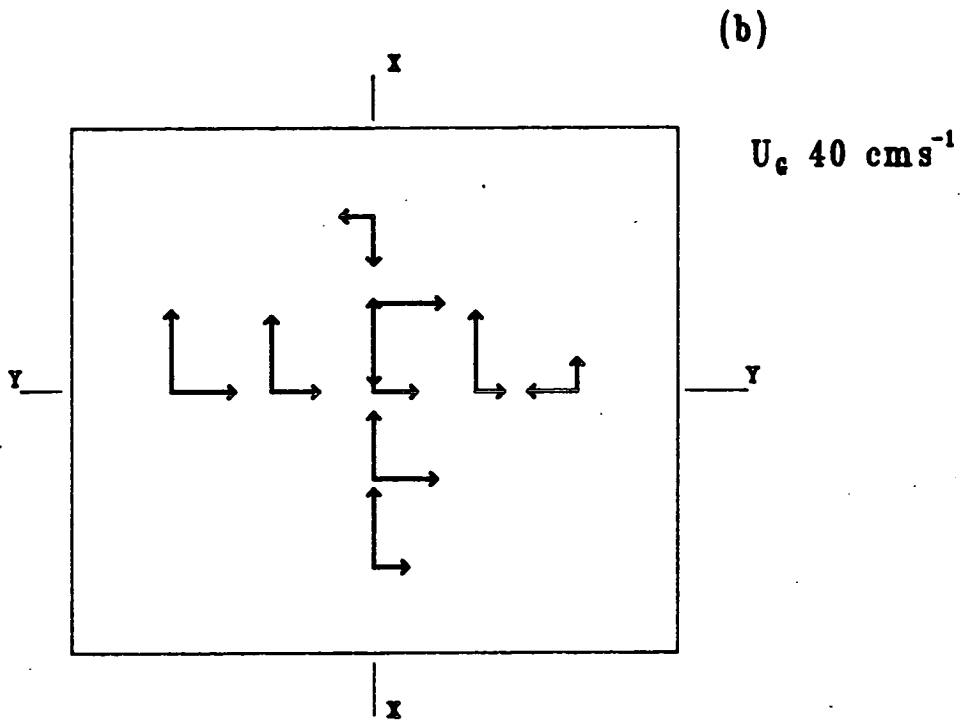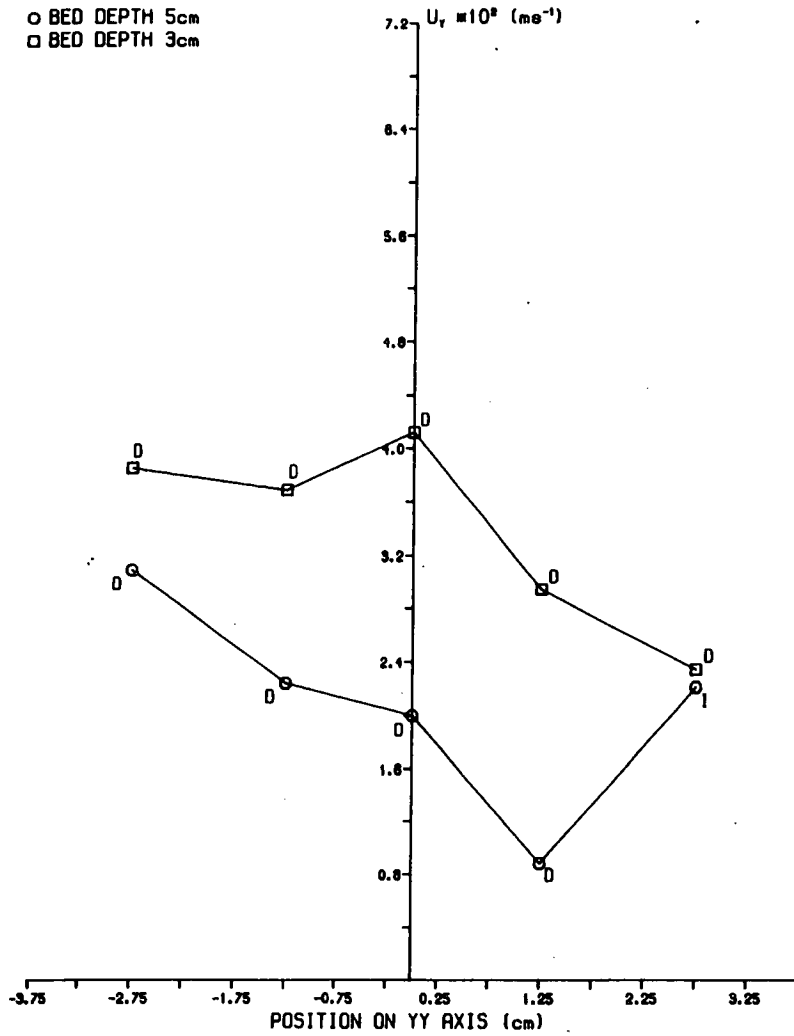
Figure 6.2.11 YY Profile of U_Y - Small Bed.

Figure 6.2.12 YY Profile of u'_Y - Small Bed.

SYSTEM PARAMETERS
U_0 0.4 m s^{-1}
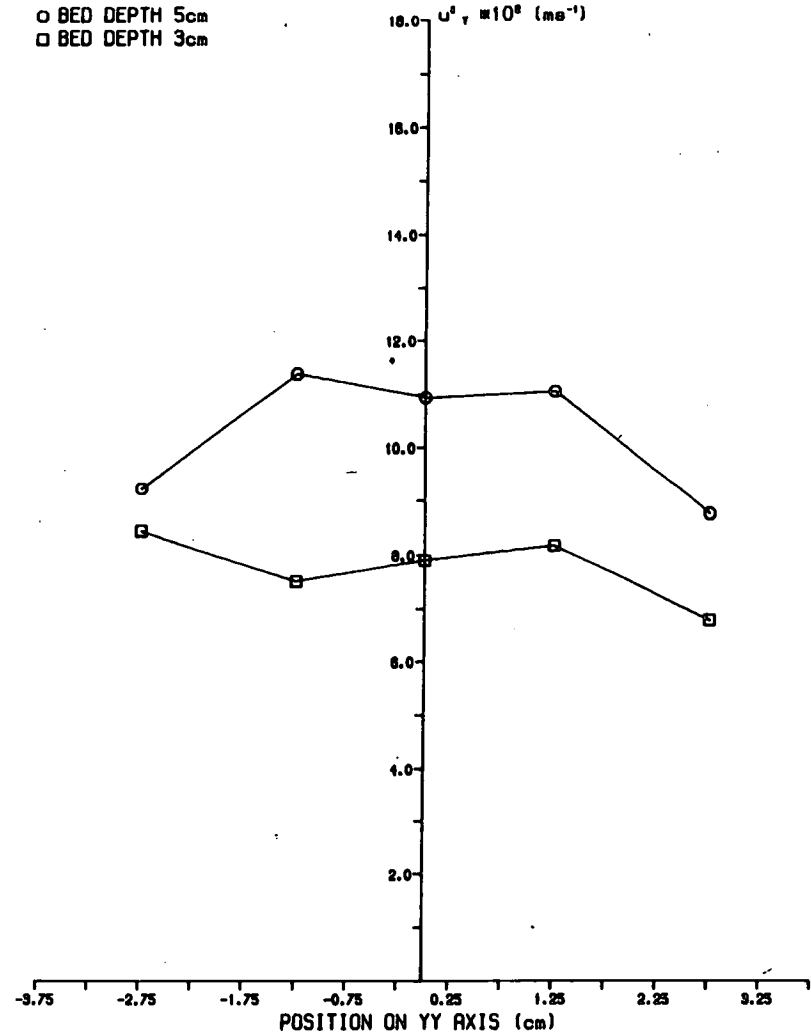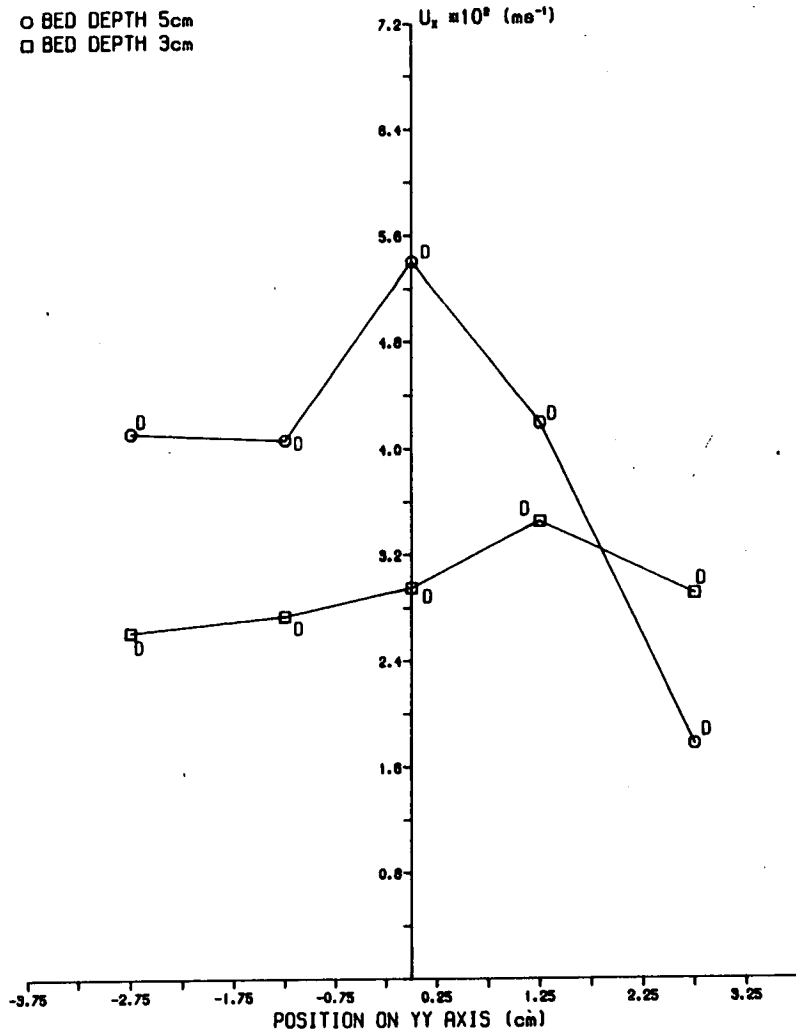Z=20cm
BED FILL BALLOTINI

o BED DEPTH 5cm
□ BED DEPTH 3cm

$U_Y \times 10^2$ (ms^{-1})

POSITION ON YY AXIS (cm)

SYSTEM PARAMETERS
U_0 0.4 m s^{-1}
Z=20cm
BED FILL BALLOTINI

o BED DEPTH 5cm
□ BED DEPTH 3cm

$u'_Y \times 10^2$ (ms^{-1})

POSITION ON YY AXIS (cm)

Figure 6.2.13 YY Profile of U_x - Small Bed.

Figure 6.2.14 YY Profile of u'_x - Small Bed.

SYSTEM PARAMETERS
U_s 0.4 m s^{-1}
Z=20cm
BED FILL BALLOTINI

o BED DEPTH 5cm
□ BED DEPTH 3cm

U_x ×10^2 (ms^{-1})

SYSTEM PARAMETERS
U_s 0.4 m s^{-1}
Z=20cm
BED FILL BALLOTINI

o BED DEPTH 5cm
□ BED DEPTH 3cm

u'_x ×10^2 (ms^{-1})

POSITION ON YY AXIS (cm)

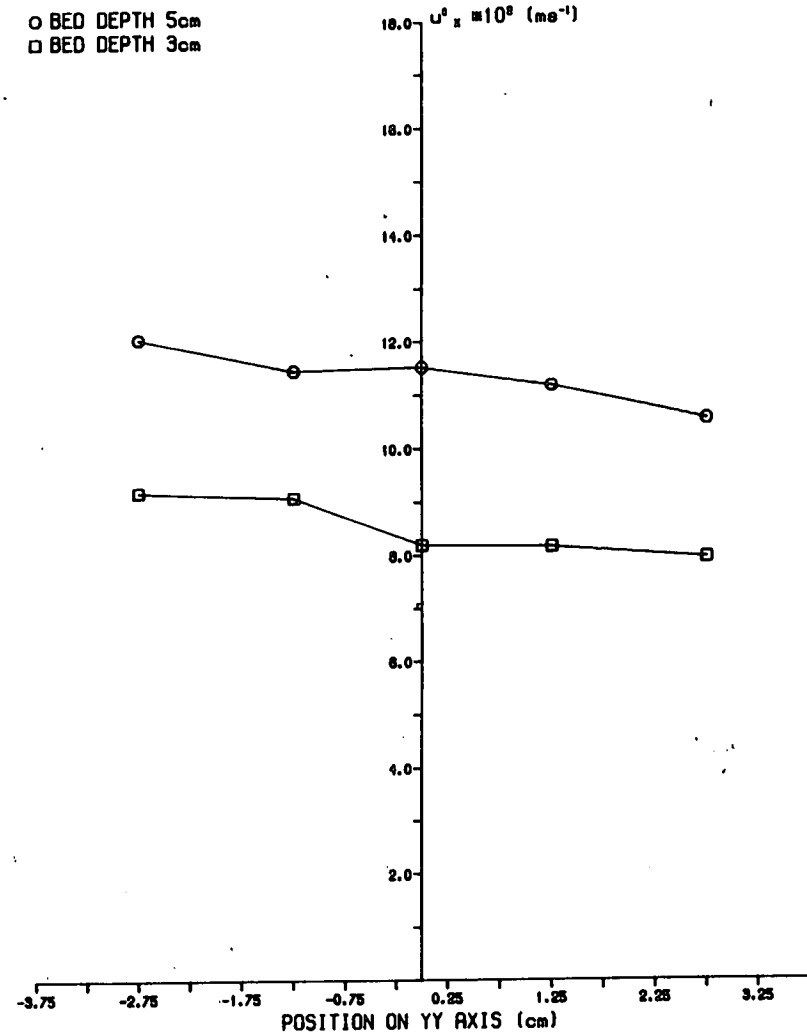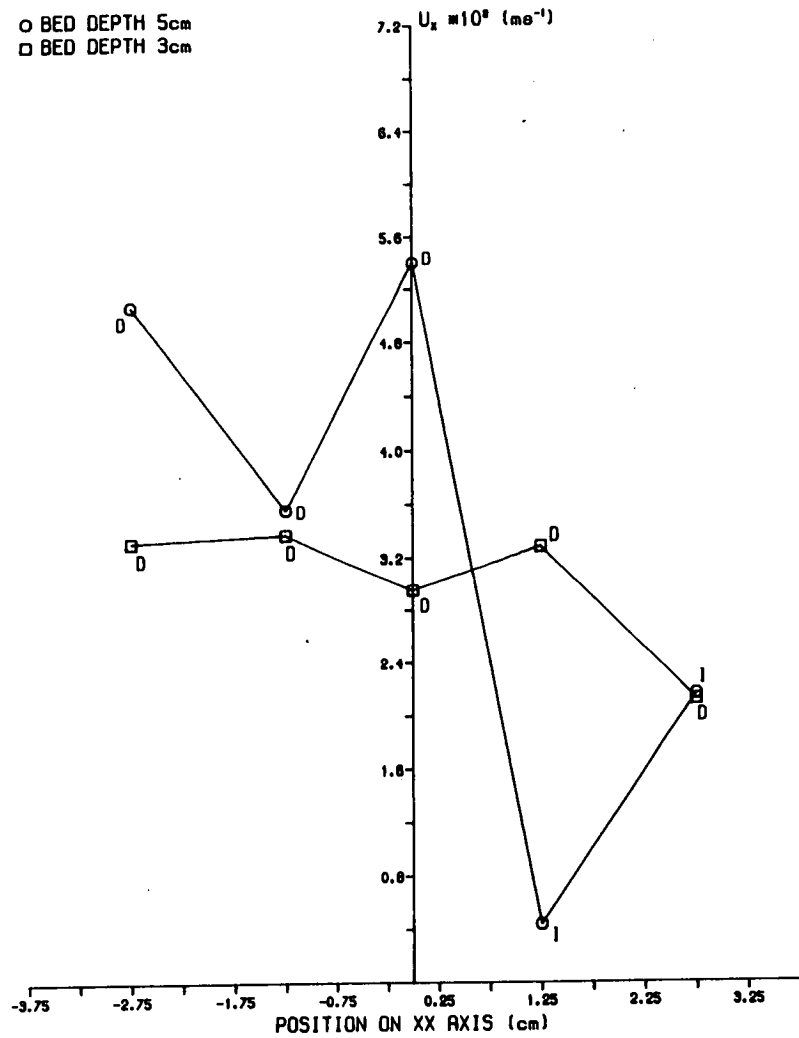POSITION ON YY AXIS (cm)

196

Figure 6.2.15 XX Profile of U_x - Small Bed.

SYSTEM PARAMETERS
U_0 0.4 m s^{-1}
Z=20cm
BED FILL BALLOTINI

o BED DEPTH 5cm
□ BED DEPTH 3cm

Figure 6.2.16 XX Profile of u$'_x$ - Small Bed.

SYSTEM PARAMETERS
U_0 0.4 m s^{-1}
Z=20cm
BED FILL BALLOTINI

o BED DEPTH 5cm
□ BED DEPTH 3cm
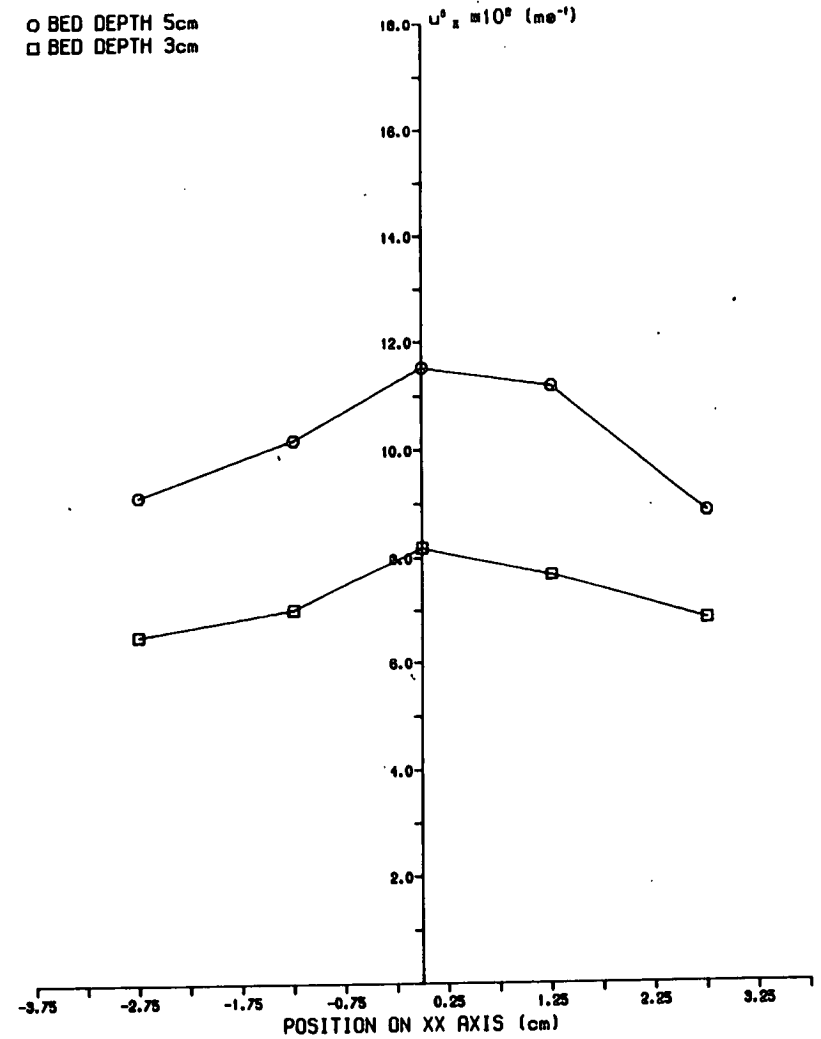
197

Figure 6.2.17 XX Profile of U_Y - Small Bed.
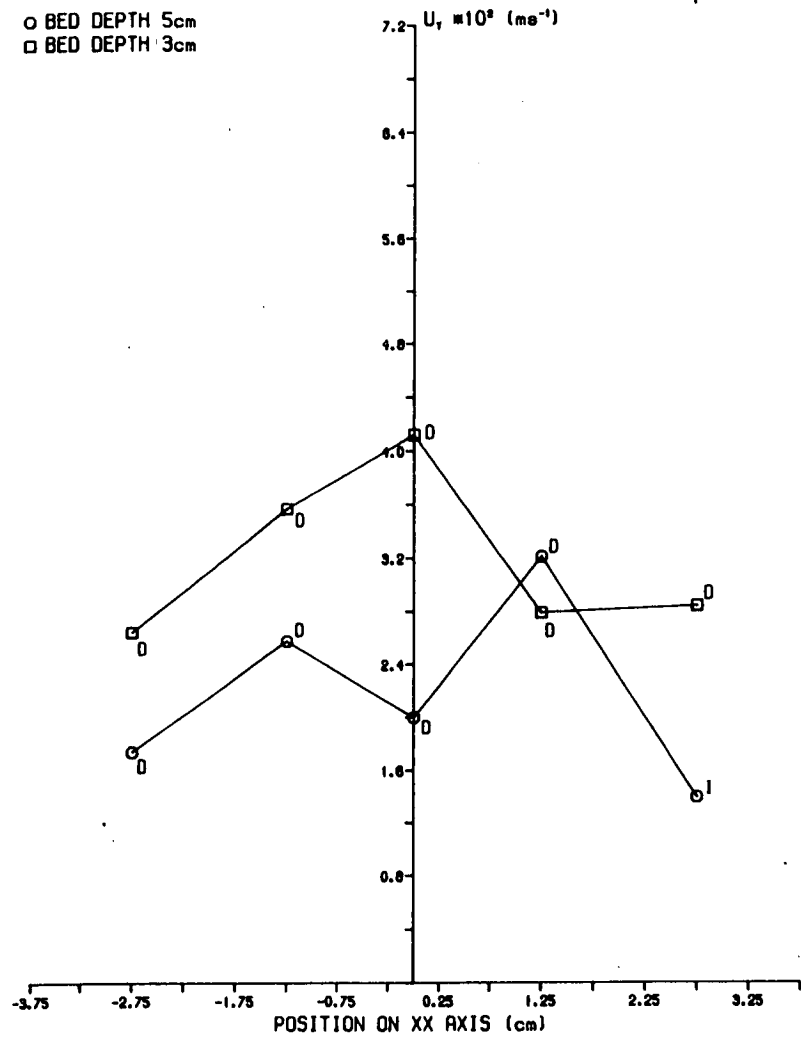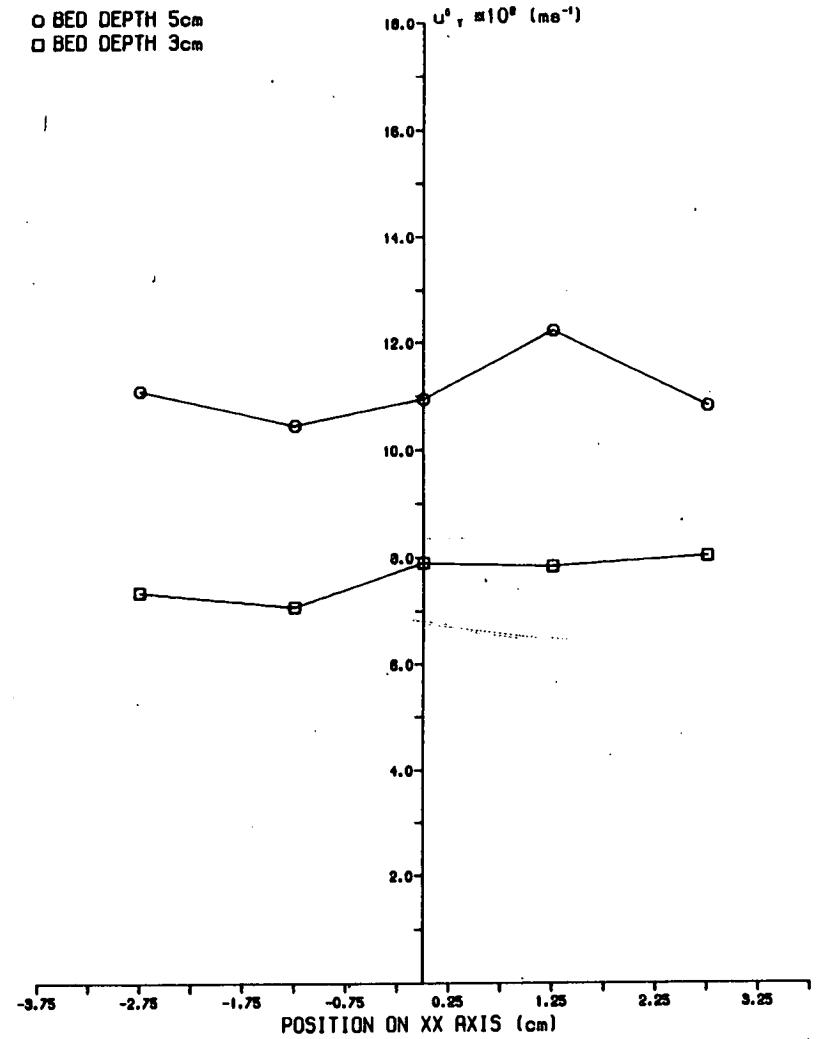
Figure 6.2.18 XX Profile of u'_Y - Small Bed.

SYSTEM PARAMETERS
U_0 0.4 m s^{-1}
Z=20cm
BED FILL BALLOTINI

o BED DEPTH 5cm
□ BED DEPTH 3cm

U_Y ×10^2 (ms^{-1})

POSITION ON XX AXIS (cm)

SYSTEM PARAMETERS
U_0 0.4 m s^{-1}
Z=20cm
BED FILL BALLOTINI

o BED DEPTH 5cm
□ BED DEPTH 3cm

u'_Y ×10^2 (ms^{-1})

POSITION ON XX AXIS (cm)

198

Pattern of Average Transverse Velocity Variation across
Freeboard of Small Bed, Depth 3 cm, at Freeboard Height =
20 cm.

(a)

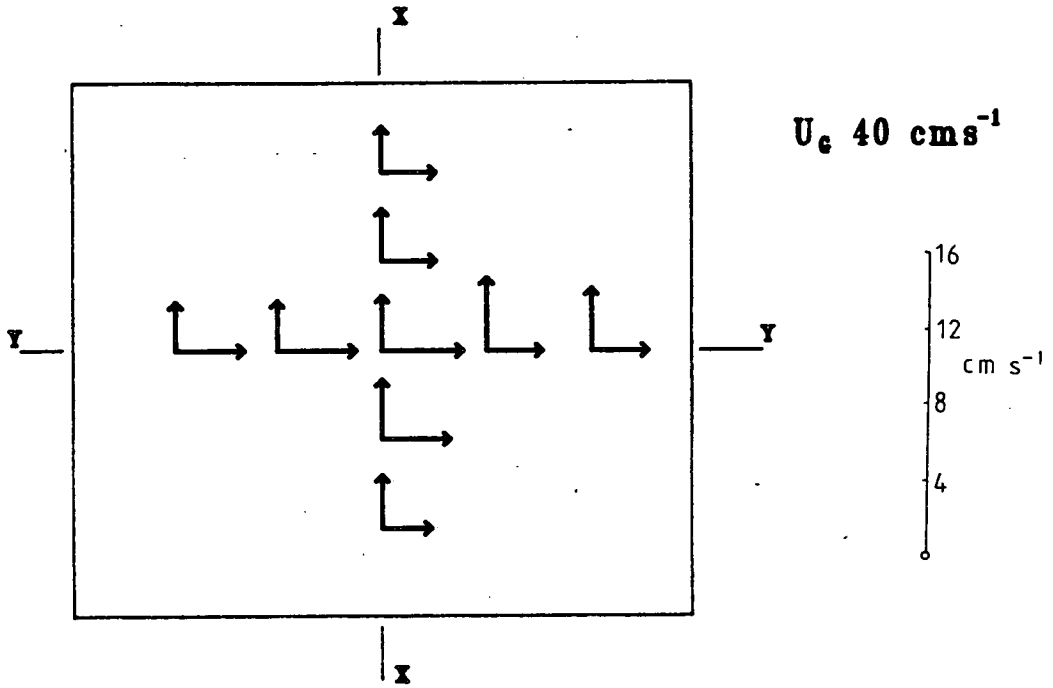U_c **40 cms^{-1}**

Figure 6.2.19

(b)

U_c **30 cms^{-1}**

Figure 6.2.20 YY Profile of U_Y - Small Bed.

Figure 6.2.21 YY Profile of u'_Y - Small Bed.

SYSTEM PARAMETERS
BED DEPTH 3cm
U_e 0.4 m s^{-1}
BED FILL BALLOTINI

o Z 20cm
□ Z 29.5cm
△ Z 40cm

SYSTEM PARAMETERS
BED DEPTH 3cm
U_e 0.4 m s^{-1}
BED FILL BALLOTINI

o Z 20cm
□ Z 29.5cm
△ Z 40cm

POSITION ON YY AXIS (cm)

POSITION ON YY AXIS (cm)

Figure 6.2.22 YY Profile of U_x - Small Bed.

SYSTEM PARAMETERS
BED DEPTH 5cm
U_s 0.4 m s^{-1}
BED FILL BALLOTINI

o Z 20cm
□ Z 29.5cm
△ Z 40cm

U_x #10^2 (ms^{-1})
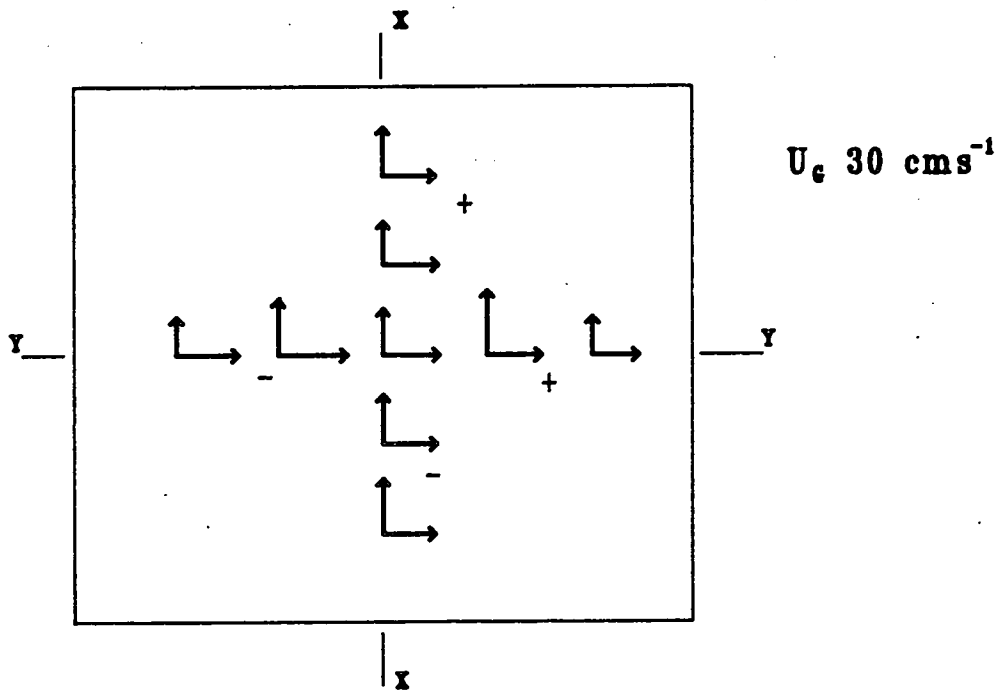
POSITION ON YY AXIS (cm)

Figure 6.2.23 YY Profile of u'_x - Small Bed.

SYSTEM PARAMETERS
BED DEPTH 5cm
U_s 0.4 m s^{-1}
BED FILL BALLOTINI

o Z 20cm
□ Z 29.5cm
△ Z 40cm

u'_x #10^2 (ms^{-1})

POSITION ON YY AXIS (cm)
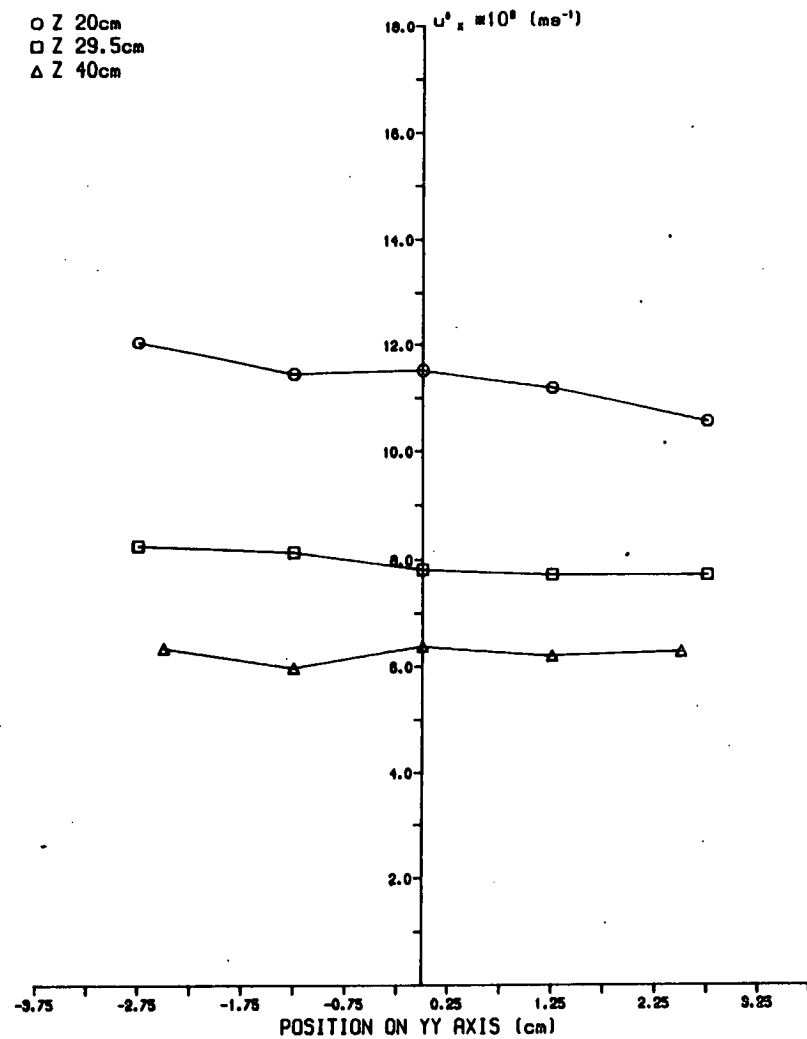
Figure 6.2.24 XX Profile of U_x - Small Bed.

SYSTEM PARAMETERS
BED DEPTH 5cm
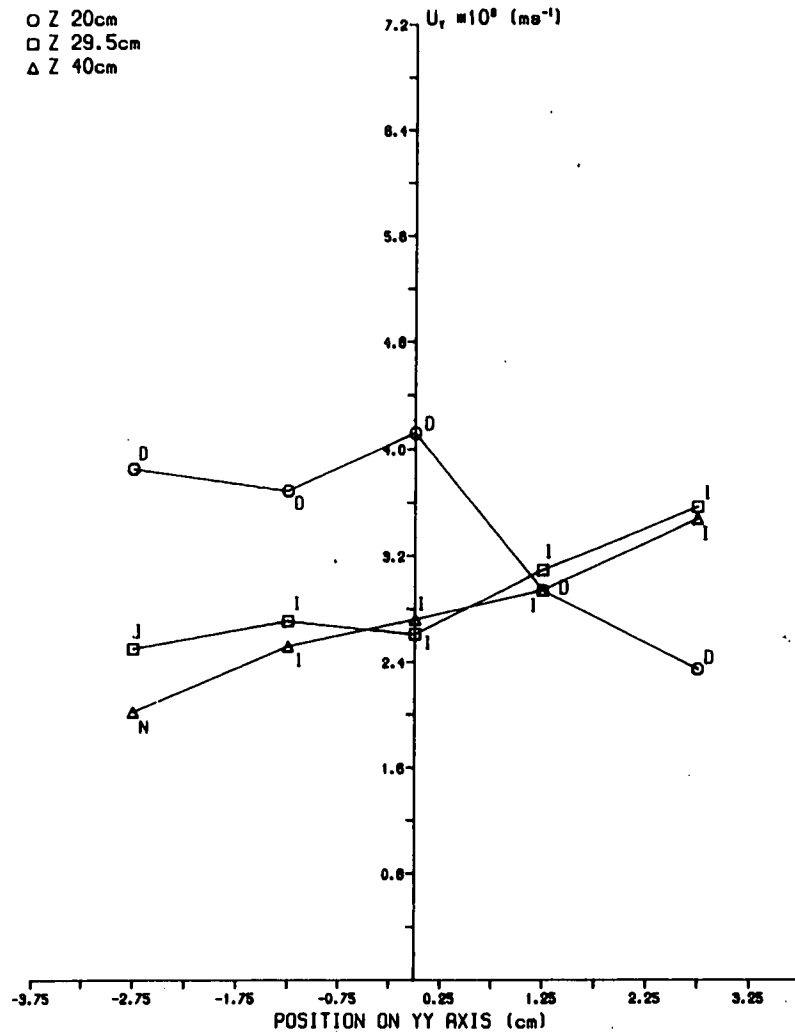U_s 0.3 m s⁻¹
BED FILL BALLOTINI

o Z 20cm
□ Z 29.5cm
△ Z 40cm
◇ Z 47.5cm
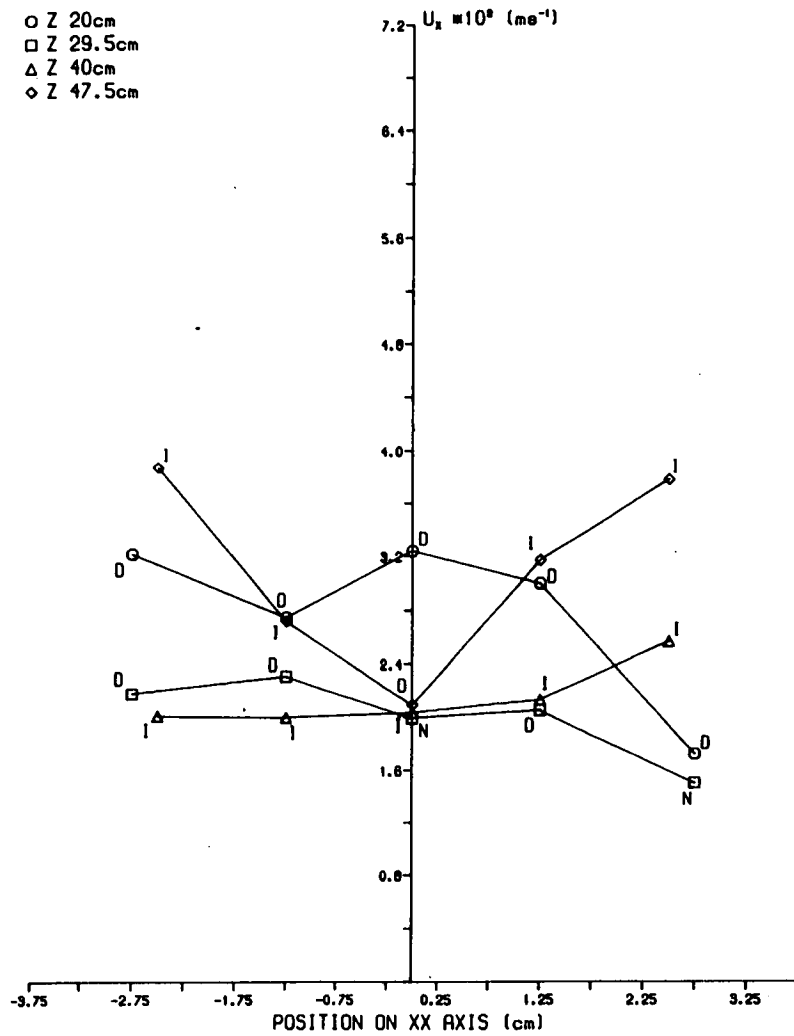
Figure 6.2.25 XX Profile of u'_x - Small Bed.

SYSTEM PARAMETERS
BED DEPTH 5cm
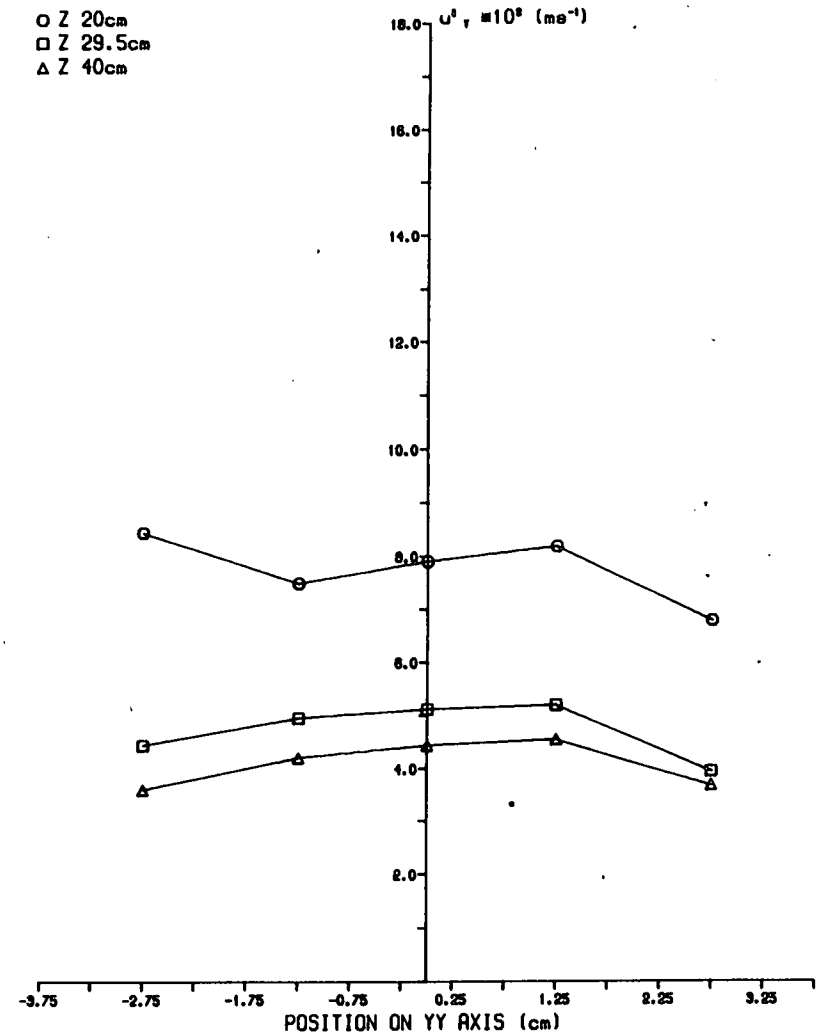U_s 0.3 m s⁻¹
BED FILL BALLOTINI

o Z 20cm
□ Z 29.5cm
△ Z 40cm
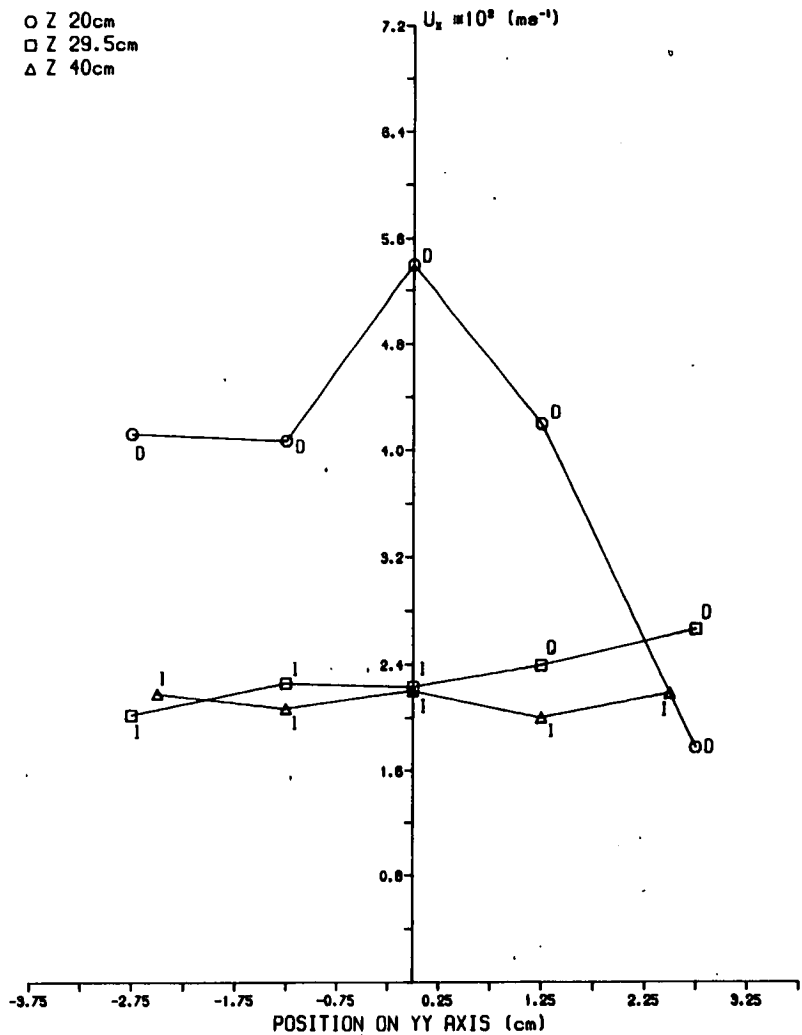◇ Z 47.5cm
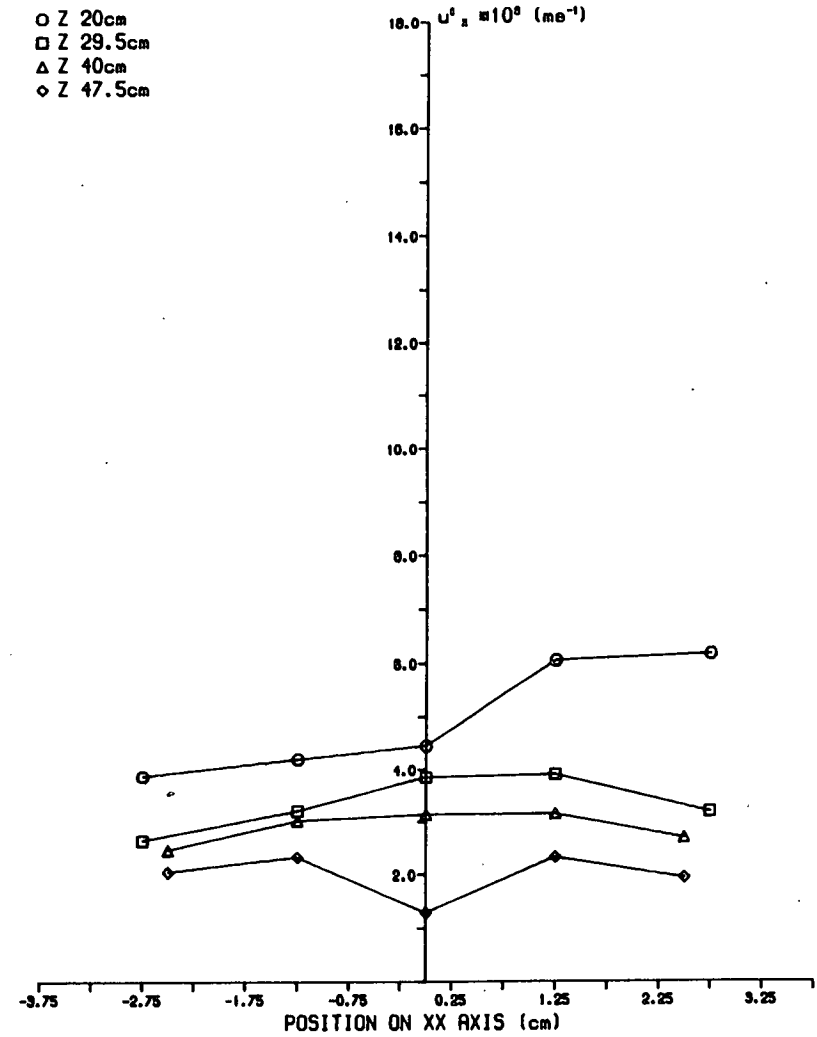
Figure 6.2.26 XX Profile of U_Y - Small Bed.
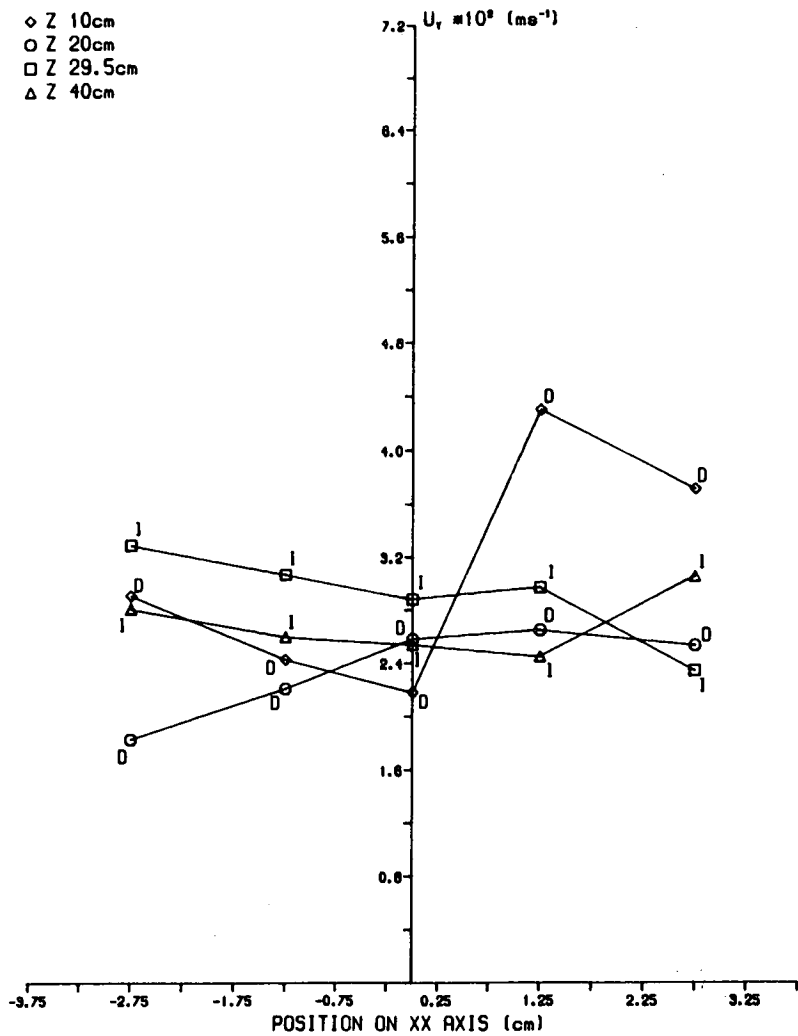
Figure 6.2.27 XX Profile of u'_Y - Small Bed.

SYSTEM PARAMETERS
BED DEPTH 3cm
U_8 0.3 m e^{-1}
BED FILL BALLOTINI

◇ Z 10cm
O Z 20cm
□ Z 29.5cm
△ Z 40cm

U_Y #10^2 (me^{-1})

POSITION ON XX AXIS (cm)

SYSTEM PARAMETERS
BED DEPTH 3cm
U_8 0.3 m e^{-1}
BED FILL BALLOTINI

◇ Z 10cm
O Z 20cm
□ Z 29.5cm
△ Z 40cm

u'_Y #10^2 (me^{-1})

POSITION ON XX AXIS (cm)

203
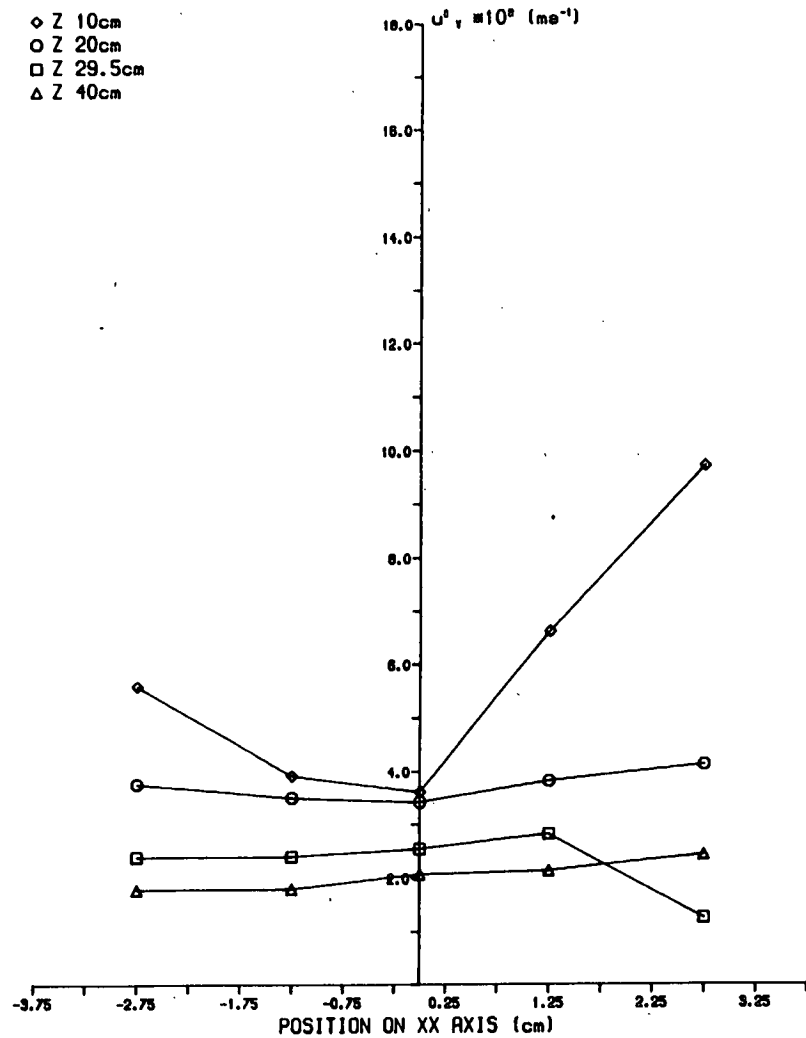
Pattern of Average Transverse Velocity Variation across
Freeboard of Small Bed, Depth 3 cm, at Freeboard Height =
40 cm.

Figure 6.2.28

Figure 6.3.1 YY Profile of U_Y - Large Bed.

SYSTEM PARAMETERS
BED DEPTH 60cm
Z 120cm
BED FILL SAND

o U_6 3 cm s^{-1}
□ U_6 4 cm s^{-1}

U_Y ×10^3 (ms^{-1})

14.4

12.8

11.2

9.6

8.0

6.4

4.8

3.2

1.6

-24   -16   -8   8   16   24
POSITION ON YY AXIS (cm)
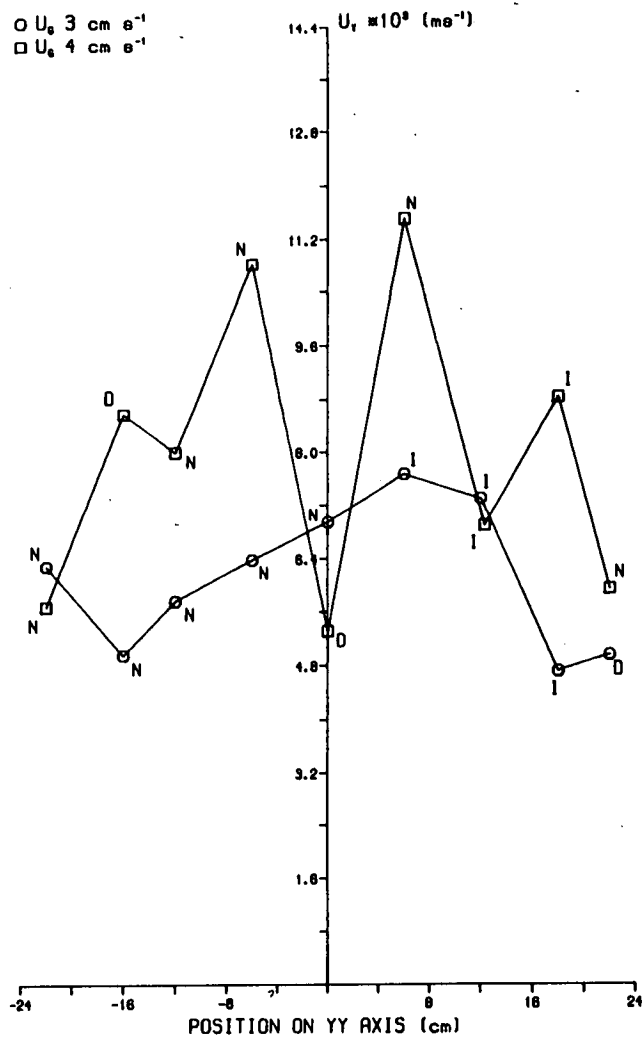
Figure 6.3.2 YY Profile of u'_Y - Large Bed.

SYSTEM PARAMETERS
BED DEPTH 60cm
Z 120cm
BED FILL SAND

o U_6 3 cm s^{-1}
□ U_6 4 cm s^{-1}

u'_Y ×10^3 (ms^{-1})

27

24

21

18

15

12

9

6

3

-24   -16   -8   8   16   24
POSITION ON YY AXIS (cm)
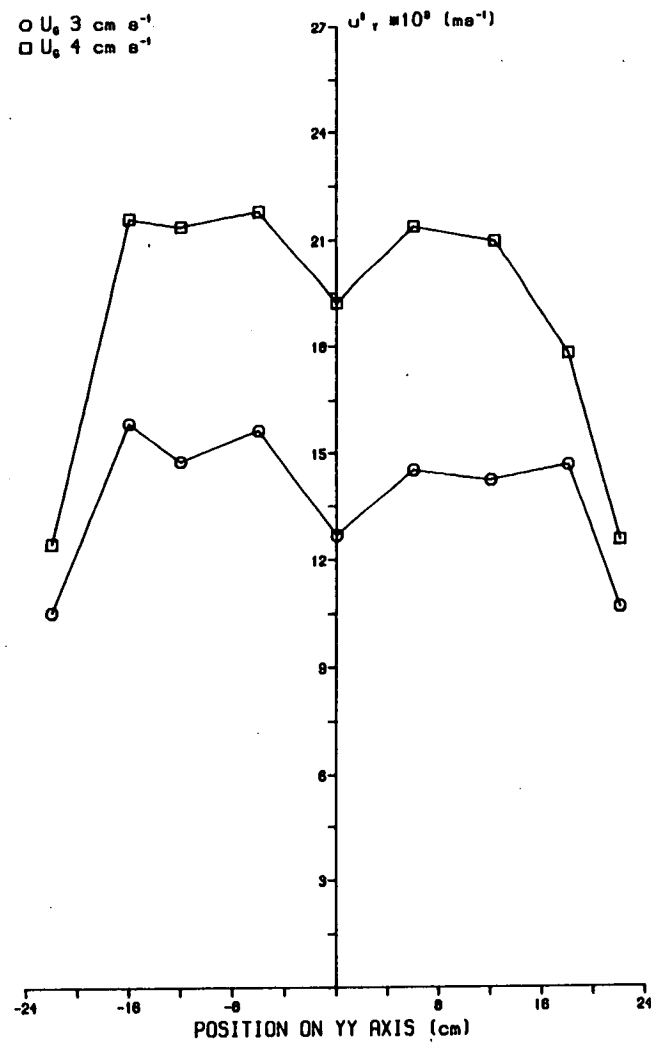
Figure 6.3.3 YY Profile of U_x - Large Bed.

SYSTEM PARAMETERS
BED DEPTH 60cm
Z 120cm
BED FILL SAND

o U_6 3 cm s^{-1}
□ U_6 4 cm s^{-1}

$U_x \times 10^3$ (m s^{-1})

POSITION ON YY AXIS (cm)
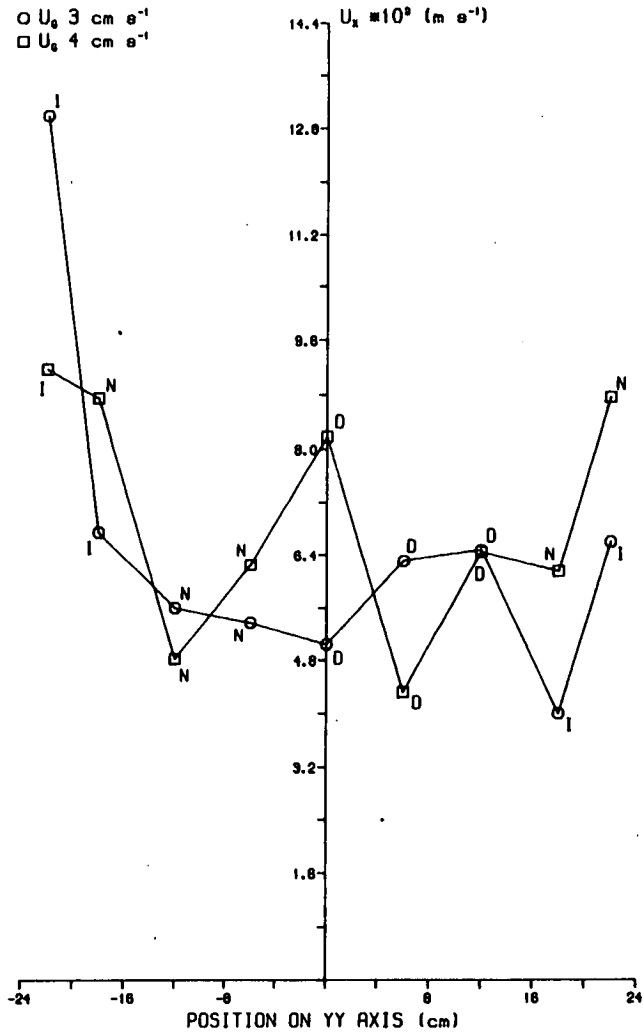
Figure 6.3.4 YY Profile of u'_x - Large Bed.

SYSTEM PARAMETERS
BED DEPTH 60cm
Z 120cm
BED FILL SAND

o U_6 3 cm s^{-1}
□ U_6 4 cm s^{-1}

$u'_x \times 10^3$ (m s^{-1})

POSITION ON YY AXIS (cm)

Figure 6.6 XX Profile of u'_x - Large Bed.

SYSTEM PARAMETERS
BED DEPTH 60cm
Z 120cm
BED FILL SAND

○ U_0 3 cm s^{-1}
□ U_0 4 cm s^{-1}

POSITION ON XX AXIS (cm)

$\overline{u'^2_x}$ x10^6 (m s^{-1})

Figure 6.5 XX Profile of U_x - Large Bed.

SYSTEM PARAMETERS
BED DEPTH 60cm
Z 120cm
BED FILL SAND

○ U_0 3 cm s^{-1}
□ U_0 4 cm s^{-1}

POSITION ON XX AXIS (cm)

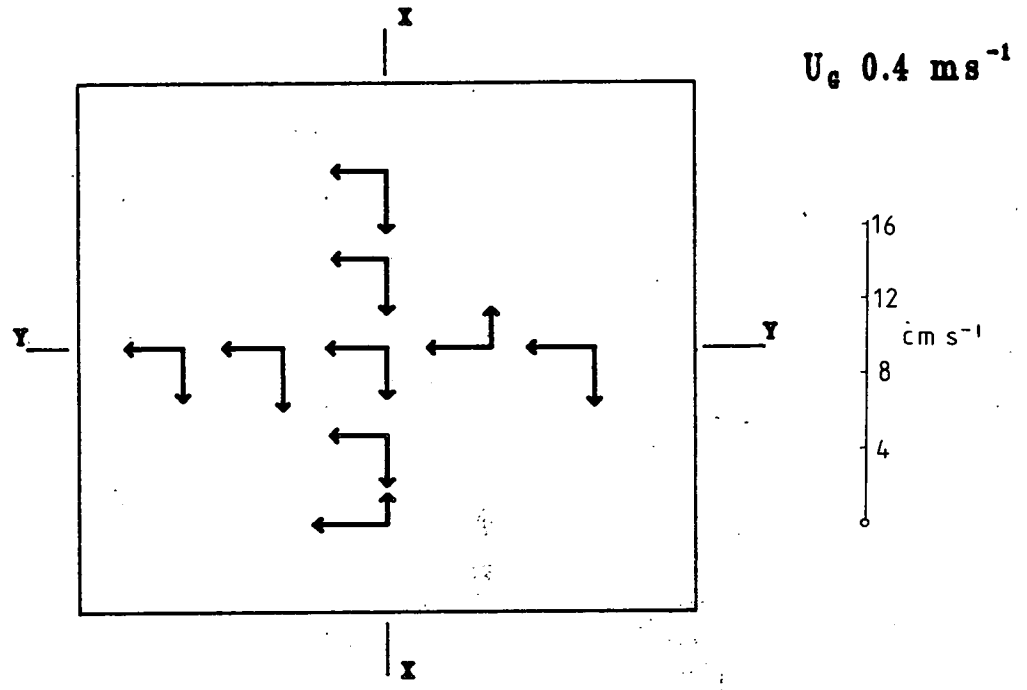U_x x10^6 (m s^{-1})
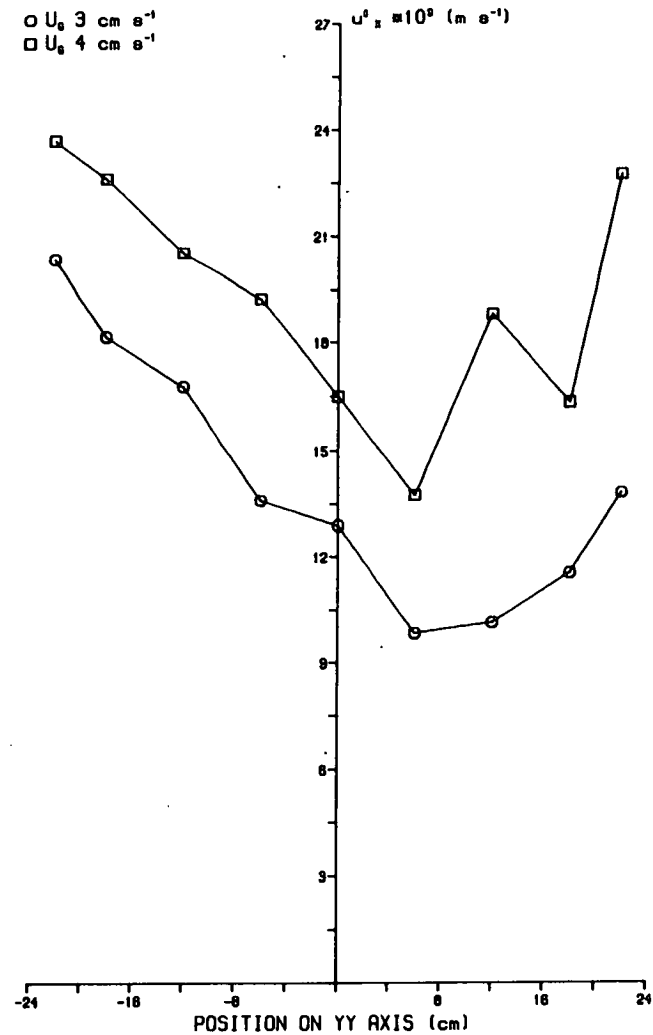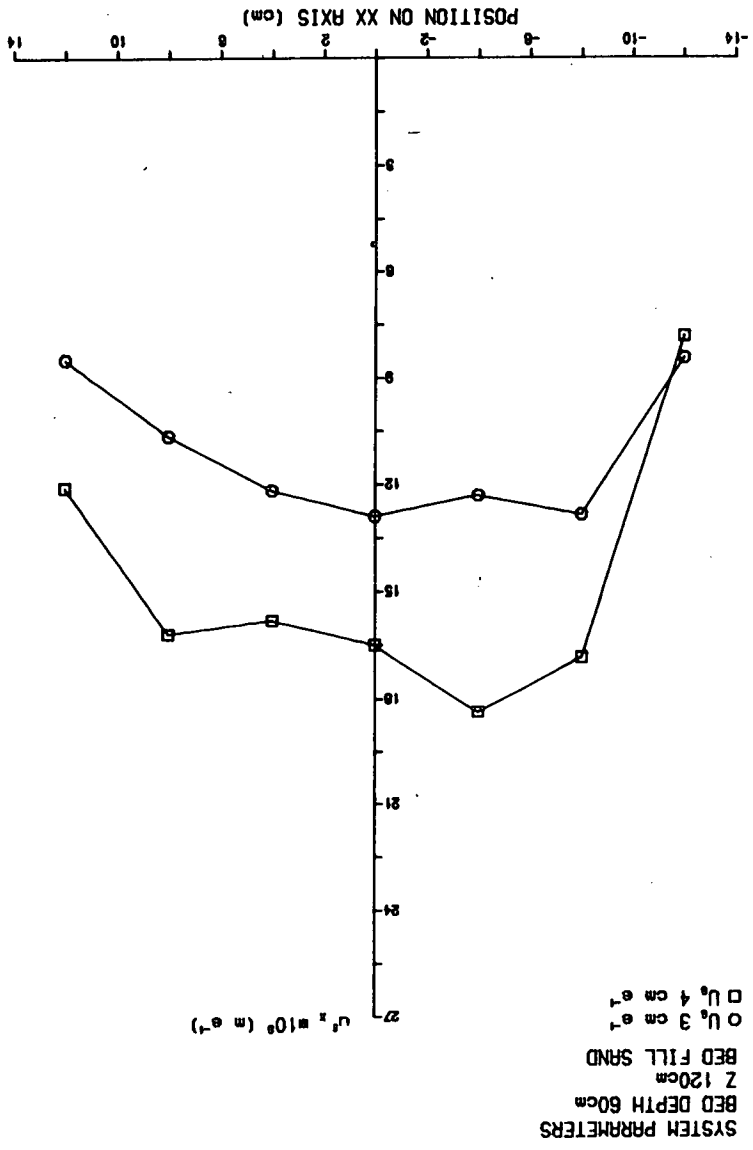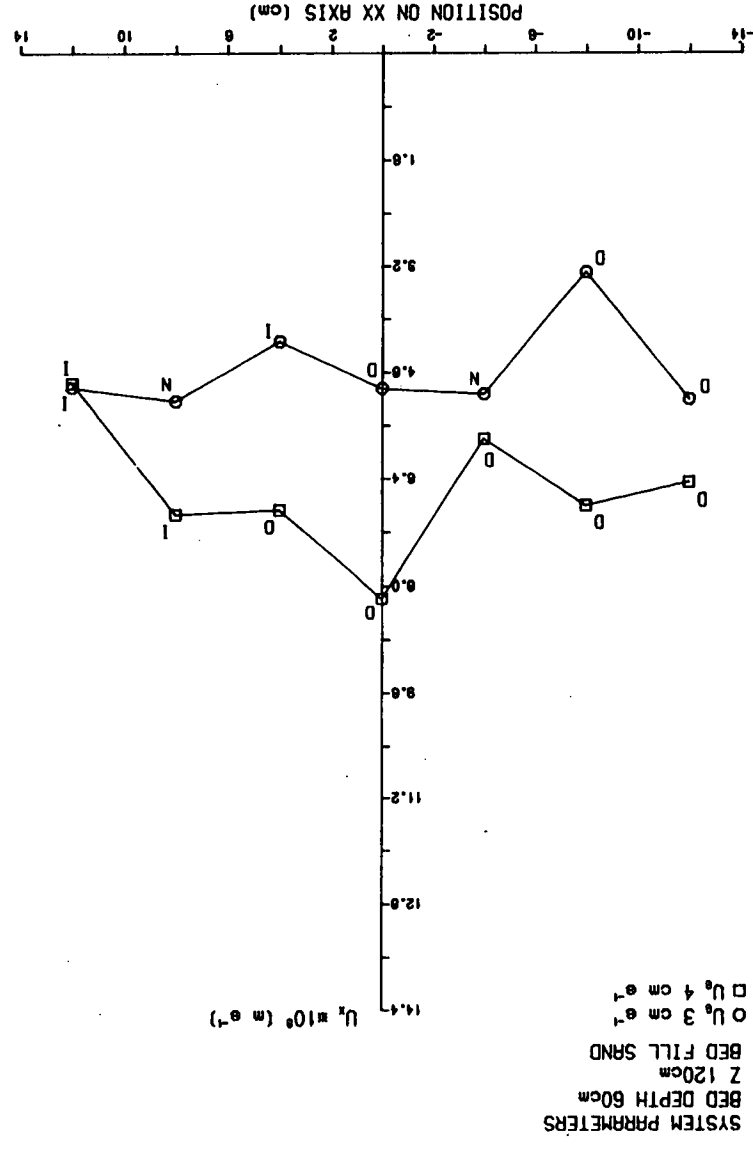
Figure 6.3.7 XX Profile of U_Y - Large Bed.

Figure 6.3.8 XX Profile of u'_Y - Large Bed.

SYSTEM PARAMETERS
BED DEPTH 60cm
Z 120cm
BED FILL SAND

o U_6 3 cm s^{-1}
□ U_6 4 cm s^{-1}

U_Y ×10^3 (m s^{-1})

SYSTEM PARAMETERS
BED DEPTH 60cm
Z 120cm
BED FILL SAND

o U_6 3 cm s^{-1}
□ U_6 4 cm s^{-1}

u'_Y ×10^3 (m s^{-1})

POSITION ON XX AXIS (cm)

POSITION ON XX AXIS (cm)

208

Pattern of Average Transverse Velocity Variation across Freeboard of Large Bed, Depth 60 cm, at Freeboard Height = 120 cm.
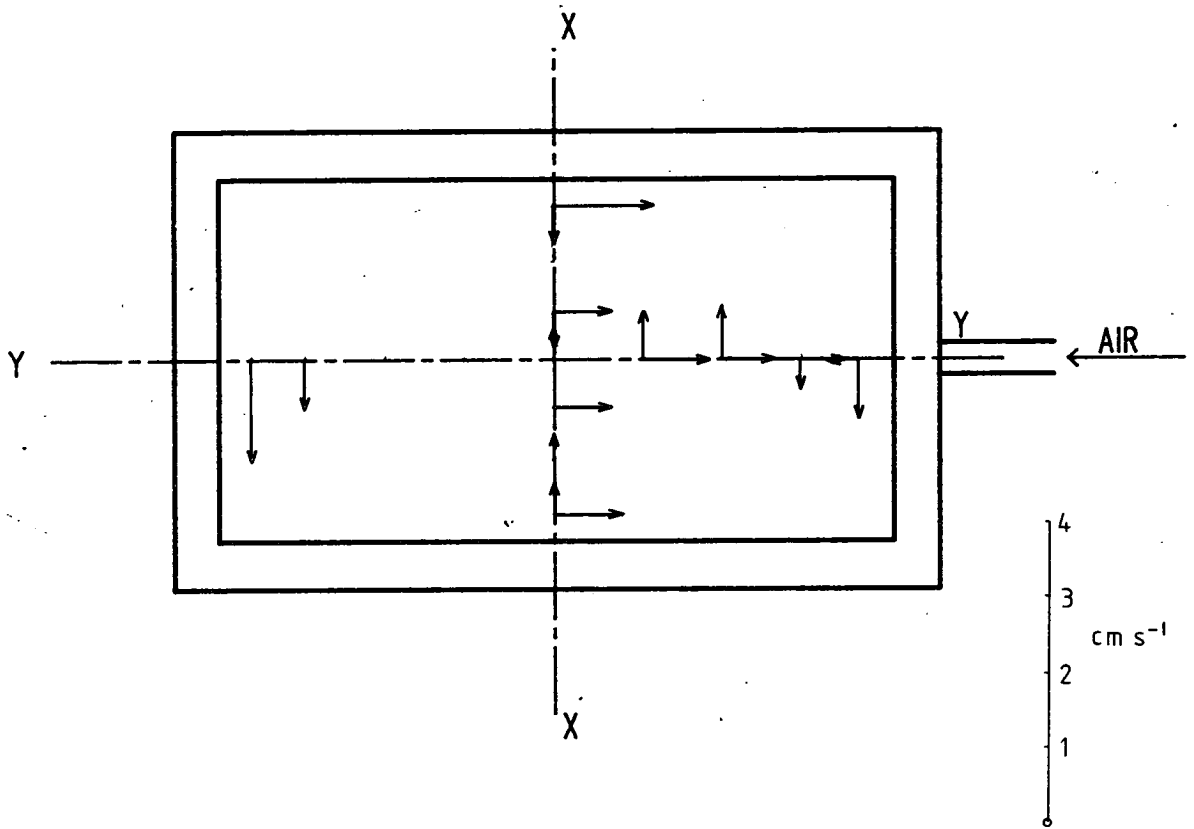
Figure 6·3·9

Figure 6.3.10 YY Profile of U_Y - Large Bed.

SYSTEM PARAMETERS
U_0 3 cm s^{-1}
Z' 60cm
BED FILL SAND

o BED DEPTH 30cm
□ BED DEPTH 60cm

U_Y $\times 10^8$ (m s^{-1})

POSITION ON YY AXIS (cm)
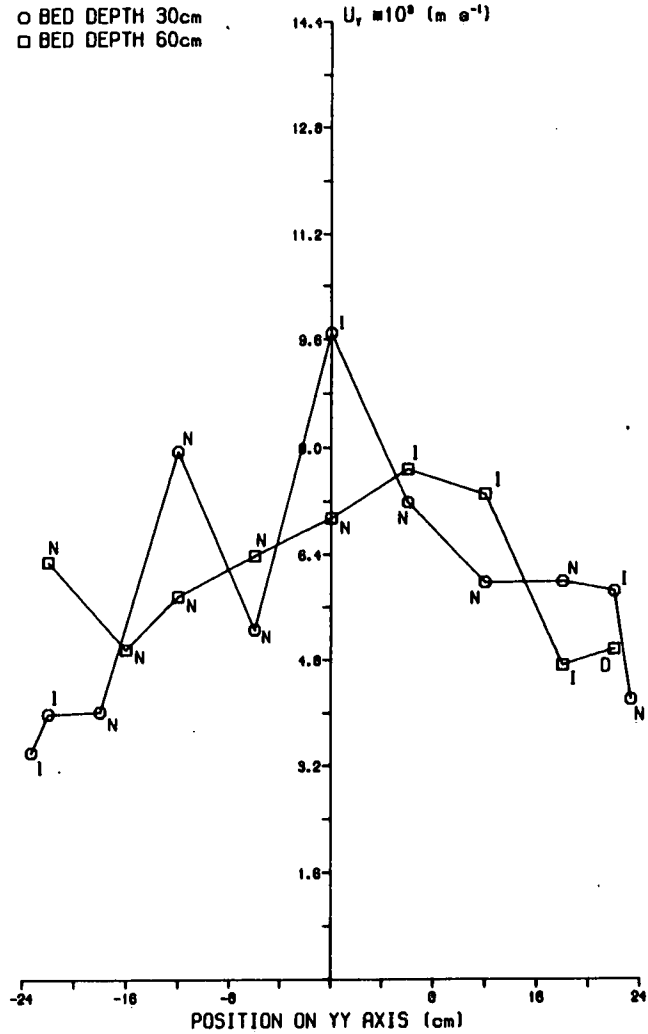
Figure 6.3.11 YY Profile of u'_Y - Large Bed.

SYSTEM PARAMETERS
U_0 3 cm s^{-1}
Z' 60cm
BED FILL SAND

o BED DEPTH 30cm
□ BED DEPTH 60cm

u'_Y $\times 10^8$ (m s^{-1})

POSITION ON YY AXIS (cm)
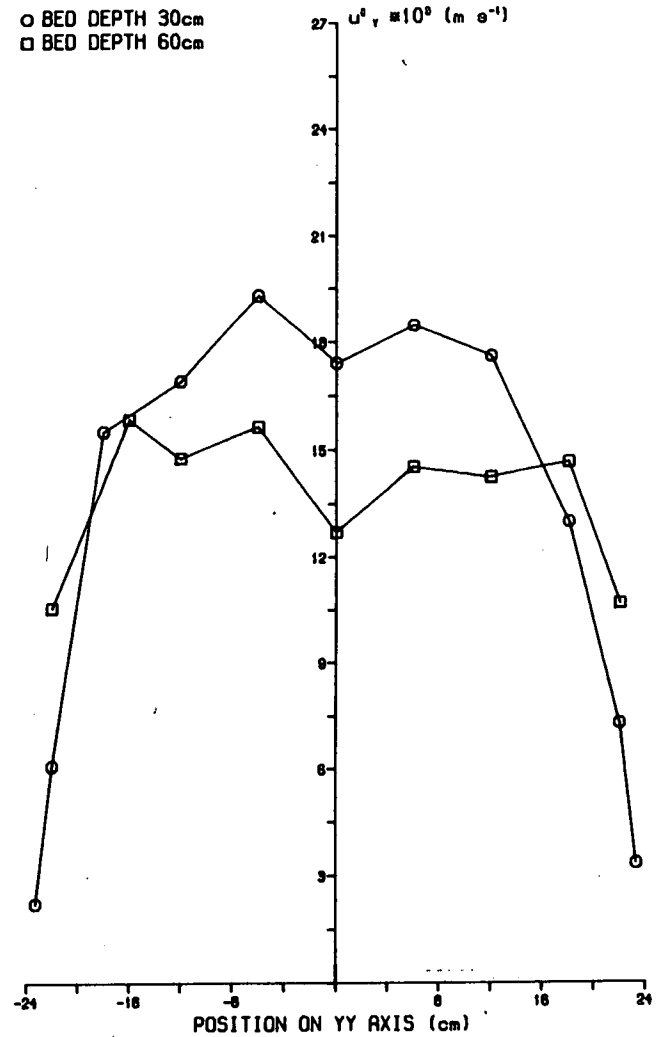
Figure 6.3.12 YY Profile of U_Y - Large Bed.

SYSTEM PARAMETERS
U_a 4 cm a^{-1}
Z^a 60cm
BED FILL SAND

o BED DEPTH 30cm
□ BED DEPTH 60cm

U_Y ×10^a (m a^{-1})

POSITION ON YY AXIS (cm)
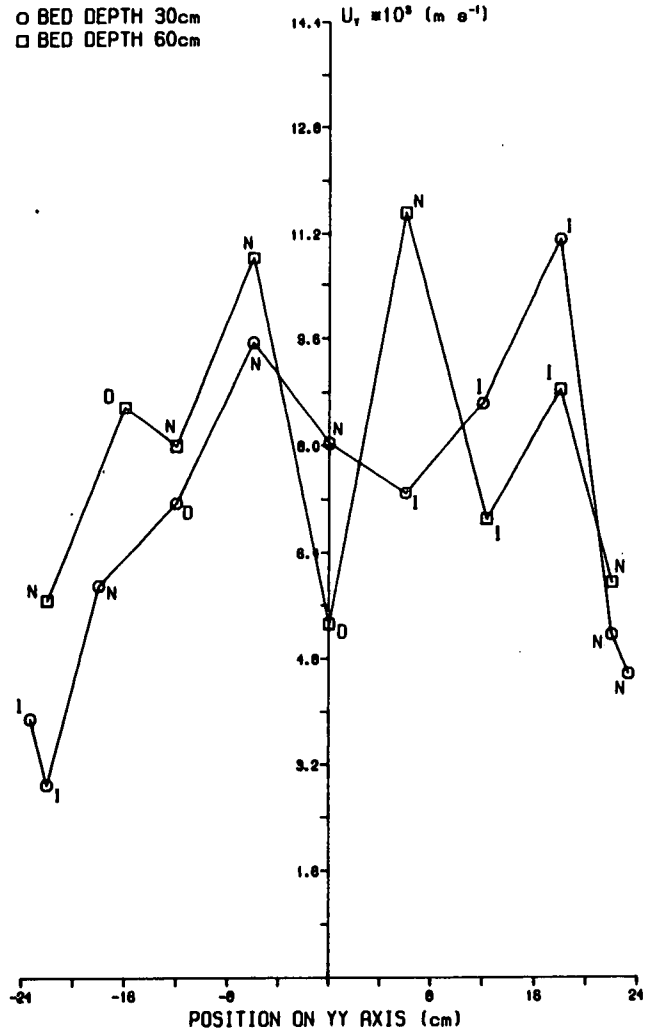
Figure 6.3.13 YY Profile of u'_Y - Large Bed.

SYSTEM PARAMETERS
U_a 4 cm a^{-1}
Z^a 60cm
BED FILL SAND

o BED DEPTH 30cm
□ BED DEPTH 60cm

u'_Y ×10^a (m a^{-1})

POSITION ON YY AXIS (cm)
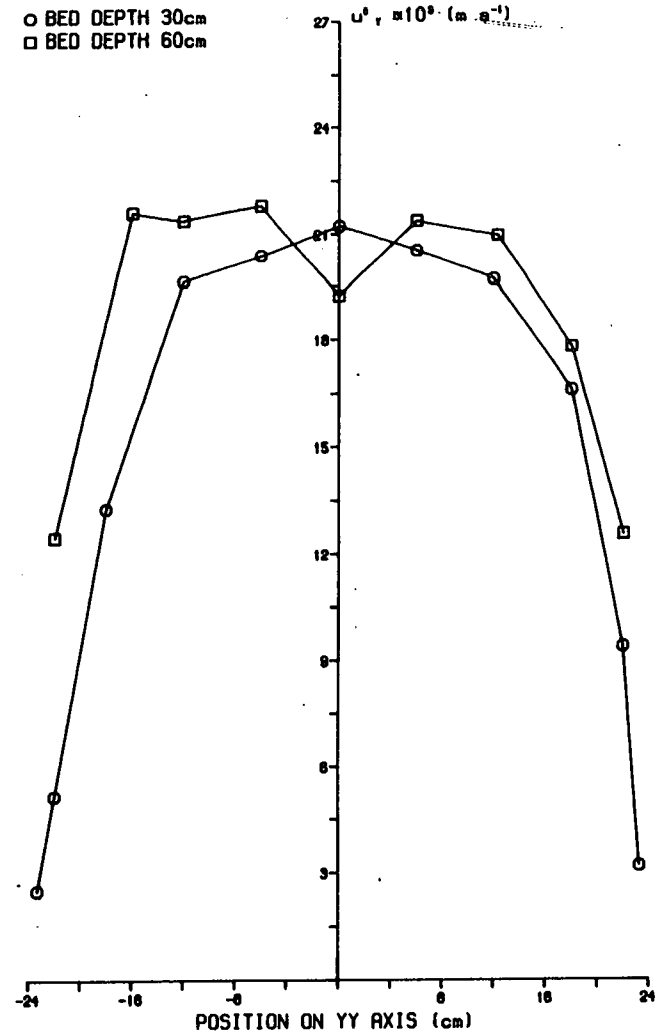
Figure 6.3.14 YY Profile of U_Y - Large Bed.

SYSTEM PARAMETERS
BED DEPTH 60cm
U_G 4 cm s^{-1}
BED FILL SAND

o Z 120cm
□ Z 150cm
△ Z 180cm

U_Y ✳10^9 (m s^{-1})

POSITION ON YY AXIS (cm)

Figure 6.3.15 YY Profile of u'_Y – Large Bed.

SYSTEM PARAMETERS
BED DEPTH 60cm
U_G 4 cm s^{-1}
BED FILL SAND

o Z 120cm
□ Z 150cm
△ Z 180cm

u''_Y *10^9 (m s^{-1})

POSITION ON YY AXIS (cm)

Figure 6.3.16 YY Profile of U_x - Large Bed.

SYSTEM PARAMETERS
BED DEPTH 60cm
U_s 4 cm s^{-1}
BED FILL SAND

○ Z 120cm
□ Z 150cm
△ Z 180cm

U_x *10^s (m s^{-1})

POSITION ON YY AXIS (cm)
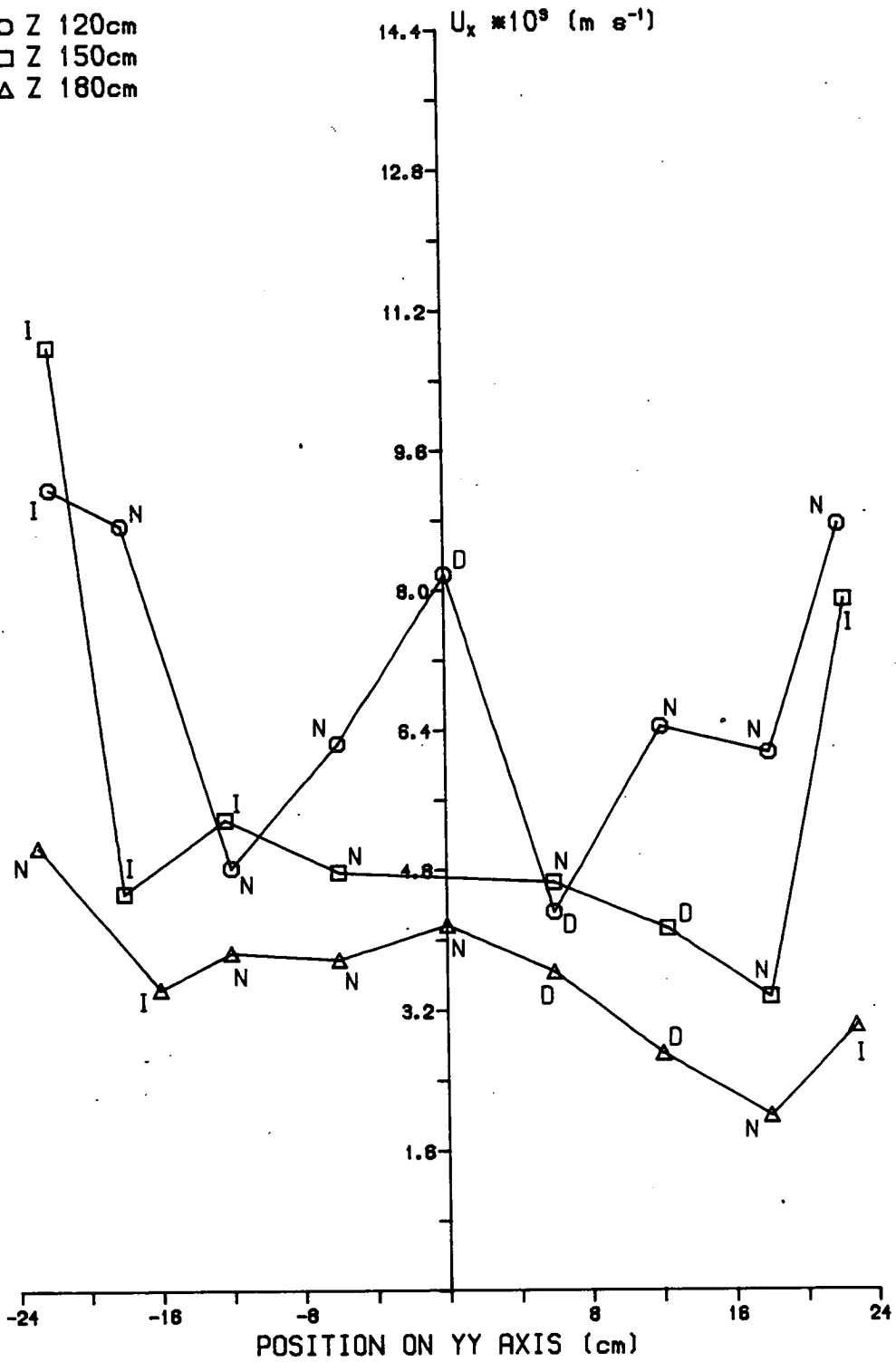
Figure 6.3.17 YY Profile of u'_x - Large Bed.

SYSTEM PARAMETERS
BED DEPTH 60cm
U_G 4 cm s^{-1}
BED FILL SAND

o Z 120cm
□ Z 150cm
△ Z 180cm

POSITION ON YY AXIS (cm)
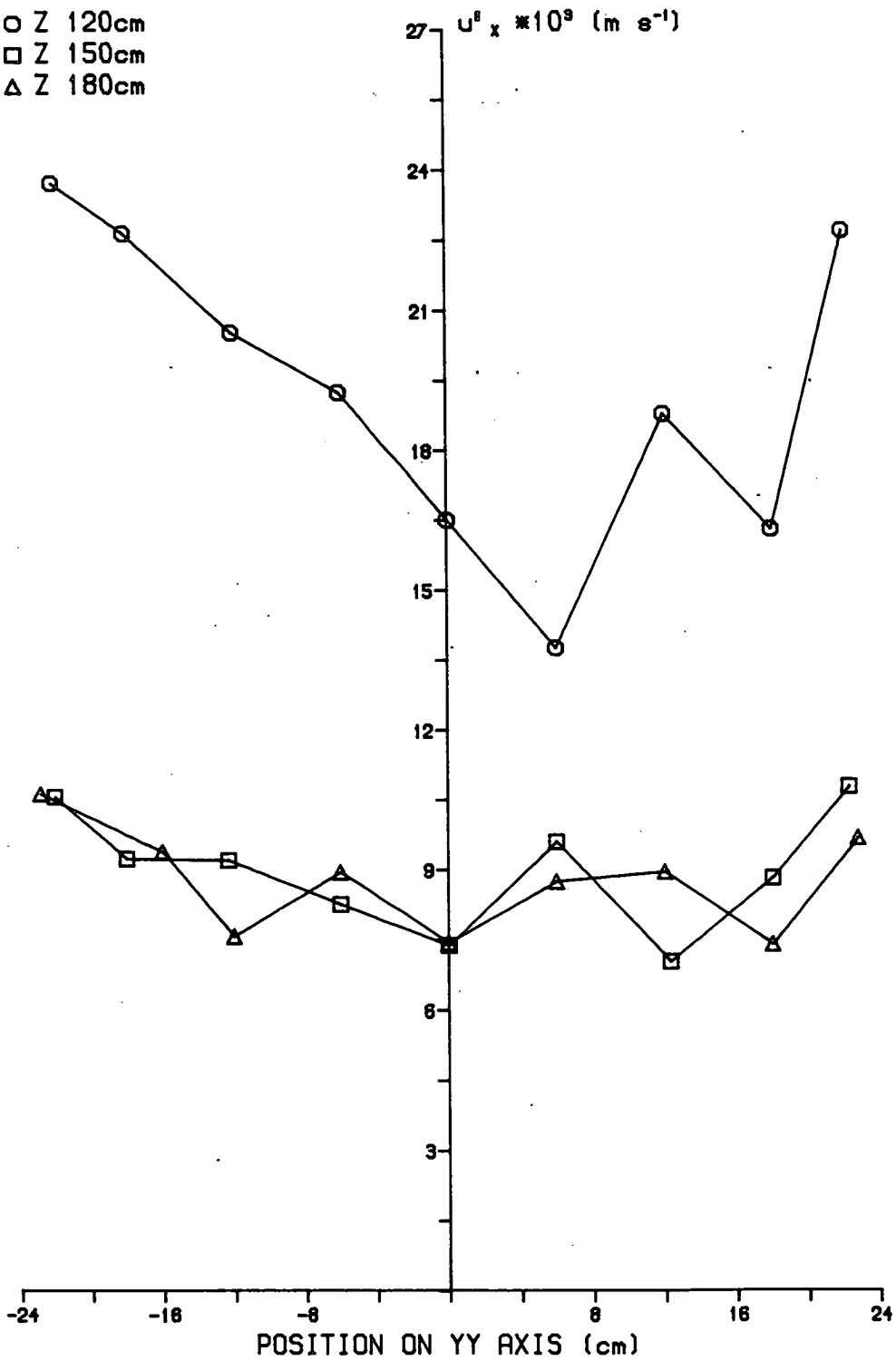
Figure 6.3.18 YY Profile of U_Y - Large Bed.

SYSTEM PARAMETERS
BED DEPTH 30cm
U_G 3 cm s^{-1}
BED FILL SAND

O Z 90cm
□ Z 120cm
△ Z 150cm
◇ Z 180cm

U_Y *10^3 (m s^{-1})

POSITION ON YY AXIS (cm)

216
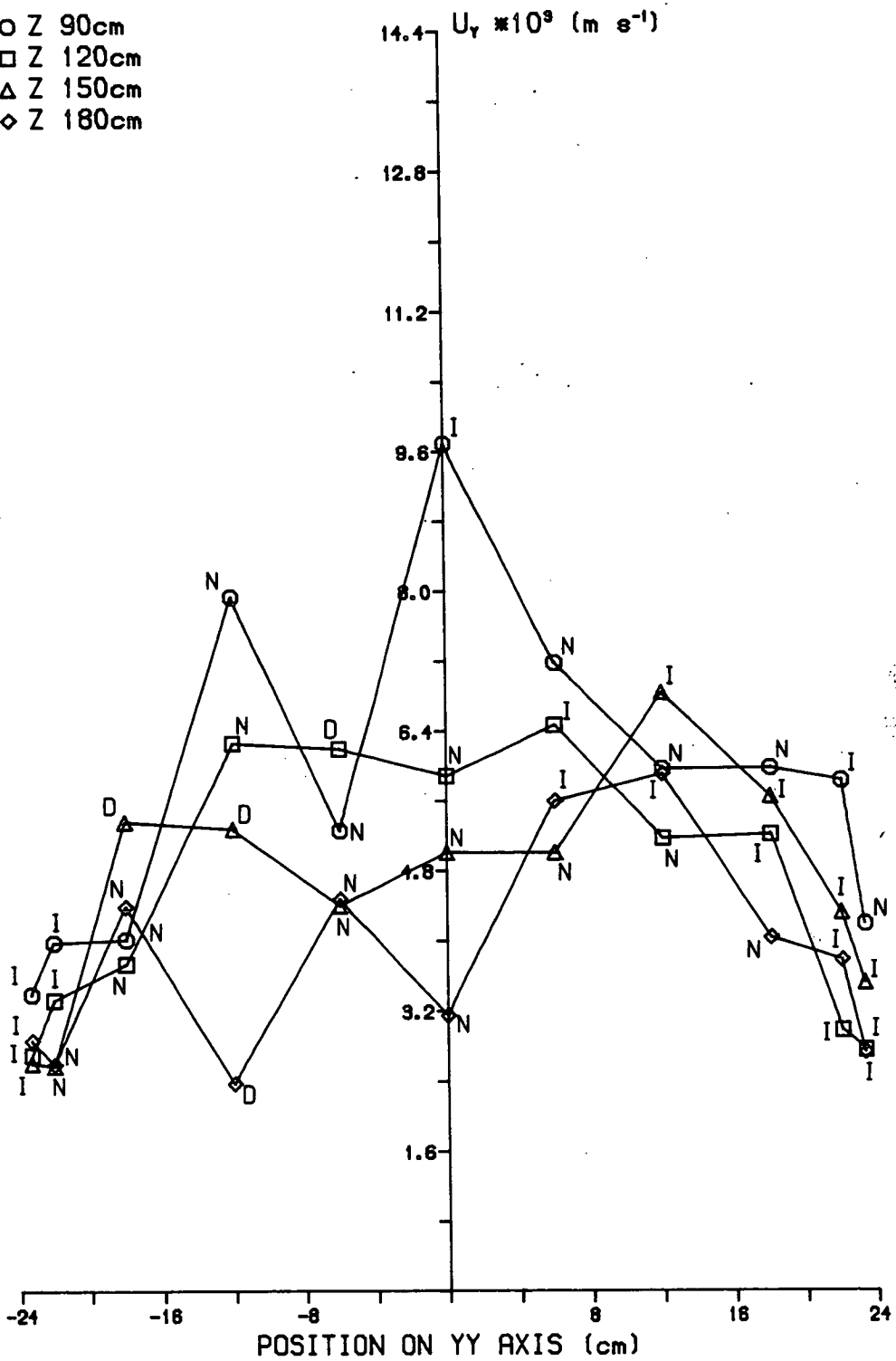
Figure 6.3.19 YY Profile of u′$_Y$ - Large Bed.

SYSTEM PARAMETERS -
BED DEPTH 30cm
U$_6$ 3 cm s^{-1}
BED FILL SAND

o Z 90cm
□ Z 120cm
△ Z 150cm
◇ Z 180cm

u″$_Y$ *10^3 (m s^{-1})

POSITION ON YY AXIS (cm)
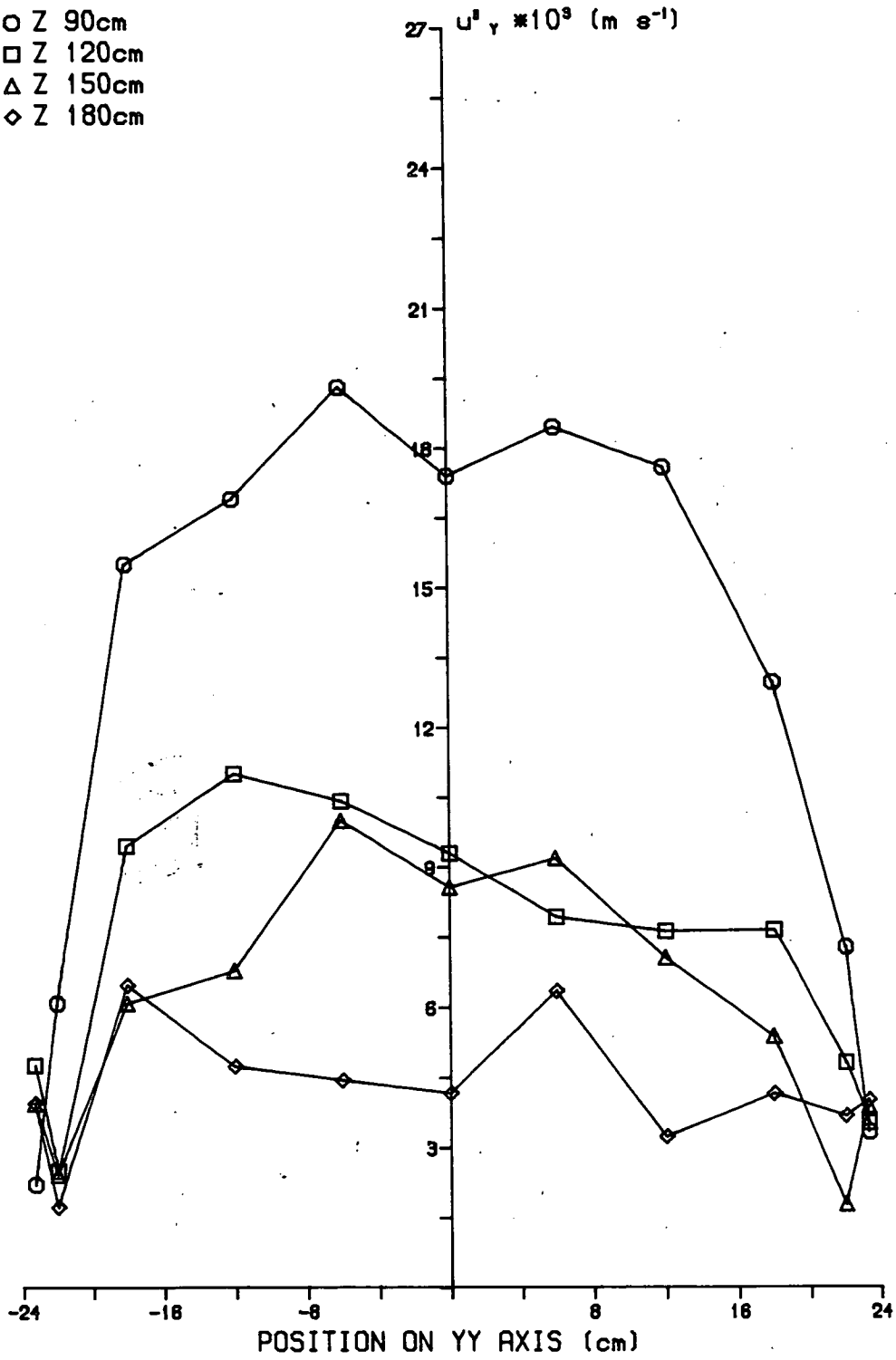
Figure 6.3.20 YY Profile of U_Y - Large Bed.
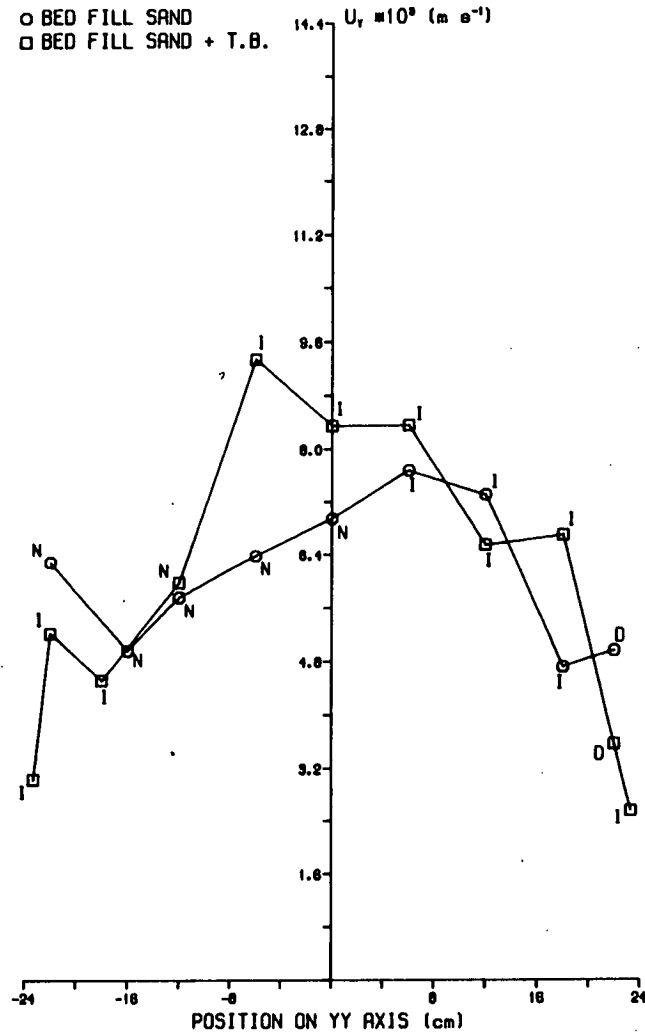
Figure 6.3.21 YY Profile of u'_Y - Large Bed.
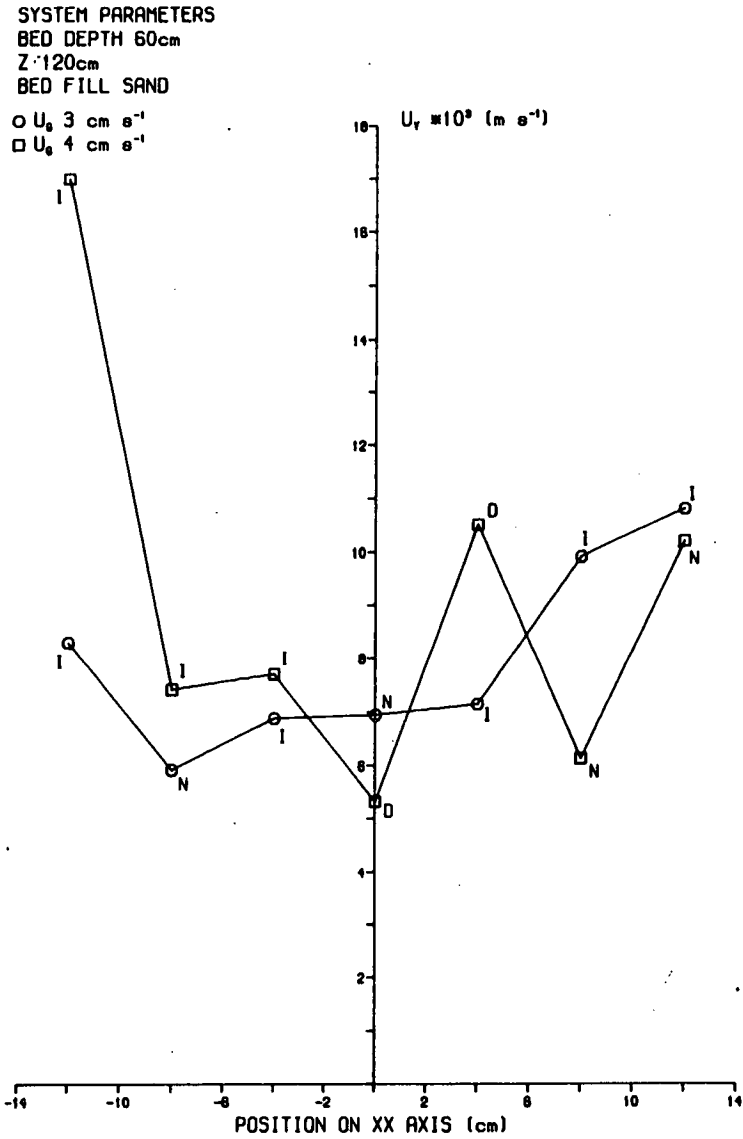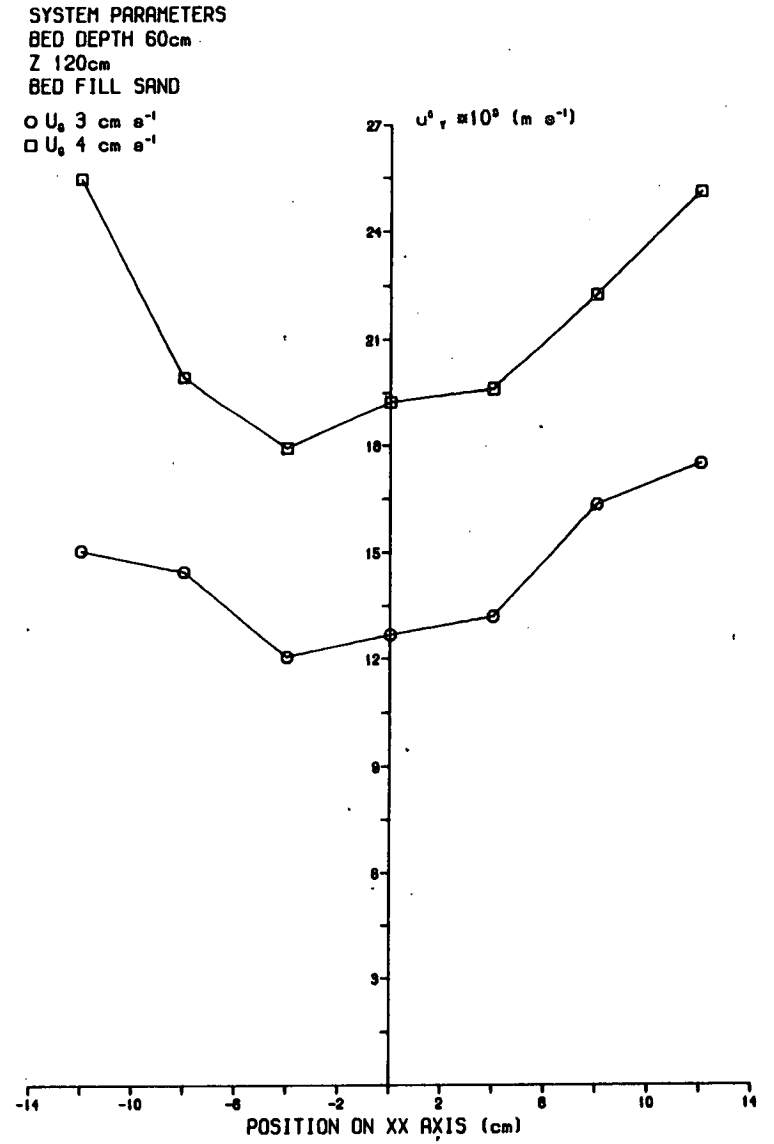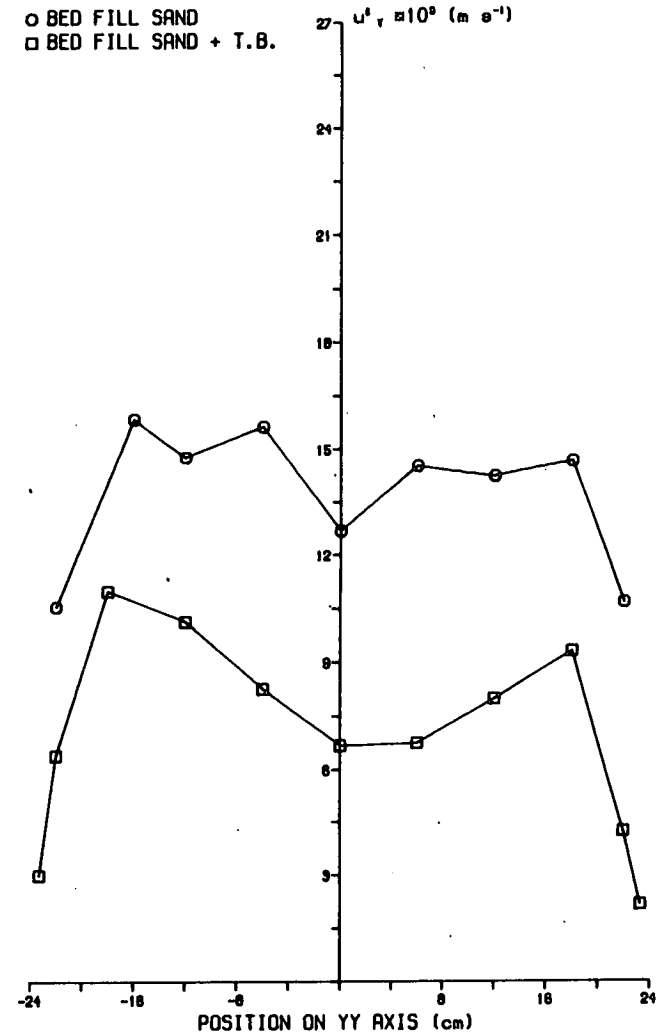
Figure 6.3.22 YY Profile of U_Y - Large Bed.

SYSTEM PARAMETERS
BED DEPTH 60cm
Z 120cm
U_0 4 cm s^{-1}

o BED FILL SAND
□ BED FILL SAND + T.B.

U_Y x10^9 (m s^{-1})

POSITION ON YY AXIS (cm)
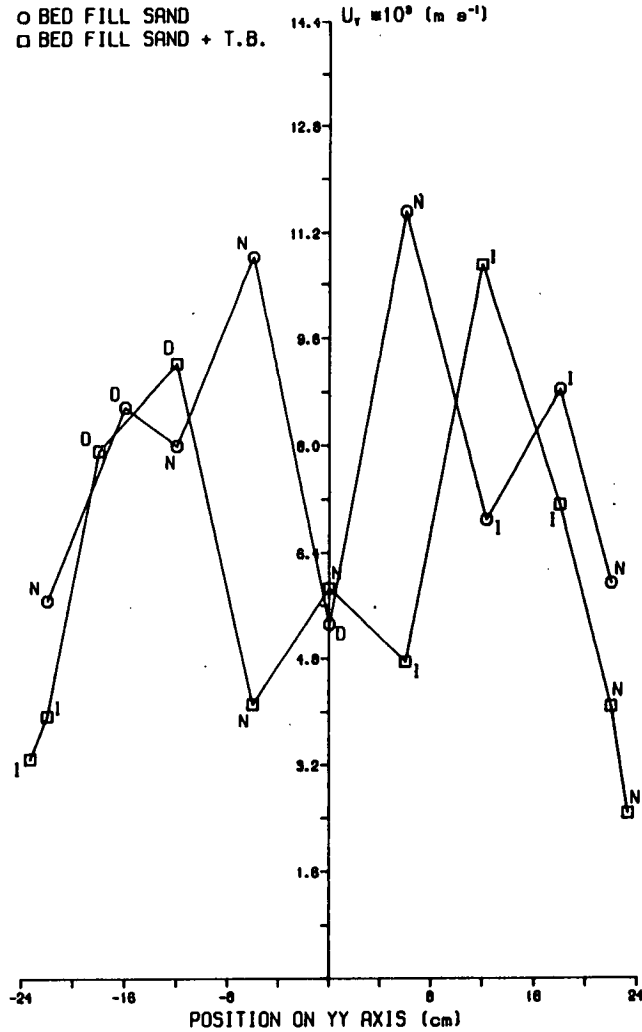
Figure 6.3.23 YY Profile of u'_Y - Large Bed.

SYSTEM PARAMETERS
BED DEPTH 60cm
Z 120cm
U_0 4 cm s^{-1}

o BED FILL SAND
□ BED FILL SAND + T.B.

u'_Y x10^9 (m s^{-1})

POSITION ON YY AXIS (cm)
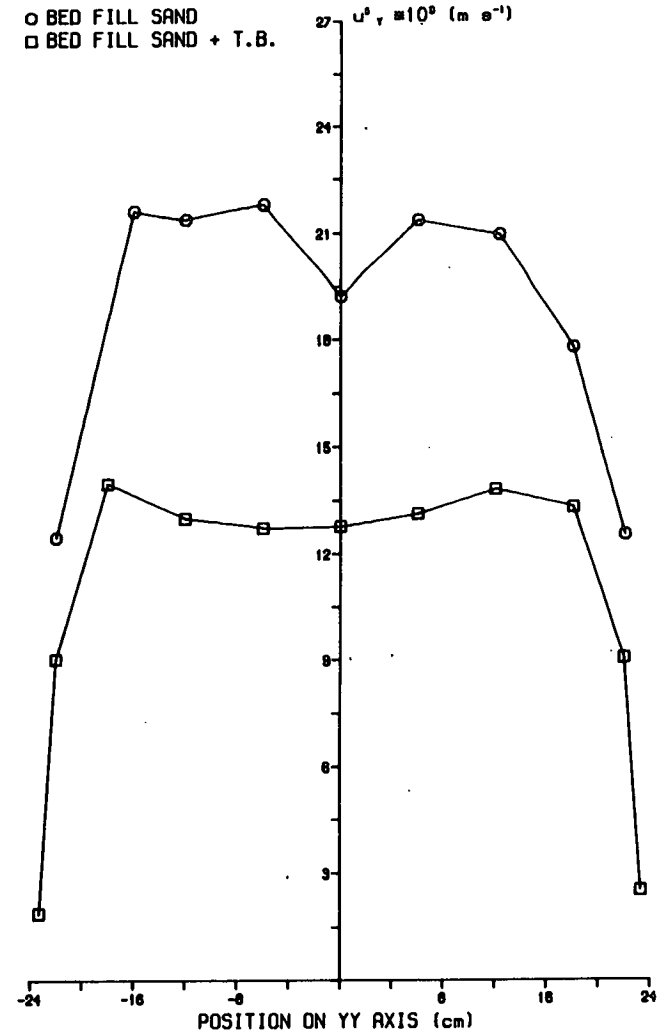
Figure 6.3.24 Profile of U_Y Along and Parallel to the XX Axis.

SYSTEM PARAMETERS
BED DEPTH 60cm
Z 180cm
U_e 3 cm e^{-1}
BED FILL SAND

o XX AXIS
□ Y=-18cm AXIS

$U_Y \times 10^9$ (m e^{-1})

POSITION (cm)
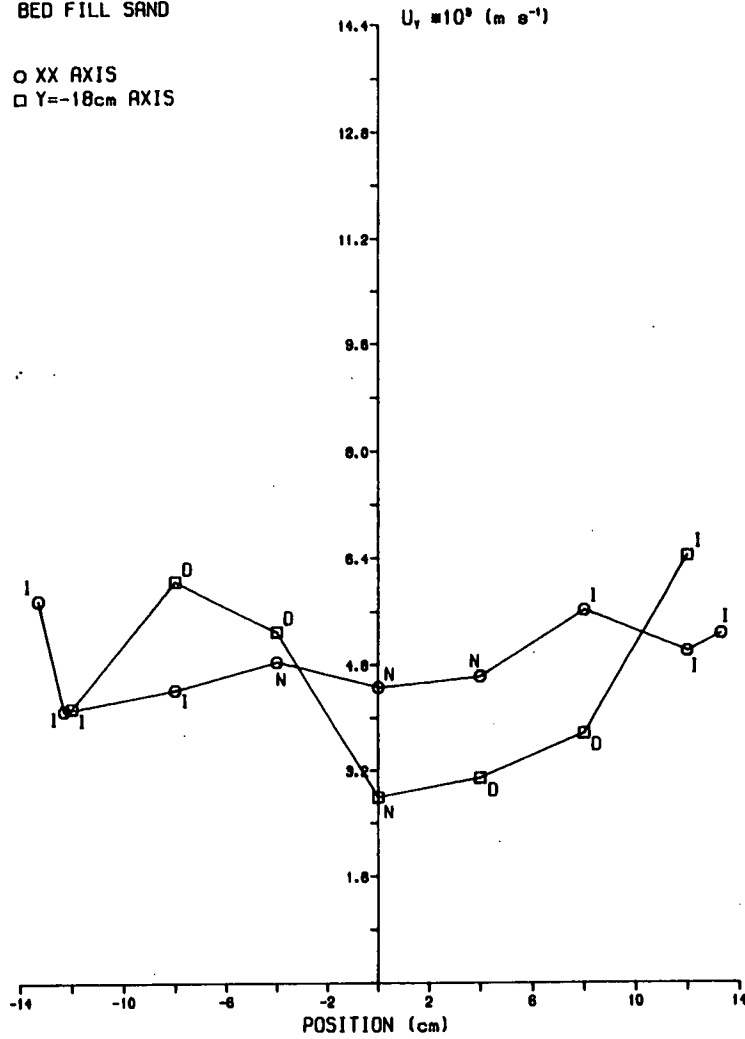
Figure 6.3.25 Profile of u'_Y Along and Parallel to the XX Axis.

SYSTEM PARAMETERS
BED DEPTH 60cm
Z 180cm
U_e 3 cm e^{-1}
BED FILL SAND

o XX AXIS
□ Y=-18cm AXIS

$u'_Y \times 10^9$ (m e^{-1})

POSITION (cm)
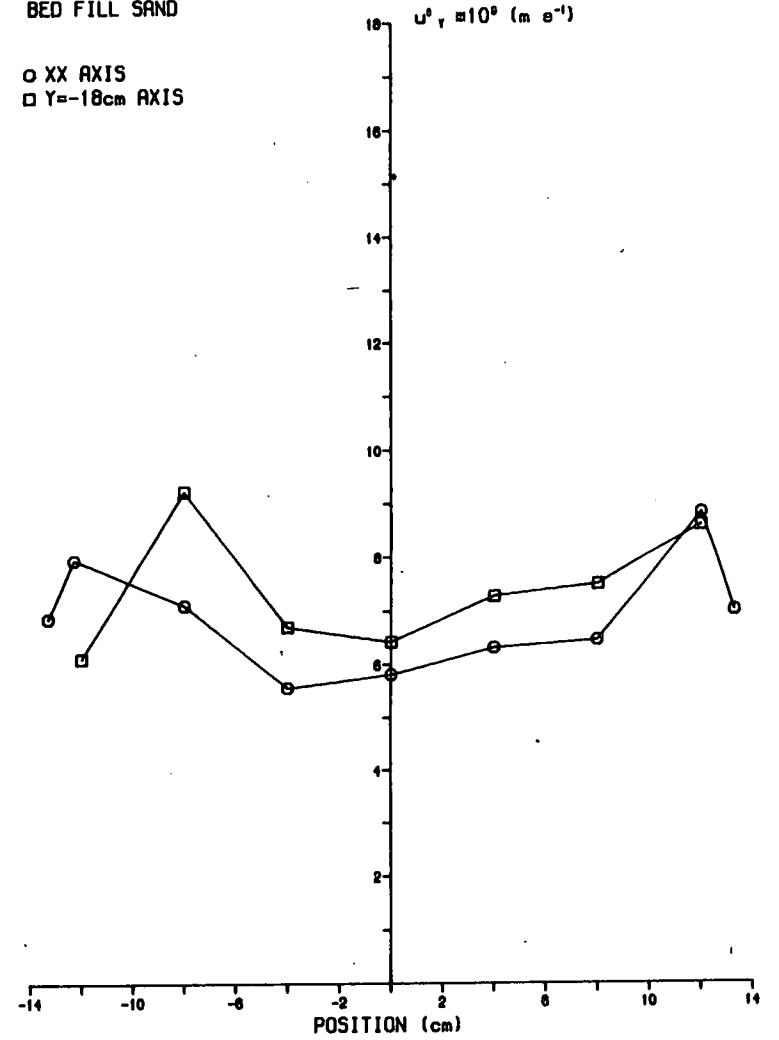
Figure 6.3.26 Profile of U_Y Along and Parallel to the YY Axis.

SYSTEM PARAMETERS
BED DEPTH 60cm
Z 150cm
U_8 3 cm s^{-1}
BED FILL SAND + T.B.

o YY AXIS
□ X=-8cm AXIS

U_Y ✻10^3 (m s^{-1})

POSITION (cm)
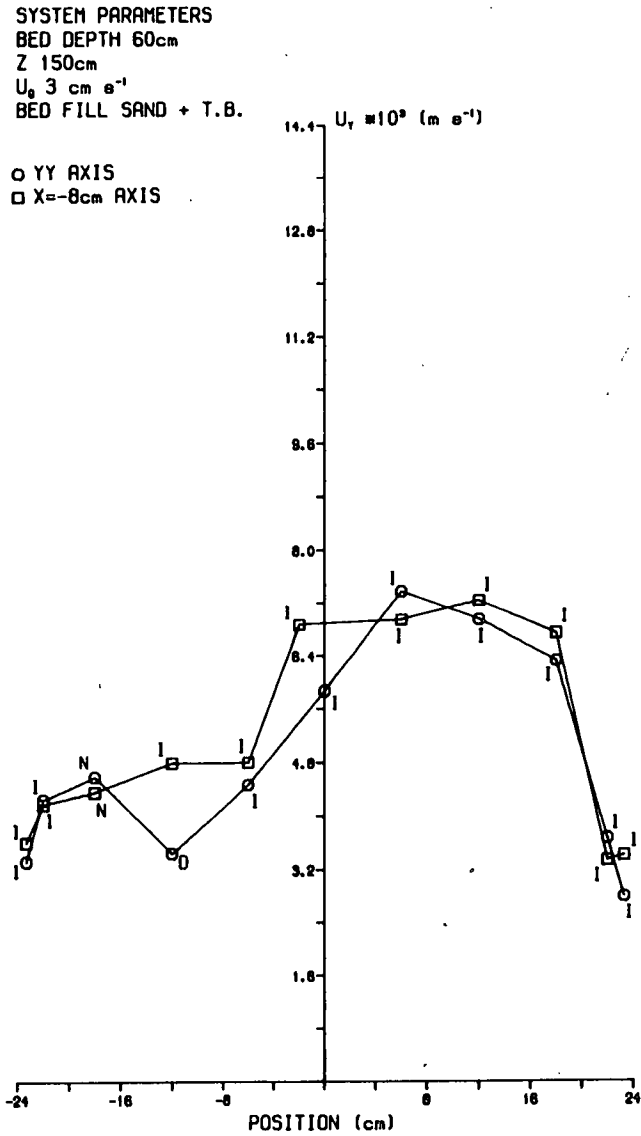
Figure 6.3.27 Profile of u'_Y Along and Parallel to the YY Axis.

SYSTEM PARAMETERS
BED DEPTH 60cm
Z 150cm
U_8 3 cm s^{-1}
BED FILL SAND + T.B.

o YY AXIS
□ X=-8cm AXIS

u'_Y ✻10^3 (m s^{-1})

POSITION (cm)
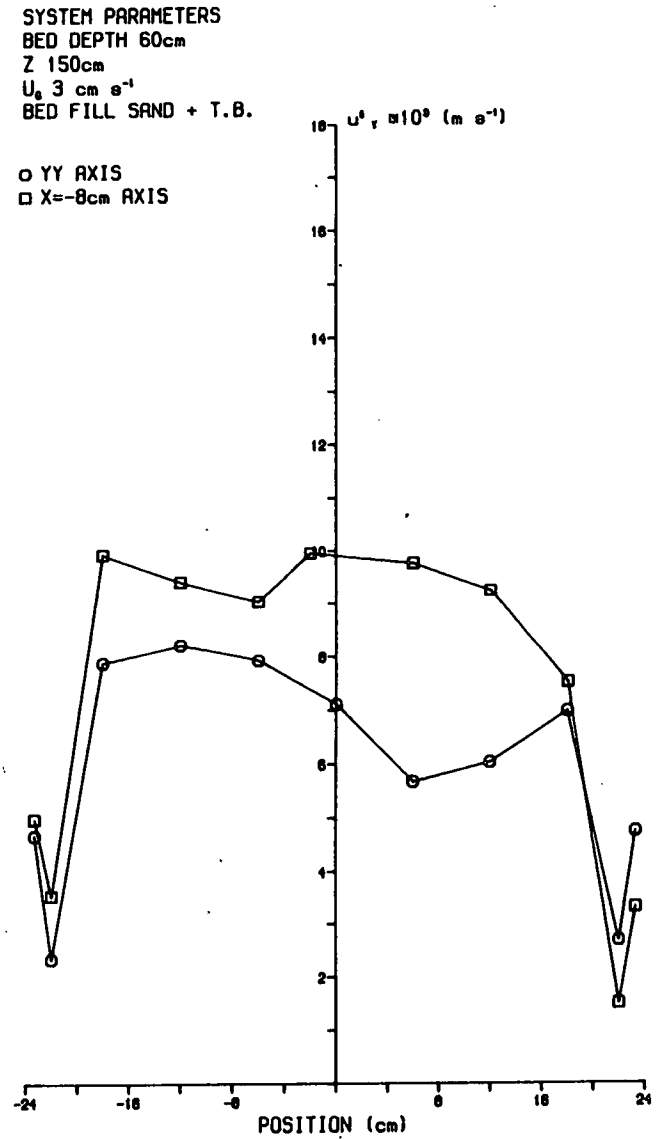
Figure 6.3.28 Profile of U_x Along and Parallel to the YY Axis.

SYSTEM PARAMETERS
BED DEPTH 60cm
Z 180cm
U_e 3 cm s^{-1}
BED FILL SAND

o YY AXIS
□ X=-8cm AXIS

U_x ×10⁹ (m s⁻¹)

POSITION (cm)
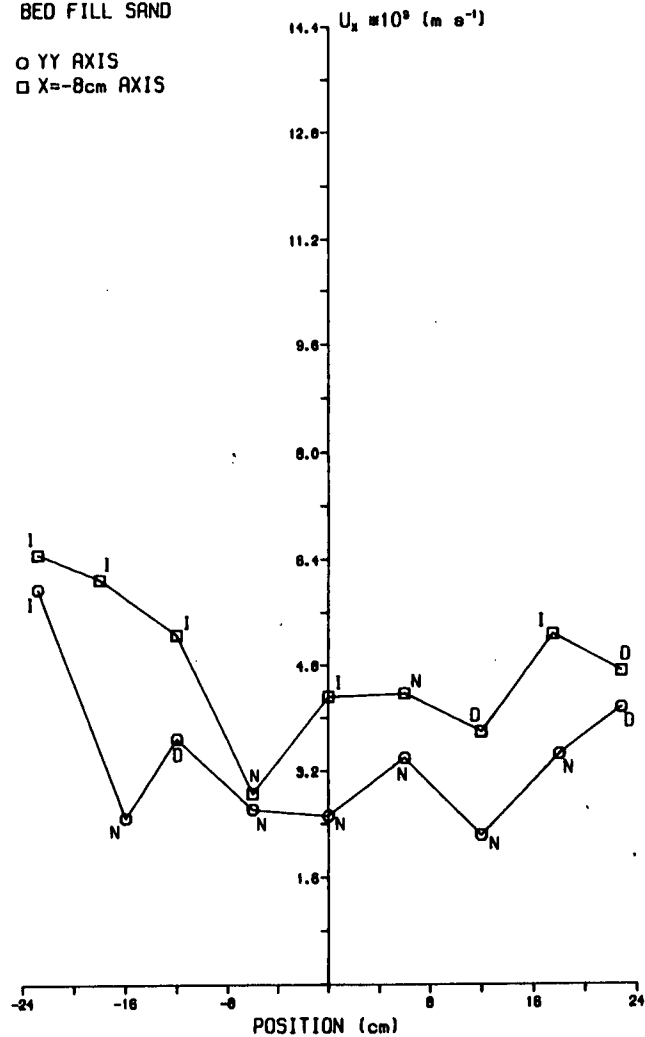
Figure 6.3.29 Profile of u'_x Along and Parallel to the YY Axis.

SYSTEM PARAMETERS
BED DEPTH 60cm
Z 180cm
U_e 3 cm s^{-1}
BED FILL SAND

o YY AXIS
□ X=-8cm AXIS

u'_x ×10⁹ (m s⁻¹)
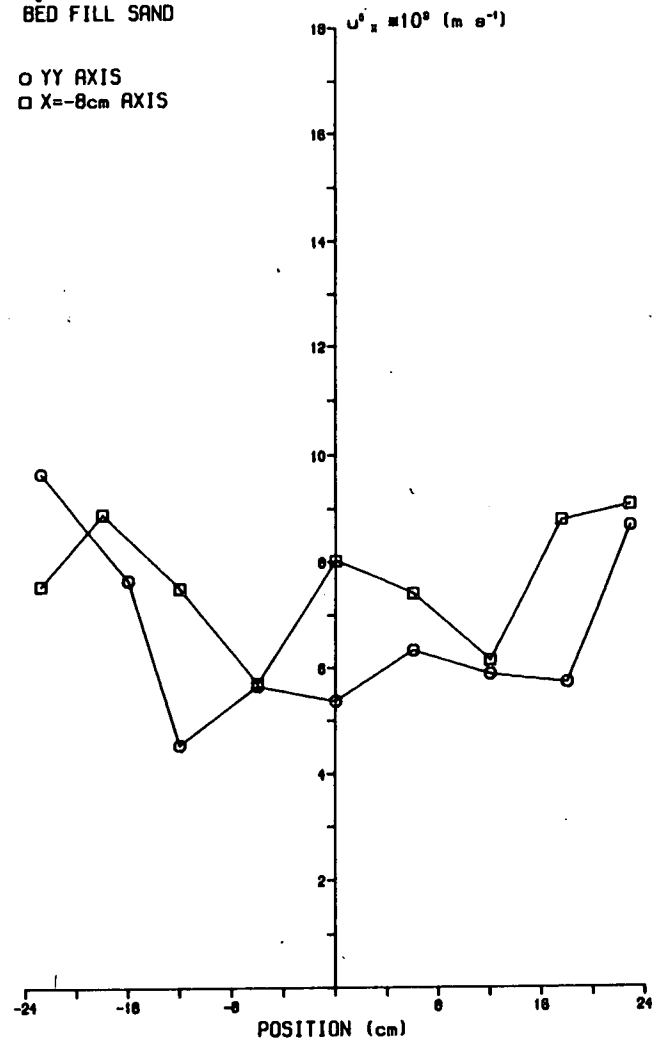
POSITION (cm)

Figure 6.3.30 YY Profile of U_Y - Large Bed.

SYSTEM PARAMETERS
BED DEPTH 30cm
Z 150cm
BED FILL CATALYST

O U_6 16.4 cm s^{-1}

U_Y $\times 10^2$ (m s^{-1})

POSITION ON YY AXIS (cm)
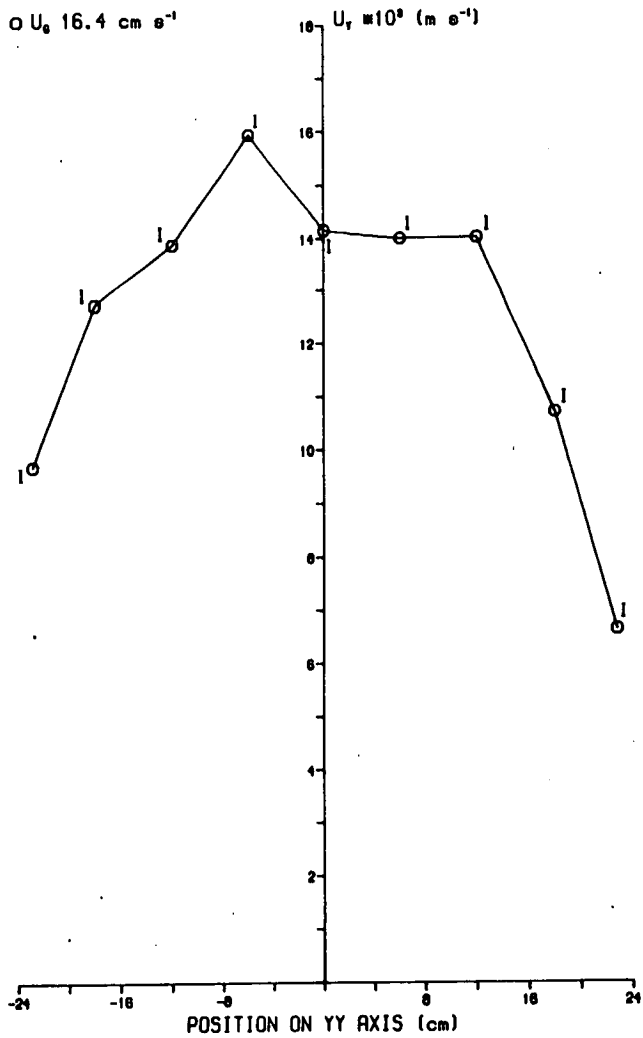
Figure 6.3.31 YY Profile of u'_Y - Large Bed.

SYSTEM PARAMETERS
BED DEPTH 30cm
Z 150cm
BED FILL CATALYST

O U_6 16.4 cm s^{-1}

u'_Y $\times 10^2$ (m s^{-1})

POSITION ON YY AXIS (cm)
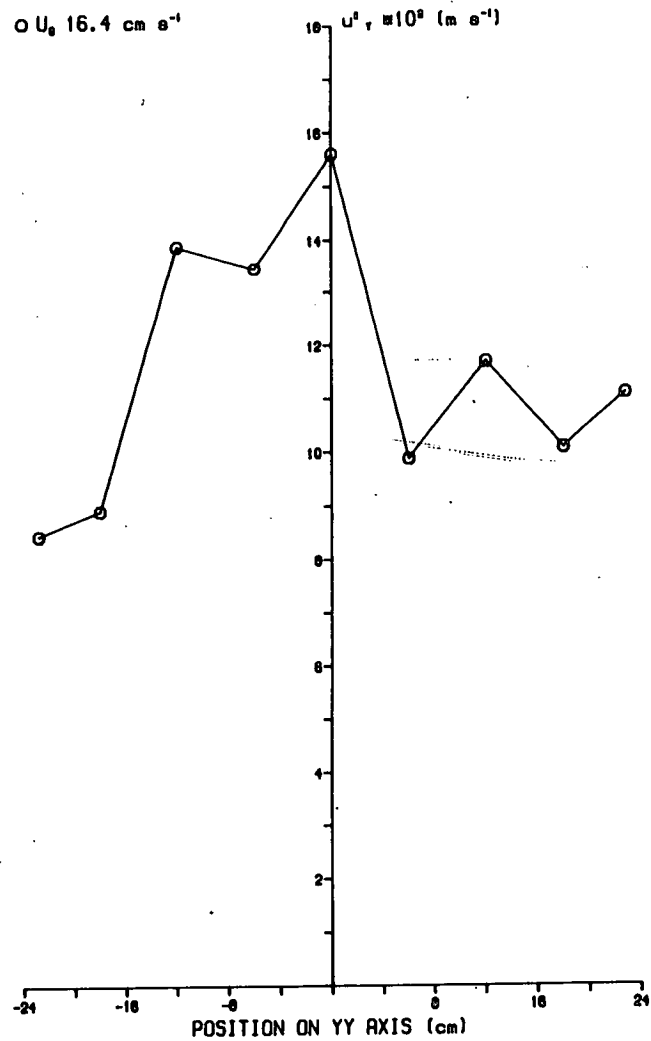
Position (cm)	u'_X (ms^{-1})	u'_Y (ms^{-1})	u'_Z (ms^{-1})
2.75	$8.83 * 10^{-2}$	$10.80 * 10^{-2}$	$12.30 * 10^{-2}$
1.25	$11.80 * 10^{-2}$	$12.21 * 10^{-2}$	$13.10 * 10^{-2}$
0	$11.53 * 10^{-2}$	$10.94 * 10^{-2}$	$12.60 * 10^{-2}$
-1.25	$10.20 * 10^{-2}$	$10.46 * 10^{-2}$	$13.10 * 10^{-2}$
-2.75	$9.17 * 10^{-2}$	$11.11 * 10^{-2}$	$12.10 * 10^{-2}$

Table 6.2.1 Bed Depth 5cm, Superficial Flow 0.4 ms^{-1}, Freeboard Height 20cm and Reference Axis XX.

Variation of rms Fluctuating Velocity Components with Position on the XX Axis at Two Freeboard Heights – Small Bed, Depth 5 cm.

Position (cm)	u'_X (ms^{-1})	u'_Y (ms^{-1})	u'_Z (ms^{-1})
2.75	$5.50 * 10^{-2}$	$7.03 * 10^{-2}$	$7.70 * 10^{-2}$
1.25	———	$6.31 * 10^{-2}$	$7.04 * 10^{-2}$
0	$6.38 * 10^{-2}$	$6.19 * 10^{-2}$	$6.80 * 10^{-2}$
-1.25	$5.85 * 10^{-2}$	$6.40 * 10^{-2}$	$6.96 * 10^{-2}$
-2.75	$5.09 * 10^{-2}$	$6.69 * 10^{-2}$	$7.54 * 10^{-2}$

Table 6.2.2 Bed Depth 5cm, Superficial Flow 0.4 ms^{-1}, Freeboard Height 40cm and Reference Axis XX.

Position (cm)	u'_X (ms^{-1})	u'_Y (ms^{-1})	u'_Z (ms^{-1})
2.75	$6.82 * 10^{-2}$	$8.01 * 10^{-2}$	$8.06 * 10^{-1}$
1.25	$7.66 * 10^{-2}$	$7.83 * 10^{-2}$	$8.26 * 10^{-2}$
0	$8.19 * 10^{-2}$	$7.90 * 10^{-2}$	$9.20 * 10^{-2}$
-1.25	$7.02 * 10^{-2}$	$7.08 * 10^{-2}$	$7.72 * 10^{-2}$
-2.75	$6.54 * 10^{-2}$	$7.36 * 10^{-2}$	$7.88 * 10^{-2}$

Table 6.2.3 Bed Depth 3cm, Superficial Flow 0.4 ms^{-1}, Freeboard Height 20cm and Reference Axis XX.

Variation of rms Fluctuating Velocity Components with Position on the XX Axis at Two Freeboard Heights - Small Bed, Depth 3 cm.

Position (cm)	u'_X (ms^{-1})	u'_Y (ms^{-1})	u'_Z (ms^{-1})
2.75	$3.86 * 10^{-2}$	$4.89 * 10^{-2}$	$6.52 * 10^{-2}$
1.25	$4.81 * 10^{-2}$	$4.49 * 10^{-2}$	$5.68 * 10^{-2}$
0	$5.28 * 10^{-2}$	$4.43 * 10^{-2}$	$6.00 * 10^{-2}$
-1.25	$5.09 * 10^{-2}$	$4.11 * 10^{-2}$	$5.49 * 10^{-2}$
-2.75	$4.16 * 10^{-2}$	$4.87 * 10^{-2}$	$6.79 * 10^{-2}$

Table 6.2.4 Bed Depth 3cm, Superficial Flow 0.4 ms^{-1}, Freeboard Height 40cm and Reference Axis XX.

Variation of rms Fluctuating Velocity Components with Position on the YY Axis - Large Sand Bed.

Position (cm)	u'_X (ms^{-1})	u'_Y (ms^{-1})	u'_Z (ms^{-1})
22	13.82 * 10^{-3}	10.67 * 10^{-3}	13.57 * 10^{-3}
18	11.54 * 10^{-3}	14.67 * 10^{-3}	16.73 * 10^{-3}
12	10.41 * 10^{-3}	14.24 * 10^{-3}	14.57 * 10^{-3}
6	9.83 * 10^{-3}	14.52 * 10^{-3}	12.19 * 10^{-3}
0	12.90 * 10^{-3}	12.69 * 10^{-3}	10.96 * 10^{-3}
-6	13.61 * 10^{-3}	15.64 * 10^{-3}	11.51 * 10^{-3}
-12	16.76 * 10^{-3}	14.78 * 10^{-3}	16.42 * 10^{-3}
-18	18.16 * 10^{-3}	15.86 * 10^{-3}	20.11 * 10^{-3}
-22	20.35 * 10^{-3}	10.56 * 10^{-3}	18.03 * 10^{-3}

Table 6.3.1 Bed Depth 60cm, Superficial Flow 3 cms^{-1}, Freeboard Height 120cm and Reference Axis YY.

Variation of rms Fluctuating Velocity Components with Position on the YY Axis - Large Sand Bed.

Position (cm)	u'_X (ms^{-1})	u'_Y (ms^{-1})	u'_Z (ms^{-1})
23.3	————	$4.33 * 10^{-3}$	$8.37 * 10^{-3}$
22	$8.67 * 10^{-3}$	$1.61 * 10^{-3}$	$3.05 * 10^{-3}$
18	$5.72 * 10^{-3}$	$4.65 * 10^{-3}$	$9.23 * 10^{-3}$
12	$5.88 * 10^{-3}$	$5.47 * 10^{-3}$	$4.85 * 10^{-3}$
6	$6.33 * 10^{-3}$	$5.05 * 10^{-3}$	$6.93 * 10^{-3}$
0	$5.37 * 10^{-3}$	$5.81 * 10^{-3}$	$6.43 * 10^{-3}$
-6	$5.66 * 10^{-3}$	$4.74 * 10^{-3}$	$5.81 * 10^{-3}$
-12	$4.55 * 10^{-3}$	$5.30 * 10^{-3}$	$9.27 * 10^{-3}$
-18	$7.66 * 10^{-3}$	$6.26 * 10^{-3}$	$9.76 * 10^{-3}$
-22	$9.67 * 10^{-3}$	$2.27 * 10^{-3}$	$17.27 * 10^{-3}$
-23.3	————	$4.04 * 10^{-3}$	$6.00 * 10^{-3}$

Table 6.3.2 Bed Depth 60cm, Superficial Flow 3 cms^{-1}, Freeboard Height 180 cm and Reference Axis YY.

Variation of rms Fluctuating Velocity Components with Position on the YY Axis - Large Sand Bed.

Position (cm)	u'_X (ms^{-1})	u'_Y (ms^{-1})	u'_Z (ms^{-1})
22	$22.73 * 10^{-3}$	$12.54 * 10^{-3}$	$24.17 * 10^{-3}$
18	$16.32 * 10^{-3}$	$17.77 * 10^{-3}$	$20.12 * 10^{-3}$
12	$18.79 * 10^{-3}$	$20.96 * 10^{-3}$	$20.52 * 10^{-3}$
6	$13.76 * 10^{-3}$	$21.37 * 10^{-3}$	$16.72 * 10^{-3}$
0	$16.50 * 10^{-3}$	$19.24 * 10^{-3}$	$14.61 * 10^{-3}$
-6	$19.25 * 10^{-3}$	$21.80 * 10^{-3}$	$16.46 * 10^{-3}$
-12	$20.53 * 10^{-3}$	$21.40 * 10^{-3}$	$19.63 * 10^{-3}$
-18	$22.65 * 10^{-3}$	$21.63 * 10^{-3}$	$21.12 * 10^{-3}$
-22	$23.73 * 10^{-3}$	$12.48 * 10^{-3}$	$29.09 * 10^{-3}$

Table 6.3.3 Bed Depth 60cm, Superficial Flow 4 cms^{-1}, Freeboard Height 120cm and Reference Axis YY.

Variation of rms Fluctuating Velocity Components with Position on the YY Axis - Large Sand Bed.

Position (cm)	u'_X (ms^{-1})	u'_Y (ms^{-1})	u'_Z (ms^{-1})
23.3	————	$3.79 * 10^{-3}$	$8.21 * 10^{-3}$
22	$9.70 * 10^{-3}$	$2.59 * 10^{-3}$	$8.78 * 10^{-3}$
18	$7.42 * 10^{-3}$	$7.41 * 10^{-3}$	$6.73 * 10^{-3}$
12	$8.96 * 10^{-3}$	$7.41 * 10^{-3}$	$7.56 * 10^{-3}$
6	$8.75 * 10^{-3}$	$6.90 * 10^{-3}$	$8.71 * 10^{-3}$
0	$7.44 * 10^{-3}$	$6.67 * 10^{-3}$	$7.10 * 10^{-3}$
-6	$8.95 * 10^{-3}$	$7.82 * 10^{-3}$	$7.12 * 10^{-3}$
-12	$7.58 * 10^{-3}$	$7.61 * 10^{-3}$	$6.87 * 10^{-3}$
-18	$9.39 * 10^{-3}$	$7.12 * 10^{-3}$	$11.37 * 10^{-3}$
-22	$10.64 * 10^{-3}$	$2.98 * 10^{-3}$	$10.91 * 10^{-3}$
-23.3	————	$3.32 * 10^{-3}$	$3.61 * 10^{-3}$

Table 6.3.4 Bed Depth 60cm, Superficial Flow 4 cms^{-1}, Freeboard Height 180 cm and Reference Axis YY.

Variation of Vertical and Transverse Average and rms
Fluctuating Velocity Components with Position on the YY
Axis - Large Catalyst Bed, Same Conditions.

Position (cm)	U_Y (ms^{-1})	U_Z (ms^{-1})
0	$1.415 * 10^{-2}$	$20.3 * 10^{-2}$
-6	$1.595 * 10^{-2}$	$21.0 * 10^{-2}$
-12	$1.39 * 10^{-2}$	$21.8 * 10^{-2}$
-18	$1.275 * 10^{-2}$	$21.2 * 10^{-2}$
-22.8	$0.97 * 10^{-2}$	$14.1 * 10^{-2}$

Table 6.3.5 Bed Depth 30cm, Superficial Flow 16.4 cms^{-1}, Freeboard Height 150cm and Reference Axis YY.

Position (cm)	u'_Y (ms^{-1})	u'_Z (ms^{-1})
0	$15.61 * 10^{-3}$	$28.9 * 10^{-3}$
-6	$13.47 * 10^{-3}$	$27.35 * 10^{-3}$
-12	$13.69 * 10^{-3}$	$32.6 * 10^{-3}$
-18	$8.92 * 10^{-3}$	$38.75 * 10^{-3}$
-22.8	$8.46 * 10^{-3}$	$42.2 * 10^{-3}$

Table 6.3.6

Chapter 7
Analysis and Discussion of Results

7.1 Initial Levels of Turbulence and Decay of Turbulence

The dependence of fluctuations in gas velocity in the freeboard above fluidised beds on the rise velocity of bubbles in the bed was assumed and tested in Chapter 5. The assumption was used to explain the effect of fluidising conditions on the turbulence intensity measured by L.D.A.

In this section expected values of bubble rise velocity are compared to initial values of turbulence intensity i.e. values at $Z'=0$. The method used to estimate the bubble rise velocity was as follows:

<u>1</u> The bubble diameter in the bed was estimated using the bubble size correlation of Mori and Wen [51], Equation 2.1.

<u>2</u> Bubble rise velocity was estimated from the equation of Davidson and Harrison [14], Equation 2.3, using the bubble diameter estimate given by part one. The magnitude of gas velocity fluctuations in the freeboard may be given by the absolute bubble rise velocity minus the minimum fluidising velocity:

$$u^* = (U_G - U_{MF}) + 0.711(gd_e)^{1/2} - U_{MF} \qquad (7.1)$$

Pemberton and Davidson [61] assume that "ghost" bubbles are formed in the freeboard with an initial velocity equal to the absolute bubble rise velocity at the surface of the bed. An estimate of the value of the rms fluctuating velocity at the surface of the bed can be obtained by extrapolation of the rms fluctuating velocity vs. height above static bed surface plot to zero. The magnitude of the velocity fluctuations, u^*, will be given by twice the rms value of the velocity fluctuations, u'. It is possible therefore to compare the estimate of the magnitude of the gas velocity fluctuations predicted by equation (7.1) and the value obtained experimentally.

The decay of turbulence was analysed by two methods outlined by Pemberton and Davidson [61]:

1 Assume ghost bubbles are formed in the freeboard which increase in size due to entrainment of bulk fluid, and the velocity of the ghost bubble therefore decreases. The change in volume with time is given by the expression suggested by Maxworthy [48] for vortex rings. The magnitude of velocity fluctuations should decrease according to the relationship:

$$u^* = u^*_0 \exp(-\beta_1 Z') \qquad (7.2)$$

where β_1 maybe predicted by:

$$\beta_1 = -3\sqrt{(\pi \upsilon)}/4u_0^{1/2}a_0^{3/2} \qquad (7.2a)$$

and υ = Kinematic viscosity,
u_0 = Initial ghost bubble velocity (given by equation 7.1),
a_0 = Initial ghost bubble radius (given by equation 2.1).

2 Decay of Isotropic turbulence based on the expression for pipe flow given by Brodkey [6], with the characteristic dimension of turbulence taken as the bubble diameter:

$$\varepsilon' = 7.36 \ u'^3/d_e \qquad (7.3)$$

where ε' = Turbulent energy dissipation rate,
        u' = rms fluctuating velocity.

The rms velocity fluctuations should vary with distance from the bed surface, Z', according to the relationship referred to in Chapter 2, equation (2.48).

Figure 7.1.1 shows the decay of axial turbulence under various fluidising conditions in the small bed fluidising glass ballotini beads. Table 7.1.1 shows the results obtained by Linear Regression Analysis, as described by

Chatterjee and Price [8], of the data of Figure 7.1.1 assuming an exponential decay of the form given in Equation (7.2). The regression coefficient is nearly one for each set of experimental conditions which indicates that the curve fit is good. Table 7.1.2 shows the value of u^* predicted by Equation (7.1) and the value of β_1 predicted by Equation (7.2a).

The magnitudes of the velocity fluctuations at the bed surface obtained by extrapolation are of the same order of magnitude as the values predicted by Equation (7.1). The values of β obtained by regression analysis, however, show significant difference from the values of β_1 predicted by Equation (7.2a). The values are of the same order of magnitude for a superficial fluidising velocity of 0.4 m s^{-1} and a bed depth of 5 cm, but for subsequent fluidising conditions under which the bubble diameter and relative bubble rise velocity are smaller the predicted value, β_1, tends to get larger whereas the values obtained by regression analysis of the experimental data tend to get smaller. This implies that small, slow moving vortex rings in this system do not entrain large amounts of bulk fluid and do not therefore loose their momentum. At a superficial fluidising velocity of 0.3 m s^{-1} and a bed depth of 3 cm there is very little decay of axial turbulence intensity with freeboard height (Figure 7.1.1).

Table 7.1.3 shows the value of the gradient obtained by regression analysis of the data in Figure 7.1.1 plotted as $1/u'$ vs. Z' in accordance with the decay of isotropic turbulence (Equation 2.48). It is apparent that the rate of decay is much less than that predicted by Equation (2.48). The turbulence in the freeboard of gas fluidised beds is generated by bursting gas bubbles, and the turbulence intensities are much greater than those expected for pipe flow at the same superficial flow. The value of U_G in equation (2.48) for the flow in the

freeboard of the fluidised beds is low relative to the turbulence intensities measured. Therefore, the rate of decay, which for pipe flow is due to viscous stresses, is overestimated.

Figure 7.1.2 shows the decay of axial turbulence under various fluidising conditions for round sand fluidised in the large rectangular bed. Table 7.1.4 shows the results obtained by linear regression analysis of the data given in Figure 7.1.2, assuming an exponential decay of the form given by Equation (7.2). Table 7.1.5 shows the initial value of the gas velocity fluctuations predicted by Equation (7.1), and the value of β_1 predicted by the vortex ring model, Equation (7.2a).

The value of u^* obtained by extrapolation of the experimental data to zero Z' is much less than the values of u^* predicted by the bubble rise velocity model. This may be because of the mechanism of bubble eruption in this relatively large fluidised system suggested in Section 5.3.5. The resultant velocity of a ghost bubble will be lower than predicted by the bubble rise velocity in the bed because of the horizontal components of gas velocity that exist when bubbles burst at the surface of the bed.

In addition, comparison of the experimental values of u^* to the values predicted by the bubble rise velocity model shows that the trends under different fluidising conditions are not in agreement. For example, the initial value of u^*, found by extrapolation of the experimental data, for a fluidised bed of depth 30 cm and superficial fluidising velocity 3 cm s^{-1}, is greater than the initial value for a fluidised bed of depth 60 cm and superficial fluidsing velocity 3 cm s^{-1}, whereas the converse is predicted by the bubble rise velocity model. This behaviour was found in Section 5.3.2, at a freeboard height, Z', of 60 cm (Figure 5.3.7), and may be a result of the assumption that bubble rise velocity is solely

dependent on the bubble diameter which does not take into account the manner by which the bubble reached its volume.

The values of the exponential decay constant obtained by regression analysis of the experimental data are of the same order of magnitude as those predicted by Equation (7.2a). However, the trend in the values of the decay constants is again not in agreement. The values obtained experimentally are low when the initial fluctuations in gas velocity are low, whereas the predicted value of the decay constant is high when the initial magnitude of gas velocity fluctuation is low. The behaviour of vortex rings in the freeboard of gas fluidised beds may be different from the behaviour of vortex rings in the system used by Maxworthy [48], on which Equation (2.48) is based.

Table 7.1.6 shows the results obtained by regression analysis for the gradient of the plot of $1/u'$ vs. Z', based on the decay of isotropic turbulence. This value is considerably lower than the values of gradient predicted by Equation (2.48). This is probably because the values of turbulence are very high for the superficial flow as the fluctuations are forced by bursting gas bubbles. The difference is considerable in this case because U_G, the superficial flow, is relatively small. The Reynolds Number for the gas flow is approximately 800, and very little turbulence would be expected in pipe flow under these conditions.

In conclusion, although there are differences between current theory and experimental results the vortex ring model gives the best description of the gas flow in the freeboard of fluidised beds. Improved methods of predicting the growth of vortex rings in the freeboard are necessary, as the analysis based on the expression proposed by Maxworthy [48] does not predict the

behaviour found experimentally.

A factor which may also be important is the amplitude of pressure fluctuations expected in the fluidised bed. The magnitude of pressure fluctuations is related to both the bed density and the size of the bubbles which are the source of the pressure fluctuations, and are larger at larger superficial fluidising velocities (Section 2.1.5). The initial velocity of the bubble phase gas after eruption may also be correlated with the amplitude of the pressure fluctuations. Fan et. al. [19] showed that the intensity of pressure fluctuations was proportional to the parameter $(M_a/2A)(U_G - U_{MF})$, equation (2.5). The experimental values of u^*_0 found in this work and in the work of Pemberton [60] are plotted against this parameter in Figure 7.1.3. The values of u^*_0 seem to be dependent on the parameter. For systems with low values of this parameter, for example the large bed fluidising sand in this work, there is likely to be a relatively large difference between the bubble rise velocity at the surface of the bed and the magnitude of the gas velocity fluctuations. This was found to be the case, (Table 7.1.4 and Table 7.1.5). For systems with larger values of this parameter, for example Pemberton's [60] 0.3 m square bed the difference may be relatively small. In fact, Pemberton found that the agreement between the relative bubble rise velocity at the bed surface and the initial magnitude of gas velocity fluctuations found by extrapolation of experimental data was good.

7.2 Implications for Particle Motion

In most practical fluidised systems significant entrainment and elutriation of bed material occurs as a result of particle ejection and the range in particle diameter of the bed material. The motion of the ejected particles in the freeboard will depend on the initial particle velocity, the size of the particle and the properties of the turbulent gas flow. According to Launder and Spalding [37] the local structure of turbulence can be identified by two properties, the local mean velocity and the length scale of the turbulent motion. According to Hinze [32] the method used to describe turbulent flow fields is a scale in time and a scale in space. The magnitudes of these scales will be dependent on the dimensions of the system. In fluidised systems bubble induced turbulence exists in the freeboard, and it is desirable to be able to predict the motion of particles in the turbulent flow. The properties of the flow in various systems have been investigated in some detail in Chapters 5 and 6. The extension of this investigation to the motion of particles in turbulent gas streams is dicussed in this section.

The behaviour of a particle in a turbulent gas flow will depend on its size. Small particles will follow the turbulent velocity fluctuations whereas velocity fluctuations will not be induced in large particles. The behaviour of particles of different sizes in turbulent flows has been discussed by Hinze [32], Pemberton [60], Clift et. al. [12], Clift and Gauvin [10] and Abrahamson [2]. Small and large particles are classified relative to the length scale of turbulence. Clift and Gauvin [10] outline criteria for the classification of particles given below:

(a) The diameter of the particle, d_p, should be much less than the characteristic dimension of the flow field. This is given by Kolmogoroff's length scale, η. The expression for η is given by Hinze [32]:

$$\eta = (\upsilon^3/\varepsilon')^{0.25}$$

where υ = Kinematic viscosity of the fluid,

ε' = Turbulent energy dissipation per unit mass.

The turbulent energy dissipation per unit mass may be estimated by analogy to pipe flow (Equation 7.3).

(b) The Turbulent Reynolds Number, $(N_{Re})_t$, of the particle should be small, in other words:

$$d_p u'/\upsilon < 1$$

where u' = rms fluctuating velocity.

(c) The particle relaxation time, θ_p, should be much less than the characteristic time of the flow field, which may be given by the Kolmogoroff Time, θ_k. Therefore:

$$\theta_p = d_p^2/9\upsilon[2(\varrho_p/\varrho_g) + 1]$$

$$\theta_k = \eta^2/\upsilon$$

Table 7.2.1 shows the initial values of the Kolmogoroff length scale for the turbulent flow above fluidised beds of round sand. The value of turbulence intensity used was that found experimentally (Table 7.1.4). The size distribution of the round sand is given in Table 4.1. All the particle diameters are less than the characteristic length of the turbulent flow field, therefore criterion (a) is satisfied. Table 7.2.2 shows the turbulent Reynolds number of the particle (taking d_p as 100 µm), the particle relaxation time and the characteristic time of the turbulent flow field, θ_k. The particle turbulent Reynolds number is less than 1 for each set of fluidisation

conditions and therefore criterion (b) is partially satisfied. The particle relaxation time, again based on a particle diameter of 100 μm, is much larger than the characteristic time of the turbulent flow field, and criterion (c) is therefore not satisfied. Only for very small particles, <1μm, will the particle relaxation time be less than the Kolmogoroff Time. It is likely therefore that the particles of sand will not follow the turbulent motion of the gas flow. In this case the major problem is predicting the drag force experienced by the particles as a result of their motion in the turbulent gas stream.

Clift and Gauvin [10] present correlations for the drag coefficients of spheres in terms of a relative turbulence intensity, I_R, defined by:

$$I_R = u'/V_r$$

where V_r is the velocity of a particle relative to the fluid.

Knowing the value of this parameter the value of the particle critical Reynolds Number, $d_p V_r/\upsilon$, may be estimated and the appropriate correlation for C_D, the drag coefficient, selected. The effect of acceleration was also discussed, which is relevent in the freeboard of fluidised beds for relatively large particles that are projected upwards with an initially high velocity which decreases with height and time until velocity is reversed and the particle falls towards the bed. Uhlherr and Sinclair [71] give a correlation for C_D at low values of the particle Reynolds number defined above.

Clift and Gauvin [10] describe the equation of motion for a particle in a turbulent gas flow, and it should be possible to predict the trajectories of particles based on

this. The experimental results presented in this work show that the turbulent flow field in the freeboard of gas fluidised beds can be far from simple. Large variations in local mean velocities can exist, as shown in Chapter 5 which make the solution for particle motion rather complicated. In addition, the turbulence may not be homogeneous, as found for fluidised beds of round sand, and the turbulence may exhibit a high degree of anisotropy, as found for fluidised beds of catalyst. The prediction of particle motion is therefore a very complex problem unless simplifying assumptions are made, which do not seem reasonable in the light of experimental evidence given in this work.

Pemberton [60] assumed that a secondary mechanism of particle disengagment was due to transfer of particles towards the walls in the freeboard. It was assumed that low gas velocity existed in this region and particles would therefore tend to fall back towards the bed. In Chapter 6 extensive information on the horizontal components of the gas flow were presented. In general it was found that mean velocities existed in the horizontal direction, but, particularly for fluidised beds of round sand, the mean velocities at many positions had no dominant direction. Pemberton [60] used a particle mass transfer coefficient to model the horizontal motion (Section 2.2.4).

A comparison of this value with a limited number of horizontal particle velocity measurements done in this work is possible. Consider the large bed fluidising round sand. The bed depth was 30 cm and superficial flow was 3 cm s^{-1}. At a freeboard height, Z, of 120 cm the

turbulence intensity will be given by an equation of the form:

$$u' = u'_0 \exp(-\beta Z') \qquad (7.4)$$

Using the experimentally determined values of the parameters u'_0 and β from Table 7.1.4 a value for the turbulence intensity is obtained. Substituting this value into equation (2.43) the value of the particle mass transfer coefficient, k_g, given is:

$$k_g = 1.89 * 10^{-4} \text{ m s}^{-1}$$

Table 7.2.3 shows the mean particle velocities, V_Y, measured over a 50 second experiment duration at position +6 cm on the YY axis for the experimental conditions described above. Each velocity is labelled I which implies that the dominant direction is in the +ve Y direction. The value of the relative turbulence intensity, v''_Y, expresses the range of velocities measured over the experiment duration. The mean velocity estimates from runs 1 and 4 are similar and are nearly two orders of magnitude greater that the particle mass transfer coefficient. TThey are, on the other hand, commensurate with the measured values of the horizontal component of mean gas velocity. The mean velocity estimates from the remaining runs show a large deviation, but this illustrates the unsteady nature of the particle motion. It should also be kept in mind that the particles whose velocities were measured may have been of different sizes and as a result may have behaved differently.

It seems therefore that the value of the particle mass transfer coefficient predicted by equation (2.43) for particles in the turbulent gas flow is orders of magnitude less than the values of particle velocity measured in the freeboard of the large bed fluidising sand.

In the later stages of research the Laser Doppler Anemometer System was further developed to enable particle counts to be made in the freeboard region (Section 3.4.3). In view of the particle velocities measured and the properties of the gas flow horizontally the variation in particle count over the freeboard is of interest. Figure 7.2.1 shows the number of particles detected over a five minute experiment duration on the YY axis for superficial fluidising velocities of 3 and 4 cm s^{-1}. The bed depth was 30 cm and the freeboard height, Z, was 120 cm. At both superficial flows more particles were detected near the walls which is consistent with the view that particles are transferred towards the walls by horizontal components of velocity. The profile for the vertical component of velocity at this postion in the freeboard is given in Figure 5.3.11. There is relatively high velocity near the walls with a region of low velocity less than 1 cm from the wall (Figure 5.3.13). Particles transferred towards the walls will therefore be acted on by relatively high gas velocities before reaching the region of low gas velocity near the wall and may therefore be carried upwards by the gas flow. Figure 7.2.1 also shows the increase in particle count with increase in superficial flow expected because of increased bubbling activity in the dense bed.

To summarize the preceding section in the context of improved mechanistic models of entrainment:

1 The concentration of solids, C_i, mass flux of solids, E_i and particle velocity, V_z, are related by the following equation:

$$C_i = E_i / V_z \qquad (7.5)$$

It does not seem reasonable to disregard the effect of turbulence on the drag experienced by particles in the gas flow. Reference is made to this subject in Chapter 8 as a recommendation for further work. The prediction of particle velocity of a particular size fraction with in creasing distance from the bed surface would need to take into account the relationship between turbulence intensity and distance from the bed surface analysed in Section 7.1. This may be possible using current numerical integration techniques. Unfortunately, the development of such methods has not been possible due to the complexity of the problem and pressure of time.

2 The rates of transfer of particles horizontally in the freeboard appear to be greater than currently predicted. However, the nature of their motion may be such that the use of a single predicted value is unresasonable. The relatively small amount amount of data obtained on horizontal particle velocities indicates that the statistical properties of the velocity fluctuations support the above observation.

7.3 Experimental Velocity Profiles

Previous work done on velocity profiles has been performed by researchers named in Section 2.3.1.

Pemberton [60] found that the axial vertical component of velocity decreased exponentially with increase in freeboard height (Section 2.3.1). He explained this by assuming that at low freeboard height turbulence was relatively high and the transfer of particles to the wall region of the freeboard would consequently be large. The particles would fall downwards at the walls, entrain gas and cause gas recirculation. By continuity the gas flow had to be greater at the centre of the cross section. The behaviour of the bubble phase gas after bubble eruption was not considered to explain the velocity profile. The bed depths used were such that the ratio of bed depth to vessel diameter was in the range 2.8 - 3.55 i.e. the beds were very deep. Under these fluidising conditions bubbling activity was probably concentrated at the centre of the bed surface and because the minimum fluidising velocity was quite large the extent to which bubble phase gas was transferred horizontally would be limited. The velocity profile would therefore show a maximum at the centre of the freeboard cross section at low freeboard height.

Levy [41] found that velocity profiles at low freeboard height had a dip profile with maxima at the walls (Section 2.3.1). The minimum fluidising velocities of the materials used were relatively large, and the assumption that bubble phase gas was transferred to the corresponding region in the freeboard after bubble eruption is reasonable (Section 5.4). The beds used were shallow and bubbling activity was presumably concentrated near the walls in the dense bed. Larger local gas velocities would therefore be expected near the walls in the freeboard.

It may be possible to use the streamline functions characteristic of vortex rings to model the experimental gas velocity profiles found in this study and the work of Levy [41] and Pemberton [60]. In addition, the minimum fluidising velocity may have the following effect:

1 For low U_{MF}, the vortex pair may generate circulation that has upward motion near the wall and downwards motion at the centre of the cross section (Figure 7.3.1a).

2 For relatively large U_{MF} the vortex pair may generate circulation that has downwards motion near the wall and upwards motion at the centre of the cross section (Figure 7.3.1b).

It should be emphasised that Figure 7.3.1 is not an attempt to accurately represent flow streamlines, but is an attempt to show schematically a possible explanation of the gas velocity profiles found experimentally. Again, further development of such mathematical models has been the victim of time. The subject is referred to in Chapter 8 as a recommendation for further work.

Figure 7.1.1 Variation of u´$_z$ Along Z Axis for Two Fluidising Velocities and Bed Depths - Small Bed.
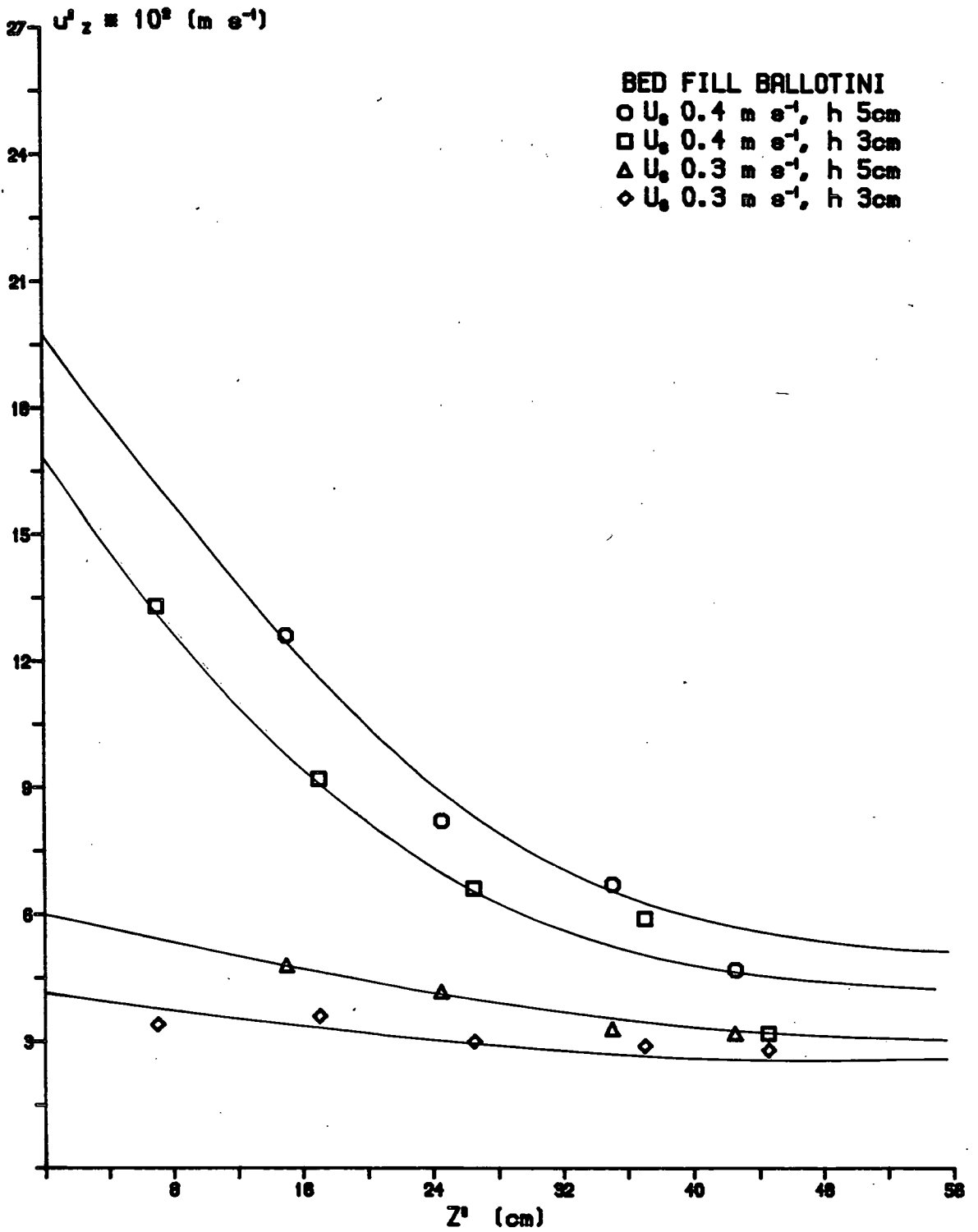
Figure 7.1.2 Variation Along Z Axis of Transverse Component
of rms Fluctuating Velocity for Two Fluidising Velocities
and Bed Depths - Large Sand Bed.
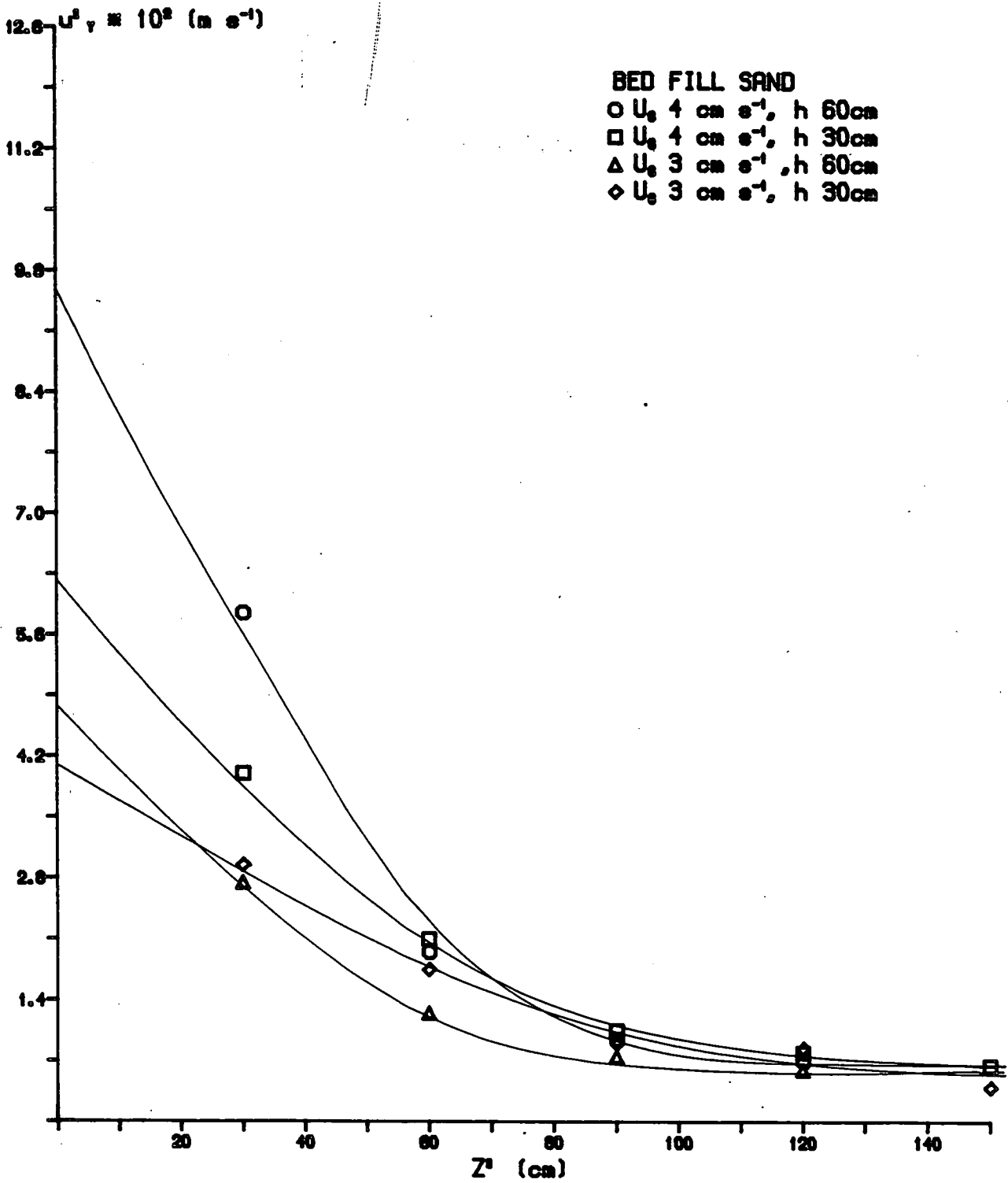
Figure 7.1.3 Variation of Amplitude of Velocity Fluctuations at Bed Surface with Fan's Pressure Fluctuation Parameter.
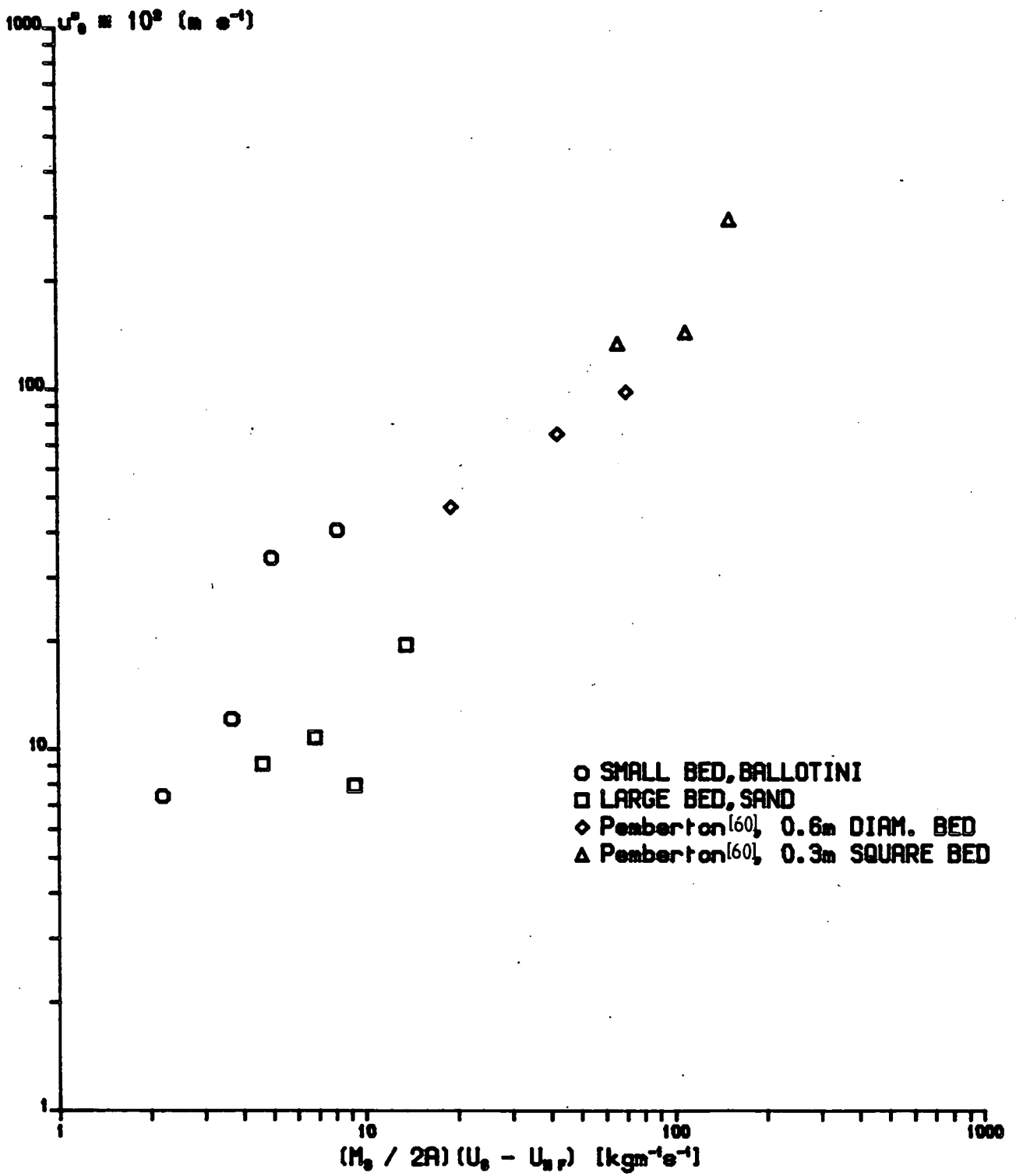
Figure 7.2.1 Variation of Sand Particle Frequency with Position on the YY Axis for Large Sand Bed.

SYSTEM PARAMETERS
BED DEPTH 30cm
Z 120cm
BED FILL SAND

O U_s 3 cm s^{-1}
☐ U_s 4 cm s^{-1}

N_p (5min^{-1})

POSITION ON THE YY AXIS (cm)
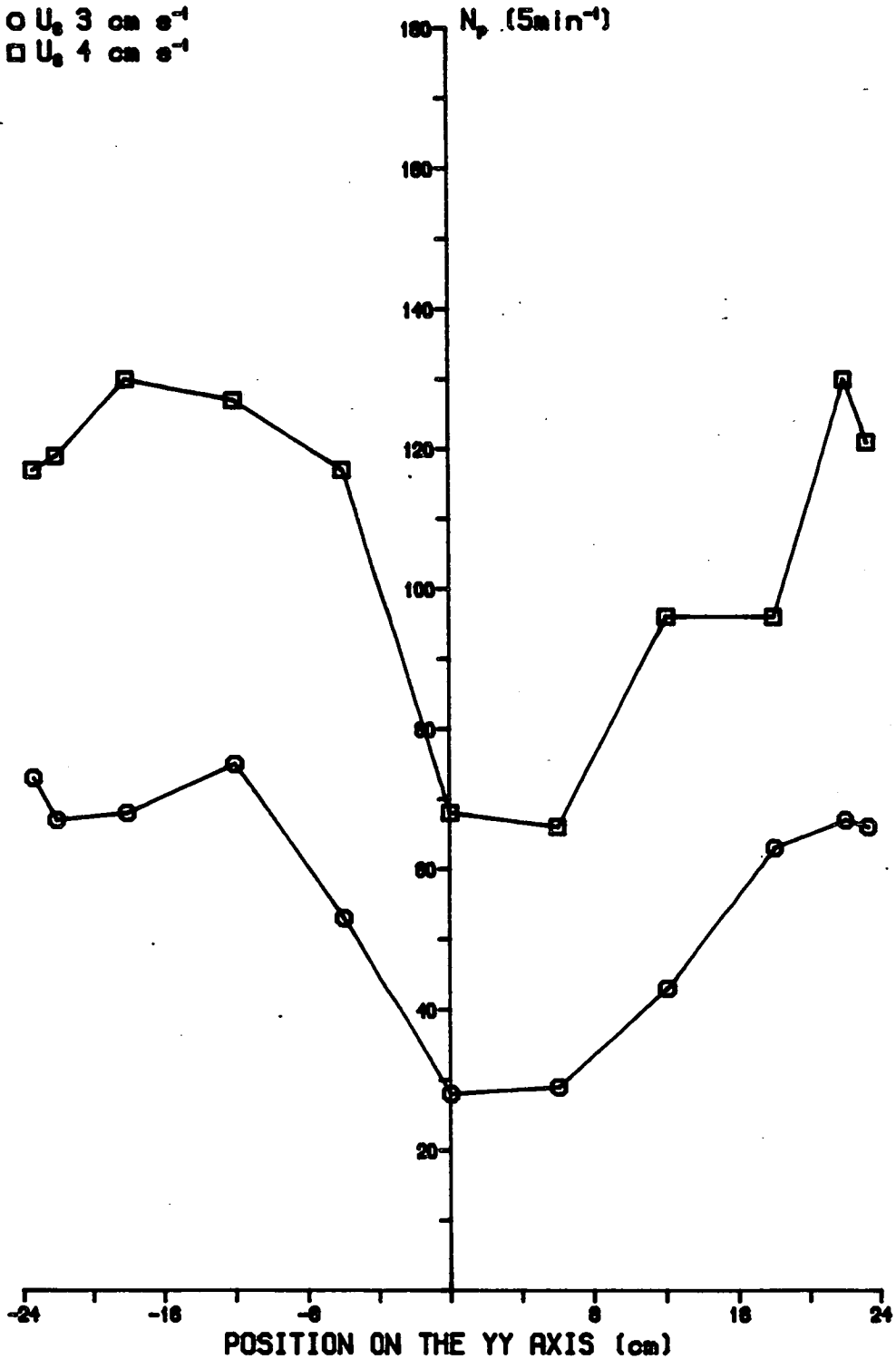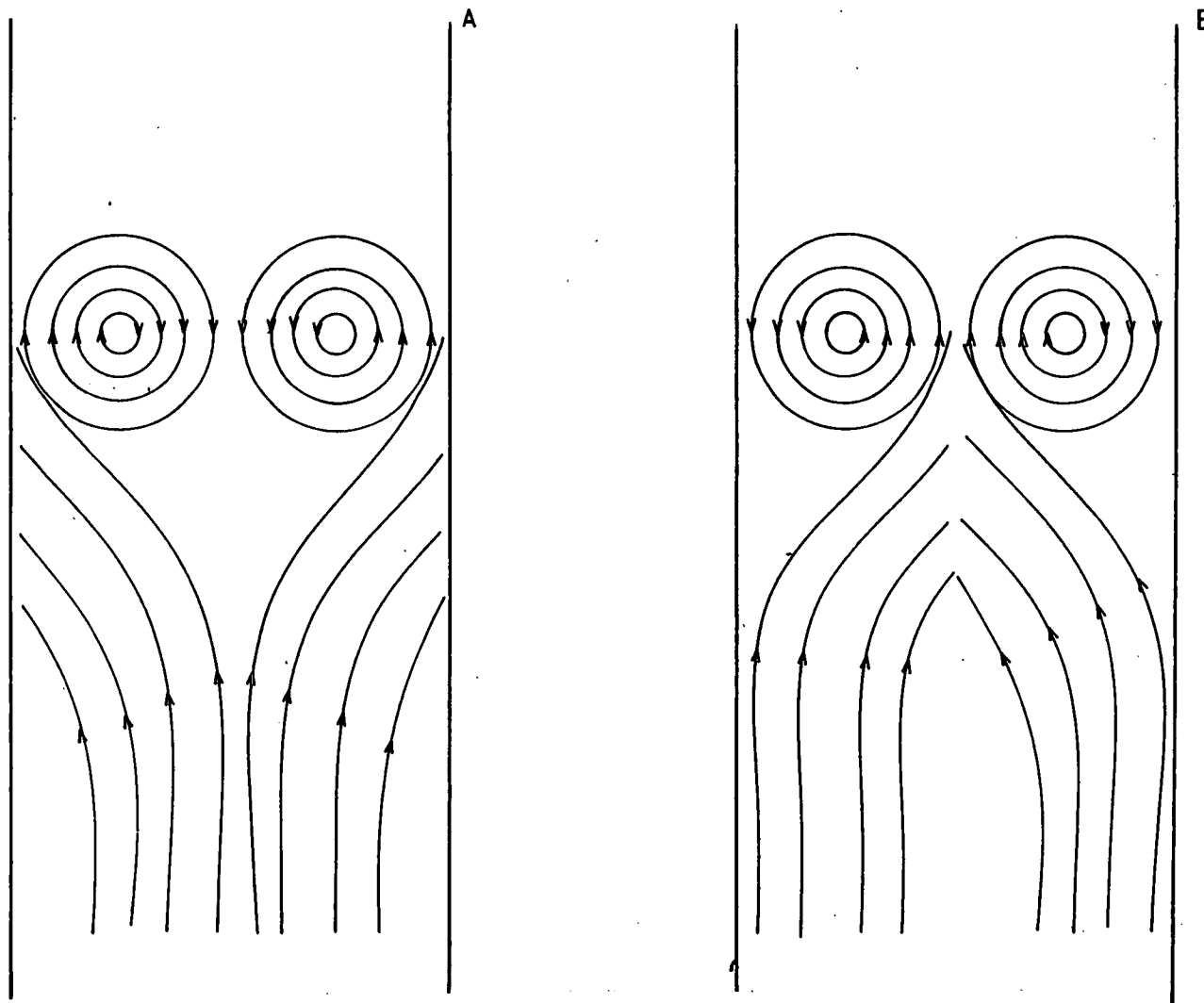
Figure 7.3.1 Possible Gas Flow Patterns in Freeboard of a Fluidised Bed.

Values of Velocity Fluctuation at Bed Surface and Rate of Decay of Turbulence in Freeboard Calculated from Fig. 7.1.1 - Small Bed.

U_G (ms^{-1})	h (cm)	u'_{z0} (ms^{-1})	u^*_{z0} (ms^{-1})	β (m^{-1})	R^2
0.4	5	0.2027	0.4054	-3.38	0.97
0.4	3	0.1697	0.3394	-3.43	0.94
0.3	5	0.0606	0.1212	-1.58	0.97
0.3	3	0.0370	0.0740	-0.64	0.79

Table 7.1.1

Quantities Corresponding to those of Table 7.1.1, Calculated from Mori and Wen's Correlation - Small Bed.

U_G (ms^{-1})	h (cm)	d_e (cm)	u (ms^{-1})	β_1 (m^{-1})
0.4	5	2.86	0.337	-5.68
0.4	3	2.25	0.294	-8.72
0.3	5	1.55	0.137	-22.33
0.3	3	1.06	0.089	-48.99

Table 7.1.2

Co mparison of Measured Rate of Decay of Freeboard
Turbulence with that Calculated from Theory of Pemberton
and Davidson - Small Bed.

U_G (ms^{-1})	h (cm)	Gradient[1]	R^2	Gradient[2]
0.4	5	45.30	0.96	214
0.4	3	55.13	0.83	272
0.3	5	40.94	0.96	527
0.3	3	20.29	0.81	770

(1) Gradient from Linear Regression Analysis of data in
Figure 7.1.1 plotted as $1/u'$ vs. Z'.

(2) Gradient expected from Equation (2.47) i.e. $2.45/(U_G d_e)$.

Table 7.1.3

Values of Velocity Fluctuation at Bed Surface and Rate of Decay of Turbulence in Freeboard Calculated from Fig. 7.1.2 - Large Bed.

U_G (cms^{-1})	h (cm)	u'_0 (ms^{-1})	u^*_0 (ms^{-1})	β	R^2
4.0	60	0.0976	0.1952	2.36	0.94
4.0	30	0.0539	0.1078	1.53	0.94
3.0	60	0.0397	0.0794	1.69	0.94
3.0	30	0.0455	0.0910	1.57	0.96

Table 7.1.4

Quantities Corresponding to those of Table 7.1.4, Calculated from Mori and Wen's Correlation - Large Bed.

U_G (cms^{-1})	h (cm)	d_e (cm)	u (ms^{-1})	β_1 (m^{-1})
4.0	60	7.27	0.621	1.03
4.0	30	4.10	0.481	2.77
3.0	60	6.13	0.568	1.39
3.0	30	3.47	0.425	3.78

Table 7.1.5

Comparison of Measured Rate of Decay of Freeboard Turbulence with that Calculated from Theory of Pemberton and Davidson - Large Bed.

U_G (cms^{-1})	h (cm)	Gradient[1]	R^2	Gradient[2]
4.0	60	144	0.99	842
4.0	30	112	0.99	1494
3.0	60	148	0.99	1332
3.0	30	164	0.86	2353

(1) Gradient from Linear Regression Analysis of data in Figure 7.1.2 plotted as $1/u'$ vs. Z'.
(2) Gradient expected from Equation (2.47) i.e. $2.45/(U_G d_e)$.

Table 7.1.6

Length Scale, η of Freeboard Turbulence, Calculated from Experimental Data using Brodkey's Expression for Energy Dissipation.

U_G (cms^{-1})	h (cm)	d_e (cm)	u'_0 (ms^{-1})	η (μm)
4.0	60	7.27	0.0976	593
4.0	30	4.10	0.0539	675
3.0	60	6.13	0.0397	940
3.0	30	3.47	0.0455	735

Table 7.2.1

Particle Relaxation Time, θ_p, and Kolmogoroff Time, θ_k, for Large Sand Bed Conditions.

U_G (cms^{-1})	h (cm)	$(N_{Re})_t$	θ_p (s)	θ_k (s)
4.0	60	0.54	0.308	0.019
4.0	30	0.30	0.308	0.025
3.0	60	0.22	0.308	0.049
3.0	30	0.25	0.308	0.030

Table 7.2.2

Sand Particle Velocity Measurements.

Run Number	Mean Particle Velocity, V_Y (ms^{-1})	V''_Y (%)
1	$9.07 * 10^{-3}$	53.3
2	$6.43 * 10^{-4}$	670.6
3	$4.91 * 10^{-3}$	116.5
4	$8.88 * 10^{-3}$	35.4

Table 7.2.3

Chapter 8
General Conclusions and Recommendations

One of the characteristics of gas fluidised beds is entrainment of solids into the freeboard space above the bed surface. It is now generally accepted that the contribution to conversion of the freeboard region in, for example, a fluidised bed catalytic cracker regenerator is significant [20]. The motion of solid particles after entrainment will be dependent on the structure of the gas flow. The motion of particles will in turn determine the residence time of the particles in the freeboard and therefore the conversion expected. If the local gas velocity is large enough particles may be carried out of the system, or in other words, they may be elutriated. Knowledge of the mean gas velocity profile over the cross section is necessary to be able to predict rates of elutriation reliably.

The development of a doppler difference L.D.A. system to operate in gas flows containing entrained solids has proved to be a very useful tool in measuring the structure of flow in the freeboard region of gas fluidised beds. The results obtained appear to satisfy continuity and complement results obtained previously [41].

A number of conclusions can be drawn from the data obtained which have been used to explain some of the results published in the literature. These can be summarized as follows:

1 Vertical mean velocity profiles have been found to be dependent on bed depth. This in turn implies that the velocity profiles are dependent on the spatial distribution of bubbling at the bed surface. Furthermore, the velocity profiles appear to be dependent on the minimum fluidising velocity which may dictate the behaviour of bubble phase gas after eruption at the bed surface.

2 The turbulence intensity profiles are dependent on the distance from the containing walls and the mean velocity gradient. The turbulence intensity profile may also be

affected by the distribution of bubble rise velocities in the bed due to particle circulation patterns, particularly at low freeboard height.

3 From the results obtained for turbulence intensity in the freeboard in the presence and absence of an immersed tube bank in the dense phase, positive evidence is given that turbulence intensity in the freeboard is dependent on the bubble rise velocity in the dense phase.

4 The form of the vertical mean gas velocity profiles appears to be independent of superficial fluidising velocity and the presence of an immersed tube bank in the range investigated.

5 The vertical mean gas velocity profiles, particularly under low bed depth conditions, seem to be dependent on height above the bed surface. The presence of horizontal components of gas velocity may be assumed to explain this.

6 Drift velocities have been shown to exist in the freeboard space of fluidised beds. The magnitude and dominant direction are dependent on the operating conditions, such as bed depth, superficial fluidising velocity and freeboard height.

7 Transverse components of particle velocity tend to be orders of magnitude greater than particle mass transfer coefficients calculated from turbulent diffusion theory. This may be because drift velocities are superimposed on the turbulent diffusion effect (See Chapter 7).

8 The turbulence in the freeboard of fluidised beds has been found to:

(a) be nearly isotropic for fluidised beds of glass ballotini and round sand.

(a) exhibit a large degree of anisotropy for fluidised beds of catalyst.

The measurements of turbulence intensity horizontally show similar trends to those measured vertically.

These findings are directly relevant in predicting the behaviour of entrained solids in the freeboard space above fluidised beds. This relevance can be summarized as follows:

1 The shape of the velocity profile in the freeboard at various heights will dictate the relative particle velocity contained in the equation of motion, Equation (2.32). The distance to which particles that are entrained but not elutriated travel may therefore be predicted. If there is a large variation in the magnitude of the local mean gas velocity, as found above fluidised beds of round sand, the range of particles that may be elutriated is increased.

2 The existence of large velocity fluctuations in the gas flow above fluidised beds has been confirmed. The implications for particle motion have been discussed in Chapter 7. In previous attempts to predict particle motion the assumption that the effect of turbulence is negligible has been made. This assumption seems open to question.

3 The transfer of particles horizontally in the freeboard may be a secondary mechanism of disengagement. Particles which are transferred towards the walls may reach the low gas velocity region in the vicinity of the solid boundary, and as a result fall downwards towards the bed. The shape of the gas velocity profile is also relevent in this context. Particles transferred towards the walls in the freeboard space above fluidised beds of round sand will in many cases be acted on by large gas velocities before reaching the low velocity region. Conversely, any particles transferred to the (relatively) low velocity axial region would tend to fall back towards the bed. However, above fluidised beds of catalyst the gas velocity is nearly constant in the central region, and particles transferred horizontally may reach the low gas velocity region in the vicinity of the walls directly.

Development of a Model to Predict Particle Entrainment

Particles are ejected into the freeboard region by a number of mechanisms which have been described in Chapter 2. Various equations exist (Section 2.2.3) which attempt to predict the initial rate of ejection. In any entrainment model one of these, or a superior development, would be used to obtain an estimate for this.

The initial value of particle entrainment from the dense phase is much greater than the ultimate value of carry over from the system. The reason for this is that the freeboard region acts as a kind of filter. The particles which are carried over are those which have a low enough terminal velocity, or find themselves in a region of high enough gas velocity, to be carried downstream to a region where return to the dense phase is impossible. Particles which, on the other hand, have a high terminal velocity, or find themselves in regions of low, or even downward, gas flow fall back towards the dense phase and are re-engaged.

In order to predict which of the ejected particles are returned to the dense phase and which are carried over it is necessary to follow the trajectories of particles originating from different positions on the bed surface. If sufficient trajectories were investigated the proportion which do not return to the bed would indicate the fraction of ejected particles that were ultimately carried over. From this an accurate prediction of carry over could be made.

Previous work along these lines has been based on a simplified model of gas flow in the freeboard region in which a constant gas velocity core region is surrounded by a wall zone of much reduced gas velocity or even reversed flow. Particles with terminal velocities less than the

mean upward gas velocity in the central core will be carried over, unless they are transferred to the wall region. The rate of transfer to the wall has been predicted by pseudo - diffusional models based on measurements of turbulence of the gas flow. Transfer of particles from the low velocity wall zone to the central core region has been assumed to be improbable [33].

In the light of the results of this work and that of Levy and Lockwood [42] this model must be regarded as an oversimplification. It is clear that in some, but not all, cases a crater type gas velocity profile develops with low velocity at the centre of the cross section and in a thin boundary layer region near the wall but relatively high upward local velocities in a region adjacent to the wall. The movement of particles in the horizontal direction has in many cases been shown to be towards the wall and at a rate much higher than is predicted by diffusional models based on measurements of the gas turbulence. A systematic drift of the gas in the horizontal direction, mostly towards the walls, has been identified in these cases.

The effect of such flow patterns in the freeboard region is likely to be enhanced carry over rates. Despite the region of low gas velocity at the centre of the cross section ejected particles will be carried by horizontal components of mean gas velocity, as well as turbulence induced diffusion, towards the walls. Particles moving in this direction will encounter increasing turbulence and upward gas velocity whose influence will be to carry them rapidly upwards and almost to ensure their eventual escape from the freeboard region. No escape of particles from the region of high gas velocity to the more stagnant regions near the bed axis has been detected and carry over as a whole will therefore be correspondingly high.

Such "crater like" profiles, however, do not exist in all fluidised systems. The range of parameters investigated in this work is not great enough to enable the form of the velocity profiles to be predicted in any fluidised system, but it seems, on the basis of these observations, that the crater type profiles are more likely to be present above fluidised beds of particles with relatively low minimum fluidising velocities (<1 cm s^{-1}) in apparatus of relatively large size. Unfortunately, this appears to be precisely the type of system operated in many industrial situations. Smaller beds, or beds of particles with higher minimum fluidising velocities, seem to have freeboard velocity profiles similar to those observed by Pemberton and Davidson [61] and Horio et. al. [33].

In order to construct predictive models for particle entrainment rates from fluidised beds the following extra information is needed.

$\underline{1}$ Reliable means of predicting in any system what type of freeboard region velocity profile will be encountered. Given the baffling nature of the "crater type" velocity profile and its development this must wait for a plausable physical explanation.

$\underline{2}$ Some servicable expression must be found for the stream function characteristic of such crater type profiles. Such an expression would allow the prediction of vertical and horizontal components of velocity at any point in the freeboard space. Some attempts were made in the course of this work to do this by means of assuming a double (or toroidal) vortex system held steady by the upward superficial fluidising gas flow. Insurmountable difficulties were however encountered with this approach due to the instability of any such system in the proximity of a solid restraining wall.

$\underline{3}$ In addition, expressions for the distribution of turbulence in the freeboard space would have to be developed. Given the results of the investigations in this

work these would be related to the rise velocity and spatial distribution of bubbles bursting at the surface of the bed.

<u>4</u> Measurements of horizontal particle velocities could then be compared with the predictions of (2) and (3) above. This would resolve the question of whether the horizontal movement of particles can be entirely explained in terms of known local gas flow parameters or whether some other as yet undiscovered influence is at work.

<u>5</u> Further work on drag coefficients between gas and particles in the turbulent region would also be useful to answer the question whether or not the particles can be expected to follow the fluctuations of gas velocity in this region. If not, the spatial integration of particle trajectories will be a laborious business.

<u>6</u> In the absence of such information it is not at present possible to develop a predictive model of particle entrainment from gas solid fluidised beds. It is clear that further work along the lines suggested above should be performed.

Recommendations for Further Work

<u>1</u> Investigation of the possibility of developing the L.D.A. system further to enable the size of particles to be deduced would provide a facility for obtaining entrainment data by a non-intrusive method. The technique is potentially very powerful as the phenomenon could be investigated in real time. The development of such a facility may be possible based on the "Pulse Rate" theory outlined in Chapter 4.

<u>2</u> It would be of interest to study the effect of gas velocity fluctuations on the motion of solid particles. From existing literature available it seems that the drag experienced by the particle is affected, if the particle is of a size such that fluctuations in velocity are not induced. The investigation could initially be carried out in a simplified flow system.

<u>3</u> The development of mathematical models to predict the mean velocity profiles found experimentally above fluidised beds is highly desirable. The use of vortex ring theories may be possible. In addition, the effect of minimum fluidising velocity would have to be taken into account.

Nomenclature

a   Constant in equations (2.2), (2.10) and (2.22).

a   Freeboard exponential coefficient, equation (2.13).

a' Specific interface area between ascending and descending zones, averaged over the cross section.

a_0 Initial value of ghost bubble radius.

a'_0 Amplitude of coefficient that represents uncorrelated data.

AI   Total number of input pulses to correlator.

a_1 Beam profile coefficient.

A   Constant in equation (2.13)

A   Cross sectional area of the bed.

b   Constant in equations (2.2), (2.12) and (2.14).

b_0 Constant in equation (2.13).

B   Constant in equation (2.19).

C   Concentration of fines in bed after time t.

C   Constant in equations (2.12), (2.19), (2.20) and (2.21).

C_0 Initial concentration of fines.

C_0 Drag coefficient.

d_p Diameter of a particle.

d_{pi} Diameter of the ith size fraction of bed material.

d_e Equivalent diameter of bubble.

D_t Diameter or equivalent diameter of fluidised bed.

E Entrainment rate (kg m^{-2} s^{-1}).

E' Entrainment rate (kg s^{-1})

E_0 Initial entrainment rate.

f Frequency obtained from a power spectrum.

f_b Bubble frequency.

f_w Fraction of bubble volume occupied by wake.

Δf Differential doppler shift in two beam system.

$\Delta f'$ Frequency of scattered radiation by Fringe Model.

$F^*(k)$ Discrete fourier transform of N real data points F(N).

g Gravitational constant.

g_1 Amplitude of first turning point in a.c.f.

g_2 Amplitude of second turning point in a.c.f.

g_3 Amplitude of third turning point in a.c.f.

G Gas mass flow rate.

$G(\tau)$ Autocorrelation function (a.c.f.).

h   Bed depth.

I_R Relative turbulence intensity, Section 7.2.

j $\sqrt{-1}$.

k_0 Characteristic wave number of energy containing eddies.

k_g Particle mass transfer coefficient.

K_0 Incident wave vector of laser beam.

k_{01} Incident wave vector of first split laser beam.

k_{02} Incident wave vector of second split laser beam.

k_s Scattered wave vector of scattered radiation.

l   Effective diffusion length.

L   Characteristic length of turbulence.

m   Wave number power index of turbulent energy spectrum.

m_1 Fringe visibiity.

M_s Mass of solids in a fluidised bed.

N   Number of data points in a.c.f. and power spectrum.

N_σ Number of fringes in beam radius.

$(N_{Re})_t$ Turbulent Reynolds Number.

N_p Number of particles counted in five minutes.

n   Constant in equation (2.46).

$P(\omega)$ Power spectrum.

Q   Gas volumetric flow rate.

Re_p Particle Reynolds Number, equation (2.26).

r_1 Distance between apex of bulge and bubble centre at the bed surface.

R_{b1} Bubble radius at the bed surface, equation (2.27).

r_0 Laser beam radius at the waist.

$r(z)$ Beam radius at distance z from source.

$R(z)$ Radius of curvature at the wave front.

Sh   Turbulent Sherwood Number.

St   Stokes Number.

s   Fringe spacing.

TS   Total number of samples taken to give a.c.f.

t   Time

T   Sample time set in the correlator.

t_{av} Average time of each turning point in a.c.f.

$Turb_{app}$ Turbulence estimate from a.c.f. obtained when

using phase modulation.

$Turb_t$ Turbulence estimate corrected to take into account phase modulation.

u' rms value of fluctuations in velocity

u^* Magnitude of fluctuations in velocity.

U_a Absolute bubble rise velocity.

U_G Superficial gas velocity.

U_{MF} Minimum fluidising velocity.

U_X Component of velocity in the X direction.

U_Y Component of velocity in the Y direction.

U_Z Component of velocity in the Z direction.

U_t Terminal velocity of particle.

U_1 Estimate of velocity obtained directly from a.c.f.

U_2 Velocity taking into account turbulence effects and fringe visibility.

u''_{12}, u''_{23} Independent estimates of turbulence estimated from a.c.f.

U_C Velocity equivalent of modulator frequency.

V Scattering centre velocity.

V_r Relative particle velocity.

V_z Component of particle velocity in Z direction.

V_Y Component of particle velocity in Y direction.

V''_Y Relative turbulence intensity of particle velocity fluctuations.

V_h Particle ejection velocity radially.

V_1 Particle velocity in phase 1 of Kunii and Levenspiel's model [35].

V_2 Particle velocity in phase 2 of Kunii and Levenspiel's model [35].

V_3 Particle velocity in phase 3 of Kunii and Levenspeil's model [35].

X   Position on XX axis (Figures 4.1 and 4.3).

X   Weight of fines in bed at time t.

Y   Position on YY axis (Figures 4.1 and 4.3).

z   Distance above distributor.

z′   Distance above static bed surface.

z   Distance from source of laser beam

Greek Letters

α_g Diffusivity of gas.

α_p Diffusivity of particles.

β Decay constant from linear regression analysis.

β_1 Decay constant predicted by vortex ring model.

ΔP Pressure drop across bed.

$\Delta\upsilon$ Doppler shift of radiation scattered by particle crossing a single laser beam.

ϵ Volume fraction in the freeboard.

ϵ' Rate of turbulent energy dissipation.

ϵ_{MF} Bed voidage at minimum fluidising velocity.

ζ Volume of particles ejected per unit bubble volume.

η Kolmogoroff length scale.

θ Incident angle of laser beams.

θ' Angle of ejection of particles from the bed surface.

θ_k Kolmogoroff time.

θ_p Particle relaxation time.

λ Wavelength of laser light.

λ' Friction coefficient due to particles bouncing

against walls and each other.

μ Dynamic viscosity.

ϱ_g Density of gas.

ϱ_p Density of solids.

υ Kinematic viscosity.

ϕ Divergance of laser beam.

References

1. Abbiss, J B., Chubb, T W and Pike, E R.,
Optics and Laser Technology, Dec 1974, p.249.

2. Abrahamson, J., Chem. Eng. Sci., 1975, 30, p.1371

3. Agarwal, J K and Johnson E M.
   T.S.I. Quarterly July-September 1981.

4. Andrews, J M., Ind. Eng. Chem., 1960, 52, p.85

5. Bachovchin, D M., Beer J M. and Sarofim, A F.
   A.I.Ch.E. Symp. Ser. 1981, 77, No 205

6. Brodkey, R S., "Turbulence in Mixing Operations"
   1975, Academic Press.

7. Baskakov, A P., Shuvalov, V Y, Berg, B V.
   Chem. Eng. Sci., 1984, 39 No 3, p.407

8. Chatterjee, S. and Price, B., "Regression Analysis
   by Example" 1977, Wiley

9. Chen, T P. and Saxena, S C., in "Fluidisation"
   edited by Davidson, J F. and Keairns, D L.
   1978, Cambridge University Press.

10. Clift, R. and Gauvin, W H., in "Proceedings of
    Chemica 70", 1970, 1, p.14; Butterworths.

11. Clift, R. and Grace, J R.
    Chem. Eng. Prog. Symp. Ser., 1970, 66 No 105, p.14

12. Clift, R., Grace, J R. and Weber,
    "Bubbles, Drops and Particles" 1977, Academic Press

275

13. Colakyan, N., Catipovic, N., Jovanovic, G. and
    Fitzgerald, T., A.I.Ch.E. Symp. Ser., 1981, 77,
    No 205, p.66

14. Davidson, J F. and Harrison, D., "Fluidised Particles"
    1963, Cambridge University Press.

15. De Lasa, H I. and Grace, J R.
    A.I.Ch.E. Journal, 1979, 25 No 6, p.984

16. Do, H T., Grace, J R. and Clift, R.
    Powder Tech., 1972, 6, p.195.

17. Durst, F., Melling, A. and Whitelaw, J H.
    "Principles and Practise of Laser Doppler Anemometry"
    1981, Academic Press.

18. Fan, L T., Ho T-C., Hiroka, S. and Walawender, W P.,
    A.I.Ch.E. Journal, 1981, 27 No 3, p.388

19. Fan, L T., Hiroka, S. and Shin, S H.,
    A.I.Ch.E. Journal, 1984, 30 No 2, p.346

20. Ford, W D., Reineman, R C., Vasolos, I A. and Fahrig, R J.,
    Chem. Eng. Prog., 1977, 73 No 4, p.92.

21. Fournol, A B., Bergougnou, M A. and Baker, G G J.,
    Can. J. Chem. Eng., 1973, 26 No 1, p.401.

22. Geldart, D., Powder Tech., 1970/71, 4, p.41

23. Geldart, D., Cullinan, J., Georghiades, S., Gilvray, D.
    and Pope, D J., Trans. Inst. Chem. Eng., 1979, 57
    p.269.

24. George, S E. and Grace, J R., Can. J. Chem. Eng.,

1981, <u>49</u>, p.279.

25. George, S E. and Grace, J R., A.I.Ch.E. Symp. Ser.,
    1978, <u>74</u> No 176, p.67.

26. Glicksman, L R., Chem. Eng. Sci., 1984, <u>39</u> No 9,
    p.1373.

27. Guha, S K., Kumar, A. and Sen Gupta, P.,
    Can. J. Chem. Eng., 1972, <u>50</u> No 5, p.602.

28. Hanesian, D. and Rankell, A., I and EC Fundamentals,
    1968, <u>7</u>, p.452.

29. Hatano, H. and Ishida, M., J. Chem. Eng. Japn.,
    1981, <u>14</u>, p.306.

30. Hatano, H. and Ishida, M., Powder Tech., 1983,
    <u>35</u>, p.201.

31. Hatano, H., Okuma, T. and Ishida, M.,
    J. Chem. Eng. Japn., 1984, <u>17</u> No 5, p.491.

32. Hinze, J O. "Turbulence", 1975, Mc Graw Hill

33. Horio, M., Taki, A., Hsieh, Y S. and Muchi, I.,
    in "Fluidisation" edited by Grace, J R. and
    Matsen, J M., 1980, p509 Plenum Press.

34. Hsieh, Y S, Taki, A., Horio, M. and Muchi, I.,
    Kagaku, Kogaku Ronbunshu, 1980, <u>13</u> No 2, p.171.

35. Kunii, D. and Levenspiel, O., J. Chem. Eng. Japn.,
    1969, <u>2</u>, p.84.

36. Kato, K. and Wen, C Y., Chem. Eng. Sci., 1969,
    <u>24</u>, p.1351.

37. Launder, B E. and Spalding, D B., "Lectures in Mathematical Models of Turbulence", 1972, Academic Press.

38. Leung, L S., Powder Tech., 1972, $\underline{6}$, p.189.

39. Leva, M., Chem. Eng. Prog., 1951, p.39.

40. Leva, M. and Wen, C Y., Chapter 14, "Fluidisation", Edited by Davidson, J F. and Harrison, D., 1971.

41. Levy, Y., Ph.D. Thesis, University of London, 1981.

42. Levy, Y. and Lockwood, F C., A.I.Ch.E. Journal, 1983, $\underline{29}$ No 6, p.889.

43. Levy, E K., Caram, H S., Dille, J C. and Edelstein, S., A.I.Ch.E. Journal, 1983, $\underline{29}$ No 3, p.383.

44. Lewis, W K., Gilliland, E R. and Lang, P M., Chem. Eng. Prog. Symp. Ser., 1962, $\underline{58}$ No 38, p.65.

45. Lin, J S., Chen, M M. and Chao, B T., A.I.Ch.E. Journal, 1985, $\underline{31}$ No 3, p.465.

46. Lin L., Sears J T. and Wen, C Y., Powder Tech., 1980, $\underline{27}$, p.105.

47. Matsumo, Y., Kage, H., Nagamitsu, T., Yamaguchi, H. and Higashitani, K., Powder Tech., 1982, $\underline{33}$ No 1, p.65.

48. Maxworthy, T., J. Fluid Mech., 1972, $\underline{51}$ No 1, p.15.

49. Merrick, D. and Highley, J., A.I.Ch.E. Symp. Ser., 1974, $\underline{70}$ No 157, p.366.

50. Mojtahedi, W., Ph.D. Thesis, University of
    Edinburgh, 1983.

51. Mori, S. and Wen, C Y., A.I.Ch.E. Journal, 1975,
    21, p.109.

52. Morooka, S., Kawaguishi K. and Kato, Y.,
    1980, Powder Tech., 26, p.75.

53. Nazemi, A M., Bergougnou, M A. and Baker, G G J.,
    A.I.Ch.E. Symp. Ser., 1974, 141, p.98.

54. Nicastro, M T. and Glicksman, L R., Chem. Eng. Sci.,
    1984, 39 No 9, p.1381.

55. Ogden, D M. and Stock, D E., In "Laser Velocimetry
    and Particle Sizing" edited by Thompson, H D. and
    Stevenson, W H., 1979, Hemisphere Publishing
    Corporation, p.496.

56. Ohki, K. and Shirai, T.,
    Fluidisation Technology, 1976, 1, p.95.

57. Orcutt, J C. and Carpenter, B H., Chem. Eng. Sci.,
    1971, 26, p.1049.

58. Osberg, G L. and Charlesworth, D H.,
    Chem. Eng. Prog., 1951, 47, p.566.

59. Parks, W H., Kang, W K., Capes, C E. and Osberg, G L.,
    Chem. Eng Sci., 1969, 24, p.851.

60. Pemberton, S T., Ph.D. Thesis, University of
    Cambridge, 1982.

61. Pemberton, S T. and Davidson, J F., Chem. Eng. Sci.,

1984, <u>39</u> No 5, p.829.

62. Peters, M H., Fan, L S. and Sweeney, T L., Chem.
    Eng. Sci., 1983, <u>38</u> No 3, p.481.

63. Rowe, P N. and Everett, D J., Trans. Instn. Chem.
    Engrs., 1972, <u>50</u>, p.55.

64. Rowe, P N. and Partridge, B A., in "Interaction
    between Fluids and Particles" (London: Instn.
    Chem. Engrs.), 1962.

65. Rowe, P N. and Yacono, C X R., Chem. Eng. Sci.,
    1976, <u>31</u>, p.1179.

66. Rudd, M J., J. Phys. E: Sci. Instrum., 1969,
    <u>2</u>, p.55.

67. Steigletz, K., "An Introduction to Discete Systems",
    1974, Wiley, p.139.

68. Skinner, D G., "The Fluidised Bed Combustion of
    Coal", 1971, Mills and Boon Ltd.

69. Tanaka, I., Shimohara, H., Hirosni, H and Tanaka, Y.,
    J. Chem. Eng. Japn., 1972, <u>5</u> No 1, p.51.

70. Thomas, W J., Grey, P J. and Watkins, S B.,
    British Chem. Eng., 1961, <u>6</u> No 2, p.176.

71. Uhlherr, P H T. and Sinclair, C G., in
    "Proceedings of Chemica '70", 1970, Butterworths,
    p.1.

72. Weinstock, J., Phys. Fluids, 1978, <u>21</u> No 6, p.887.

73. Wen, C Y. and Chen, L H., A.I.Ch.E. Journal, 1982

$\underline{28}$ No 1, p.117.

74. Wen, C Y. and Hashinger, R F., A.I.Ch.E. Journal,
    1960, $\underline{6}$ No 2, p.220.

75. Werther, J. and Molerus, O., Int. J. Multiphase
    Flow, 1973, $\underline{1}$, p.123.

76. Yates, J G., "Fundamentals of Fluidised Bed
    Chemical Processes", 1983, Butterworths.

77. Yates, J G. and Rowe, P N., Trans. Instn. Chem.
    Engrs., 1977, $\underline{55}$, p.137.

78. Yuu, S., Yasukouchi, N., Horosawa, Y. and
    Jotaki, T., A.I.Ch.E. Journal, 1978, $\underline{24}$ No 3,
    p.509.

79. Zenz, F A. and Weil, N A., A.I.Ch.E. Journal,
    1958, $\underline{4}$ No 4, p.472.